Cell Adhesion mediated by the Integrin VLA-4

Julia Schmitz

Munich 2008

Cell Adhesion mediated by the Integrin VLA-4

Julia Schmitz

Dissertation
Faculty of Physics
Ludwig–Maximilians–University
Munich

presented by
Julia Schmitz
born in
Gräfelfing

May 30th, 2008
Munich

To my family and friends: Thank you!

Contents

List of Figures

Zusammenfassung

In dieser Dissertation wurde die Adhäsion von T-Lymphozyten auf funktionalisierten Substraten untersucht, basierend auf der Interaktion von dem Lymphozyten Integrin VLA-4 mit seinem physiologischen Liganden VCAM-1.

Eine allgemein akzeptierte Annahme in der Zellbiologie ist, dass die Zelle ihr Adhäsionsverhalten über die Affinität der Adhäsionsmoleküle steuert. Wir stellten jedoch fest, dass die Widerstandsfähigkeit der Zelladhäsion unter Scherkraft durch eine Mutation des Integrins VLA-4, die die Bindung des intrazellulären Adapters Paxillin verhindert, stark beeinträchtigt wird. Aus physikalischer Sicht ist es einsichtig, dass die Mechanik des Kraftübertragenden Glieds die Stärke von molekularen Bindungen beeinflusst. Wir entwickelten ein viskoelastisches Modell für die Analyse von kraftspektroskopischen Experimenten an transmembranen Adhäsionsrezeptoren, um die mechanischen Eigenschaften der Rezeptorverankerung in der Zelle zu quantisieren. Mit diesem Modell konnten wir nach der VLA-4 Aktivierung mit Magnesium feine Unterschiede in der Nano-Umgebung der Integrine feststellen. Numerische Simulationen basierend auf diesem Modell zeigen, dass die Zelle ihre Adhäsivität über die Mechanik der Rezeptorverankerung genauso effektiv einstellen kann, wie über die Rezeptoraffinität. Diese Methode wird tatsächlich von der Zelle genutzt: Die physiologische Aktivierung des Integrins VLA-4 durch das Chemokin SDF-1 verursachte hauptsächlich eine drastische Versteifung der Integrinverankerung.

Um die Zelladhäsion im Blutstrom zu beschreiben, die von einzelnen Adhäsionsmolekülen verursacht wird, entwickelten wir ein weiteres Modell, das die molekularen Bindungseigenschaften auf das zelluläre Adhäsionsverhalten extrapoliert. Wir fanden heraus, dass die Stimulierung mit Magnesium nicht die Dissoziationsrate erniedrigt, sondern bindungsunfähige Integrine aktiviert. Anhand unseres Modells konnten wir die verlängerte Adhäsion in der Durchflusskammer durch multiple Bindungen erklären.

Mit einer neuartigen opto-mechanischen Kombination aus AFM und TIRF wurde ausserdem das Herausziehen von Membranschläuchen aus der Zelle beobachtet. Damit konnte zwischen einem adhärenten Mikrovillus und einem benachbarten, nicht-adhärenten Mikrovillus unterschieden werden. Mit affinitätssensitiven Fluoreszenzfarbstoffen wurden ausserdem Affinitätsänderungen des Integrins auf der Zelle nachgewiesen.

In einem weiteren Projekt in Kollaboration mit Daniel König und Ralf Jungmann wurden die Dissipation und der Q-Faktor eines nicht-linearen Einzel-Elektron-Transistors mittels Kraftmikroskopie und Selbstoszillation ermittelt.

Abstract

The main objective of this thesis is the interaction between the lymphocyte adhesion receptor, the integrin VLA-4, and its endothelial ligand VCAM-1 investigated by atomic force spectroscopy.

It is a common paradigm that the cell regulates its adhesiveness by altering the affinity state of adhesive receptors like integrins. However, we found that a mutation in the β cytoplasmic tail of VLA-4 integrins – which impaired the binding of the intracellular adaptor protein paxillin without affecting the affinity or the distribution of the integrin – diminished the cellular adhesion strengthening in the shear flow. From a physical point of view this is in line with the well-known influence of the mechanics of the force-transmitting linker on the strength of isolated adhesive bonds. We developed a viscoelastic model to quantify the mechanics of the cellular anchorage of adhesive transmembrane receptors. With this model we were able to detect subtle differences in the nano-environment of integrins upon stimulation with magnesium. Furthermore, we demonstrated in simulations that the mechanical modulation of the receptor anchorage provides a highly effective tool for adjusting the cellular adhesiveness besides the established affinity regulation. It will be shown that the mechanical regulation of the cellular adhesiveness is indeed employed by nature: The major result of the physiological activation of the integrin VLA-4 with the chemokine SDF-1 is a stiffening of the receptor anchorage. Since cell adhesion in the blood flow is mediated by single adhesion molecules, we present a model which extrapolates the molecular properties to the adhesive behaviour of the cell in the shear flow. We found that the exogenous activation of the integrin VLA-4 with magnesium activates resting integrins on the cell surface, rather than affecting the dissociation rate of the receptor. With our model, the highly increased cellular adhesion times observed in flow chamber assays could be explained by the presence of multiple bonds, whereas classical interpretations of these ensemble measurements would suggest a reduced molecular dissociation rate. Furthermore, an opto-mechanical examination of unspecific and specific cell adhesion was performed by a combined setup of an atomic force microscope (AFM) and a total internal reflection fluorescence (TIRF) microscope. We were able to distinguish between the adherent tether and an adjacent protruding microvillus. In addition, we showed that changes in the integrin affinity can be detected with affinity-sensitive dyes.

In an unrelated project in collaboration with Daniel König and Ralf Jungmann, the dissipation and the Q-factor of an impacting nanomechanical single-electron transistor were determined by atomic force microscopy and self-oscillations.

Chapter 1

Introduction

Cell adhesion is an omnipresent phenomenon in all living organisms. For vertebrates, a tightly regulated cell adhesion is indispensable for embryogenesis and development, but also for the homeostasis of the organism. In order to achieve maximum control, specific cell adhesion is mediated by single adhesion molecules. The different receptors can be addressed selectively by their respective ligands and are specifically activated. To tackle the diverse and demanding tasks in the organism, the different adhesion receptors act in concert and complement one another.

In general, cells can be divided according to their constitutional adhesiveness in adherent cells (e.g. epithelial cells) and in non-adherent cells (e.g. lymphocytes). While epithelial cells are inherently adhesive and induce apoptosis if detached from the substrate, lymphocytes, in contrast, must not randomly stick to surfaces or other cells. However, both cell types can actively regulate their adhesiveness to suit the situation. This thesis focusses on the adhesion of lymphocytes. The main objective was the interaction between the lymphocyte adhesion receptor, the integrin VLA-4 (also called $\alpha_4\beta_1$), and its endothelial ligand VCAM-1 investigated by atomic force spectroscopy (Fig. 1.1).

In this introductory section, basic aspects will be outlined which are a prerequisite for, or related to our work. To this end, I will briefly sketch the biological background of lymphocyte adhesion, the various peculiar features of the integrin adhesion receptors and the physical principles of single-molecule force spectroscopy and of the forced unbinding of receptor/ligand bonds.

1.1 Extravasation of Lymphocytes

One example for a physiological process requiring a controlled cell adhesion is the recruitment of T-lymphocytes from the bloodstream. Lymphocytes are white blood cells, important for the induction and for the regulation of immune responses. In order to survey the homeostasis of the organism, lymphocytes circulate between the bloodstream, the lymphatic system and the peripheral tissues [6]. To switch from the passive transport in the bloodstream to an active and directed motion mediated by cell-cell and cell-matrix in-
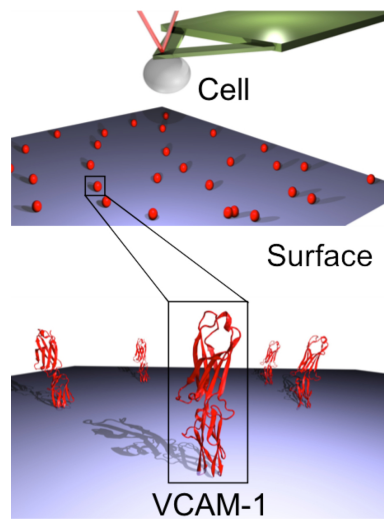
Figure 1.1: The experimental setup: The lymphocyte presenting the integrin VLA-4 was immobilised on the cantilever of an AFM. The substrate was coated with the isolated integrin ligand, VCAM-1.

teractions, these cells have to strictly regulate their adhesiveness. In the case of an injury or inflammation in the tissue, activating signal molecules (e.g. chemokines) are secreted by the adjacent endothelium. Sensing these signals, the lymphocytes can exit the bloodstream to access the target site in the tissue.

1.1.1 Adhesion Cascade

The extravasation of lymphocytes is a multi-step process [7, 8]. If the lymphocytes in the bloodstream incidentally come into contact with the endothelium lining of the vessel wall, they are possibly captured and start to roll on the endothelial cells (Fig. 1.2). This process is mediated by selectins and integrins – two important classes of cellular adhesion receptors. Rolling interactions require a dynamic equilibrium of bond formation and bond dissociation. On the leading edge, new bonds are formed, whilst on the rear end, the bonds break up at a comparable rate. During this process, the lymphocytes are slowed down so that signal molecules presented on the endothelium can be detected. Chemokines, for instance, bind to G-protein coupled receptors on the lymphocytes and thus trigger different intracellular signalling pathways [9]. This induces a rapid activation of the integrins and the stoppage of the lymphocytes by firm adhesion to the endothelium. Then, adhesion strengthening followed by cellular spreading is induced, enabling the lymphocyte to leave the bloodstream and to extravasate to the target tissue [10]. The recruitment of lymphocytes from the bloodstream is tightly regulated by varying the kind and the number both of the signal molecules and of the adhesive ligands expressed on the endothelium. This
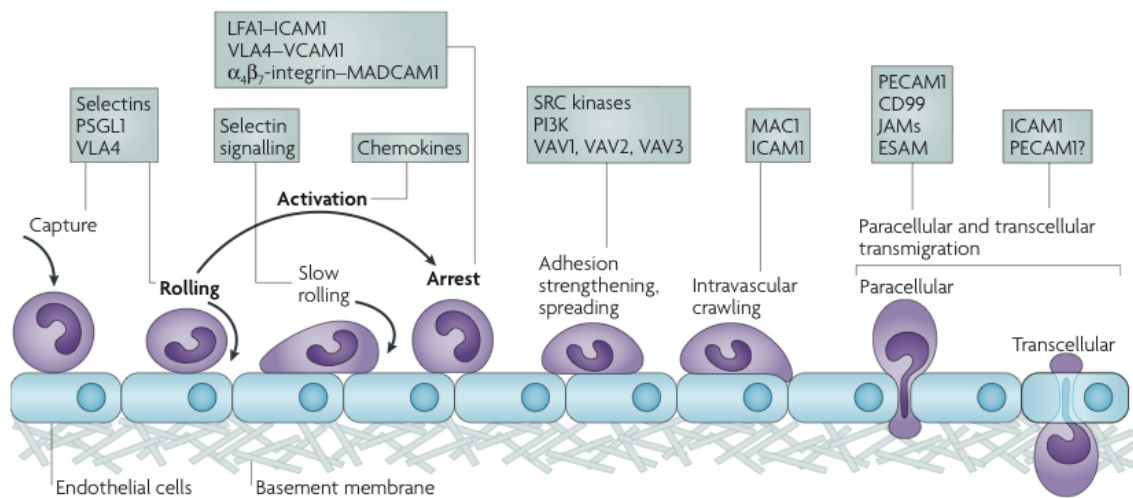
Figure 1.2: The recruitment of lymphocytes from the blood stream: The initial rolling process slows the lymphocytes down, so that they can react to inflammatory signals displayed on the endothelium. In the case of injury or inflammation in the adjacent tissue, the lymphocytes start to adhere strongly to the vessel wall and extravasate into the tissue (figure taken from ref. [1]).

combinatory control leads to the high selectivity of the immune system [8].

1.1.2 Cellular Adhesiveness

During the adhesion cascade preceding the extravasation of lymphocytes, the cells adapt their adhesiveness from initial weak rolling interactions to strong adhesion. Since all these interactions are mediated by cellular adhesion receptors, the cell has to modulate the adhesive properties of the molecules in order to encounter the different mechanical and kinetic requirements for these modes of adhesion.

Avidity

At whole cell level, the adhesiveness mediated by one specific receptor species is described by the avidity [11]. Thus, the avidity depends on the binding properties of the single molecules, but also on the distribution on the cell surface [12]. It can be increased, for instance, by enhancing the expression level of the receptor on the cell. Since this results in more receptor molecules being displayed on the cell surface, the probability for bond formation is greater, raising at the same time the cellular adhesiveness. Another possibility for increasing the adhesiveness is the activation of resting receptors. For some adhesion receptors, as for integrins, a large reservoir of inactive receptors is present on the cell surface [13]. Activating some or all of them changes the number of active receptors available

for binding. Furthermore clustering the receptors will concentrate the molecules at the site of adhesion, thereby increasing the cellular adhesiveness without changing the number of expressed or active receptors on the cell surface.

Affinity

The affinity of the single receptor molecule can likewise be modulated. The affinity is related to the ratio of the binding and dissociation rate and describes the kinetics of binding soluble ligands. Thus, it refers to the free energy of the interaction in equilibrium [14]. The affinity for the ligand is changed, e.g., after conformational rearrangements in the binding pocket of the receptor. Regardless of whether these changes affect the binding rate or the dissociation rate, an increased binding and/or a reduced dissociation will both result in a higher affinity.

Anchorage

A less apparent way to modulate the cellular adhesion is the anchorage of the adhesive receptor in the cell. On the one hand, the anchorage of the receptor molecules determines the lateral mobility of the receptor on the cell surface [11]. This is of fundamental importance for the binding between molecules, which in the case of cell adhesion are both constrained to different surfaces. Hence, an altered anchorage of the receptor will affect its diffusivity in the membrane and, thus, the two-dimensional binding kinetics of a surface-bound receptor/ligand pair.

On the other hand, the receptor anchorage will determine the mechanics of force loading. In the bloodstream, the adherent cell experiences a force, which is transmitted to the adhesive receptor/ligand bond. The force loading of the bond will depend on the anchorage of the transmembrane receptor in the cell. It will differ for receptors diffusing freely in the membrane, for receptors clustered with other molecules by their cytoplasmic ends, or for receptors attached to the cytoskeleton (Fig. 1.3). Likewise, the mechanics of the membrane environment also influences the force loading [2]. If the receptors are located in lipid rafts or in a membrane compartment with many actin binding proteins, the surroundings of the receptors will be stiffer. Thus, not only direct intracellular modifications of the receptor itself, but also the nano-environment of the receptor both exert an influence on the force loading. Since – as discussed below in section 1.3.2 – the force loading of a molecular bond determines the bond strength, all these processes affecting the mechanics of the receptor anchorage will modulate the cellular adhesiveness.

1.2   Integrins

Integrins constitute a large class of cell adhesion receptors. These transmembrane receptors are vital for the development and homeostasis of the organism, as for instance in the embryogenesis, in the maintenance of the skin integrity, in blood clotting and in immune responses [10, 15]. In particular, they play a crucial role in all reactions of leukocytes to
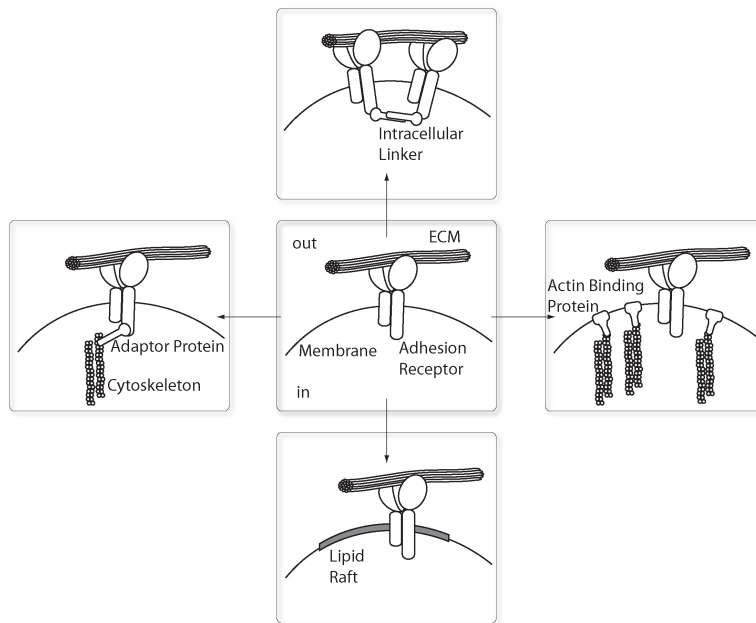
Figure 1.3: The cellular anchorage of integrins: Integrins can be either freely diffusing in the membrane (*middle*), attached to the cytoskeleton (*left*) or clustered by intracellular proteins (*top*). But the nano-environment also affects the receptor anchorage: receptors located in lipid rafts (*bottom*) or in membrane areas with many actin-binding proteins (*right*) display a stiffer anchorage than those in other membrane compartments (figure taken from ref. [2]).

infection and injury as well as in general cell adhesion, migration and phagocytosis [16]. Since the malfunctioning of integrins causes many human diseases, e.g. asthma, cancer metastasis, multiple sclerosis and other auto-immune diseases [10], they are a focus in medical research serving as potential targets for drug design [8, 17, 18, 19].

During the adhesion cascade preceding the extravasation of lymphocytes, integrins participate in all adhesive steps from capture and rolling to firm adhesion (Fig. 1.2). This of course necessitates different time scales and functional requirements for the molecular bonds. In order to regulate dynamically the integrin-mediated adhesion, the cell can adapt all three parameters of adhesiveness described above: the avidity, the affinity and the anchorage of the receptors [14].

1.2.1 Structure

This remarkable versatility of integrins is based on the plasticity of their molecular structure. The transmembrane heterodimers are composed of an α and a β subunit, each of ca. 90-160 kDa in size. 18 α and 8 β subunits are known in mammals, which assemble non-covalently to 24 integrin receptors [7]. The α and β subunits are divided into cytoplasmic,

transmembrane and extracellular domains with peculiar structural features.

Ectodomains

In general, integrins can be classified into two groups depending on the ectodomain of the α subunit: The α subunit of the first group contains a von-Willebrand-factor-A domain [20] – also called αA domain or αI domain –, the other group lacks this domain. The crystal structure of the extracellular domains has been solved for the integrin $\alpha_V\beta_3$, which has no αA domain [21,4]. The ectodomain of the α subunit comprises four domains (Fig. 1.4, blue):
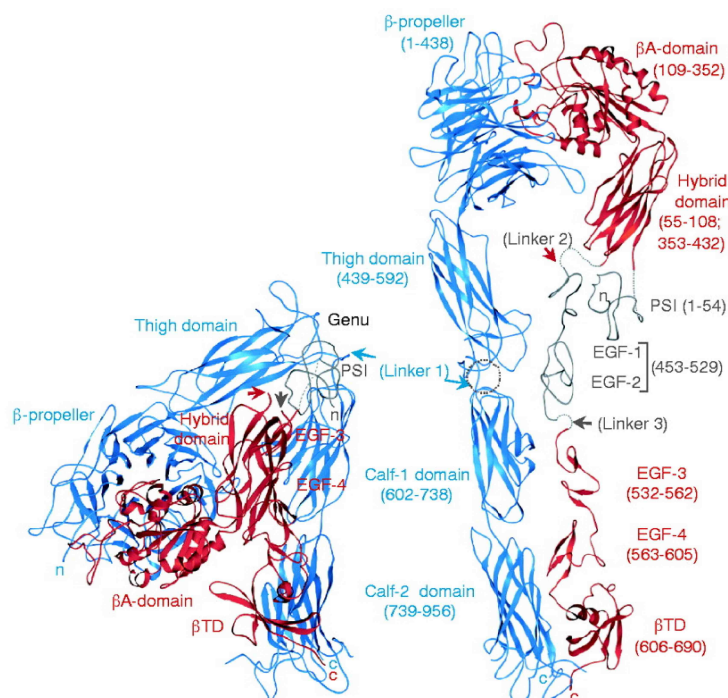
Figure 1.4: The structure of the integrin $\alpha_V\beta_3$: The α and β subunits are depicted in blue and red, respectively, and the domains are indicated. The head of the heterodimer can bend towards the membrane at the genu (*left*; figure was taken from reference [3]).

Starting from the membrane-distal end, a N-terminal 7-bladed β propeller is followed by an Ig-like Thigh domain and two large β sandwiches, Calf-1 and Calf-2. For αA integrins, the αA domain, which consists of a Rossmann fold with a central β sheet surrounded by α helices, is inserted between blade 2 and 3 of the propeller. In this introduction, however, I will focus on integrins without an αA domain, since the investigated integrin VLA-4 ($\alpha_4\beta_1$) also lacks this domain.

The extracellular part of the β subunit has eight domains (Fig. 1.2.1, red): The N-terminal PSI domain contains an Ig-like Hybrid domain, which in turn includes the βA domain [5]. The structure of the βA domain is homologous to the αA domain and contains

the ligand-specificity determining loop. Four EGF-like domains and a membrane proximal tail domain (βTD) follow the PSI domain.

The integrin heterodimer is formed by non-covalent interactions between both subunits, thereby grouping into functional sections. Hence, integrins can be structured in a globular N-terminal head connected to the membrane via two flexible legs. The assembly of the head together with glycosylation sites in the propeller stabilises the formation of the integrin heterodimer [22, 20]. The head group is formed by the propeller of the α subunit and the βA domain of the β subunit and contains the binding site for the ligand. The legs are made of the Thigh and the Calf domains of the α chain and of the PSI, Hybrid, EGF and βTD domains of the β chain. The integrin can bend at a flexible region of the legs called genu (Fig. 1.2.1), which is located between the Thigh and the Calf-1 domains on the α subunit and between the EGF-1 and the EGF-2 domains on the β subunit.

Transmembrane and Cytoplasmic Domains

The transmembrane domains of the α and β subunits each consist of a long tilted α helix spanning the membrane. In the bent state, they are densely packed by electrostatic and hydrophobic interactions into a coiled-coil structure [23, 24, 25, 26]. In the extended state, the α and β transmembrane domains become separated, which is an important feature for the signal transmission [27, 28, 29].

The cytoplasmic tails are also associated in the bent state [23]. A salt bridge connects the tails at the so-called membrane-proximal hinge region [30]. The disruption of this interaction has been shown to activate the integrins. Furthermore, the cytoplasmic domains serve as a relay station for integrating intracellular and extracellular signals. They display the recognition sequences for a large variety of intracellular signalling and cytoskeletal adaptor molecules, as kinases and phosphatases or talin, α-actinin, filamin and tensin [31, 32]. Thus, they convert cytoplasmic biochemical signals into conformational changes of the extracellular domain and vice versa. The intracellular domains are therefore required for a proper signal transmission as well as for mechanical modifications such as the formation of clusters or the anchorage of the integrin to the actin cytoskeleton.

Conformations

Integrins occur in different conformations with different affinities for the ligand (Fig. 1.5). These conformational states coexist in a dynamic equilibrium on the cell surface, which is affected by activating stimuli. The bent conformation, in which the head group is bent down towards the membrane (< 5 nm [29]), is regarded as a low affinity or resting state. Resting integrins seem to be incapable of binding their large physiological ligands due to the steric hindrance of the membrane [29, 33]. However, the binding of small peptides was actually observed [33]. The bent conformation of resting integrins is stabilised by interactions at the interface between the head and the lower legs [34], by interactions between the transmembrane helices of the α and β subunits [27] and by a membrane proximal salt bridge between the cytoplasmic domains at the so-called hinge region [7]. The

disruption of the hinge interaction between the cytoplasmic tails and the resulting spatial separation leads to the straightening of the integrin legs [28]. Likewise, the shortening of the transmembrane domains or the disruption of the head-tail interaction induces the extension of the integrin [27, 35].
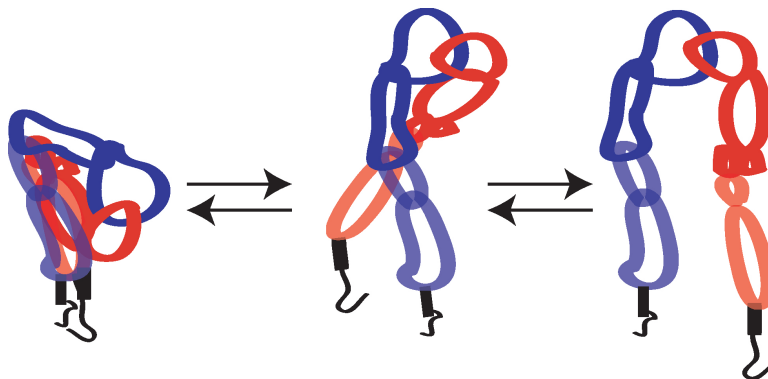
Figure 1.5: The conformational equilibrium of integrins: The bent conformation shows low affinity (*left*), the extended conformation with closed head intermediate (*centre*) and the extended conformation with open head high affinity for the ligand (*right*). The α and β subunits are depicted in blue and red, respectively.

In the extended conformation, the integrin head protrudes ca. 20 nm from the cell membrane [21]. The extended conformation exists with a closed and an open head group depending on the angle between the βA and Hybrid domains of the β subunit (Fig. 3). In the open head group, the α1 helix in the βA domain is moved inwards accompanied by a rearrangement of the β6-strand/α7-helix loop and a downward displacement of the C-terminal α7 helix (reviewed in [36]). This promotes the swing-out of the Hybrid domain [37]. Integrins in the extended conformation with an open head group show high affinity, whereas integrins with closed head display intermediate affinity for the ligand [29, 38]. The rolling interaction preceding the lymphocyte extravasation is probably mediated by integrins in the extended conformation with a closed head group, whereas the extended state with an open head group results in firm adhesion [29, 39].

Ligand Binding

The ligand binding of integrins is highly dependent upon divalent cations. On the integrin $\alpha_V\beta_3$, the α subunit contains four ion binding sites on the propeller and a fifth at the genu [40]. Furthermore, on the β subunit, a linear array of three binding sites for divalent cations is located in the ligand binding site of the βA domain [4] (Fig. 1.6). The ion binding site in the middle is called metal ion dependent adhesion site or MIDAS [21, 4]. The sites framing the MIDAS are the ADMIDAS (adjacent to MIDAS) and, on the opposite site adjacent to the β propeller, the ligand induced metal binding site or LIMBS [4].
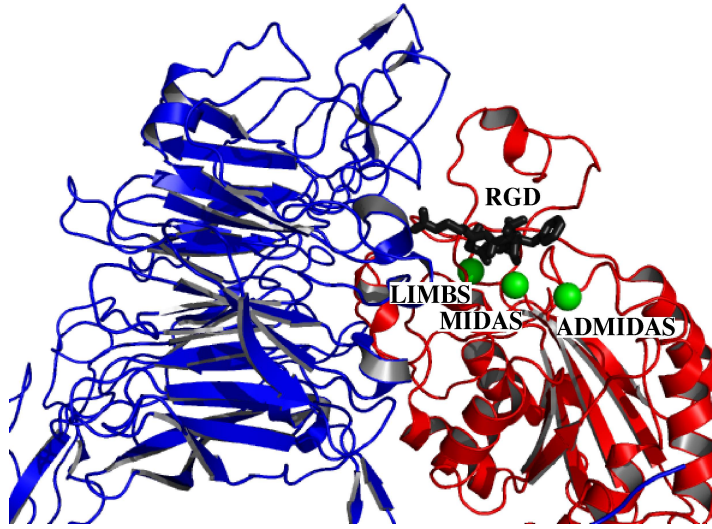
Figure 1.6: The ion binding sites: The RGD ligand (*black*) binds into the groove between the propeller of the α subunit (*blue*) and the βA domain of the β subunit (*red*). The affinity for the ligand is regulated by the cation coordination of the three ion binding sites on the β subunit (*ions in green*). The main interaction with the ligand occurs between the acidic aspartate and the MIDAS ion. The MIDAS is framed by the LIMBS and the ADMIDAS.

Many integrins form strong non-covalent bonds with RGD-containing proteins, such as fibronectin, fibrinogen and vitronectin. For αA-lacking integrins as $\alpha_V\beta_3$, the ligand binds into the cleft between the propeller and the βA domain of the head group [4, 41]. With calcium and in the absence of ligand, only the ADMIDAS is occupied by a cation, whereas the other two ion binding sites on the βA domain remain unoccupied [42]. In the closed low-affinity βA domain, the metal coordination at the ADMIDAS locks the α1 helix and the $\beta6/\alpha7$ loop (Fig. 1.7). This contact is broken by the binding of ligand or by the occupation of the MIDAS with manganese. Hence, the concerted movements of the α1 helix, the $\beta6/\alpha7$ loop and of the α7 helix become possible [37,43]. In manganese and in the presence of ligand, all three metal binding sites are occupied [4,5]. The ion incorporated at the LIMBS contributes to the stability of the liganded structure. Furthermore, structural rearrangements upon ligand binding change the metal ion coordination at the ADMIDAS, so that it is closer to the MIDAS and also improves the stabilisation of the new MIDAS ion [4]. The major interaction between the RGD ligand and the integrin $\alpha_V\beta_3$ is mediated by the contact between Asp^{RGD} and the MIDAS ion [4, 44]. The binding pocket is very shallow and, hence, does not protect this interaction from attacking water molecules [44]. However, a single water molecule is tightly coordinated to the MIDAS ion and blocks the access of free water molecules to the major interaction, thus impeding bond dissociation [44].

The MIDAS region of integrins is required for the two key interactions in the lymphocyte
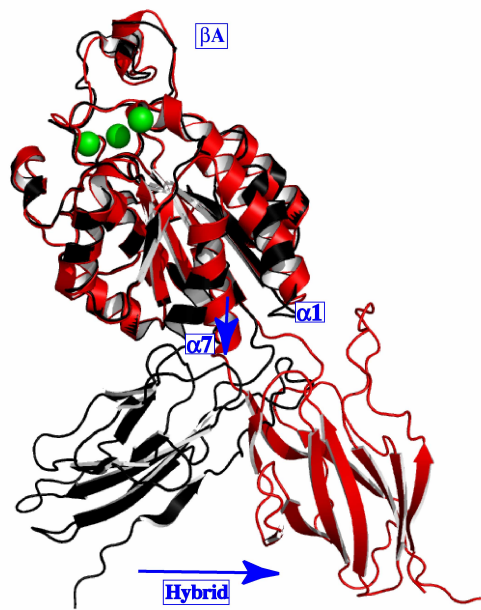
Figure 1.7: The β_3 subunit with closed and open angle of the Hybrid domain (*in black and red, respectively*): The liganded structure of ref. [4] was aligned with the structure of ref. [5]. The metal ion binding sites are indicated with green spheres. The major conformational changes affecting the $\alpha7$ and the $\alpha1$ helix are assigned by blue arrows.

recruitment from the blood stream, e.g. rolling and firm adhesion [42, 38]. The bistable regulation of these two adhesion modes is performed by the interplay of all three ion binding sites [42]: The occupation of the ADMIDAS by calcium is required for rolling adhesion [42]. This metal ion binding site therefore represents a negative regulatory site on integrins [40], responsible for the inhibition through a high concentration of calcium. In contrast, the LIMBS displays a positive regulatory site which is necessary for firm adhesion [42, 44]. By these means, integrins are capable of switching between rolling and firm adhesion.

1.2.2   Activation

Integrins are so called due to their ability to integrate information from the extracellular and the intracellular space. They can transmit signals in both directions [45] and adapt their binding properties to different requirements. The term inside-out signalling is used, if the integrins receive intracellular signals which modulate their interaction with the ligand in the extracellular space [30, 46]. Along the same lines, signal transmission from the extracellular domains of the integrin into the cell is referred to as outside-in signalling [14]. It is difficult to transmit signals and conformational changes through such long and extended structures as integrins [26]. It has however been shown that the bidirectional signalling of integrins works by coupling extracellular conformational changes to transmembrane rear-

rangements and the separation of the cytoplasmic tails [28, 26, 47]. Thus, the activation of integrins is based on structural changes.

Models for the Activation across the Cell Membrane

On resting lymphocytes, integrins are predominantly expressed in the low-affinity conformation. Upon integrin priming, they are activated from low to high affinity prior to ligand binding [16, 37]. In intracellular priming, structural modifications – such as the separation of the cytoplasmic tails [28] or of the transmembrane domains [48, 27] – lead to conformational changes in the ectodomains and induce high affinity. From the outside, integrins are readily primed by the stimulation of the extracellular domains with manganese, activating antibodies or mutations which shorten the $\alpha 7$ helix or open the head group [49, 50, 51, 52]. However, the extracellular priming by these stimuli directly induces the high-affinity conformation without the need of conformational changes in domains remote from the ligand binding site [48, 37].

Different models have been proposed to explain the signal transmission across the membrane. The switchblade model (reviewed in [34]) suggests that the integrin extension and leg separation is coupled with the swing-out of the Hybrid domain and the displacement of the $\alpha 7$ helix in the βA domain [29, 39, 5]. This swing-out can only take place after the extension of the legs due to the space required [37]. During inside-out signalling, the interactions between the cytoplasmic tails are perturbed – for example by the binding of the cytoskeletal adaptor protein talin – whereupon the cytoplasmic and the transmembrane domains separate [43]. The resulting separation of the lower legs then destabilises the interactions between the head and the legs, so that the integrin snaps open into the extended state in a switchblade-like manner. Although this is not sufficient to initiate the swing-out of the Hybrid domain directly, the equilibrium is shifted in favour of the open head [43]. The movement of the Hybrid domain would subsequently pull down the $\alpha 7$ helix in a bell-rope-like fashion [34, 53], thus inducing the remodelled ion binding site to convert the low-affinity into a high-affinity binding pocket. During outside-in signalling, ligand binding repositions the $\alpha 1$ helix, the $\beta 6/\alpha 7$ loop and the $\alpha 7$ helix [37, 53]. Since these rearrangements are tightly coupled, the induction of a high-affinity head group is linked to the piston-like downward shift of the $\alpha 7$ helix [53]. The movement of the $\alpha 7$ helix then induces the swing-out of the Hybrid domain, which in turn results in the separation of the legs and transmembrane domains [53, 5]. Thus, the initial intradomain rearrangements in the βA domain induce large interdomain conformational changes, thereby transmitting outside-in signals. The three conformational states are expected to coexist even prae ligand binding [34]: the bent state incapable of binding physiological ligands, the extended state with a closed head group representing an intermediate affinity, and the extended state with an open head group, which shows high affinity for the ligand.

Another model, the deadbolt model (reviewed in [46]), proposes that a hairpin loop in the β tail domain hinders the movement of the $\alpha 7$ helix in the βA domain, thus acting as a deadbolt [46]. During inside-out signalling, for example, the binding of talin at the cytoplasmic tails induces piston-like, seesaw [30], sliding [54] or rotational [41] movements.

This unlocks the deadbolt and accomplishes the inside-out signalling [46]. The deadbolt model suggests further that ligand binding provides enough energy to induce the swing-out of the Hybrid domain and results in varying degrees of genu-extension depending on the stimulus of outside-in signalling. Thus, the deadbolt model considers the extension and the open head group as characteristics for post-ligand outside-in signalling, whereas the activation to high affinity already results from the loss of the constraining contact between the β tail and the $\alpha 7$ helix in the βA domain [46, 37]. In the switchblade model, however, the extension and separation of the legs together with the swing-out of the Hybrid domain are regarded as necessary for activation.

Activating Stimuli

The activation of integrins ensues from extracellular or intracellular stimulation resulting in the extended state, with either a closed head group (intermediate affinity) or an open head group (high affinity).

Divalent cations have been shown to be artificial exogenous activators of integrins. In the presence of manganese, all three integrin conformations coexist in a dynamic equilibrium, whereas in calcium or in calcium and magnesium, the bent conformation is predominant [34]. Whilst calcium at the ADMIDAS exerts negative regulatory effects, manganese (but not magnesium) activates by competing with calcium at this site [42]. The occupation of the ADMIDAS with manganese shifts the ADMIDAS towards the LIMBS and favours the downward movement of the $\alpha 7$ helix [42], thus inducing high affinity. Therefore, manganese or magnesium in the absence of calcium shift the equilibrium towards the extended open conformation, whereas calcium bound to the ADMIDAS stabilises the closed head group [37, 50, 38].

Monoclonal antibodies and ligands or ligand mimics also act as extracellular stimulants [55]. Activating antibodies are mostly directed against the ligand binding region [56] or the membrane-proximal leg region [57] of the β subunit. They are thought to induce conformational changes, thus evolving their adhesion-promoting activity. Cyclic peptides containing the ligand mimicking motif RGD shift the equilibrium even more than manganese to the extended state [29]. Ligand binding triggers structural rearrangements [4] resulting in a conformation of the metal binding sites which supports the open head group [37].

In the blood stream, the physiological activation relies on complex intracellular signalling pathways triggered by the ligation of a second receptor on the lymphocyte surface. Chemokines represent potent and selective activators of integrins [9, 58]. These small polypeptides of only 8-10 kDa are displayed on the apical surface of endothelial cells and bind to G-protein coupled receptors (GPCR) on the lymphocytes [59]. GPCRs are transmembrane receptors with seven membrane-spanning domains. Their extracellular N-terminal domain determines the high specificity for their chemokine ligands, whereas the intracellular C-terminus is coupled to a G-protein. The binding of chemokines initiates intracellular signal cascades which impinge on the cytoplasmic tails of the respective integrins (for reviews see [7, 1]). Hereby, the ligation of the chemokine receptor leads to the activation of the membrane-associated G-protein trimer and the subsequent dissociation
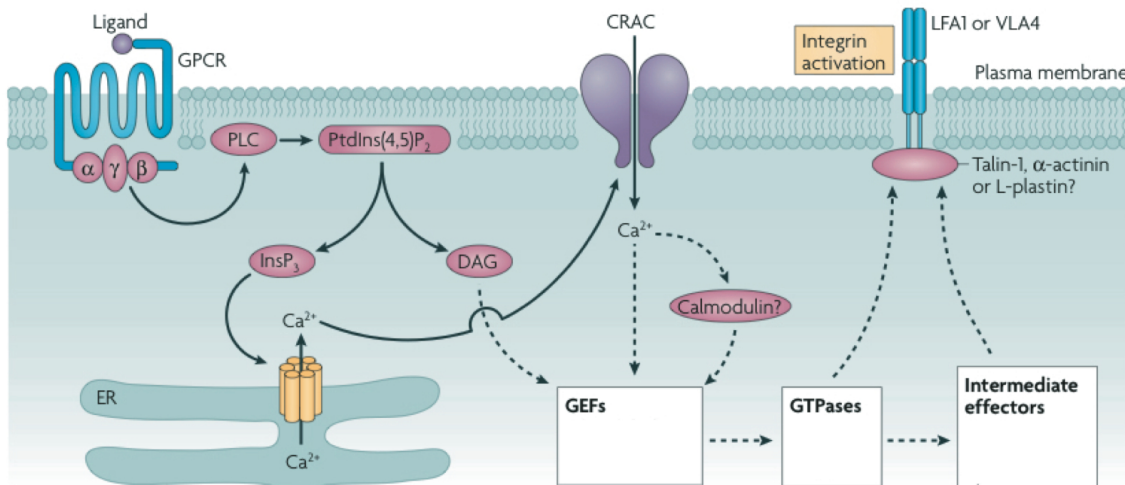
Figure 1.8: Chemokine-induced signal cascade: Signal pathways and candidate molecules which remain to be confirmed are represented with dashed lines and question marks, respectively. The chemokine binds to its GPCR hereby inducing the dissociation of the G-protein and the production of DAG and IP3. This raises the intracellular calcium level and stimulates GEFs. Further downstream, GTPases prompt the binding of adapters to the integrin cytoplasmic tails which finally activate the integrins (figure adapted from reference [1]).

of the G_α subunit from the G_β and G_γ subunits. In consequence, the phospholipase C is activated to cleave PIP2 into two second messengers, namely IP3 and DAG. IP3 triggers the calcium release from intracellular stores, thus raising the intracellular calcium level and inducing calcium influx from the extracellular space through the calcium-regulated-activated-calcium channel. Calcium and DAG possibly activate GEFs which in turn continue the cascade by stimulating GTPases. The latter finally transmit the signal either directly or via intermediate effectors to the cytoplasmic integrin tails (Fig. 1.8).

The rapid activation of integrins by chemokines is accompanied by the spatial separation of the cytoplasmic tails [28] and probably results in the extended conformation with intermediate affinity [34,60]. The final step of this inside-out signalling is most likely mediated by the binding of intracellular molecules to the cytoplasmic tails of the integrins. For instance, the binding of talin to the β tail is not only vital for the coupling of ligand-bound integrins to the cytoskeleton [61] and for the enforcement of the cytoskeletal anchorage of the integrin through the recruitment of other cytoskeletal proteins, e.g. paxillin [62]. The binding of talin via its F3 lobe of the FERM domain to the membrane-proximal NPxY motif on the β tail also plays an essential role in the final step of inside-out activation [63, 64, 28, 65, 20, 66, 67]. It was suggested, that this activation is caused by a second hydrophobic interaction between a membrane-proximal α helix of the β tail and the F3 lobe of the integrin-binding talin head (Fig. 1.9). This interaction disrupts the salt bridge be-
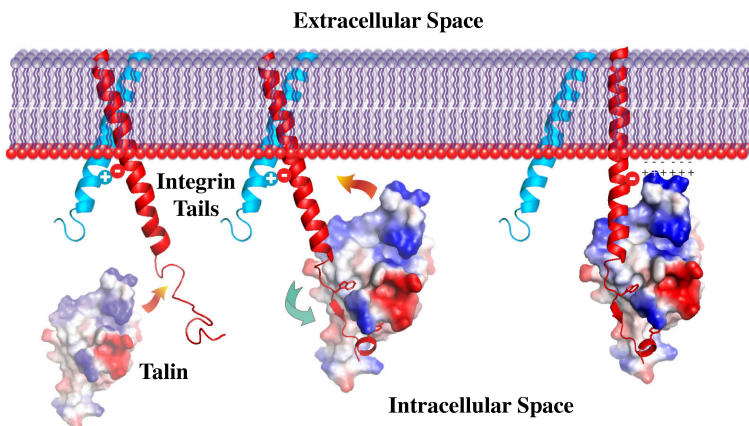
Figure 1.9: Conformational changes induced by talin binding to the β cytoplasmic tail (*red*): The main interaction is achieved by the NPxY motif on the β tail. A second membrane-proximal interaction between talin and the β subunit disrupts the salt bridge linking the two cytoplasmic tails. This results in the separation of the integrin tails and possibly induces further conformational changes in the extracellular domains (figure adapted from wikipedia).

tween the α and β tail [63], which normally stabilises the bent low-affinity conformation by clasping the α and β cytoplasmic tails. In addition, an intramembranous segment is pulled down in the cytoplasm by electrostatic interactions with the talin head [20, 68]. Thereby, the transmembrane helices are shortened and separated [69], resulting in the activation of the ectodomains.

1.3 Single-Molecule Force Spectroscopy

Integrins are designed as force-resisting receptors. In their normal environment they are always exposed to forces. Thus, the presence of forces is possibly essential for their physiological function. In addition, these cellular adhesion receptors are actively regulated by the cell and coexist in several different activation states on the cell surface. In order to dissect the properties of the coexistent states and in order to monitor the native function and regulation of integrins, single-molecule force spectroscopic experiments on living cells are desirable. Therefore, we chose the atomic force microscope in order to investigate the lymphocyte integrin VLA-4.

1.3.1 Atomic Force Microscope

The atomic force microscope (AFM) was invented by Binnig, Quate and Gerber in 1986 and belongs in the category of scanning nearfield microscopes [70]. Whereas in its early stages, the AFM was used to image surfaces at atomic resolution, it is now very popular for force

spectroscopic measurements on biological probes [71, 72, 73, 74, 75]. For this application, a laser beam is focussed on a cantilever, reflected on its back and detected by a segmented photodiode. The cantilever is mounted on a piezo element, which can precisely adjust the cantilever position with respect to the substrate. A bending of the cantilever will result in the deflection of the laser beam and therefore in a different signal in the photodiode (Fig. 1.10). With the spring constant of the cantilever, this deflection can be converted into the force which caused the bending. Amongst other force spectroscopic techniques such as biomembrane force probe and optical tweezers, the AFM has by far the highest spatial and temporal resolution.

AFM experiments can be conducted in fluid at defined temperature and pH values, mimicking the physiological conditions. In addition, it allows for a highly controlled contact between the probe and the substrate in terms of the contact time and force. Thus, the atomic force microscope represents a suitable technique for investigating such sensitive probes as living cells.

In order to investigate the adhesion of living cells mediated by the specific interaction of a particular receptor/ligand pair, the cantilever as well as the substrate have to be thoroughly prepared. Mostly, the cell is immobilised on the cantilever and the substrate is functionalized with the ligand to the cell surface receptor of interest (Fig. 1.10). Once the cell has been brought into contact with the substrate, the receptor/ligand pair can interact. During retraction, a force is loaded to the molecular bond until it ruptures. The whole cycle of approach and retraction is recorded in force-time or force-distance curves.

To further extend its abilities, the setup of an atomic force microscope can be combined with high-end optics as confocal microscopy or total internal reflection fluorescence microscopy (TIRF) [76]. The combination of AFM and TIRF, for example, allows for the observation of actions close to the substrate. After fluorescence labelling, the cell membrane or even single molecules on the cell surface can be observed in real time, while the contact can be adjusted and the mechanical parameters assessed by the AFM.

1.3.2   Forced Unbinding of Single Molecules

In thermal equilibrium, bonds are continuously dissociating and re-building activated by thermal fluctuations. The dissociation constant K_D describing this process is defined by the ration of the equilibrium dissociation rate k_{off}^0 and the association rate k_{on}.

Potential Landscape

The binding and the unbinding of the receptor/ligand pair is governed by the potential energy of the molecular bond. This potential can be imagined as an extraordinarily complicated 3-dimensional landscape. In the bound state, the molecular bond is located at the bottom of the energy funnel and surrounded by ragged energy barriers. For simplification, only the major barriers of the 3-dimensional landscape are commonly projected along the reaction coordinate x (Fig. 1.11). Under equilibrium conditions, bond dissociation is activated by thermal energy and the most probable unbinding pathway will cross the lowest
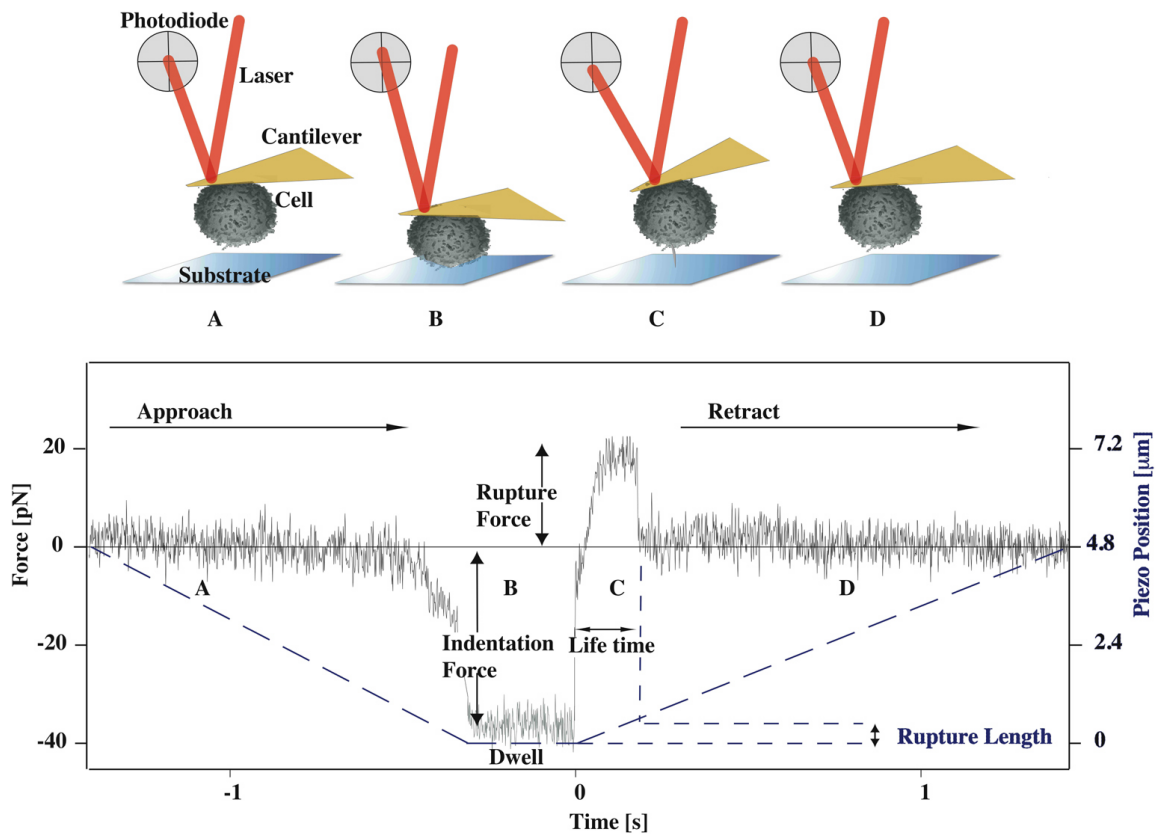
Figure 1.10: Atomic force spectroscopy: A cell is attached to the cantilever, which can be moved with respect to the functionalized substrate by a piezo element. The reflection angle of the laser beam focussed on the back of the cantilever changes if the cantilever is deflected. This is detected by a photodiode and converted into force. The different stations of an approach-retract cycle are depicted in the upper panels. The corresponding points are indicated in the recorded force curve below. For constant piezo velocity, the distance travelled is proportional to the time. Thus, the force curves can either be displayed against distance (*right axis and dashed lines*) or against time (*bottom axis*). During the approach (*A*), the force baseline is recorded. While the cell is pressed onto the substrate with a predefined indentation force for a certain dwell time (*B*), molecular bonds between the cellular receptors and their isolated ligands on the substrate may form. During retraction, the force rises (*C*) and a membrane tether is pulled from the cell until the molecular bond ruptures. Then, the force decreases down to the basal level (*D*). The height of the resulting step is called rupture force, the time until rupture is the lifetime of the bond and the position of the rupture is termed rupture length.

barrier of the landscape. Hence, the position and the height of this transition barrier T – separating the bound and the unbound state – determine the unbinding kinetics of the molecular bond.
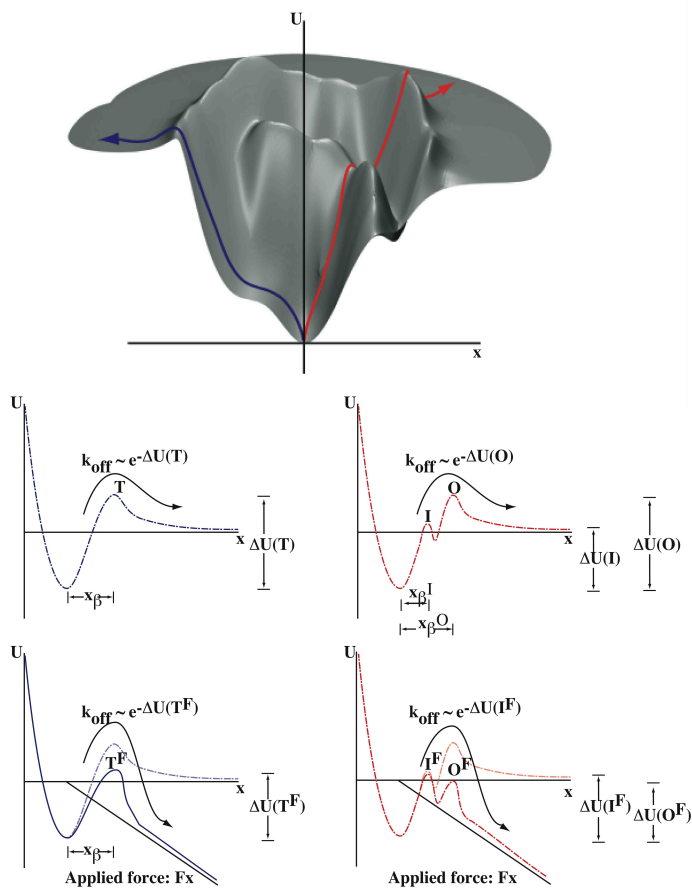
Figure 1.11: The potential landscape of a molecular bond: The 3-dimensional energy landscape (*top*) is projected along the trajectories crossing one barrier (*blue*) or two barriers (*red*). In the middle row, the equilibrium landscapes are depicted. The application of an external force F tilts the equilibrium landscape (*bottom*), thereby reducing the height of the transition barrier T. The position of the transition barrier x_β governs the susceptibility of the molecular bond to external forces. In the case of the two barriers, the higher outer barrier O determines the unbinding process in the absence of forces ($T = O$). Under the influence of force, the inner barrier I may become prominent and thus becomes the rate-limiting transition barrier ($T^F = I^F$).

The application of a force supplies mechanical energy to the system. In the picture of an energy landscape, the force tilts the binding potential. The energy barrier is thereby reduced by $-F{\cdot}x$, where F is the force acting in the direction of the barrier. Thus, the force-induced dissociation may take a different pathway through the potential landscape, crossing higher barriers than the equilibrium trajectory. The off-rate k_{off} is directly related to the barrier height $\Delta U(T^F)$. However, the reduction of the barrier height by forces depends on the position of the transition barrier T with respect to the bound state, which is also

called potential width x_β: If the transition barrier is close to the bound state, the barrier is less reduced than a transition barrier with a large potential width. Thus, the bond's susceptibility to forces is characterised by the position of the energy barrier. Furthermore, if an energy landscape comprises more than one transition barrier, the application of force possibly renders a different barrier rate-limiting for the bond dissociation ($T^F = I^F$), which is smaller, but closer to the bound state than the equilibrium transition barrier ($T = O$) (Fig. 1.11). For these reasons, the energy barriers probed in equilibrium and non-equilibrium experiments are not necessarily the same.

Theory of Forced Unbinding

In the physiological setting of lymphocytes in the blood stream, bond dissociation is not an equilibrium process since the receptor/ligand bond is subjected to external forces of the shear flow. The terms avidity and affinity are defined for equilibrium conditions and are therefore not sufficient to characterise a molecular bond under the influence of force. In cellular AFM experiments, the unbinding of the receptor/ligand bond also occurs under the influence of force as in the physiological situation. Since an external force in the direction of the unbound state tilts the equilibrium landscape and reduces the height of the transition barrier $\Delta U(T^F)$, the dissociation rate is increased. In 1978, Bell described this impact of forces on the dissociation kinetics of a molecular bond [77]. The rate of force-induced dissociation k_{off}^F is:

$$k_{off}^F = \omega \cdot e^{-\frac{\Delta U(T) - E_{mech}}{k_B T}}$$

ω is the attempt frequency of the thermally activated escape in equilibrium; $\Delta U(T)$ is the barrier height, which is reduced by the mechanical work E_{mech} performed on the system by the external force F; and $k_B T$ is the thermal energy. For $F = 0$, the equilibrium off-rate k_{off}^0 is given by:

$$k_{off}^0 = \omega \cdot e^{-\frac{\Delta U(T)}{k_B T}}$$

Thus, the dissociation rate of the molecular bond can be correlated with the applied force:

$$k_{off}^F = k_{off}^0 \cdot e^{-\frac{F}{F_\beta}} \tag{1.1}$$

$F_\beta = \frac{k_B T}{x_\beta}$ is the characteristic force of the molecular bond scaled by the thermal energy and the potential width x_β. Thus, all mechanical properties of the molecular bond are concentrated in the single parameter of the potential width x_β.

Up to now, it is assumed that the applied force is constant over time. In general, however, the forces applied to a system are hardly always constant. Thus, Evans and Ritchie expanded the static theory of Bell for the forced unbinding of a molecular bond to a dynamic theory for the dissociation kinetics in an overdamped environment (liquids) [78,77,79]. In this ansatz, they accounted for the deformation of the energy landscape and for the spatially varying friction between the molecules. Here, the force is regarded as a function of time and thus, the dissociation rate also becomes dependent on time:

$$k_{off}^{F*}(F(t)) = k_{off}^0 \cdot g(F(t)) \cdot e^{-\frac{\Delta U(F(t))}{k_B T}} \tag{1.2}$$

Here, $\Delta U(F(t))$ is the barrier height reduced by the force $F(t)$ and $g(F(t))$ is the mechanical coupling of the external force $F(t)$ into the potential landscape of the molecular bond. As shown above, an external force $F(t)$ directly affects the shape of the energy landscape. In consequence, the time dependence of the force application leads to a dependence of the molecular potential and – in particular – of the barrier height on the force loading rate $\dot{F} = \frac{\partial F}{\partial t}$. The rate of force loading on the molecular bond is governed by the mechanics of the linker transducing the applied force. In the case of cell adhesion in the blood stream, the shear force on the cell results in a tensile force on the adhesive receptor/ligand bond [80]. Hence, the mechanics of the cell and especially the mechanics of the receptor anchorage in the cell will determine the force loading and thus also the dissociation kinetics under force.

The unbinding of a molecular bond relies on a stochastic Markov process [79,81]. Hence, in force spectroscopic experiments, not a single dissociation force, but a probability distribution of rupture forces is detected. This distribution is given by:

$$p(F) = k_{off}(F(t)) \cdot e^{-\int_t k_{off}(F(t))}$$

For a constant retraction speed v, Evans and Ritchie included the influence of a non-linear elastic linker [82]:

$$p(F) = k_{off}(F) \cdot F_\beta \cdot \frac{c(F)}{v} \cdot e^{-\int_f k_{off}(F) \cdot \frac{c(F)}{v} df} \tag{1.3}$$

The mechanical compliance $c(F)$ describes the elongation of the force-exerting linker per unit force. Hence, for force spectroscopic measurements on cellular receptors, the cell mechanics will influence the dissociation kinetics and the distribution of rupture forces comparable to the basal off-rate k_{off}^0.

The most probable force of unbinding is used to characterise the bond strength. However, as mentioned above, this bond strength strongly depends on the experimental conditions, in particular on the history and rate of force loading [83]. Furthermore, the shape of the force distribution is governed by the basal off-rate k_{off}^0 and the potential width x_β of the investigated receptor/ligand bond. With the help of single-molecule force spectroscopy, insight can thus be gained into the strength, the force susceptibility and the kinetics of the receptor, if the evolution of force on the adhesive bond is known.

Chapter 2

The Mechanics of Cellular Adhesion Receptors

Cell adhesion is mostly – if not even always – exposed to forces. The molecular adhesive bonds are therefore not only subjected to their equilibrium affinity, but are also governed by the mechanics of the force-transmitting linker (see equations 1.2 and 1.3). This dependence of the bond strength on the equilibrium kinetics and the force history was termed mechanochemistry or chemomechanics [84, 85]. In the case of cell adhesion, the anchorage of the transmembrane adhesion receptors in the cell and the overall cellular mechanics will determine the mechanical properties of force loading. It is known since long, that certain receptors like integrins modulate their affinity as well as the mechanics of their anchorage for regulating their adhesiveness. Recently however, the influence of the receptor mechanics on the strength and the lifetime of the molecular bond has become the focus of attention.

This chapter concentrates on the mechanical regulation of transmembrane adhesion receptors and the influence of mechanochemistry on cell adhesion under force. Firstly, the biological importance of the integrin anchorage for the adhesion of lymphocytes under mechanical strain will be outlined with the example of the paxillin association with the α_4 subunit of the integrin VLA-4 ($\alpha_4\beta_1$) [86]. Then, it will be demonstrated, that differences in the cellular anchorage of integrin receptors are detectable when analysing the force spectroscopic data with a suitable mechanical model [2]. We compared the influence of mechanical regulation to that of affinity modulation on the bond strength and found that altering the mechanics of the receptor anchorage presents a highly effective tool for regulating the cellular adhesiveness.

2.1 Paxillin Association with the α_4 Cytoplasmic Tail regulates Adhesion Strengthening

The cytoplasmic tails of integrin heterodimers associate with a large variety of signalling and cytoskeletal adapter proteins [32] and modulate the adhesiveness of the receptors. While the intracellular ends of the β subunits contain highly conserved sequence motifs,

only very few sections tally on the α cytoplasmic tails [31, 87]. This suggests an integrin-specific assignment in signalling and anchorage functions of the α subunit. The adapter paxillin binds directly to nine residues (E983-Y991) on the cytoplasmic tail of α_4 integrins [88, 89]. The binding is regulated by the phosphorylation state of the Ser^{988} on the α_4 tail [90, 91]. Paxillin has about 68 kDa and plays a pivotal role in matrix adhesion and signalling [32]. For instance, the association of α_4 with paxillin reduces cell spreading, focal adhesion and stress fibre formation [88, 31]. On the other hand, paxillin binding to α_4 enhances not only α_4-dependent cell migration [91], but also stimulates T-cell migration mediated by the integrin LFA-1 ($\alpha_L\beta_2$). Thus, this adapter molecule is necessary for the trans-regulation of the integrin LFA-1 by VLA-4 [92, 93]. Paxillin interacts with several signalling proteins such as FAK, Src and PAK, as well as with cytoskeletal adapters, e.g. vinculin and talin [94, 95]. It would then appear that this cytoplasmic protein possibly not only participates in signalling pathways, but also plays a role as a mechanical regulator.

In order to assess the contribution of paxillin to VLA-4-mediated adhesion of T-lymphocytes, we investigated the effects of a point mutation in the α_4 cytoplasmic tail (Y991A), which inhibits the association of the integrin with paxillin [88, 31]. We found in AFM experiments that the frequency of productive VLA-4/VCAM-1 interactions was reduced for the mutant, whilst the unbinding forces were similar. This is in line with the observations that the mutant VLA-4 (Y991A) displayed an unchanged affinity to its ligand VCAM-1, although the $\alpha_4\beta_1$-dependent capture in shear flow was suppressed for Jurkat T-cells expressing mutant VLA-4. Thus, the adhesion strengthening on VCAM-1 substrates was weakened under both vertically and horizontally applied mechanical stress. This suggests that the association of paxillin to the α_4 cytoplasmic tail is necessary for the immediate post-ligand adhesion strengthening of the VLA-4 integrin under mechanical strain. Having established this we see that paxillin controls the mechanical stability of the adhesive bond, rather than regulating the affinity or the avidity of VLA-4 integrins in force-free conditions. Altogether, our findings highlight the role of mechanics in force-exposed cell adhesion: Although the attachment of integrins to the cytoskeleton was hitherto believed to reduce the cellular adhesiveness [96, 97, 98], we were able to show that this anchorage is indispensable for the force resistance of VLA-4 bonds and that it is critical for the tether stabilisation under stress.

These results have been published in the Journal of Cell Biology [86] and are reprinted in section 2.4.

2.2   The Mechanics of Transmembrane Receptors governs Cell Adhesion

The data obtained from force spectroscopic experiments do not only contain information about the bond strength of the investigated interaction. In the force-distance curves of AFM experiments, also the evolution of the force loading on the molecular bond is likewise recorded. Hence, the shape of the curve itself may reveal valuable details about the

mechanics of the force-transmitting linker. As discussed in section 1.3.2, the force loading on cellular adhesion receptors depends on the mechanics of the force-transmitting cell and of the anchorage of the receptor in the cell and will determine the adhesion strength. In order to quantify the mechanical properties of the receptor environment, we developed a viscoelastic model based on a Kelvin body (Fig. 2.1). For a constant piezo velocity, we deduced the following force-distance relationship for this model (see appendix B.3):

$$F(z) = k_t \cdot z + \mu \cdot v - \mu \cdot v \cdot e^{\frac{-k_i \cdot z}{\mu \cdot v}} \tag{2.1}$$

Here, k_t parameterises the tether stiffness, k_i characterises the initial membrane bending rigidity and the viscosity μ is determined by the slip of the membrane over cytoskeletal components.
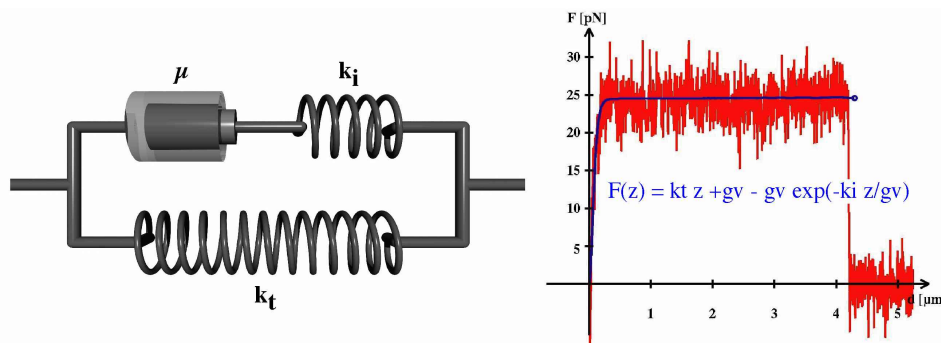
Figure 2.1: The Kelvin body: A spring with elasticity k_t is connected in parallel to a series of a second spring with k_i and a dashpot with viscosity μ. The fit of the distance-relationship F(z) (*blue*) matches the experimental force curve (*red*).

We investigated the mechanics of the lymphocyte integrin VLA-4 in two different ion conditions; one condition with physiological concentrations of magnesium and calcium (here referred to as 'resting condition'), the other with a high concentration of magnesium in the absence of calcium (here referred to as 'activating condition'). Analysing the recorded force curves with this relationship, we found that activating the integrins with concentrated magnesium in the absence of calcium alters the mechanics of the receptor environment. This can be explained by the fact that integrins are expressed in different activation states on the cell surface. Whilst the high-affinity receptors are located in lipid rafts [99, 100] and preferentially bound to cytoskeletal adapter proteins as paxillin [101], the resting receptors are randomly distributed in the membrane. Since we probe only active receptors in the AFM setup, the average mechanics of the integrin environment is altered after the activation of resting receptors. Hence, with the help of viscoelastic models, transmembrane receptors can be used as nano-probes in force spectroscopic experiments for detecting mechanical differences in the receptor surroundings.

In order to gauge the impact of a mechanical regulation compared with the conventional affinity modulation on the adhesion strength, we combined the force evolution of

our Kelvin body model (equation 2.1) with equation 1.3 and varied the mechanical and kinetic parameters in numerical simulations. Interestingly, we found that the viscosity of the receptor anchorage can tune the bond strength to the same extent as the basal off-rate of the receptor. We thus claim that the cell regulates its adhesiveness by altering the receptor mechanics as a powerful alternative to the affinity modulation.

These results have been published in the Biophysical Journal [102] and are reprinted in section 2.4.

2.3 Conclusions

In concordance with the physical theory of bond dissociation under force, we deduced that the integrin anchorage plays a pivotal role for the successful adhesion strengthening of lymphocytes under mechanical stress. Furthermore, we demonstrated that different nano-environments of the investigated receptor can be resolved by analysing force spectroscopic experiments on living cells with viscoelastic models. Numerical simulations corroborated the experimental observations that the stiffening of the receptor anchorage stabilises the molecular bond. Hence, the cell can adjust its adhesiveness very effectively by modulating the mechanics of the receptor anchorage. For this, the receptors can be attached to the cytoskeleton or relocated into membrane areas with different viscoelastic properties.

In physiological situations, forces and other mechanical stimuli are omnipresent. As a consequence, many cells are capable of 'feeling' the magnitude and the direction of forces. In addition, they possess an awareness as to the geometry and the rigidity of their surroundings and are able to react in a very distinct manner [103, 104, 105, 106, 107, 108]. Thereby, the force exerted on cellular adhesion receptors like integrins or selectins can itself act as a stimulant. For instance, it has been demonstrated in molecular dynamic simulations and in flow chamber experiments that external forces promote and accelerate conformational changes [37, 109, 110, 106]. The fascinating phenomenon of selectin catch-bonds – which grow stronger with increasing forces – is likewise triggered by a similar mechanism [84, 111, 112, 113]. Furthermore, forces or mechanical alterations of the cellular environment evoke active reactions of the whole cell [103, 114, 115]. For instance, forces control the strengthening of initial integrin adhesions to focal adhesion complexes [116] or they can induce the reorientation of cells and of stress fibres [117, 118, 119, 120]. Furthermore, the stiffness of the substrate governs the growth and migration of epithelial cells [121], the behaviour of osteoblasts [122], the progression of tumour cells [123] and the differentiation of stem cells [124]. These reactions are provoked by external forces, which can induce intracellular signal cascades [125] or transmit forces from the cell membrane to the nucleus to regulate the gene expression [126]. The force transmission to different cellular compartments depends on the cytoplasmic associations to the receptor tails [103]. This underlines the fact that the anchorage of the adhesive receptor in the cell controls the intracellular signalling as well as the force resistance of the bond. Hence, on the one hand, the receptor anchorage may regulate the mechanosensation of the cell [85, 103, 127]. On the other hand, being an effective modulator of cell adhesion, the regulation of the

receptor mechanics may also be the outcome of intracellular signal cascades. Using the transmembrane receptors as nano-probes in force spectroscopic experiments together with mechanical models will allow to scrutinise intracellular anchorage events and elucidate the mechanical regulation by the cell.

These considerations, together with other aspects of the mechanical regulation of cell adhesion, have been reviewed in Soft Matter [2] and are reprinted in section 2.4.

2.4   Publications

1. $\alpha_4\beta_1$-Dependent Adhesion Strengthening under Mechanical Strain is regulated by Paxillin Association with the α_4-cytoplasmic Domain (*published in the Journal of Cell Biology*)

2. The Viscoelasticity of Membrane Tethers and its Importance for Cell Adhesion (*Biophysical Journal, in press*)

3. Mechanical Regulation of Cell Adhesion (*Soft Matter, in press*)

α4β1-dependent adhesion strengthening under mechanical strain is regulated by paxillin association with the α4-cytoplasmic domain

Ronen Alon,[1] Sara W. Feigelson,[1] Eugenia Manevich,[1] David M. Rose,[2] Julia Schmitz,[3] Darryl R. Overby,[4,5] Eitan Winter,[1] Valentin Grabovsky,[1] Vera Shinder,[1] Benjamin D. Matthews,[4,5,6] Maya Sokolovsky-Eisenberg,[1] Donald E. Ingber,[4,5] Martin Benoit,[3] and Mark H. Ginsberg[2]

[1]Department of Immunology, The Weizmann Institute of Science, Rehovot 76100, Israel
[2]Department of Medicine, University of California, San Diego, La Jolla, CA 9209
[3]Center for Nano Science, Ludwig-Maximilians-Universität, Munich D-80799, Germany
[4]Department of Pathology and [5]Department of Surgery, Vascular Biology Program, Children's Hospital, and [6]Department of Pediatrics, Massachusetts General Hospital, Harvard Medical School, Boston, MA 02115

The capacity of integrins to mediate adhesiveness is modulated by their cytoplasmic associations. In this study, we describe a novel mechanism by which α4-integrin adhesiveness is regulated by the cytoskeletal adaptor paxillin. A mutation of the α4 tail that disrupts paxillin binding, α4(Y991A), reduced talin association to the α4β1 heterodimer, impaired integrin anchorage to the cytoskeleton, and suppressed α4β1-dependent capture and adhesion strengthening of Jurkat T cells to VCAM-1 under shear stress. The mutant retained intrinsic avidity to soluble or bead-immobilized VCAM-1, supported normal cell spreading at short-lived contacts, had normal α4-microvillar distribution, and responded to inside-out signals. This is the first demonstration that cytoskeletal anchorage of an integrin enhances the mechanical stability of its adhesive bonds under strain and, thereby, promotes its ability to mediate leukocyte adhesion under physiological shear stress conditions.

Introduction

Circulating leukocytes rapidly develop firm adhesion to vessel wall ligands through their various integrin receptors α4β7, α4β1 (VLA-4), αLβ2 (LFA-1), and αMβ2 (Mac-1; Alon and Feigelson, 2002). Integrins bind their respective endothelial ligands under shear flow at lower efficiency than selectins (Springer, 1994). Adhesive tethers form over a fraction of a second and depend on the ability of the nascent adhesive bond to withstand disruptive shear force. In contrast to selectins, all leukocyte integrins can undergo instantaneous up-regulation of their affinity or avidity to endothelial ligands upon exposure to endothelial chemokines (Kinashi, 2005). In addition, integrins can undergo conformational changes upon ligand binding (Hynes, 2002). Cytoskeletal constraints of integrins may also control integrin adhesiveness (van Kooyk and Figdor, 2000). Previous studies on leukocyte (L)-selectin function regulation have shown that preformed cytoskeletal associations of L-selectin with the actin cytoskeleton control the ability of ligand-occupied selectin to stabilize nascent tethers under shear flow and capture leukocytes under physiological shear stresses (Kansas et al., 1993; Dwir et al., 2001). This raised the possibility that specialized subsets capable of interacting with their respective endothelial ligands under physiological shear flow may also need to properly anchor to the cytoskeleton. Although selectins and integrins are structurally distinct, we hypothesized that α4 integrin bonds forming under disruptive shear stresses may share a common regulatory mechanism with L-selectin bonds. However, as alterations in cytoskeletal constraints of integrins can modify affinity, clustering, and ligand-induced conformational rearrangements (Carman and Springer, 2003), the direct contribution of integrin anchorage to adhesive outcome has been difficult to dissect.

In this study, we unraveled novel adhesive properties of an α4-tail mutant with disrupted association with the cytoskeletal adaptor paxillin (Liu et al., 1999). We found that blocking the α4–paxillin interaction markedly impaired the integrin's ability to anchor to the cytoskeleton in Jurkat T cells. Although not essential for α4β1 affinity, ligand-induced conformational

Figure 1. **The α_4(Y991A)β_1 mutant mediates poor shear-resistant adhesion to VCAM-1.** (A) JB4 Jurkat cells expressing either wt α_4 (WT) or the α_4(Y991A) mutant (Y991A) were settled for 1 min on low density VCAM-1-Fc (80 CAM sites/μm^2; left) or on sVCAM-1 coated at medium (1,480 sites/μm^2; middle) or high density (3,700 sites/μm^2; right), and their resistance to detachment by incremented shear stresses was analyzed. The fraction of cells within initially settled populations remaining bound at the end of each interval of shear increase is shown for each cell population. (B) FACS staining of ectopically expressed α_4, endogenous β_1 and α_L subunits, as well as of the β_1 activation neoepitope 15/7 on wt- and α_4(Y991A)-expressing JB4 cells, depicted with black and gray lines, respectively. (C) LFA-1–dependent adhesion of both wt- and α_4(Y991A)-expressing JB4 cells to low (80 sites/μm^2) or medium density ICAM-1–Fc (160 sites/μm^2) as well as to high density ICAM-1 (7,600 sites/μm^2), measured as in A. In each panel, the mean $\pm$ range of two experimental fields is depicted. Results in A and C are representative of six independent experiments. (D) FACS staining of VCAM-1, ICAM-1, and E-selectin on TNFα-stimulated HUVECs. Dotted lines represent staining of isotype-matched controls (left). VLA-4–dependent adhesion of JB4 cells transfected with wt α_4 (WT) or the α_4(Y991A) mutant to intact (left) or E-selectin–blocked TNFα-stimulated HUVECs (right). Resistance to the detachment of cells settled for 1 min on the monolayer was assessed as in A. Shown in parenthesis are the fractions of adherent cells that maintained rolling on the different HUVECs at 5 dyn/cm^2. LFA-1 blockage did not affect Jurkat resistance to detachment, whereas pretreatment with the $\alpha_4\beta_1$-specific blocker Bio1211 (at 1 μg/ml) resulted in complete loss of shear resistance (not depicted). Error bars represent SD.
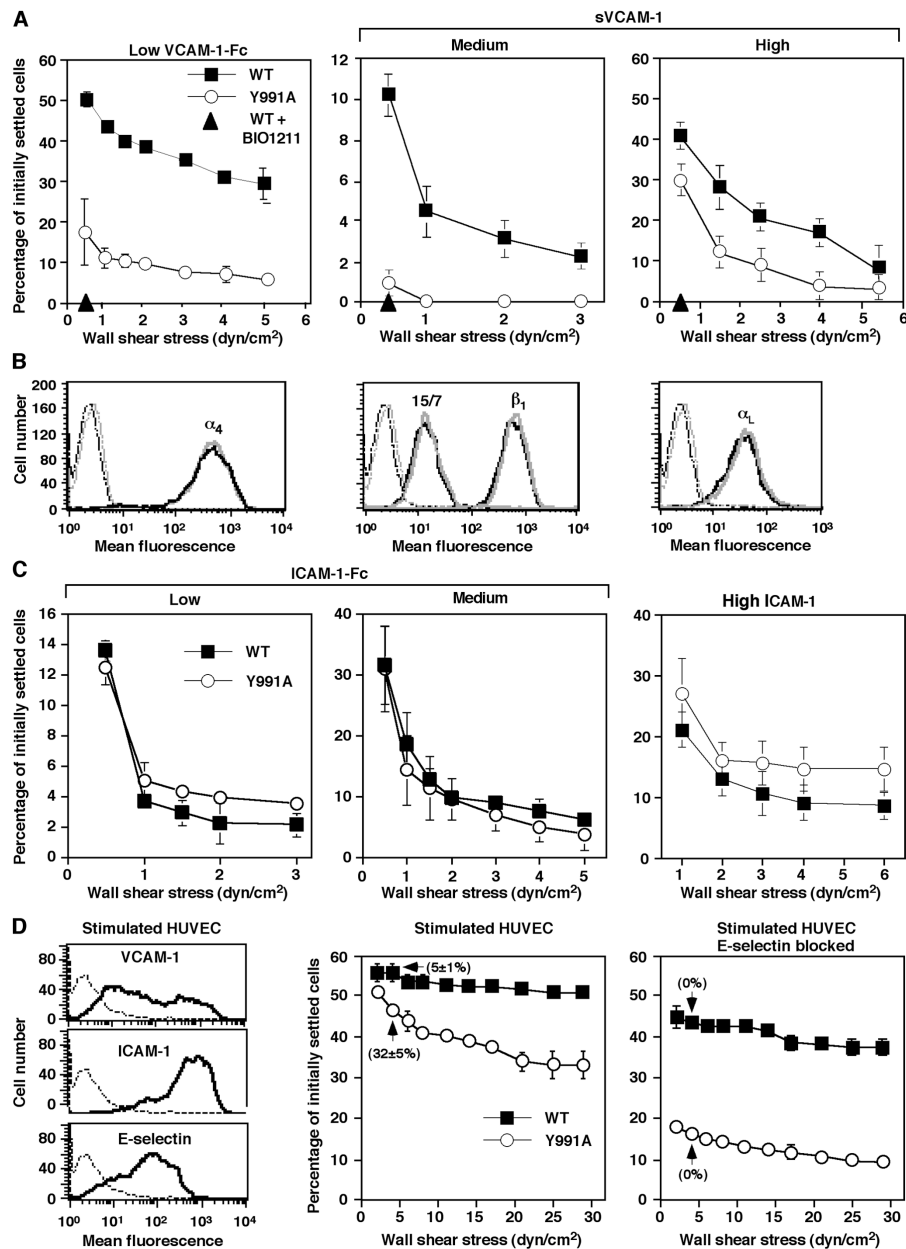
changes, surface clustering and topography, or redistribution at short static contacts, paxillin association with $\alpha_4\beta_1$ was crucial for $\alpha_4\beta_1$–VCAM-1 bonds to resist mechanical stress. These results suggest that subsecond stabilization of α_4 tethers depends on the ability of ligand-occupied α_4 integrins to properly anchor to the cytoskeleton. This work also highlights the key role of the α subunit of $\alpha_4\beta_1$ in postligand binding adhesion strengthening of the integrin under mechanical strain.

Results

Paxillin association with the α_4-cytoplasmic domain is required for cell resistance to detachment by shear stress

Paxillin binding to the α_4-cytoplasmic domain is important for integrin $\alpha_4\beta_1$ signaling but not for adhesion developed in shear-

free conditions (Rose et al., 2003). To examine the role of paxillin binding in $\alpha_4\beta_1$-mediated adhesion under shear stress, we analyzed the resistance to shear-induced detachment from the $\alpha_4\beta_1$ ligand VCAM-1 of α_4-deficient JB4 Jurkat T cells transfected with either wild-type (wt) α_4 (JB4-wt) or the paxillin binding–defective α_4(Y991A) mutant JB4-α_4(Y991A) (Rose et al., 2003). JB4-α_4(Y991A) cells were less resistant to shear-induced detachment than their JB4-wt counterparts (Fig. 1 A). Notably, bivalent VCAM-1 (VCAM-1–Fc) was much more potent than monovalent soluble VCAM-1 (sVCAM-1) in supporting $\alpha_4\beta_1$-specific adhesion (Fig. 1 A), but it still could not rescue the adhesive defect of the α_4(Y991A) mutant. These results were confirmed with multiple clones expressing similar levels of α_4 and β_1 subunits as well as the β_1 activation epitope 15/7 (Fig. 1 B and not depicted). Nevertheless, resistance to detachment from different densities of either ICAM-1–Fc or

A

B
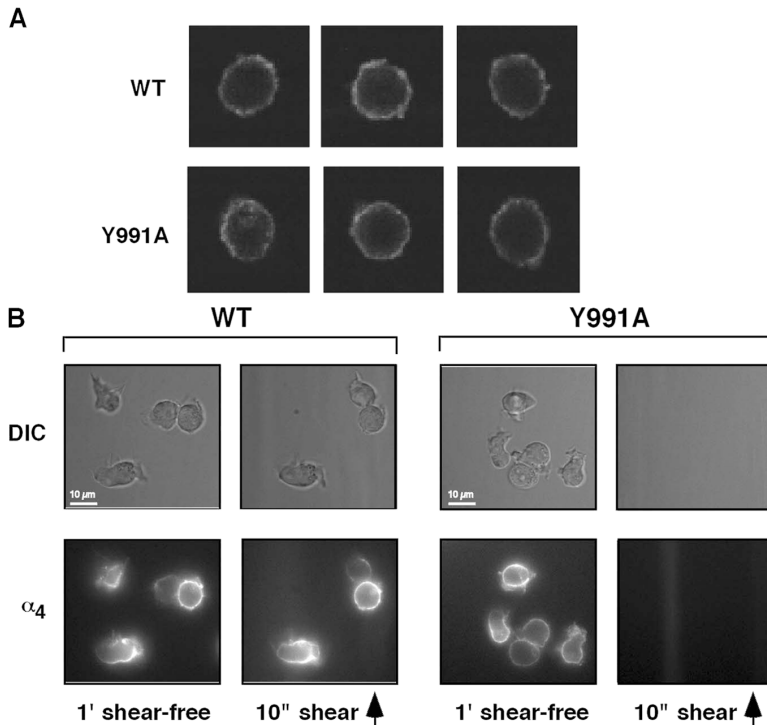
Figure 2. **The α_4(Y991A)β_1 mutant distributes normally before and during early cell spreading on VCAM-1 in shear-free conditions.** (A) wt α_4 or α_4(Y991A) is evenly distributed on the surface of JB4 cells. Confocal immunostaining of α_4 on the surface of prefixed WT or Y991A cells using the non-blocking B5G10 mAb. Three representative cells are shown for each cell type. (B) Live imaging of wt α_4 or α_4(Y991A) during short cellular contacts with VCAM-1. JB4 cells expressing wt or mutant α_4 were prelabeled with AlexaFluor488-conjugated B5G10 mAb and settled for 1 min on VCAM-1. wt or mutant α_4 were each imaged on cells that had spread on sVCAM-1 for 1 min (shear free) and were then subjected to 10 s of shear stress at 2 dyn/cm². Cell morphology was monitored in differential interface microscopy (DIC). The degree of patching was calculated by Image J analysis and was defined as having at least one region with a B5G10 staining mean intensity threefold higher than another region on the same cell. Note that shear stress on its own did not trigger wt α_4 redistribution. Shear direction is depicted by the arrow.

ICAM-1 was comparable between wt- and mutant $\alpha_4\beta_1$–expressing cells (Fig. 1 C). In agreement with these results, VLA-4–dependent adhesion to TNFα-stimulated human umbilical vein endothelial cells (HUVECs) was reduced in Jurkat cells expressing the α_4(Y991A) mutant (Fig. 1 D), in particular at shear stresses ≥ 5 dyn/cm², within the upper range of shear stresses prevailing in postcapillary venules where the majority of lymphocyte extravasation takes place (Firrell and Lipowsky, 1989). Whereas most cells expressing the wt α_4 firmly arrested on the stimulated HUVEC via their VLA-4, a significant fraction of α_4(Y991A) mutant–expressing cells failed to arrest and established endothelial (E)-selectin–dependent rolling on the HUVEC (Fig. 1 D). In the absence of functional E-selectin, the shear resistance of cells expressing the α_4(Y991A) mutant was much lower than the shear resistance of cells expressing wt α_4 (Fig. 1 D). Because the contribution of LFA-1 to Jurkat arrest was minimal, these data suggest that the Y991A α_4 mutant is deficient in establishing $\alpha_4\beta_1$-mediated shear resistance on endothelial cells expressing VCAM-1 as well as on substrates coated with isolated VCAM-1.

Notably, preformed clustering of wt and mutant α_4 subunits on JB4 cells was essentially identical (Fig. 2 A). Real time imaging of JB4 cells that adhered on VCAM-1 also showed identical cell spreading as well as the distribution of both mutant and wt α_4 during 1-min cellular contacts before shear application (WT: $n = 44$, 16% round, 54% polarized with uniform α_4, 30% polarized with patched α_4; Y911A: $n = 27$, 18% round, 52% polarized with uniform α_4, 30% polarized with patched α_4; Fig. 2 B). Notably, the strength of resistance to detachment developed by wt α_4 did not correlate with the degree of patching (Fig. 2 B) in contrast to reports on LFA-1–dependent systems (Constantin et al., 2000; Kim et al., 2004).

Thus, a mutation of the α_4 tail defective in paxillin binding prevents $\alpha_4\beta_1$-mediated resistance to shear-induced cell detachment independent of cell spreading and α_4 patching on VCAM-1.

The α_4(Y991A) mutation blocks paxillin association with the α_4 tail selectively (Liu et al., 1999). As an alternative test of the role of the α_4–paxillin interaction, we exploited a recently identified small molecule inhibitor of this interaction. The compound, designated A7B7C7, blocks the α_4–paxillin interaction and interferes with $\alpha_4\beta_1$-dependent cell migration (Ambroise et al., 2002). This inhibitor, but not a control compound (A6B6C6), attenuated the shear resistance of wt $\alpha_4\beta_1$–mediated Jurkat cell adhesion to VCAM-1 (Fig. 3 A, left) but had no effect on the residual shear resistance developed by the JB4-α_4(Y991A) cells (Fig. 3 A, right). Adhesion mediated by the $\alpha_L\beta_2$–ICAM-1 interaction was also insensitive to the inhibitor (not depicted). Knocking down paxillin expression by up to 75% using transient short inhibitory RNA (siRNA) silencing (Fig. 3 B) resulted in reduced adhesiveness of wt $\alpha_4\beta_1$–mediated Jurkat cell adhesion to VCAM-1 (Fig. 3 C), with no inhibition of adhesiveness mediated by the α_4(Y991A) mutant (Fig. 3 C). Notably, LFA-1–dependent adhesion to ICAM-1 was also insensitive to identical paxillin silencing (not depicted). Thus, both genetic and pharmacological approaches indicate that the α_4–paxillin interaction increases the resistance of $\alpha_4\beta_1$–VCAM-1 contacts to detachment by disruptive shear stresses.

Paxillin association with the α_4 subunit promotes $\alpha_4\beta_1$ anchorage to the cytoskeleton

Paxillin binds a number of actin-binding proteins such as talin and vinculin (Brown and Turner, 2004) and does so at sites distinct from the α_4-binding site (Liu and Ginsberg,
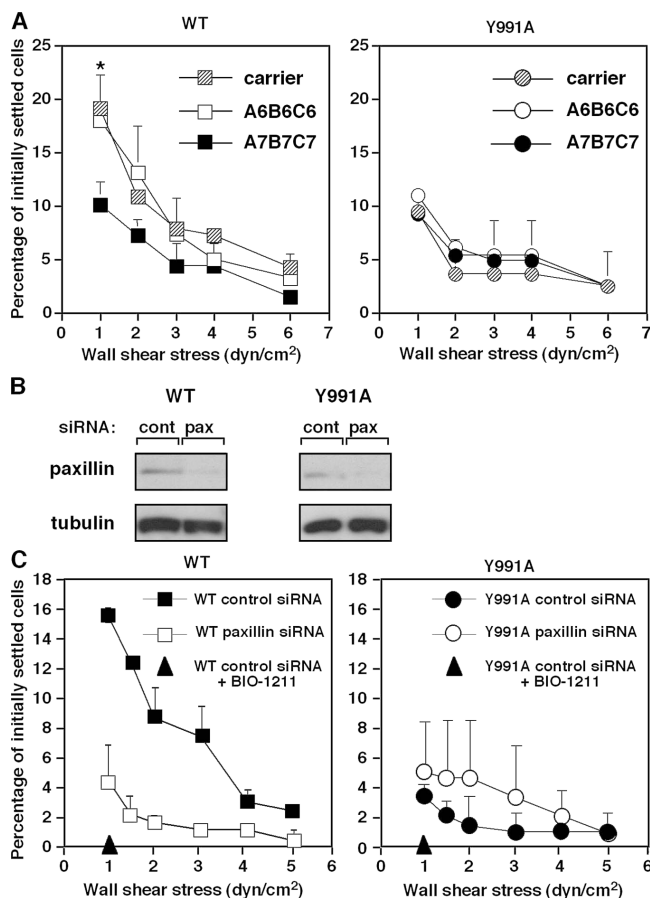
Figure 3. **Blockage of $\alpha_4\beta_1$ paxillin associations interferes with shear resistance developed by wt α_4.** (A) JB4 cells expressing either wt α_4 or α_4(Y991A) were pretreated for 15 min with A7B7C7, a cell-permeable inhibitor of paxillin binding to the α_4 tail, or with the control compound A6B6C6, both present at 5 μM. The shear resistance of carrier or compound-treated cells developed after 1-min adhesion to sVCAM-1 (2,220 sites/μm^2) was determined as in Fig. 1. Results are mean $\pm$ range of two experimental fields. The experiments depicted are each representative of four independent tests. *, P < 0.001 (a two-tailed paired t test) for control compared with A7B7C7-treated cells at 0.5 dyn/cm^2. (B) JB4 cells expressing wt α_4 were transfected with either paxillin-specific or control luciferase siRNA. Total lysates of each group were immunoblotted with paxillin- or tubulin-specific mAbs. Densitometric analysis reveals a decrease of 70 and 75% in paxillin content in JB4 expressing either wt or α_4(Y991A), respectively. (C) Paxillin silencing impairs resistance to detachment from sVCAM-1 developed by wt $\alpha_4\beta_1$ but not α_4(Y991A). The shear resistance of the indicated cells was determined as in A. Results are representative of three independent experiments. Error bars represent SD.

Figure 4. **Paxillin association with α_4 facilitates integrin anchorage to the cytoskeletal matrix.** (A) Detergent removal of nonligated wt α_4 monitored by FACS. Jurkat cells were reacted for 30 min at 4°C with FITC-conjugated anti-$\alpha_4\beta_1$ mAb (HP1/2) or isotype-matched control (dotted line). Cells were then incubated at RT in detergent-free buffer (black, −NP-40) or in buffer containing 0.05% NP-40 (gray, +NP-40). The fraction of α_4-bound mAb remaining after detergent treatment assessed by flow cytometry is shown relative to originally bound α_4 mAb. (B) The fraction of mAb-bound wt or α_4(Y991A) resistant to detergent-induced removal was compared before (white bars) and after ligation of the mAb by secondary antibody (black bars). Results are a mean of three independent experiments. Error bars represent SD.

2000). We next quantified the fraction of detergent-resistant wt α_4 or α_4(Y991A) retained on NP-40–solubilized cells using fluorescence-tagged integrin-bound α_4 mAb (Fig. 4 A). Retention of intact wt and α_4(Y991A) was similar and low (20% of the total surface α_4; Fig. 4 A). However, the addition of anti–mouse Ig to cluster the mAb-bound wt α_4 markedly increased the association of $\alpha_4\beta_1$ surface integrin with the detergent-insoluble cytoskeleton (Fig. 4 B). In contrast, the same treatment produced a negligible increase in the cytoskeletal association of α_4(Y991A)β_1 (Fig. 4 B). Thus, the α_4(Y991A) mutant fails to anchor properly to the actin cytoskeleton in Jurkat T cells.

The α_4(Y991A) mutant poorly associates with talin and does not respond to talin suppression

In light of this poor cytoskeletal anchorage of α_4(Y991A)β_1, we next compared the level of talin associated with the wt or mutant $\alpha_4\beta_1$ complex in nonadherent Jurkat cells. Notably, constitutive talin binding to the α_4(Y991A)β_1 complex was significantly reduced compared with the wt integrin, as was evident from coprecipitation analysis (Fig. 5 A). Knocking down up to 65% of the total talin content in wt $\alpha_4\beta_1$–expressing Jurkat cells (Fig. 5 B) retained integrin expression (not depicted) but resulted in significant reduction in their $\alpha_4\beta_1$-mediated shear resistance on both sVCAM-1 and VCAM-1–Fc (Fig. 5 C, left and right insets, respectively). Notably, identical suppression of talin expression in the α_4(Y991A)β_1-expressing Jurkat cells (Fig. 5 B) had no effect on their low shear resistant adhesion to identical VCAM-1 substrates (Fig. 5 C, right). These results collectively suggest that paxillin association with $\alpha_4\beta_1$ also recruits talin to the α_4–paxillin complex and may enhance talin association with the β_1 subunit tail. Thus, both paxillin and talin associations promote $\alpha_4\beta_1$-dependent cell resistance to detachment from VCAM-1 under shear stress.

α_4-Paxillin association is not required for $\alpha_4\beta_1$ avidity for VCAM-1 but increases α_4 bond stiffness

Although the affinity of integrin α_4(Y991A)β_1 to soluble VCAM-1–Fc is retained (Rose et al., 2003), we considered that Jurkat cells expressing the α_4(Y991A)β_1 mutant might fail to develop shear resistant adhesion as a result of reduced avidity for surface-bound VCAM-1. Comparing wt $\alpha_4\beta_1$ with α_4(Y991A)β_1 adhesiveness to VCAM-1–coated beads in the absence of applied shear stress, we found that JB4-wt and JB4-
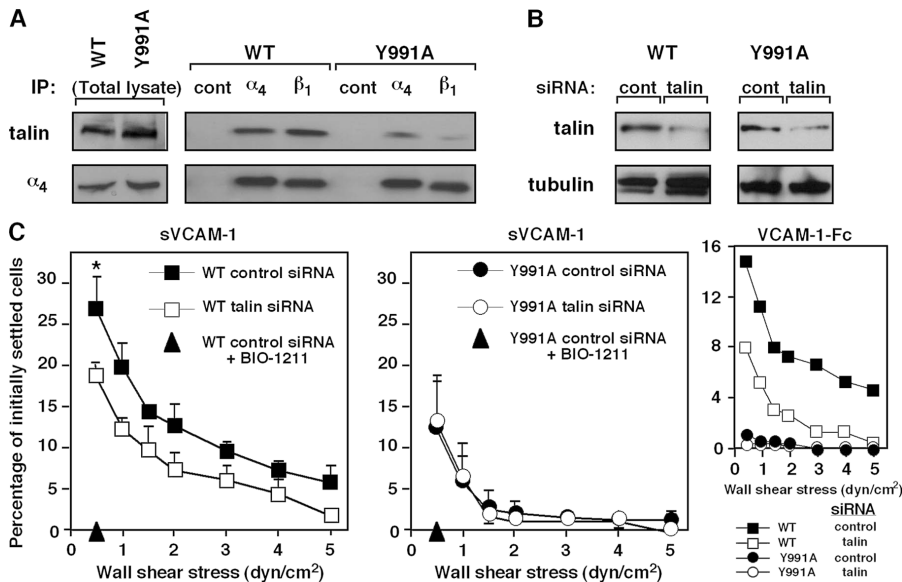
Figure 5. **The α_4(Y991A)β_1 mutant poorly associates with talin.** (A) The α_4(Y991A)β_1 complex does not properly recruit talin. Total lysates (left) or talin coprecipitating with anti-α_4, anti-β_1, or an irrelevant mouse IgG (right) from lysates of either JB4 transfected with wt α_4 or the α_4(Y991A) mutant (top). The blot was stripped and reprobed for α_4 (bottom). (B) Silencing of talin in JB4 cells expressing either wt or α_4(Y991A). The indicated cells were transfected with either talin1-specific or control siRNA. Total lysates of each group were immunoblotted with talin or tubulin-specific mAbs. Densitometric analysis reveals a decrease of 66 and 67% in talin content in JB4 expressing either wt or α_4(Y991A), respectively. (C) Talin suppression preferentially impairs wt $\alpha_4\beta_1-$ mediated resistance to detachment from sVCAM-1 (2,220 sites/μm^2). *, P < 0.03 for control compared with talin-silenced cells at 0.5 dyn/cm^2. Where indicated, cells were pretreated with the $\alpha_4\beta_1$-specific blocker BIO1211. (inset) Effect of talin suppression on resistance to detachment from VCAM-1–Fc (30 CAM sites/μm^2) of JB4 cells expressing either wt or α_4(Y991A). In each panel, the mean $\pm$ range of two experimental fields is depicted. Results are representative of three independent experiments. Error bars represent SD.

α_4(Y991A) cells bound identically to magnetic beads coated with increasing site densities of VCAM-1–Fc (Fig. 6 A), which is supportive of the normal adhesion of α_4(Y991A)β_1-expressing cells under static conditions. Nevertheless, when VCAM-1–coated beads that bound to JB4-wt cells were exposed to abrupt mechanical stress, these beads were displaced significantly less than beads prebound to JB4-α_4(Y991A) cells (Fig. 6 B and Fig. S1, available at http://www.jcb.org/cgi/content/full/jcb.200503155/DC1). α_4 resistance to displacement required an intact actin cytoskeleton, as JB4-wt cells pretreated with the F-actin–severing drug cytochalasin D exhibited even greater displacement in response to abrupt magnetic stress (Fig. 6 C). These findings, together with the shear-based detachment assays (Fig. 1), collectively suggest that paxillin association with the $\alpha_4\beta_1$ heterodimer and an intact actin cytoskeleton are both required for ligand-occupied $\alpha_4\beta_1$ to develop stress-resistant adhesive bonds.

Paxillin association with the α_4 tail augments α_4-mediated T cell capture on VCAM-1 and MadCAM-1 under shear flow

The $\alpha_4\beta_1$ and $\alpha_4\beta_7$ integrins mediate leukocyte capture under physiological shear flow (Alon et al., 1995; Berlin et al., 1995). Therefore, we compared the ability of mutant α_4(Y991A) versus wt α_4 to support $\alpha_4\beta_1$-dependent T cell capture by monovalent and bivalent VCAM-1 under continuous shear flow. Consistent with its defective resistance to shear force, α_4(Y991A)β_1 mediated reduced cell capture and arrest on a large range of densities of either monovalent (sVCAM) or bivalent (VCAM-Fc) VCAM-1 (Fig. 7, A and B). This differential behavior was also manifested at different levels of shear stress that were tested (Fig. 7 B, first two panels). Notably, whereas disruption of the

actin cytoskeleton by cytochalasin D resulted in marked inhibition of both cell capture and arrest mediated by wt $\alpha_4\beta_1$, cytochalasin D had no effect on the residual adhesions mediated by the α_4(Y991A)β_1 mutant (Fig. 7 A). Interestingly, the duration of individual $\alpha_4\beta_1$ tethers, which is a measure of integrin affinity to the ligand (Feigelson et al., 2001), was not altered upon the loss of paxillin binding (Fig. 7 A). Thus, for optimal cell capture under shear flow, the α_4 tail of $\alpha_4\beta_1$ requires associations with the intact actin cytoskeleton.

Jurkat cells express low levels of the β_7 integrin subunit; thus, >95% of their α_4-integrin subunits are found in $\alpha_4\beta_1$ heterodimers. Nevertheless, JB4-wt cell capture on high density of the bivalent $\alpha_4\beta_7$-integrin ligand MadCAM-1–Fc (Berlin et al., 1993) was inhibited by the anti-$\alpha_4\beta_7$ antibody Act-1 (unpublished data). The JB4-α_4(Y991A) cells formed fivefold fewer tethers on MadCAM-1 than JB4-wt cells, with a diminished fraction of tethers followed by immediate arrests (Fig. 7 B, right). Thus, paxillin association with the α_4 subunit enhances the ability of α_4 to promote adhesive tethers in the context of both β_1 and β_7 integrins under continuously applied disruptive shear stress.

Preferential localization of receptors to microvilli increases their availability for interactions with counter ligands under shear flow (von Andrian et al., 1995). Electron microscopic analysis of wt α_4 and the α_4(Y991A)-tail mutant revealed identical distribution of these variants to microvillar compartments (82 $\pm$ 4% for wt α_4, $n = 222$; 80 $\pm$ 6% for the α_4(Y991A) mutant, $n = 196$; Fig. 5 C). Furthermore, a higher ratio of the α_4(Y991A)-tail mutant localized on microvillar tips than wt α_4 (a 4.5 tip/base ratio for the mutant vs. only 1.8 tip/base ratio for wt α_4). The number and size of microvillar projections in JB4-wt and JB4-α_4(Y991A) cells were also comparable (Fig. 7 C). Thus, the enhanced ability of wt $\alpha_4\beta_1$ to
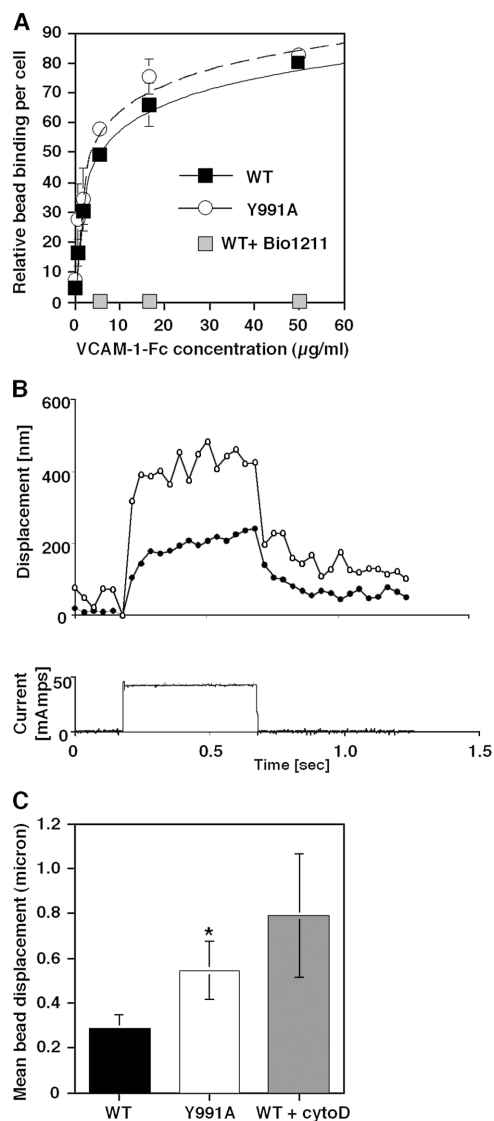
Figure 6. **The α_4(Y991A)β_1 mutant exhibits normal avidity under shear-free conditions but develops lower bond stiffness under applied force.** (A) Binding of either wt or Y991A $\alpha_4\beta_1$-expressing cells to M-280 protein A Dynabeads coated with 2D VCAM-1–Fc. Relative bead binding was determined by side scattering analysis. Bead binding in the presence of 1 µg/ml of the $\alpha_4\beta_1$-specific blocker Bio1211 is shown in gray squares. Results are representative of three independent experiments. (B, top) Representative bead displacement measured from an α_4(Y991A)-expressing cell (open circles) and a wt α_4–expressing cell (closed circles) during a 500-ms force pulse of ∼100 pN. (bottom) Electromagnetic current waveform corresponding to the displacement response. (C) VCAM-1–coated magnetic bead displacement in response to magnetic force pulse. VCAM-1 beads bound on the surface of JB4 cells expressing wt or α_4(Y991A) as well as on cytochalasin D–treated JB4 cells expressing wt α_4 were exposed for 0.5 s to the force pulse as described in the supplemental Materials and methods and Fig. S1 (available at http://www.jcb.org/cgi/content/full/jcb.200503155/DC1). For each experimental group, 8–10 cells were analyzed, and results are the mean ± SD (error bars) of all displacement curves. All samples were confirmed by side scattering analysis to bind a similar number of VCAM-1 beads. A two-tailed unpaired t test for mean bead displacements on wt and α_4(Y991A)-expressing JB4 cells yielded $P < 0.06$. One representative experiment of three.

promote adhesive tethers under shear flow was not the result of its preferential distribution to cellular microvilli or to increased localization on microvillar tips.

The α_4(Y991A)β_1 mutant fails to generate productive adhesive bonds with VCAM-1 under disruptive forces

To examine the effects of disrupting the α_4–paxillin interaction at a single molecule level and in the presence of an external force other than shear stress, we next measured the force of unitary adhesive interactions between wt $\alpha_4\beta_1$ or the α_4(Y991A)β_1 mutant and immobilized VCAM-1 by atomic force microscopy (AFM). JB4-wt or JB4-α(Y991A) cells were coupled to the end of an AFM cantilever (Fig. 8 A) and lowered onto a VCAM-1–Fc-coated surface. After a 0.5-s contact, the frequency of productive adhesive events and their strength were analyzed by the degree of deflection experienced by the cantilever during its retraction from the adhesive substrate. Both cell types detached from the VCAM-1 substrate through single jumps, suggesting the breakage of individual bonds during cantilever retraction (Fig. 8 B). The adhesion frequencies of all experiments were maintained below 30%, a level assumed to reflect single $\alpha_4\beta_1$–VCAM-1 interactions (Zhang et al., 2004). The specificity of the adhesive events detected in this system were confirmed by a similar 70% reduction in total binding events by the blockade of wt $\alpha_4\beta_1$ with Bio1211 (Lin et al., 1999) or by omission of VCAM-1 from the substrate (Fig. 8 C and not depicted). As indicated by the force histograms derived for JB4-wt or JB4-α_4(Y991A) cells (Fig. 8 C), the frequency of productive adhesive events developed by α_4(Y991A)β_1 was up to 10-fold lower than those developed by $\alpha_4\beta_1$ after background subtraction. The distribution of unbinding (rupture) forces measured for the two integrin variants was, however, similar (Fig. 8 C). Thus, paxillin association with the α_4 subunit dramatically augments the ability of $\alpha_4\beta_1$ to form adhesive tethers that resist disruptive forces irrespective to whether these forces are applied during a vertical force loading (AFM) or during cell rotation (shear stress).

Paxillin association with α_4 augments shear resistance of integrin tethers independent of ligand-induced conformational changes

The aforementioned data suggest that paxillin binding to α_4 is required for mechanical stabilization of cell attachments rather than for cytoplasmic induction of high affinity integrin conformations. Ligand binding to integrins can induce conformational changes in the integrin, resulting in high affinity conformations (Du et al., 1991; Shimaoka et al., 2002). Therefore, we considered the possibility that the reduced tether formation by the α_4(Y991A) mutant could reflect defective, instantaneous ligand-induced conformational changes in the integrin under shear stress. We first verified that the $\alpha_4\beta_1$ ligand Bio1211 provoked similar conformational changes in $\alpha_4\beta_1$ and α_4(Y991A)β_1 under shear-free conditions, as indicated by the identical induction of the β_1 ligand–induced binding site reporter 15/7 epitope by increasing doses of the monovalent $\alpha_4\beta_1$-specific ligand Bio1211 (Fig. 9 A; Lin et al., 1999). We next tested the intrinsic attachment efficacy of either wt α_4 or the α_4Y991A mutant to surface-immobilized α_4 mAb in the absence of ligand occupancy of the integrin. Notably, the HP1/2 mAb binding to α_4 integrins is not sensitive to their affin-

Figure 8. α_4(Y991A)β_1 **fails to stabilize bonds ruptured by an AFM probe.** (A) Schematic representation of the experimental system. JB4 cells were coupled to an AFM cantilever tip via an anti-CD43 mAb. VCAM-Fc was immobilized onto the substrate as in previous figures. (B) Representative AFM force–displacement curves acquired with wt α_4–expressing JB4 cells (top) or α_4(Y991A)-expressing cells (middle) approaching the VCAM-1–Fc-bearing substrate. A force–displacement curve of wt α_4–expressing JB4 approaching a control substrate devoid of VCAM-1 is indicated in the bottom curve. (C) Force histograms of $\alpha_4\beta_1$–VCAM-1 unbinding forces measured under a fixed loading rate of 0.33 nN/s. The number of productive adhesive interactions and their unbinding force distribution are depicted. Background binding is depicted by the dashed line. The mean unbinding force (UF) values of 10 independent experiments are indicated near each histogram. Pulling velocity was 3 μm/s, and the cell–substrate contact time was 0.5 s. A representative result of 10 independent experiments is depicted.

ity to or rearrangement by native ligands (Feigelson et al., 2001) and, thus, should be insensitive to intrinsic or ligand-induced affinity changes under shear stress. Notably, in the presence of shear flow, the α_4(Y991A) mutant formed adhesive tethers to immobilized HP1/2 mAb much less efficiently than wt α_4 (Fig. 9 B), as was observed for VCAM-1 (Fig. 1). In addition, adhesive contacts generated by the α_4(Y991A) mutant after 1 min of static contact also exhibited poor resistance to detachment by increasing shear forces relative to wt α_4–mediated contacts (Fig. 9 C). Thus, paxillin association with the α_4-integrin tail enhances the ability of the integrin subunit to generate resistance to detachment forces independently of ligand-induced conformational rearrangements under shear stress conditions.

Figure 7. **Paxillin association with the α_4-cytoplasmic tail facilitates tethering mediated by $\alpha_4\beta_1$ and $\alpha_4\beta_7$ under shear flow without altering α_4 distribution on microvilli.** (A) Tethering (transient or followed by immediate arrest) of Jurkat cells expressing either wt α_4 (WT) or the α_4(Y991A) mutant (Y991A) to immobilized VCAM-1. The mean duration of transient tethers is shown in parenthesis above bars. Where indicated, cells were pretreated with 20 μM cytochalasin D (cyto D) or carrier (carr). Error bars represent SD. (B) Tethering under shear flow of Jurkat cells mediated by either WT or Y991A to distinct α_4-integrin ligands. Tethers (transient or arrest) were determined under the indicated shear stresses on surfaces coated with either monomeric 7D VCAM-1 (sVCAM-1), dimeric 7D VCAM-1 (VCAM-1–Fc), or high density MadCAM-Fc. In each panel, the mean ± range of two experimental fields is depicted. All tethers to VCAM-1 were blocked in the presence of the α_4-integrin mAb HP1/2 (not depicted). All tethers to MadCAM-1 were blocked by the anti-$\alpha_4\beta_7$ antibody Act-I (not depicted). Results in A and B are representative of five and four independent experiments, respectively. (C) Surface distribution of wt α_4 (WT) or the α_4(Y991A) mutant on JB4 Jurkat cells monitored by immunoelectron microscopy. Insets show lower magnification images. The boxed areas depict the cellular areas enlarged. Prefixed cells were stained with the nonblocking α_4-specific mAb B5G10.

Washed cells were stained with rabbit anti–mouse Ig and 5 nm gold particle–conjugated goat anti–rabbit as described in Materials and methods. Gold particles are marked by arrowheads. Photomicrographs are representative of 20–30 cells.
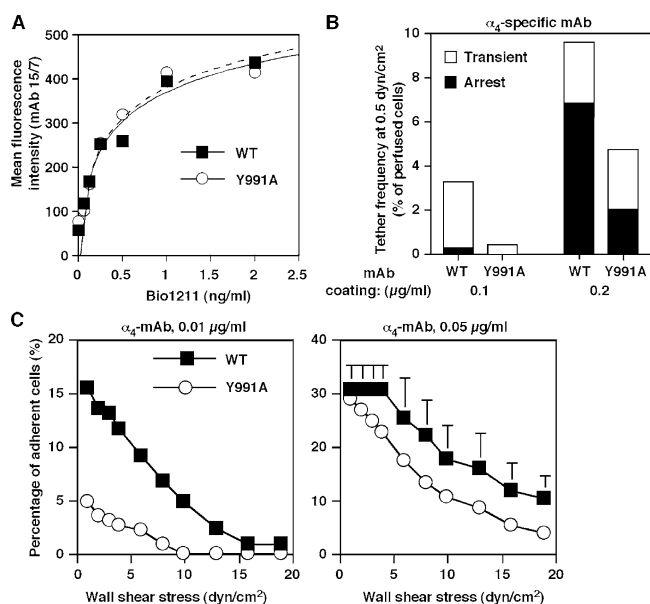
Figure 9. **Paxillin association with α$_4$ integrins stabilizes adhesive tethers to immobilized α$_4$-specific mAbs independent of ligand-induced rearrangements.** (A) Dose-dependent induction of the 15/7 epitope by the α$_4$β$_1$-specific ligand Bio1211 on wt α$_4$ or α$_4$(Y991A)–expressing Jurkat cells. (B) Reduced tethering and firm adhesion of the α$_4$(Y991A) mutant to immobilized α$_4$ mAb (HP1/2) under shear flow. Frequency of tethers and their categories were determined as in Fig. 7. (C) Strength of adhesion developed by JB4 expressing either wt or α$_4$(Y991A) settled for 1 min on low or high density mAb. Experiments in A and B are each representative of three independent experiments. Error bars represent SD.

Figure 10. **The α$_4$(Y991A)β$_1$ mutant responds to phorbol ester and SDF-1 inside-out signals but develops poor adhesiveness in stimulated T cells under shear flow.** Adhesion of JB4 cells expressing wt α$_4$ or α$_4$(Y991A) mutant to sVCAM-1 (2,960 sites/μm^2) left intact (−) or stimulated by 1 min PMA pretreatment or by cell encounter with SDF-1α coimmobilized at 2 μg/ml. (A) Resistance to detachment after 1 min of static contact analyzed as in Fig. 1. Values are mean ± range of two experimental fields. (B) Capture and arrest under continuous shear flow. Frequency of tethers and their categories were determined as in Fig. 7. The experiments in A and B are each representative of four independent tests.

The α$_4$(Y991A)β$_1$ mutant responds to inside-out stimulation but develops weaker adhesions to VCAM-1 under shear flow

Cellular stimulation by various agonists increases integrin adhesiveness in various contexts (Hynes, 2002). We next examined the effects of two prototypic agonists, PMA, a direct agonist of diacyl glycerol–dependent PKCs, and the chemokine SDF-1 (CXCL12) on mutant and wt α$_4$. Exposure of JB4-α$_4$(Y991A) cells to soluble PMA or to immobilized SDF-1 resulted in enhanced resistance to detachment from VCAM-1–bearing surfaces (Fig. 10 A), although the overall adhesion strength developed by the α$_4$(Y991A) mutant was lower than that developed by the intact integrin. Further analysis of adhesive tethers formed on VCAM-1 at subsecond contacts also indicated that the ability of initial α$_4$(Y991A)β$_1$-dependent Jurkat tethers to convert to immediate firm arrests was enhanced by PMA (Fig. 10 B). Likewise, JB4-α$_4$(Y991A) cells efficiently responded to in situ subsecond signals from SDF-1 with a twofold elevated frequency of α$_4$β$_1$-dependent tethers on VCAM-1 (Fig. 10 B, right). However, overall SDF-1–stimulated tethers mediated by α$_4$(Y991A) cells remained lower than wt α$_4$–mediated tethers. Thus, although the mutant α$_4$ underwent robust activation in response to both chemokine and PMA inside-out signals, its impaired cytoskeletal associations resulted in overall reduced adhesion to VCAM-1 under shear stress.

Discussion

This study shows that the disruption of paxillin binding to the integrin α$_4$ tail abrogates its anchorage to the actin cytoskeleton and impairs the ability of integrin ligand bonds to withstand immediate rupture by shear stress, an AFM-pulling device, or abruptly applied magnetic force. Despite normal distribution on the cell surface and retained avidity to immobilized VCAM-1, in the presence of applied forces, this anchorage-deficient mutant poorly mediates tether formation and rapid adhesion strengthening on its ligand. Paxillin-dependent cytoskeletal anchoring of ligand-occupied α$_4$ integrins may thus underlie their unique capacity to resist disruptive forces and support leukocyte adhesion under shear flow. Thus, although cytoskeletal constraints of integrins were predicted to restrict mobility and clustering on the cell surface and reduce cell adhesiveness (Kucik et al., 1996; Yauch et al., 1997; Kim et al., 2004), we propose that α$_4$ integrins must retain correct cytoskeletal associations to resist immediate rupture by shear stresses exerted at leukocyte contacts with target blood vessels. Our findings indicate that α$_4$-integrin anchorage to the cell cytoskeleton is critical for nascent adhesive contacts to resist immediate rupture by shear stress, but it is not required for integrin binding to the ligand nor for ligand-induced conformational rearrangements in the absence of external force. The anchorage deficiency of the α$_4$-tail mutant resulted in an inability to develop

adhesion to a high affinity mAb, which binds the integrin independently of affinity to native ligands (Feigelson et al., 2001; Kinashi et al., 2004). Altogether, these data suggest that paxillin associations with the α_4 tail control (a postligand occupancy anchorage step that is critical for tether stabilization under stress), which is a mechanical property underlying the ability of lymphocytes to capture and arrest on endothelial α_4-integrin ligands under shear flow. Our experiments on cytokine-activated endothelial cells also predict an increased contribution of this α_4–paxillin association to T cells interacting with endothelial beds expressing α_4-integrin ligands in the absence of endothelial selectins.

Integrin affinity is controlled by β-subunit associations with the talin head domain (Tadokoro et al., 2003) and by Rap1 (Kinashi, 2005) via effectors such as RAPL (regulator of adhesion and cell polarization enriched in lymphoid tissues; Katagiri et al., 2004). The effect of RAPL requires α-tail sequences (Katagiri et al., 2004) that are distant from the paxillin-binding site on α_4 (Liu and Ginsberg, 2000). The retained affinity of the α_4(Y991A) mutant and its capacity to mediate static adhesion suggest that lack of paxillin association with the α_4-integrin tail does not interfere with Rap1-dependent signals whether mediated through RAPL or other Rap1 effectors. The reduction in talin association with α_4(Y991A)β_1 did not alter basal $\alpha_4\beta_1$ affinity for VCAM-1 (Rose et al., 2003), suggesting that the paxillin-mediated association of talin with $\alpha_4\beta_1$ does not contribute to affinity modulation. On the other hand, the extent of these cytoskeletal associations and an intact actin cytoskeleton critically determine the mechanical strength of $\alpha_4\beta_1$ VCAM-1 bonds (i.e., tether formation, adhesion strengthening, and resistance to mechanical stress). Thus, we propose that the ability of α_4 integrins to translate ligand occupancy into immediate mechanical stability of subsecond adhesive contacts requires paxillin and talin-mediated linkages of $\alpha_4\beta_1$ to the actin cytoskeleton. The regulation of $\alpha_4\beta_1$ adhesiveness by talin has never been addressed, especially not under shear stress conditions. The finding that talin suppression impairs the strengthening of wt $\alpha_4\beta_1$ bonds under strain is reminiscent of results reporting the involvement of talin1 in ligand-driven $\alpha_5\beta_1$-cytoskeletal bonds in fibroblasts (Jiang et al., 2003). Although different integrins may anchor differently to the cytoskeleton in distinct cell types, this involvement of talin in both α_4- and α_5-integrin associations with the actin cytoskeleton is consistent with the notion that talin, apart from its role in integrin affinity regulation (Tadokoro et al., 2003), is a key postligand occupancy adaptor that promotes integrin bond stabilization in distinct mechanical contexts and cellular environments.

Our results highlight the role of the α-integrin subunit rather than the β subunit in postligand binding adhesion strengthening of the $\alpha_4\beta_1$–VCAM-1 bond under mechanical strain. Previous findings suggested that a nearly complete truncation of the α_4-cytoplasmic tail impairs $\alpha_4\beta_1$ adhesion strengthening without altering initial cell capture to VCAM-1 under shear flow (Alon et al., 1995; Kassner et al., 1995). This truncation of the α_4-integrin tail also reduced integrin mobility (Yauch et al., 1997) and may have increased integrin cytoskeletal anchorage via the intact $\beta 1$ subunit, although this was not experimentally demon-

strated. Therefore, in these earlier studies, it was impossible to distinguish between the contributions of α_4 anchorage versus mobility to rapid mechanical stabilization of α_4 integrin–mediated tethers. Our present results provide the first direct evidence for a positive role of α_4 anchorage for the earliest stabilization events of $\alpha_4\beta_1$–VCAM-1 bonds subjected to mechanical strain.

In addition to the α_4 Y991 residue, the phosphorylation level of the α_4 serine 988 has been shown to control the degree of α_4 association with paxillin (Han et al., 2001). A dephosphorylated serine variant mimicked by the phosphodeficient mutant α_4 S988A was reported to bind paxillin at enhanced levels (Nishiya et al., 2005). Interestingly, this phosphodeficient mutant did not properly anchor to the cytoskeleton and supported reduced adhesiveness to VCAM-1 (unpublished data). These findings, together with the paxillin-silencing data of this study, suggest that paxillin binding to the α_4 subunit is required but is insufficient to anchor α_4 to the cytoskeleton. Thus, α_4 phosphorylation, which is postulated to attenuate paxillin binding to the α_4 subunit, is in fact required, at least at a basal level, for proper cytoskeletal α_4 association and productive adhesiveness under shear stress. Overphosphorylation of α_4, which reduces paxillin association, may, on the other hand, attenuate both anchorage and adhesiveness. Studies are ongoing to address both the positive and negative effects of serine phosphorylation on α_4 anchorage and function under strain.

α_4 association with paxillin enhances the activation of the focal adhesion kinases FAK and PYK-2 after $\alpha_4\beta_1$ ligation (Liu et al., 1999; Rose et al., 2003). This association also restricts Rac activation at the leading edge via recruitment of the Arf GTPase-activating protein (Nishiya et al., 2005). Nevertheless, at 1-min contacts with VCAM-1, cells expressing the α_4-tail mutant spread normally on VCAM-1. Suppression of tyrosine phosphorylation or inhibition of PYK-2 activity in Jurkat T cells had no effect on $\alpha_4\beta_1$-mediated adhesion strengthening developed under shear stress (unpublished data). Thus, the ability of paxillin association with $\alpha_4\beta_1$ to enhance integrin anchorage to the cytoskeleton and promote mechanical stability of adhesive tethers at short-lived contacts is distinct from its roles in focal adhesion turnover and Rac deactivation during cell spreading on VCAM-1–containing substrates (Nishiya et al., 2005). Altogether, our findings suggest that modulating mechanical properties of α_4 integrins by the inhibition of specific associations between α_4-cytoplasmic tails and the cytoskeleton may be a selective strategy to fine tune integrin-mediated adhesion under shear stress without altering integrin affinity.

Materials and methods

Reagents and antibodies
Recombinant seven-domain human VCAM-1 (sVCAM-1) was provided by B. Pepinsky (Biogen, Cambridge, MA). VCAM-1–Fc fusion protein containing seven-domain VCAM-1 fused to IgG was generated as described previously (Rose et al., 2000). VCAM-1–Fc constructed from domains 1 and 2 of VCAM-1 fused to Fc, termed 2D VCAM-1–Fc, was provided by B. Pepinsky. Affinity-purified human full-length spleen-derived ICAM-1 was a gift from T. Springer (Harvard University, Boston, MA). ICAM-Fc and SDF-1α were purchased from R&D Systems. BSA (fraction V), poly-L-lysine, and Ca^{2+}/Mg^{2+}-free HBSS were obtained from Sigma-Aldrich. Human serum albumin (fraction V) and PMA were purchased from Calbiochem.

The α_4-integrin function–blocking HP1/2 mAb, the E-selectin–blocking mAb BB11, the β_1-specific TS2/16 mAb, the α_4-specific nonblocking 5BG10 mAb (all provided by B. Pepinsky), the β_1-integrin subunit mAb 15/7 (provided by T. Yednock, Elan Pharmaceuticals, San Francisco, CA; Yednock et al., 1995), and the anti-$\alpha_4\beta_7$ Act-1 (a gift from M.J. Briskin, Millennium Pharmaceuticals, Cambridge, MA) were all used as purified Ig. Antitalin mAb (clone 8d4) was purchased from Sigma-Aldrich. Anti-paxillin mAb (clone 349) was purchased from BD Transduction Laboratories. Goat polyclonal anti-α_4 Ab (clone C-20) was purchased from Santa Cruz Biotechnology, Inc.

Cell culture and flow cytometry
Jurkat cells deficient in α_4 (JB4) were stably transfected with either wt α_4 or α_4(Y991A) cDNA as described previously (Liu et al., 1999). Cells were subcloned, and multiple clones expressing identical levels of α_4 and β_1 subunits were taken for functional analysis. Clones were maintained in RPMI 1640 medium supplemented with 10% heat-inactivated FCS, 2 mM L-glutamine, 1 mM sodium pyruvate, 100 mM nonessential amino acids, and antibiotics (Biological Industries). Primary HUVECs were established as previously described (Shamri et al., 2005). HUVECs were left intact or stimulated for 4 h with 0.1 ng/ml TNF-α (R&D Systems) before experiments. Staining and FACS analysis were performed as previously described (Feigelson et al., 2003).

Immunofluorescence staining and immunoelectron microscopy
For α_4-integrin immunostaining, Jurkat cells were washed in PBS and incubated with 10 μg/ml anti-α_4 B5G10 mAb for 30 min at 4°C. Cells were washed once with PBS + 5 mM EDTA and twice with PBS/0.1% BSA, and α_4 integrins were stained with AlexaFluor546-conjugated anti–mouse Ab (Invitrogen) and fixed in 3% PFA in PBS (30 min at RT). Control cells were fixed before mAb incubation steps. Cells were attached to poly-L-lysine–coated glass slides, and coverslips were mounted with elvanol overnight and analyzed with a confocal microscope (TE300; Nikon) and a laser-scanning system (model 2000; Bio-Rad Laboratories).

α_4 localization was assessed by immunoelectron microscopy as previously described (Chen et al., 1999). In brief, cultured Jurkat cells were washed and prefixed in 0.1 M phosphate buffer, pH 7.4, containing 2% PFA and 0.05% glutaraldehyde. Washed cells in H/H medium (HBSS containing 2 mg/ml BSA and 10 mM Hepes, pH 7.4, supplemented with 1 mM CaCl$_2$ and 1 mM MgCl$_2$) were incubated with 10 μg/ml anti-α_4 B5G10 mAb for 40 min at 22°C. Washed cells were stained with 10 μg/ml rabbit anti–mouse Ig, washed, and incubated for 45 min with 5 nm gold particle–conjugated goat anti–rabbit (Aurion). Ultrathin sections (70–90 nm) of 40–60 cells for each experimental group were examined with an electron microscope (Tecnai 12; FEI) under 120 kV, and images were taken using a CCD camera (Megaview 3; Soft Imaging System). In each experimental group analyzed, the number of α_4-specific gold particles on microvillar projections was compared with that on adjacent cell body compartments of identical dimensions.

siRNA-mediated silencing of paxillin and talin
Silencing of talin expression in Jurkat cells was achieved by a talin1-specific 21-nucleotide siRNA (Dharmacon) corresponding to positions 6,043–6,063 relative to the talin1 mRNA start codon (Shamri et al., 2005). Silencing of paxillin was conducted as described previously (Nishiya et al., 2005). Control transfections were performed with a fluorescein-labeled 21-nucleotide duplex directed to Luciferase GL2. Transfection of T cells was performed by electroporation using the Nucleofection system (Amaxa). Transfected cells were maintained in culture medium. Talin and paxillin expression monitored by immunoblotting was maximally suppressed 72 h posttransfection, and time points were chosen for subsequent functional assays. Immunoprecipitation of α_4 was performed as previously described (Feigelson et al., 2003).

Quantification of integrin anchorage to the cytoskeleton
Cells were stained with 10 μg/ml of the FITC-conjugated anti-α_4 mAb HP1/2 at 4°C for 30 min, washed twice with H/H medium supplemented with 1 mM CaCl$_2$ and 1 mM MgCl$_2$, and left either untreated or cross-linked with secondary antibodies at 4°C for 30 min followed by two washes as described previously (Geppert and Lipsky, 1991; Evans et al., 1999). All cells were then incubated at RT for 30 min with the cytoskeletal stabilizing buffer (CSB; 50 mM NaCl, 2 mM MgCl$_2$, 0.22 mM EGTA, 13 mM Tris, pH 8.0, 1 mM PMSF, 10 mM iodacetamide, and 2% FCS) alone or supplemented with 0.1% NP-40. The intact cells or their recovered detergent-insoluble cytoskeletal fractions were washed in detergent-free CSB, fixed in 1% PFA/PBS, and analyzed by flow cytometry. Under these con-

ditions, the majority of detergent-treated cells retain their shape and size. The ratio of mean fluorescence intensity recovered in detergent-treated cells divided by that of cells not exposed to the detergent yields the fraction of mAb-bound α_4 integrin that is resistant to detergent extraction; i.e., anchored to the (detergent resistant) cytoskeletal fraction of the cell.

VCAM-1 microbead–binding assays and integrin bond stiffness
Protein A–coated magnetic M-280 Dynabeads (Dynal) were coated at RT with various concentrations (0.004–1 μg/ml) of 2D VCAM-Fc in H/H binding medium, washed according to the manufacturer's instructions, and stored on ice. Cells and VCAM-1–coated beads were mixed at RT for 1 min in binding medium at a concentration of 10^7 cells/ml at a cell/bead ratio of 1:8 followed by a threefold dilution in binding medium. The cellular side scatter, distinguishing between bead-bound and bead-free cells, was analyzed immediately in a FACScan flow cytometer (Becton Dickinson). Background binding determined with protein A–coated beads was <10% of the maximal binding observed at VCAM-1 saturation and was subtracted from the total binding results.

The mechanical stiffness of $\alpha_4\beta_1$/VCAM-1 adhesions was measured by electromagnetic pulling cytometry using VCAM-1–coated beads (Matthews et al., 2004). The detailed method is described in supplemental material (available at http://www.jcb.org/cgi/content/full/jcb.200503155/DC1).

AFM measurements
All force measurements were conducted at 35 $\pm$ 2°C using a previously described AFM apparatus (Benoit et al., 2000). In brief, a microfabricated Si$_3$N$_4$ cantilever tip (Park Scientific Instruments) was coated with 0.1 mg/ml of the anti-CD43 mAb (R&D Systems). The spring constants of the cantilevers used were determined at $\sim$4.7 $\pm$ 0.6 mN/m. A single cell was immobilized on the cantilever tip shortly before experimentation. The device was mounted with a piezo-actuator (Piezosystem Jena) on an inverted optical microscope (Carl Zeiss MicroImaging, Inc.) containing a heating stage. A diode laser beam focused on the sensor was used to measure the displacement of the cantilever by the laser beam deflection on a two-segment photodetector. The cell adhering to the cantilever was positioned above an adhesive substrate coated with 2D VCAM-1–Fc captured via human IgG Fc mAb (Jackson ImmunoResearch Laboratories). The cantilever was lowered until the sensor detected a contact force equal to a preselected value (typically 50 pN). After the contact was established for a dwelling time of 500 ms, the cell-bearing cantilever was lifted up by the piezo-actuator, and the de-adhesion force was monitored by a force–distance plot (Fig. 5 B). From this plot, the last detectable de-adhesion force was calculated. For each cell, $\sim$50–200 force–distance plots were collected within $\sim$30 min. All de-adhesion events collected in at least 10 independent experiments were presented in histograms (Fig. 5 C).

Laminar flow adhesion assays
Purified ligands or mAbs were coated on polystyrene plates as previously described (Grabovsky et al., 2000). Site densities of coated sVCAM-1 and VCAM-1–Fc were determined as previously described (Grabovsky et al., 2000; Sigal et al., 2000). The polystyrene plates were each assembled on the lower wall of the flow chamber (260-um gap) as previously described (Dwir et al., 2000; Feigelson et al., 2001). Cells were washed with cation-free H/H medium, resuspended in binding medium (H/H medium supplemented with 1 mM CaCl$_2$ and 1 mM MgCl$_2$), and perfused through the flow chamber at the desired shear stress. To disrupt actin cytoskeleton, cells were pretreated for 15 min with 20 μM cytochalasin D (Calbiochem) or carrier solution (0.1% DMSO). All flow experiments were conducted at 37°C. Tethers were defined as transient if cells attached briefly (<2 s) to the substrate and as arrests if they immediately arrested and remained stationary for at least 5 s of continuous flow. Frequencies of adhesive categories within differently pretreated cells or rates of cell accumulation on adhesive substrates were determined as a percentage of cells flowing immediately over the substrates, as previously described (Grabovsky et al., 2000). To assess rapid development of integrin avidity to the ligand at 1-min stationary contacts, cells were allowed to settle onto the substrate for 1 min at stasis. Flow was then initiated and increased step-wise every 5 s by a programmed set of rates. At the indicated shear stresses, the number of cells that remained bound was expressed relative to the number of cells originally settled on the substrate. Over 95% of tethers to VCAM-1 were blocked by pretreating cells with 10 μg/ml of the α_4-blocking mAb HP1/2. Live imaging of α_4 on Jurkat cells prelabeled with AlexaFluor488-conjugated B5G10 mAb that settled on VCAM-1 was conducted with Delta Vision Spectris RT (Applied Precision). α_4 patching was quantified using Image J software (National Institutes of Health).

References

Alon, R., and S. Feigelson. 2002. From rolling to arrest on blood vessels: leukocyte tap dancing on endothelial integrin ligands and chemokines at subsecond contacts. *Semin. Immunol.* 14:93–104.

Alon, R., P.D. Kassner, M.W. Carr, E.B. Finger, M.E. Hemler, and T.A. Springer. 1995. The integrin VLA-4 supports tethering and rolling in flow on VCAM-1. *J. Cell Biol.* 128:1243–1253.

Ambroise, Y., B. Yaspan, M.H. Ginsberg, and D.L. Boger. 2002. Inhibitors of cell migration that inhibit intracellular paxillin/alpha4 binding: a well-documented use of positional scanning libraries. *Chem. Biol.* 9:1219–1226.

Benoit, M., D. Gabriel, G. Gerisch, and H.E. Gaub. 2000. Discrete interactions in cell adhesion measured by single-molecule force spectroscopy. *Nat. Cell Biol.* 2:313–317.

Berlin, C., E.L. Berg, M.J. Briskin, D.P. Andrew, P.J. Kilshaw, B. Holzmann, I.L. Weissman, A. Hamann, and E.C. Butcher. 1993. $\alpha_4\beta_7$ integrin mediates lymphocyte binding to the mucosal vascular addressin MAdCAM-1. *Cell.* 74:185–195.

Berlin, C., R.F. Bargatze, J.J. Campbell, U.H. von Andrian, M.C. Szabo, S.R. Hasslen, R.D. Nelson, E.L. Berg, S.L. Erlandsen, and E.C. Butcher. 1995. α_4 integrins mediate lymphocyte attachment and rolling under physiologic flow. *Cell.* 80:413–422.

Brown, M.C., and C.E. Turner. 2004. Paxillin: adapting to change. *Physiol. Rev.* 84:1315–1339.

Carman, C.V., and T.A. Springer. 2003. Integrin avidity regulation: are changes in affinity and conformation underemphasized? *Curr. Opin. Cell Biol.* 15:547–556.

Chen, C., J.L. Mobley, O. Dwir, F. Shimron, V. Grabovsky, R.L. Lobb, Y. Shimizu, and R. Alon. 1999. High affinity VLA-4 subsets expressed on T cells are mandatory for spontaneous adhesion strengthening but not for rolling on VCAM-1 in shear flow. *J. Immunol.* 162:1084–1095.

Constantin, G., M. Majeed, C. Giagulli, L. Piccio, J.Y. Kim, E.C. Butcher, and C. Laudanna. 2000. Chemokines trigger immediate β_2 integrin affinity and mobility changes: differential regulation and roles in lymphocyte arrest under flow. *Immunity.* 13:759–769.

Du, X.P., E.F. Plow, A.L. Frelinger 3rd, T.E. O'Toole, J.C. Loftus, and M.H. Ginsberg. 1991. Ligands "activate" integrin alpha IIb beta 3 (platelet GPIIb-IIIa). *Cell.* 65:409–416.

Dwir, O., G.S. Kansas, and R. Alon. 2000. An activated L-selectin mutant with conserved equilibrium binding properties but enhanced ligand recognition under shear flow. *J. Biol. Chem.* 275:18682–18691.

Dwir, O., G.S. Kansas, and R. Alon. 2001. The cytoplasmic tail of L-selectin regulates leukocyte capture and rolling by controlling the mechanical stability of selectin:ligand tethers. *J. Cell Biol.* 155:145–156.

Evans, S.S., D.M. Schleider, L.A. Bowman, M.L. Francis, G.S. Kansas, and J.D. Black. 1999. Dynamic association of L-selectin with the lymphocyte cytoskeletal matrix. *J. Immunol.* 162:3615–3624.

Feigelson, S.W., V. Grabovsky, E. Winter, L.L. Chen, R.B. Pepinsky, T. Yednock, D. Yablonski, R. Lobb, and R. Alon. 2001. The src kinase p56Lck upregulates VLA-4 integrin affinity: implications for rapid spontaneous and chemokine-triggered T cell adhesion to VCAM-1 and fibronectin. *J. Biol. Chem.* 276:13891–13901.

Feigelson, S.W., V. Grabovsky, R. Shamri, S. Levy, and R. Alon. 2003. The CD81 tetraspanin facilitates instantaneous leukocyte VLA-4 adhesion strengthening to VCAM-1 under shear flow. *J. Biol. Chem.* 278:51203–51212.

Firrell, J.C., and H.H. Lipowsky. 1989. Leukocyte margination and deformation in mesenteric venules of rat. *Am. J. Physiol.* 256:H1667–H1674.

Geppert, T.D., and P.E. Lipsky. 1991. Association of various T cell-surface molecules with the cytoskeleton. Effect of cross-linking and activation. *J. Immunol.* 146:3298–3305.

Grabovsky, V., S. Feigelson, C. Chen, R. Bleijs, A. Peled, G. Cinamon, F. Baleux, F. Arenzana-Seisdedos, T. Lapidot, Y. van Kooyk, et al. 2000. Subsecond induction of α_4 integrin clustering by immobilized chemokines enhances leukocyte capture and rolling under flow prior to firm adhesion to endothelium. *J. Exp. Med.* 192:495–505.

Han, J., S. Liu, D.M. Rose, D.D. Schlaepfer, H. McDonald, and M.H. Ginsberg. 2001. Phosphorylation of the integrin alpha 4 cytoplasmic domain regulates paxillin binding. *J. Biol. Chem.* 276:40903–40909.

Hynes, R.O. 2002. Integrins: bidirectional, allosteric signaling machines. *Cell.* 110:673–687.

Jiang, G., G. Giannone, D.R. Critchley, E. Fukumoto, and M.P. Sheetz. 2003. Two-piconewton slip bond between fibronectin and the cytoskeleton depends on talin. *Nature.* 424:334–337.

Kansas, G.S., K. Ley, J.M. Munro, and T.F. Tedder. 1993. Regulation of leukocyte rolling and adhesion to high endothelial venules through the cytoplasmic domain of L-selectin. *J. Exp. Med.* 177:833–838.

Kassner, P.D., R. Alon, T.A. Springer, and M.E. Hemler. 1995. Specialized functional properties of the integrin α_4 cytoplasmic domain. *Mol. Biol. Cell.* 6:661–674.

Katagiri, K., N. Ohnishi, K. Kabashima, T. Iyoda, N. Takeda, Y. Shinkai, K. Inaba, and T. Kinashi. 2004. Crucial functions of the Rap1 effector molecule RAPL in lymphocyte and dendritic cell trafficking. *Nat. Immunol.* 5:1045–1051.

Kim, M., C.V. Carman, W. Yang, A. Salas, and T.A. Springer. 2004. The primacy of affinity over clustering in regulation of adhesiveness of the integrin $\alpha_L\beta_2$. *J. Cell Biol.* 167:1241–1253.

Kinashi, T. 2005. Intracellular signalling controlling integrin activation in lymphocytes. *Nat Rev Immunol.* 5:546–559.

Kinashi, T., M. Aker, M. Sokolovsky-Eisenberg, V. Grabovsky, C. Tanaka, R. Shamri, S. Feigelson, A. Etzioni, and R. Alon. 2004. LAD-III, a leukocyte adhesion deficiency syndrome associated with defective Rap1 activation and impaired stabilization of integrin bonds. *Blood.* 103:1033–1036.

Kucik, D.F., M.L. Dustin, J.M. Miller, and E.J. Brown. 1996. Adhesion-activating phorbol ester increases the mobility of leukocyte integrin LFA-1 in cultured lymphocytes. *J. Clin. Invest.* 97:2139–2144.

Lin, K., H.S. Ateeq, S.H. Hsiung, L.T. Chong, C.N. Zimmerman, A. Castro, W.C. Lee, C.E. Hammond, S. Kalkunte, L.L. Chen, et al. 1999. Selective, tight-binding inhibitors of integrin $\alpha_4\beta_1$ that inhibit allergic airway responses. *J. Med. Chem.* 42:920–934.

Liu, S., and M.H. Ginsberg. 2000. Paxillin binding to a conserved sequence motif in the α_4 integrin cytoplasmic domain. *J. Biol. Chem.* 275:22736–22742.

Liu, S., S.M. Thomas, D.G. Woodside, D.M. Rose, W.B. Kiosses, M. Pfaff, and M.H. Ginsberg. 1999. Binding of paxillin to α_4 integrins modifies integrin-dependent biological responses. *Nature.* 402:676–681.

Matthews, B.D., D.R. Overby, F.J. Alenghat, J. Karavitis, Y. Numaguchi, P.G. Allen, and D.E. Ingber. 2004. Mechanical properties of individual focal adhesions probed with a magnetic microneedle. *Biochem. Biophys. Res. Commun.* 313:758–764.

Nishiya, N., W.B. Kiosses, J. Han, and M.H. Ginsberg. 2005. An α_4 integrin-paxillin-Arf-GAP complex restricts Rac activation to the leading edge of migrating cells. *Nat. Cell Biol.* 7:343–352.

Rose, D.M., P.M. Cardarelli, R.R. Cobb, and M.H. Ginsberg. 2000. Soluble VCAM-1 binding to α_4 integrins is cell-type specific and activation dependent and is disrupted during apoptosis in T cells. *Blood.* 95:602–609.

Rose, D.M., S. Liu, D.G. Woodside, J. Han, D.D. Schlaepfer, and M.H. Ginsberg. 2003. Paxillin binding to the α_4 integrin subunit stimulates LFA-1 (integrin $\alpha_L\beta_2$)-dependent T cell migration by augmenting the activation of focal adhesion kinase/proline-rich tyrosine kinase-2. *J. Immunol.* 170:5912–5918.

Shamri, R., V. Grabovsky, J.M. Gauguet, S. Feigelson, E. Manevich, W. Kolanus, M.K. Robinson, D.E. Staunton, U.H. von Andrian, and R. Alon. 2005. Lymphocyte arrest requires instantaneous induction of an extended LFA-1 conformation mediated by endothelium-bound chemokines. *Nat. Immunol.* 6:497–506.

Shimaoka, M., J. Takagi, and T.A. Springer. 2002. Conformational regulation of integrin structure and function. *Annu. Rev. Biophys. Biomol. Struct.* 31:485–516.

Sigal, A., D.A. Bleijs, V. Grabovsky, S.J. van Vliet, O. Dwir, C.G. Figdor, Y. van Kooyk, and R. Alon. 2000. The LFA-1 integrin supports rolling adhesions on ICAM-1 under physiological shear flow in a permissive cellular environment. *J. Immunol.* 165:442–452.

Springer, T.A. 1994. Traffic signals for lymphocyte recirculation and leukocyte emigration: the multistep paradigm. *Cell.* 76:301–314.

Tadokoro, S., S.J. Shattil, K. Eto, V. Tai, R.C. Liddington, J.M. de Pereda, M.H.

Ginsberg, and D.A. Calderwood. 2003. Talin binding to integrin beta tails: a final common step in integrin activation. *Science.* 302:103–106.

van Kooyk, Y., and C.G. Figdor. 2000. Avidity regulation of integrins: the driving force in leukocyte adhesion. *Curr. Opin. Cell Biol.* 12:542–547.

von Andrian, U.H., S.R. Hasslen, R.D. Nelson, S.L. Erlandsen, and E.C. Butcher. 1995. A central role for microvillous receptor presentation in leukocyte adhesion under flow. *Cell.* 82:989–999.

Yauch, R.L., D.P. Felsenfeld, S.K. Kraeft, L.B. Chen, M.P. Sheetz, and M.E. Hemler. 1997. Mutational evidence for control of cell adhesion through integrin recruitment, independent of ligand binding. *J. Exp. Med.* 186: 1347–1355.

Yednock, T.A., C. Cannon, C. Vandevert, E.G. Goldbach, G. Shaw, D.K. Ellis, C. Liaw, L.C. Fritz, and L.I. Tanner. 1995. $\alpha_4\beta_1$ integrin-dependent cell adhesion is regulated by a low affinity receptor pool that is conformationally responsive to ligand. *J. Biol. Chem.* 270:28740–28750.

Zhang, X., S.E. Craig, H. Kirby, M.J. Humphries, and V.T. Moy. 2004. Molecular basis for the dynamic strength of the integrin $\alpha_4\beta_1$/VCAM-1 interaction. *Biophys. J.* 87:3470–3478.

Viscoelasticity of membrane tethers

The Viscoelasticity of Membrane Tethers and its Importance for Cell Adhesion

Julia Schmitz, Martin Benoit, Kay-Eberhard Gottschalk˙

Applied Physics and Biophysics
Ludwig-Maximilians University
Amalienstr 54
80799 Munich, Germany

˙corresponding author
email: kay.gottschalk@physik.uni-muenchen.de
fon: +49-89-2180 3436
fax: +49-89-2180 2050

Keywords:

cell mechanics, viscoelasticity, nano-environment, AFM, integrin, Kelvin body;

Abstract

Cell adhesion mechanically couples cells to surfaces. The durability of individual bonds between the adhesive receptors and their ligands in the presence of forces determines the cellular adhesion strength. For adhesive receptors like integrins, it is a common paradigm that the cell regulates its adhesion strength by altering the affinity state of the receptors. However, the probability distribution of rupture forces is not only dependent on the affinity of individual receptor-ligand bonds, but also on the mechanical compliance of the cellular anchorage of the receptor. Hence, by altering the anchorage, the cell can regulate its adhesion strength without changing the affinity of the receptor. Here, we analyze the anchorage of the integrin VLA-4 with its ligand VCAM-1. For this purpose, we develop a model based on the Kelvin body, which allows one to quantify the mechanical properties of the adhesive receptor's anchorage using atomic force microscopy on living cells. As we demonstrate, the measured force curves give valuable insight into the mechanics of the cellular anchorage of the receptor, which is described by the tether-stiffness, the membrane rigidity and the membrane viscosity. The measurements relate to a tether stiffness of $k_t=$ 1.6μN/m, an initial membrane rigidity of $k_i=$260μN/m and a viscosity of μ=5.9μN·s/m. Integrins exist in different activation states. When activating the integrin with Mg^{2+}, we observe altered viscoelastic parameters of k_t=0.9μN/m, k_i=190μN/m and μ=6.0μN·s/m. Based on our model, we postulate that anchorage-related effects are common regulating mechanisms for cellular adhesion beyond affinity regulation.

Introduction

Cell-to-surface or cell-to-cell adhesion is of critical importance for a large variety of cellular events. It is fundamental in homing of T-lymphocytes and in cancer metastasis. During homing, the T-lymphocytes experience shear stress of the blood stream and adhere against external forces. The adhesiveness of cells is tightly regulated and involves a variety of force-resisting receptors like selectins and integrins. Our understanding how different conformational states of integrins relate to different adhesion properties has been greatly improved by a combined effort of structural and cell biologists (1,2). While the focus has been on conformational switching between affinity states, the influence of cytoskeletal anchorage as well as of integrin clustering has also been investigated (3-5). The latter events change the mechanical environment of the receptor (6). It is conceivable that changing the receptor's cellular anchorage influences the adhesive behavior of the cell against external forces, even without changing the equilibrium affinity of the receptor to its ligand (7). We focus here on the anchorage of the integrin VLA-4 in Jurkat cells. VLA-4 is one of the key adhesive receptors on T-lymphocytes and is involved in both lymphocyte rolling and arrest (6,8). In our experimental setup, the VLA-4 receptor serves as a local nano-probe to investigate the viscoelasticity of its environment. For using a single receptor as a probe for its environment, single-molecule techniques are required. Atomic force spectroscopy (AFM) is ideally suited to probe cell adhesion events on the level of individual molecules. It is capable of measuring and analyzing single receptor-ligand bonds on living cells under physiological conditions (9-12). Usually, AFM on cells has been employed to analyze the distribution of rupture forces of a given receptor-ligand pair (12-16). From this, one gets important insight on the energy landscape of the respective bond (16,17). Yet, the AFM data contain more information than only the rupture forces. When retracting cells from adhesive

surfaces, the history of force development up to the point of cell-to-surface bond breakage is measured with high precision (Figure 1). This force-distance relationship is dictated by the energy landscape of the receptor-ligand bond, but also includes the mechanical anchorage of the receptor in the cellular membrane. Thoroughly analyzing the force development can therefore reveal the mechanical properties of the anchorage. As noted earlier (12,18-22), the force-distance curves correspond to microvillus stretching and membrane tether pulling. Membrane tethers are small membrane tubes with a diameter on the order of tens of nm, which are fed from the membrane reservoir of the cell, when pulled out. The force-distance relationship of pulling tethers has the characteristics of viscoelastic solids (22). Thus, the interpretation of the force curves should follow models, which describe the viscoelasticity of cells. One well-established model for viscoelastic bodies is the Kelvin body (Figure 2) (23-25). We show that the cell behaves like a Kelvin body under our experimental conditions. Hence, we can use VLA-4 expressed on Jurkat cells as a nano-probe for the viscoelastic properties of the cellular anchorage in close vicinity to this receptor.

To investigate changes in the environment of force-resisting receptors, we tested two different conditions: integrins on cells in a physiological buffer and integrins on cells in a buffer that is known to artificially activate integrins (26). Mechanical differences in the anchorage between these two setups are possible: for resting cells in physiological buffer, the vast majority of integrins is kept in an inactive state and not available for binding. This allows the immune cell to circulate freely in the blood stream. Due to both statistical fluctuations and the requirement to probe the vessel-wall, a small subset of integrins is nevertheless always in a binding competent state. These integrins have been postulated to be distributed to the proximity of lipid rafts (27-29), which are thought to be stiffer than the average lipid bilayer membrane. When artificially activating the integrins with an activating buffer, nearly all integrins become binding competent. Therefore, after artificial activation, the majority of the binding competent integrins will not be located in the proximity of lipid rafts, but distributed all over the cell. Therefore, we expect to measure a differing nano-environment. Here, we show that the average nano-environment of Mg^{2+}-activated integrin receptors is indeed different from the nano-environment of resting receptors. Further on, from the force-distance relationship obtained from the Kelvin body model, we analytically determine the compliance of membrane tethers. The compliance describes the elastic response of the cell to external forces (30). The compliance is also fundamentally determining the distribution of rupture forces (7). The knowledge of the compliance allows us to gauge the influence of the rheological parameters on this distribution of rupture forces, which directly influences the force-persistence of the cell-to-surface adhesion.

In summary, we have developed a model for the description of force-distance curves derived from cellular AFM measurements. We show that we can detect subtle differences in the membrane environment of the receptors. We conclude that the anchorage of receptors in the cellular membrane can be used as a regulator of receptor adhesiveness, without the need to change the receptor conformation. Hence, the cell can regulate its adhesiveness by altering the receptor anchorage on top of modulating the affinity of the receptor to its ligand through conformational changes.

Materials and Methods

3

Reagents

BSA (fraction V), HSA (fraction V) and Ca^{2+}/Mg^{2+}-free HBSS were purchased from Sigma-Aldrich. BIO1211 was a gift from Blake Pepinsky (Biogen Inc. Cambridge MA). Recombinant human VCAM-1 (seven domains), recombinant human SDF-1alpha and anti-human CD43mAb were obtained from R&D Systems.

Surface preparation

To prepare the substrate for the AFM experiment, spots were incubated on the lid of a Petri dish with 0.0125 μg/ml or 0.025 μg/ml VCAM-1 and 2 μg/ml HSA as carrier protein together with an heat-inactivated chemokine as inert spacer (8,15). The site density of VCAM-1 was equivalent to 50 sites/μm^2 and 100 sites/μm^2, respectively (8). After adsorption over night at 4°C, the spots were washed four times with PBS (Ca^{2+}/Mg^{2+}-free) and quenched with 2% HSA in PBS for >60 minutes at 4°C.

Cell culture

Jurkat cells were cultured in RPMI1640 medium (Biochrom AG) supplemented with 10% heat-inactivated FCS, 2 mM L-glutamine and penicillin/streptomycin in 5% CO_2 at 37°C. The cells were washed with 5 mM EDTA and then transferred to HBSS medium (2 mg/ml BSA, 10 mM HEPES, 1 mM of $CaCl_2$ and $MgCl_2$ or 5 mM $MgCl_2$ and no Ca^{2+}).

AFM Measurements

All experiments were conducted at 36±1°C in HBSS medium as described (9). The spring constant of the cantilever was determined by the thermal fluctuation method (31,32); one leg was broken from the C Lever (Park Scientific Instruments). The tip was snapped. 30 minutes before the experiment, the cantilever was incubated with 0.1 mg/ml of anti-human CD43mAb at room temperature. A cell was attached on the cantilever, positioned over the VCAM-1 spot and pressed onto the coated Petri dish for 300 ms at ~50 pN. Then, the cantilever with the cell was retracted from the surface at a velocity of 3.6 μm/s . This lies within the range of physiological velocities for lymphocytes in the blood stream (33). Two setups were tested: in one setup, physiological buffer conditions with 1 mM Ca^{2+}/Mg^{2+} were used, in the second setup, the integrins were artificially activated (26) by a buffer with 5 mM Mg^{2+} in the absence of Ca^{2+}. 50-100 force-distance curves were registered per cell and at eight cells per setup were probed (Table I). Controls to test the specificity of the interactions were performed on uncoated Petri dish and by adding BIO1211 in experiments on VCAM-1 coated substrates. At a concentration of 1 μg/ml this peptidomimetic blocks binding (34). BIO1211 was added 10 min before the measurement.

Mechanical Models

The force distance relationships of the three standard viscoelastic models (Maxwell body, Voigt body, Kelvin body – Figure 2) have been tested for the condition of a constant retract velocity. The Maxwell body and the Voigt body can be regarded as special cases of the third model, the Kelvin body. For the analysis of our data, we transformed the differential equation for the Kelvin body into a time-dependency of the force under the boundary condition of a constant retraction velocity. This yields (23):

$$\frac{dF(t)}{dt} = -\frac{k_i}{\mu}\left(F(t) - k_t \cdot z - \mu \cdot \left(1 + \frac{k_t}{k_i}\right) \cdot \frac{dz}{dt} \right) \qquad \text{(equation 1)}.$$

Here, $F(t)$ is the force depending on the time, k_i is the spring constant of the spring in series to the dashpot, μ is the viscosity of the dashpot and k_t is the spring constant of the spring parallel to the dashpot. If the retract velocity $v = \dfrac{dz}{dt}$ is constant, the time t can be expressed in terms of the position z as $t = \dfrac{z}{v}$. With the boundary condition $F(0) = 0$, equation (1) can be integrated to

$$F(z) = k_t \cdot z + \mu \cdot v - \mu \cdot v \cdot e^{\frac{-k_i \cdot z}{\mu \cdot v}} \qquad \text{(equation 2)}.$$

With this equation, we fitted all force curves having a single rupture event and obtained distributions for the viscoelastic parameters. For fitting, all parameters were restraint to be larger than zero. We tested the significance of the differences between the two setups with the Mann-Whitney U-test.

Simulation of the Force Distributions

In order to test the quality of the used model to describe the viscoelastic anchorage of molecular bonds under external load, we calculated the expected force distribution from the measured rupture length distribution. To this end, we used the measured viscoelastic parameters and recalculated the distribution of rupture forces from the measured distribution of rupture length using equation (2). To better simulate the experimental conditions, we added a random force noise of ±8pN.

Results and Discussion

Specificity of Adhesion of our Measurements.

To be in the single-molecule regime, adhesion rates on the order of 30% are required (9). The adhesion rates are 26% under resting conditions and 39% under activating conditions (Table I), being a) in the desired range and demonstrating b) that the activation of integrins leads to an increased adhesion. Recently, it has been argued that it is highly nontrivial to pull tethers from specific contacts (35) as opposed to non-specific contacts. Since the surface is only adhesive if functionalized with VCAM-1, and since the cellular adhesion can be blocked by the specific integrin blocker BIO1211 (Figure 3), we ensured the integrin-mediated specificity of the cell-to-surface adhesion. Moreover, to guarantee that we are in a single-molecule regime, we used a highly diluted ligand density of only 50-100 sites/µm². At this density, the average distance between the ligands is larger than the average diameter of a microvillus of 100 nm (36).

Mechanical models for viscoelastic bodies.

Three simple models are common for the description of viscoelastic bodies, the Maxwell body, the Voigt body and the Kelvin body (Figure 2) (25). The Kelvin body consists of a spring with spring constant k_t parallel to a series of a dashpot with viscosity μ and a second spring with spring constant k_i . In our setup, the first spring with spring constant k_t describes the stiffness of the membrane tether pulled from the cell membrane; the second spring describes the bending

5

rigidity of the cellular membrane and the dashpot represents the viscous contribution of the receptor-anchoring membrane. The Voigt and the Maxwell bodies are special cases of the Kelvin body, with $F_{Maxwell} = \lim\limits_{k_t \to 0}(F_{Kelvin})$ for the Maxwell body and $F_{Voigt} = \lim\limits_{k_i \to \infty}(F_{Kelvin})$ for the Voigt body. Fitting a typical force curve with equation (2) reveals that only the Kelvin body is a good model for the description of our force-distance relationship (Figure 2). By fitting our data , we can analyze the nano-viscoelastic properties k_i, k_t and μ in the vicinity of the receptor. Due to the higher number of free parameters, the Kelvin model naturally fits the force curves better. Yet, also from a biophysical point of view it is important to include a spring modelling a tether stiffness: it has been shown that also static tethers without a viscous contribution act like a spring with a certain spring constant (22), which cannot be modelled in a Maxwell body.

The viscoelastic parameters of the cellular membrane.

We measured the cellular adhesion mediated by the interaction of the integrin VLA-4 with VCAM-1 both under physiological conditions and under the integrin-activating condition of 5 mM Mg^{2+} in the absence of Ca^{2+}. Only force curves with single rupture events were taken into account. Each single rupture was fitted according to equation (2). From the median of the distributions of the fit parameters, we determined the respective parameter value. Since the values are potentially dependent on the length of the force curves, we used different minimum lengths (Figure 4). The median of the viscosity μ with a minimum length of l>600nm is 6.0 μN·s/m for Mg^{2+}-activated integrins and for resting integrins 5.9 μN·s/m. k_i, the initial bending rigidity of the membrane, is decreased after activation from 260 μN/m to 190 μN/m. k_t decreases from 1.6 μN/m to 0.9 μN/m under activating conditions (Table II). A Mann-Whitney test of the distributions shows that for a minimum length of l> 300nm or l > 600nm, only the initial bending rigidity is significantly different. For ruptures with tethers longer than 800 nm, also the tether stiffness becomes significantly different between the two setups, although the absolute value hardly changes with increasing cut-off length. This shows that k_t becomes better defined for longer ruptures. Although it would be desirable to test even longer ruptures, the number of ruptures with a rupture-length of ≥ 1mm is too small to obtain statistically significant distributions.

While no cut-off dependent differences in μ or k_t can be detected, k_i is higher, if we include ruptures with a length between 300 nm to 600 nm, than if we exclude these ruptures. This may have different reasons: the molecular bonds of stiffly anchored receptors potentially break earlier due to the faster force loading. Hence, a stiffer environment induces shorter ruptures. Furthermore, k_t is ill defined for short ruptures. Since the initial slope is the sum of k_i and k_t, an ill-defined k_t influences k_i. In our fit-procedure, k_t is initially set to k_t=0; if due to the shortness of the rupture k_t is not well defined, k_i will be artificially higher.

The initial slope of the force curve might be influenced by the cortex tension, which causes the (negative) pushing force of the cell when compressed. To test the correlation between cortex tension and initial bending rigidity, we compared the slope before zero force with ki for each setup. The cell stiffness, which is described by the slope before zero force, is related to the cortex tension. The two slopes (before and ki) are significantly different in both setups (Figure 4). Comparing the slopes before zero forces of the Ca^{2+}/Mg^{2+} setup with the slope before zero forces of the Mg^{2+} setup shows, that the slopes before zero force are not influenced by the ion-composition of the buffer. This is reasonable, since the treatment with Mg^{2+} should not lead to a global change in the cellular mechanics, but should only be observable when pulling on the activated integrins.

6

A weak dependency of the initial bending rigidity with the cellular stiffness is observed as expected (Figure 4).

We also compared the distributions of the medians per single cell. To this end, we calculated the significance of the difference between the distributions of the medians per single cell. The initial bending rigidity, but not the tether reset force constant or the viscosity, is significantly different between the two setups when statistically testing the cell-to-cell variations (Figure 5).

What is a plausible molecular reason for the altered nano-environment of Mg^{2+}-activated receptors? It is commonly assumed that the cell bears a reservoir of resting receptors on its surface. These receptors are binding-incompetent and not observed in our experiments. Yet, even for resting cells, a subset of receptors is binding competent. These receptors have been postulated to be located in lipid rafts (27). The binding-incompetent receptors, on the other hand, are distributed in other membrane areas. Mg^{2+}-activation activates the resting receptors, which are not in rafts. Since lipid rafts are rich in cholesterol and do have different viscoelastic properties, it is reasonable to assume that the receptors probed after Mg^{2+}-stimulation are located in an environment with less rigidity.

Yet, the tether populations we are probing are not homogeneous: before activation, not all binding-competent receptors will be located in the vicinity of lipid rafts, and after activation, a fraction of the integrins will still be located within lipid rafts. Other effects might further lead to inhomogeneities: activated integrins may be clustered or attached to the cytoskeleton. Also these alterations of the intra-cellular attachment will influence the viscoelasticity measured by pulling on the integrins.

In principle, it should be possible to resolve the different environments and to gauge the ratio of the respective populations. Unfortunately, due to the subtle differences between the environments, we are unable to statistically detect the subpopulations in the setups. The probing of inhomogeneous populations in each setup blurs the true differences between the varying environments.

Evaluation of the Model

Equation (2) gauges the force at a certain rupture length, provided that the viscoelastic parameters are known. Hence, it is a good test of the model to try to re-calculate the distribution of rupture forces from the measured rupture lengths, using the obtained viscoelastic parameters. The fit between the experimentally measured force distribution and the distribution re-calculated from the distribution of rupture lengths is a good indicator of the performance of the model. As shown in Figure 6, the re-calculated force distributions and the measured force distributions are in very good agreement.

We then went on to test the model on data obtained by Evans et al, who analyzed the extraction of P-selectin mediated membrane tethers from primary T-lymphocytes using a micropipette assay (40). Equation (2) fits the force-distance relationship measured by Evans and co-workers both for normal cells and for cells treated with Latrunculin A (Figure 7). Our fit reveals that treatment with Latrunculin, a drug that impairs cytoskeletal development, renders the cell significantly softer. Interestingly, the membrane viscosity of these cells is only half the value of that of the untreated cells. On first sight, this is surprising, since Latrunculin does not change

the membrane composition. Yet, it has been observed before that the membrane viscosity is dominated by the slip of the membrane over intra-cellular components rather than by intra-membrane slipping events (22), in line with our observations here.

Equation (2) describes the influence of the pulling velocity on the expected rupture forces. To test whether our model is able to reproduce experimental data over a large range of pulling velocities, we used the velocity-dependent measurements of Evans and co-workers. To compare our model with these data, we performed a Monte Carlo simulation of ruptures at different velocities. For small distance intervals $dz=v \cdot dt$, where v is the pulling velocity and dt a small time interval, we calculated the rupture probability as $p_r = 1 - \exp(-k_{off}^F \cdot dz)$. Then, a random number n_{random} was generated. If $n_{random} > p_r$, the bond was broken and the rupture force saved, otherwise, the distance was incremented by dz. The off-rate under force k_{off}^F was defined as $k_{off}^F = k_{off}^0 \cdot \exp(\dfrac{F(z) \cdot x_b}{k_b T})$, with $F(z)$ as described by our model. This kind of simulations has been shown to accurately reproduce AFM data (37). $F(z)$ was calculated for each distance according to equation (2) with the viscoelastic parameters obtained from the fit to the single force-distance curve (Table II, data by Evans). The values for k_{off}^0 and x_b were taken from an earlier single-molecule AFM-study of isolated P-selectin by Fritz et al. (37) as $k_{off}^0 = 0.0022 s^{-1}$ and $x_b = 2.3 \text{ Å}$.

The simulation is in good agreement with the data of Evans et al. up to velocities of 50 μm/s, although our approach tends to underestimate the forces at low velocities (Figure 7) and at the very high velocity of 150 μm/s (data not shown). The failure of our model to reproduce the data at very high velocities is not surprising, since at these velocities different barriers may be probed, so that the kinetic parameters are not accurate any more (7,13,16,17). Still, it is encouraging that we can use data from isolated single molecules and the viscoelastic parameters obtained from a single force-distance curve on a cell to reasonably estimate the expected rupture forces of a given receptor/ligand pair on living cells over a range of velocities of over two orders of magnitude.

How do the viscoelastic parameters compare to other experiments? The range of measured parameters is large and spans orders of magnitude (for a recent review, see (38)). In general, the viscosity is recorded as μ_{eff}, which corresponds to the here recorded viscosity according to $\mu = 2 \cdot \pi \cdot \mu_{eff}$. The membranes of red blood cells have a significantly higher viscosity than the values observed here, in the range of $\mu_{eff}=34$pN·s/μm (39). Membrane surface viscosities for vesicles of lipid membranes are in the range of 0.001 pN·s/μm (40), while neuronal growth cones have been measured to have a viscosity $\mu_{eff}=0.137$pN·s/μm (19,20). For primary T-lymphocytes, a μ_{eff} of 1.6 pN·s/μm has been reported by Xu et al. (41). The viscosity obtained from the fit to Evans et al. data is in excellent agreement with the data by Xu et al.: 9.1 pN·s/μm corresponds to $\mu_{eff}=1.4$pN·s/μm. Our viscosity value measured for the integrin-bound membrane tethers on Jurkat cells of ~5-6 pN·s/μm ($\mu_{eff}=0.8$-1.0pN·s/μm) is lower than the value reported by Xu et al. and the value obtained from the fit to Evans data. Xu et al. and Evans et al. used the PSGL-1 receptor P-selectin on primary T-cells in a micropipette manipulation assay, whereas we used the VLA-4/VCAM-1 pair and Jurkat cells. These are cancerous cells, which are softer and have a less developed cytoskeleton, which might reduce the viscous slip of the membrane over the cytoskeleton (22). Experiments at lower ambient temperatures might also increase μ_{eff}, compared to our experiments performed at 36°C.

The stiffness of the tethers is described by k_t. This stiffness has been estimated before by Li et al. for outer hair cells (OHC) using optical tweezers (22). In these earlier studies, differences in the tether stiffness between tethers pulled from the lateral wall and tethers pulled from the basal end of OHC have been observed. The stiffness of the tethers was determined as 0.0037 pN/nm for the lateral wall and 0.0045 pN/nm for the basal end. These differences have been attributed to the higher cholesterol content of the membrane at the basal end compared to the lateral wall. These values are similar to the values of k_t=0.001–0.002pN/nm measured in our setup. The fit to Evans data yields a k_t of 0.008 pN/nm, slightly higher than the other values.

Stretching of the molecular connection between the cell and the cantilever as well as the deformations of the whole cell can influence the force distance relationship and therefore have an effect on the measured parameters. In our cell, the cell is attached to the cantilever via an antibody. The typical size of an antibody is on the order of a few nanometers, while the typical size of cells is on the order of micrometers. Hence, stretching the antibody will not significantly affect the measurement. The initial bending rigidity, on the other hand, will certainly contain contributions from the deformation of the whole cell. These contributions are well described by our model, demonstrated by the good agreement between data and fit.

Theoretical Analysis of the Force-Distance Relationship: the Compliance.

The mechanical compliance describes how much a system elongates under an applied force. It is important for the force absorption by the system and influences the distribution of rupture forces (7). To better understand the effect of the different parameters on the mechanical compliance, we isolated z in equation (2) and differentiated it to obtain the analytical expression:

$$c(f) = \frac{\partial z}{\partial f} = -\frac{g \cdot v}{k_i}\left(\frac{k_i \cdot LambertW(A)}{k_t \cdot g \cdot v \cdot (1 + LambertW(A))} - \frac{k_i}{k_t \cdot g \cdot v}\right) \qquad \text{(equation 3)},$$

with $A = \dfrac{k_i}{k_t} \cdot \exp\left(\dfrac{k_i \cdot (g \cdot v - f)}{k_t \cdot g \cdot v}\right)$. Hence, the knowledge of the viscoelastic parameters allows the calculation of the force-dependent compliance. Whereas k_t changes the compliance in the high-force regime, k_i changes the compliance in the low-force regime (Figure 8). The viscosity changes the transition point between these two regimes. This demonstrates that by altering the anchorage properties in a well-defined manner, the cell can fine-tune the mechanical response to high forces, the response to low forces and the transition between these two responses.

Theoretical Analysis of the Force-Distance Relationship: the Distribution of Rupture Forces.
The distribution of rupture forces is not only dependent on the energy landscape of the receptor ligand bond, but also on the elastic compliance of the linkage between receptor and the force-exerting environment (7). In cellular adhesion events, the cell itself constitutes this linkage. Therefore, changes in compliance caused by altered viscoelastic parameters should also influence the distribution of rupture forces. The distribution of rupture forces is given by (7):

$$p(f) = \frac{koff^F \cdot f_b}{v} \cdot c(f) \cdot \exp\left(-\int_0^f \frac{koff^F}{v} \cdot c(f') \cdot df'\right) \qquad \text{(equation 4)},$$

where $koff^F = koff^0 \cdot \exp(f/f_b)$ is the off-rate under force, $koff^0$ the basal off-rate, $f_b = \dfrac{k_b T}{\gamma}$ the characteristic force of the bond and γ the potential width. Thus, with the compliance described by equation (3), the effect of the viscoelastic parameters on the distribution of rupture forces can be gauged. Equation (4) cannot be solved analytically, when using the compliance described by equation (3). Hence, we calculated the distribution numerically for different values of k_i, k_t and μ. At a given affinity state, the viscosity of the membrane sets the force scale of the rupture and modulates very effectively the most probable rupture force (Figure 9). At a given viscosity, both k_i and k_t can fine-tune the distribution of rupture forces and thus the adhesiveness of the cell.

Biological Implications.

One of the features of our force curves is the long plateau of equal force before the rupture. Similar force plateaus preceding the tether rupture have been observed before (12,18,22,42,43). Still, the shape of the reported force curves differs between different cells, different receptors and pulling speeds. Hence, although the Kelvin body is a good model for the here investigated T-cells, it might not be appropriate for other cell types or experimental setups. In particular, a strong initial tether formation force ranging from ~100 pN to 500 pN has been observed for adherent cells like OHC cells, before the force drops to the plateau value (22). For OHC, the plateau value of ~100 pN is significantly higher than the here observed 20-25 pN, demonstrating that the tether force is strongly correlated to the overall architecture of the cell. Therefore, an in-depth analysis of the force curves leading to membrane tethers will give insight into different cellular architectures.

Many other models have successfully been employed to analyze the deformability of cells (for a review, see (38)). The advantage of the Kelvin body is its simplicity. As shown above, it is the simplest linear solid capable of describing the observed force-distance relationship. This does not imply that other models, treating for instance the cell as liquid drop, may not also be applicable.

When analyzing the force curves with our model, the shape of the force curve characterizes the viscoelastic parameters of the membrane in close vicinity to the probed receptor. Hence, the receptor serves as a nano-probe of its membrane environment. The gathered data thus offer the unique possibility to analyze changes in the receptor anchorage. This is particularly interesting for adhesive cellular receptors like integrins, which dynamically change their mode of anchorage depending on their phosphorylation states as well as on specific associations with cytoskeleton adaptor molecules (44). Future studies on the physiological activation of integrins with chemokines will use the here-described analysis to gain better insight into the involved processes. It has been observed that the attachment of membrane components to the cytoskeleton has a significant impact on the rupture forces (45-47). Hence, the effects of physiological activation involving cytoskeletal attachment are expected to be much stronger than the subtle effect observed here.

The integrin VLA-4 is involved both in rolling as well as in firm arrest (8). These divers tasks are associated with different affinity states of the integrin. Our results indicate that the slow-down can additionally be maintained by changes in the compliance of the receptor's cellular anchorage. Changing the compliance of the system has the same influence on the distribution of rupture forces and therefore on the adhesiveness of cells as has changing the off-rate (equation 4).

Hence, modulating the stiffness of the receptor-environment either intra-cellularly or extra-cellularly can be used as a regulator of cell-adhesion or of force-based signalling. Different lines of evidence suggest that this additional level of regulation is indeed utilized by cells. It has recently been shown that the mechanical properties of the extracellular matrix influence the development of stem cells (48). In addition, it has been reported that the extracellular matrix stiffness is a crucial factor for the migration of tumor cells (49). Furthermore, a paradigm in integrin signalling states that chemoattractants lead to a cytoskeletal attachment of the integrins (6). This will certainly lead to a lowered compliance and hence to increased rupture forces, even in the absence of further conformational changes. Furthermore, integrins are re-distributed to lipid rafts after activation of the cell (27). Lipid rafts have altered membrane properties, expressed for example in a higher viscosity (50). As shown here, this redistribution alone will influence the integrin-mediated adhesiveness of the cell. These arguments corroborate that the mechanical compliance of the membrane or the extracellular matrix is indeed a factor in cellular behaviour, and that it is actively modulated in addition to the affinity state of the receptor ligand bonds.

Conclusions

Not only the technical innovations in single-molecule force measurements, but also the increased understanding of the physical background leading to the observed force-distance curves have greatly advanced our understanding of the material properties of single molecules (51). Refined theoretical models have helped to interpret the complex data obtained from these measurements (52-56). For single-molecule studies of isolated molecules, models like the worm-like chain model or the freely-rotated chain model have enabled the field to analyze not only the rupture forces, but also the history of force evolution in order to obtain interesting parameters like the persistence length of single molecules (7,17,57,58). For cells, these models have been lacking. Our presented data show that a Kelvin body based model is well suited to interpret single-molecule measurements on living cells. With such a model, we can not only describe the observed force-distance relationship, but also obtain a tool to possibly scrutinize cellular receptors from the outside for intra-cellular changes in the anchorage of these receptors. Hence, the here introduced interpretation of single-molecule force measurements can help to thoroughly analyze the bio-mechanics of cellular activation events.

References

1. Xiao, T., J. Takagi, B. S. Coller, J. H. Wang, and T. A. Springer. 2004. *Structural basis for allostery in integrins and binding to fibrinogen-mimetic therapeutics. Nature 432:59-67.*

2. Xiong, J. P., T. Stehle, B. Diefenbach, R. Zhang, R. Dunker, D. L. Scott, A. Joachimiak, S. L. Goodman, and M. A. Arnaout. 2001. *Crystal structure of the extracellular segment of integrin alpha Vbeta3. Science 294:339-345.*

3. van Kooyk, Y. and C. G. Figdor. 2000. *Avidity regulation of integrins: the driving force in leukocyte adhesion. Curr Opin Cell Biol 12:542-547.*

4. Grabovsky, V., S. Feigelson, C. Chen, D. A. Bleijs, A. Peled, G. Cinamon, F. Baleux, F. Arenzana-Seisdedos, T. Lapidot, Y. van Kooyk, R. R. Lobb, and R. Alon. 2000. *Subsecond induction of alpha4 integrin clustering by immobilized chemokines stimulates leukocyte tethering and rolling on endothelial vascular cell adhesion molecule 1 under flow conditions. J Exp Med 192:495-506.*

5. Gottschalk, K. E. and H. Kessler. 2004. *A computational model of transmembrane integrin clustering. Structure 12:1109-1116.*

6. Alon, R. and M. L. Dustin. 2007. *Force as a facilitator of integrin conformational changes during leukocyte arrest on blood vessels and antigen-presenting cells. Immunity 26:17-27.*

7. Evans, E. and K. Ritchie. 1999. *Strength of a weak bond connecting flexible polymer chains. Biophys J 76:2439-2447.*

8. Alon, R., S. W. Feigelson, E. Manevich, D. M. Rose, J. Schmitz, D. R. Overby, E. Winter, V. Grabovsky, V. Shinder, B. D. Matthews, M. Sokolovsky-Eisenberg, D. E. Ingber, M. Benoit, and M. H. Ginsberg. 2005. *Alpha4beta1-dependent adhesion strengthening under mechanical strain is regulated by paxillin association with the alpha4-cytoplasmic domain. J Cell Biol 171:1073-1084.*

9. Benoit, M., D. Gabriel, G. Gerisch, and H. E. Gaub. 2000. *Discrete interactions in cell adhesion measured by single-molecule force spectroscopy. Nat Cell Biol 2:313-317.*

10. Benoit, M. and H. E. Gaub. 2002. *Measuring cell adhesion forces with the atomic force microscope at the molecular level. Cells Tissues Organs 172:174-189.*

11. Eibl, R. H. and V. T. Moy. 2005. *Atomic force microscopy measurements of protein-ligand interactions on living cells. Methods Mol Biol 305:439-450.*

12. Sun, M., J. S. Graham, B. Hegedus, F. Marga, Y. Zhang, G. Forgacs, and M. Grandbois. 2005. *Multiple membrane tethers probed by atomic force microscopy. Biophys J 89:4320-4329.*

13. Li, F., S. D. Redick, H. P. Erickson, and V. T. Moy. 2003. Force measurements of the alpha5beta1 integrin-fibronectin interaction. Biophys J 84:1252-1262.

14. Grandbois, M., W. Dettmann, M. Benoit, and H. E. Gaub. 2000. Affinity imaging of red blood cells using an atomic force microscope. J Histochem Cytochem 48:719-724.

15. Zhang, X., A. Chen, D. De Leon, H. Li, E. Noiri, V. T. Moy, and M. S. Goligorsky. 2004. Atomic force microscopy measurement of leukocyte-endothelial interaction. Am J Physiol Heart Circ Physiol 286:H359-367.

16. Zhang, X., S. E. Craig, H. Kirby, M. J. Humphries, and V. T. Moy. 2004. Molecular basis for the dynamic strength of the integrin alpha4beta1/VCAM-1 interaction. Biophys J 87:3470-3478.

17. Evans, E. and K. Ritchie. 1997. Dynamic strength of molecular adhesion bonds. Biophys J 72:1541-1555.

18. Evans, E., V. Heinrich, A. Leung, and K. Kinoshita. 2005. Nano- to microscale dynamics of P-selectin detachment from leukocyte interfaces. I. Membrane separation from the cytoskeleton. Biophys J 88:2288-2298.

19. Hochmuth, F. M., J. Y. Shao, J. Dai, and M. P. Sheetz. 1996. Deformation and flow of membrane into tethers extracted from neuronal growth cones. Biophys J 70:358-369.

20. Shao, J. Y. and R. M. Hochmuth. 1996. Micropipette suction for measuring piconewton forces of adhesion and tether formation from neutrophil membranes. Biophys J 71:2892-2901.

21. Shao, J. Y., H. P. Ting-Beall, and R. M. Hochmuth. 1998. Static and dynamic lengths of neutrophil microvilli. Proc Natl Acad Sci U S A 95:6797-6802.

22. Li, Z., B. Anvari, M. Takashima, P. Brecht, J. H. Torres, and W. E. Brownell. 2002. Membrane tether formation from outer hair cells with optical tweezers. Biophys J 82:1386-1395.

23. Barakat, A. I. 2001. A model for shear stress-induced deformation of a flow sensor on the surface of vascular endothelial cells. J Theor Biol 210:221-236.

24. Bausch, A. R., F. Ziemann, A. A. Boulbitch, K. Jacobson, and E. Sackmann. 1998. Local measurements of viscoelastic parameters of adherent cell surfaces by magnetic bead microrheometry. Biophys J 75:2038-2049.

25. Fung, Y. C. 1993. Biomechanics; Mechanical Properties of Living Tissues. New York: Springer.

26. Spillmann, C., D. Osorio, and R. Waugh. 2002. Integrin activation by divalent ions affects neutrophil homotypic adhesion. Ann Biomed Eng 30:1002-1011.

27. Leitinger, B. and N. Hogg. 2002. *The involvement of lipid rafts in the regulation of integrin function. J Cell Sci 115:963-972.*

28. Shirakawa, J., Y. Wang, S. Tahara-Hanaoka, S. Honda, K. Shibuya, and A. Shibuya. 2006. *LFA-1-dependent lipid raft recruitment of DNAM-1 (CD226) in CD4+ T cell. Int Immunol 18:951-957.*

29. Marwali, M. R., J. Rey-Ladino, L. Dreolini, D. Shaw, and F. Takei. 2003. *Membrane cholesterol regulates LFA-1 function and lipid raft heterogeneity. Blood 102:215-222.*

30. Wojcikiewicz, E. P., X. Zhang, and V. T. Moy. 2004. *Force and Compliance Measurements on Living Cells Using Atomic Force Microscopy (AFM). Biol Proced Online 6:1-9.*

31. Florin, E. L. R., M.; Lehmann, H.; Ludwig, M.; Dornmair, C.; Moy, V.,T.; Gaub, H.-E. 1995. *Sensing specific molecular interactions with the atomic force microscope. Biosensors and Bioelectronics 10:895-901.*

32. Butt, H.-J., Jaschke, M. 1995. *Calculation of thermal noise in atomic force spectroscopy. Nanotechnology 6:1-7.*

33. Kunkel, E. J., J. L. Dunne, and K. Ley. 2000. *Leukocyte arrest during cytokine-dependent inflammation in vivo. J Immunol 164:3301-3308.*

34. Chen, C., J. L. Mobley, O. Dwir, F. Shimron, V. Grabovsky, R. R. Lobb, Y. Shimizu, and R. Alon. 1999. *High affinity very late antigen-4 subsets expressed on T cells are mandatory for spontaneous adhesion strengthening but not for rolling on VCAM-1 in shear flow. J Immunol 162:1084-1095.*

35. Hosu, B. G., M. Sun, F. Marga, M. Grandbois, and G. Forgacs. 2007. *Eukaryotic membrane tethers revisited using magnetic tweezers. Phys Biol 4:67-78.*

36. Bruehl, R. E., T. A. Springer, and D. F. Bainton. 1996. *Quantitation of L-selectin distribution on human leukocyte microvilli by immunogold labeling and electron microscopy. J Histochem Cytochem 44:835-844.*

37. Fritz, J., A. G. Katopodis, F. Kolbinger, and D. Anselmetti. 1998. *Force-mediated kinetics of single P-selectin/ligand complexes observed by atomic force microscopy. Proc Natl Acad Sci U S A 95:12283-12288.*

38. Lim, C. T., E. H. Zhou, and S. T. Quek. 2006. *Mechanical models for living cells--a review. J Biomech 39:195-216.*

39. Hwang, W. C. and R. E. Waugh. 1997. *Energy of dissociation of lipid bilayer from the membrane skeleton of red blood cells. Biophys J 72:2669-2678.*

40. *Evans, E. A. and R. M. Hochmuth. 1976. Membrane viscoelasticity. Biophys J 16:1-11.*

41. *Xu, G. and J. Y. Shao. 2005. Double tether extraction from human neutrophils and its comparison with CD4+ T-lymphocytes. Biophys J 88:661-669.*

42. *Heinrich, V., A. Leung, and E. Evans. 2005. Nano- to microscale dynamics of P-selectin detachment from leukocyte interfaces. II. Tether flow terminated by P-selectin dissociation from PSGL-1. Biophys J 88:2299-2308.*

43. *King, M. R., V. Heinrich, E. Evans, and D. A. Hammer. 2005. Nano-to-micro scale dynamics of P-selectin detachment from leukocyte interfaces. III. Numerical simulation of tethering under flow. Biophys J 88:1676-1683.*

44. *Liu, S., D. A. Calderwood, and M. H. Ginsberg. 2000. Integrin cytoplasmic domain-binding proteins. J Cell Sci 113 (Pt 20):3563-3571.*

45. *Thie, M., R. Rospel, W. Dettmann, M. Benoit, M. Ludwig, H. E. Gaub, and H. W. Denker. 1998. Interactions between trophoblast and uterine epithelium: monitoring of adhesive forces. Hum Reprod 13:3211-3219.*

46. *Afrin, R., H. Arakawa, T. Osada, and A. Ikai. 2003. Extraction of membrane proteins from a living cell surface using the atomic force microscope and covalent crosslinkers. Cell Biochem Biophys 39:101-117.*

47. *Afrin, R. and A. Ikai. 2006. Force profiles of protein pulling with or without cytoskeletal links studied by AFM. Biochem Biophys Res Commun 348:238-244.*

48. *Engler, A. J., S. Sen, H. L. Sweeney, and D. E. Discher. 2006. Matrix elasticity directs stem cell lineage specification. Cell 126:677-689.*

49. *Zaman, M. H., L. M. Trapani, A. L. Sieminski, D. Mackellar, H. Gong, R. D. Kamm, A. Wells, D. A. Lauffenburger, and P. Matsudaira. 2006. Migration of tumor cells in 3D matrices is governed by matrix stiffness along with cell-matrix adhesion and proteolysis. Proc Natl Acad Sci U S A 103:10889-10894.*

50. *Niemela, P. S., S. Ollila, M. T. Hyvonen, M. Karttunen, and I. Vattulainen. 2007. Assessing the nature of lipid raft membranes. PLoS Comput Biol 3:e34.*

51. *Hugel, T., M. Rief, M. Seitz, H. E. Gaub, and R. R. Netz. 2005. Highly stretched single polymers: atomic-force-microscope experiments versus ab-initio theory. Phys Rev Lett 94:048301.*

52. *Kessler, M., K. E. Gottschalk, H. Janovjak, D. J. Muller, and H. E. Gaub. 2006. Bacteriorhodopsin folds into the membrane against an external force. J Mol Biol 357:644-654.*

53. *Neuert, G., C. H. Albrecht, and H. E. Gaub. 2007. Predicting the rupture probabilities of molecular bonds in series. Biophys J 93:1215-1223.*

54. *Neuert, G., C. Albrecht, E. Pamir, and H. E. Gaub. 2006. Dynamic force spectroscopy of the digoxigenin-antibody complex. FEBS Lett 580:505-509.*

55. *Rief, M., F. Oesterhelt, B. Heymann, and H. E. Gaub. 1997. Single Molecule Force Spectroscopy on Polysaccharides by Atomic Force Microscopy. Science 275:1295-1297.*

56. *Clausen-Schaumann, H., M. Rief, C. Tolksdorf, and H. E. Gaub. 2000. Mechanical stability of single DNA molecules. Biophys J 78:1997-2007.*

57. *Round, A. N., M. Berry, T. J. McMaster, S. Stoll, D. Gowers, A. P. Corfield, and M. J. Miles. 2002. Heterogeneity and persistence length in human ocular mucins. Biophys J 83:1661-1670.*

58. *Evans, E. 2001. Probing the relation between force--lifetime--and chemistry in single molecular bonds. Annu Rev Biophys Biomol Struct 30:105-128.*

Tables

Table I: *Number of cells and force curves analyzed.*

	Number of cells	Total number of curves	Number of adhesions	Adhesion rate	Number of fitted curves
1mM Ca^{2+}/Mg^{2+}	8	749	195	26%	172
5mM Mg^{2+}	8	778	303	39%	278
BSA	4	170	7	4%	-
BIO1211	7	380	30	8%	-

Table II: *Median of the fit parameters to our data and to data by Evans et al.*

	Median of Resting Integrins on Jurkat			Median of Activated Integrins on Jurkat			P-selectin on primary T-cells (force-distance curves by Evans et al. (42))	
	l>300 nm	l>600 nm	l>800 nm	l>300 nm	l>600 nm	l>800 nm	- Latrunculin	+Latrunculin
μ [μN·s/m]	6.0	5.9	5.8	6.1	6.0	6.1	9.9	4.6
k_i [μN/m]	320	260	260	210	190	180	190	51
k_t [μN/m]	1.5	1.6	1.9	0.9	0.9	0.8	8.0	3.0

Figure Captions

Figure 1: *Experimental Setup*. The cell is pushed onto a surface and then retracted **(a)**. The force-distance curve is recorded with piconewton precision. **b)** A typical series of subsequent force curves is shown. A Jurkat cell immobilized on the cantilever was retracted from a VCAM-1 coated surface after 100ms contacts at an indentation force of 50 pN.
The right tail (up to 15 μm, cut at 4 μm here) of the curves was used to correct for drift and to determine the zero-force-level. For the tether model, only ruptures with tether lengths > 300 nm were taken.
From top to bottom:
double rupture (evaluated as adhesion);
short rupture (evaluated as adhesion);
double rupture (evaluated as adhesion);
no ruptures (evaluated as no adhesion);
single rupture (evaluated as adhesion and for the tether model);
no ruptures (evaluated as no adhesion),;
single rupture (evaluated as adhesion and for the tether model);
Seven no-adhesion force curves between the first three curves are omitted in the graph.
Two regimes with different slopes are especially recognized in the tether rupture (dashed lines).

Figure 2. a) *Mechanical model for cells*. The Kelvin body consists of a spring with spring constant k_t representing the tether stiffness, and parallel to this spring a series of a second spring with spring constant k_i representing the bending rigidity of the membrane and a dashpot with viscosity μ. The Voigt and the Maxwell body are simplifications of the Kelvin body. **b)** *Fit to a typical force curve*. Shown are the fits of the different models to a typical force curve.

Figure 3. *Specificity of Adhesion*. While surfaces functionalized with VCAM-1 have adhesion rates of $\geq$ 25%, the unspecific adhesion either after blocking or at surfaces functionalized only with BSA is $\leq$ 8%, demonstrating the specificity of the measured interactions. Mg^{2+} was not added when blocking with BIO1211.

Figure 4. *The distributions of the viscoelastic parameters*. Boxplots of the distributions together with the median of the respective parameter are shown. The p-value describes the probability that the distributions are identical in both setups. It has been calculated using the Mann-Whitney test. A) The distributions of the viscosity are shown for different length-cut-offs. No clear distance dependent trend is detected. B) Cut-off distance dependent distributions of the tether rigidity. Although the values do not change over cut-off distance, the significance of the difference becomes higher despite fewer ruptures. This indicates that for longer rupture lengths, the tether rigidity becomes better defined. C) Distance dependency of the initial bending rigidity. This value describes the elastic response of the membrane at the initial bending. For longer ruptures, this bending rigidity seems to decrease. D) Comparison of the bending rigidity (see lower left) and cellular stiffness. The cellular stiffness was determined by the slope of the force distance curves at region with F<0pN. In this region, the cell is compressed and works against the cantilever, depending on the stiffness of the cell. This is related to the cortex tension. E) The relation of cell-stiffness with the initial bending rigidity is shown. A weak dependency with a

correlation coefficient of R~0.4 for resting integrins and R~0.2 for Mg-activated integrins is observed.

Figure 5. *Cell-to-cell variations*. To test the cell-to-cell variations, the median was also determined for each individual cell. The boxplots show the distributions of the medians of the single cells for tethers longer than 300 μm. The initial bending rigidity is significantly different (p-value<0.05; Mann-Whitney test).

Figure 6. *Comparison of measured and simulated force distributions*. From the experimentally obtained distribution of rupture lengths, we calculated the distribution of rupture forces using the obtained viscoelastic parameters. The simulated distributions (red) are in good agreement with the experimental distributions (grey bars) under both conditions, for resting **(a)** and Mg^{2+}-activated **(b)** integrins.

Figure 7. *Fit to data by Evans et al*. **a)** Equation (2) was fitted to data by Evans et al. under two conditions, with and without Latrunculin A. **b)** The dependence of the rupture forces on the pulling velocity obtained from the experiment (red) and from a Monte-Carlo simulation with our model (black) is shown.

Figure 8. *Influence of the viscoelastic parameters on the mechanical compliance*. Clearly, two regimes are seen. The transition between the two regimes is sharp. The viscosity of the membrane determines the point of transition. The high-force regime is dominated by k_t, the low-force regime by k_i.

Figure 9. *Influence of viscoelastic parameters on distribution of rupture forces*. The distribution of rupture forces was calculated numerically according to equation (4). For a given affinity state, the force scale is set by the viscosity. At a given viscosity, both k_i and k_t can fine-tune the force resistance of the bond. The overall range in forces that can be achieved by changing the viscoelastic parameters is in the same range as caused by changes in the affinity state (k_{off}).
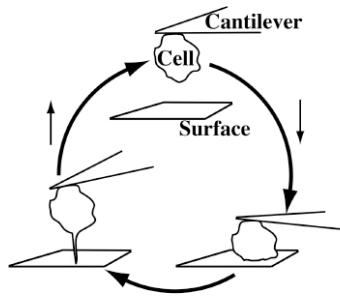
A   B

Figure 1

A

Figure 2

21

Adesion Rate
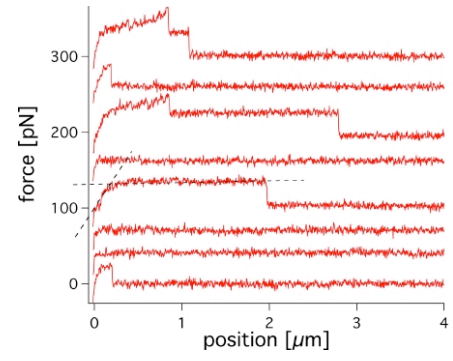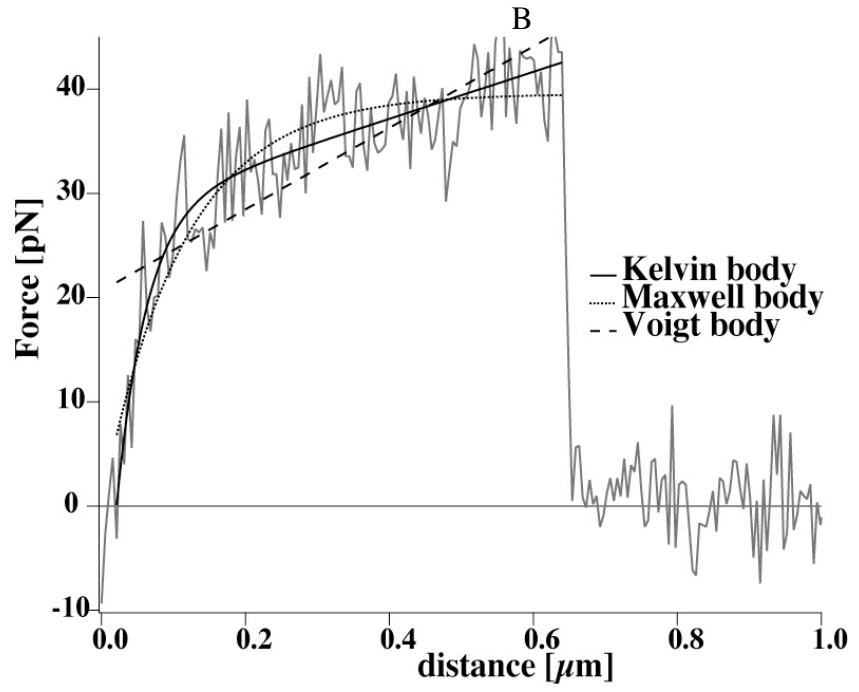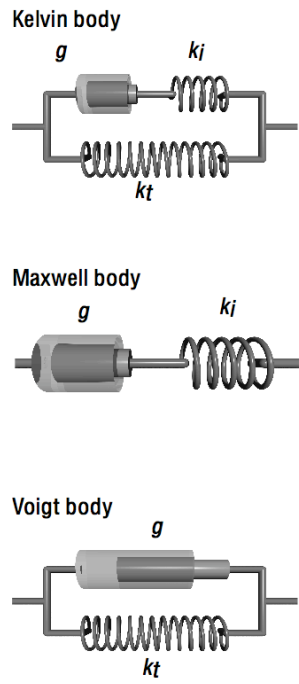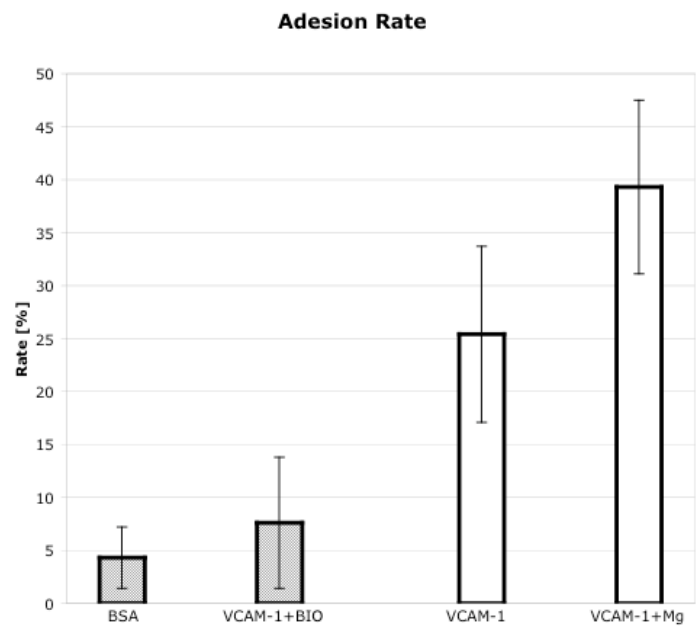
Figure 3

A
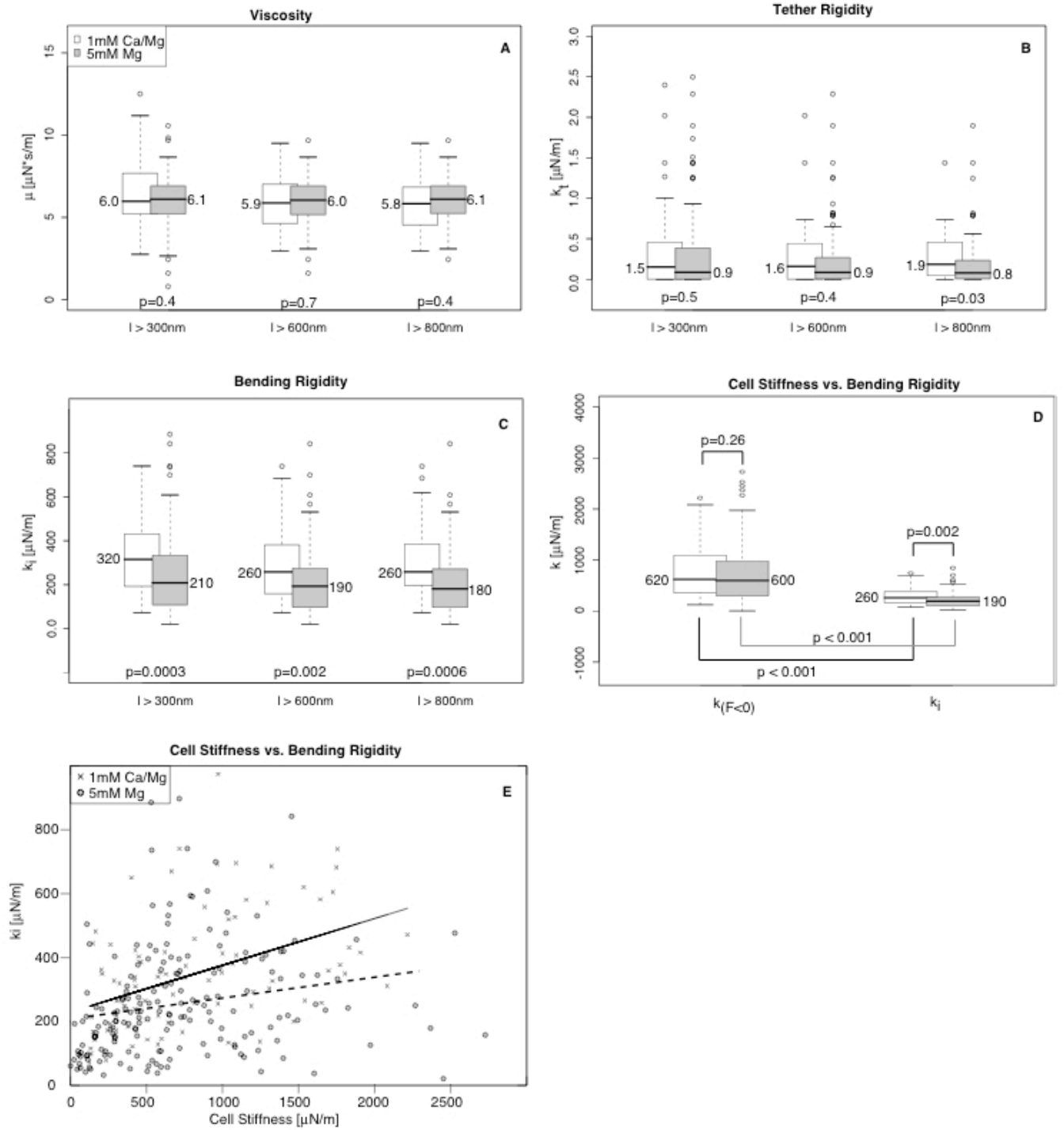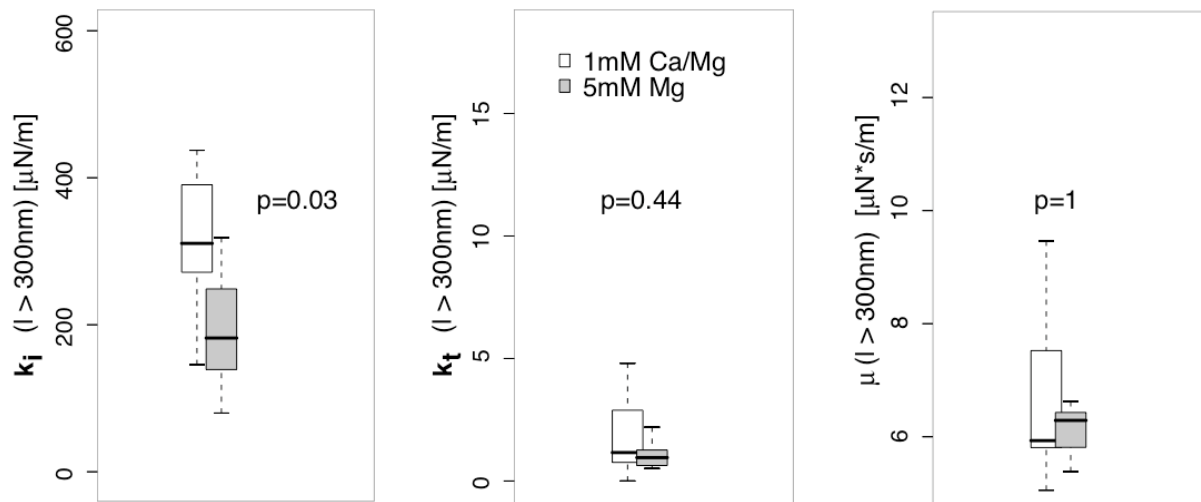
Figure 4

Figure 5

A
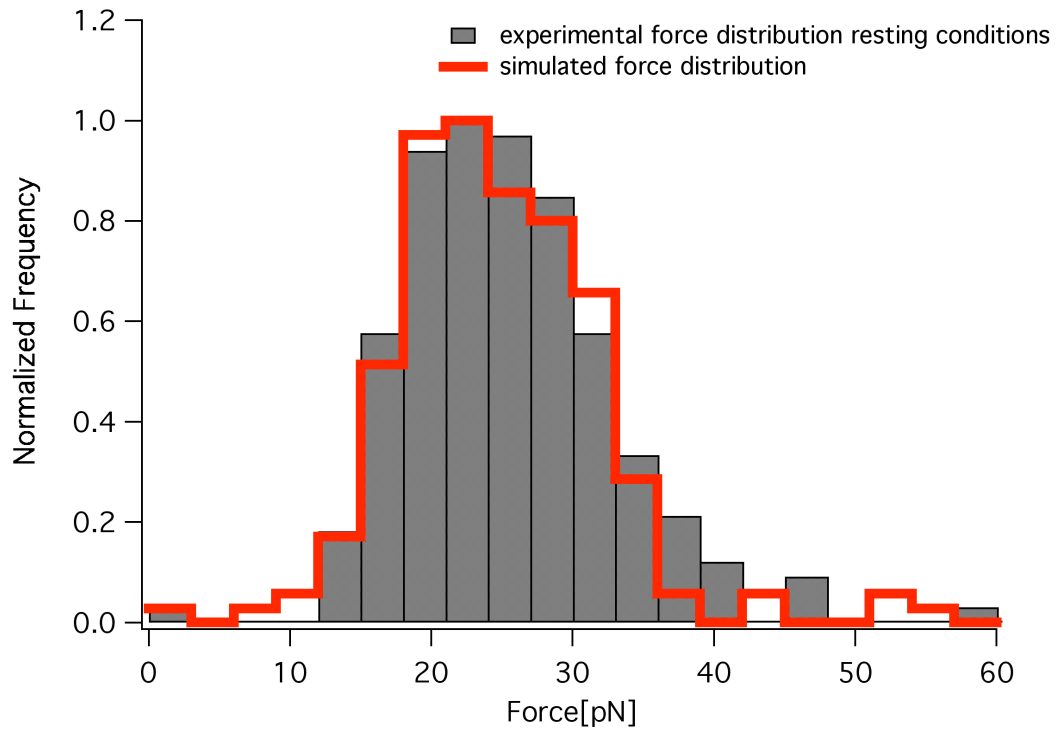
B
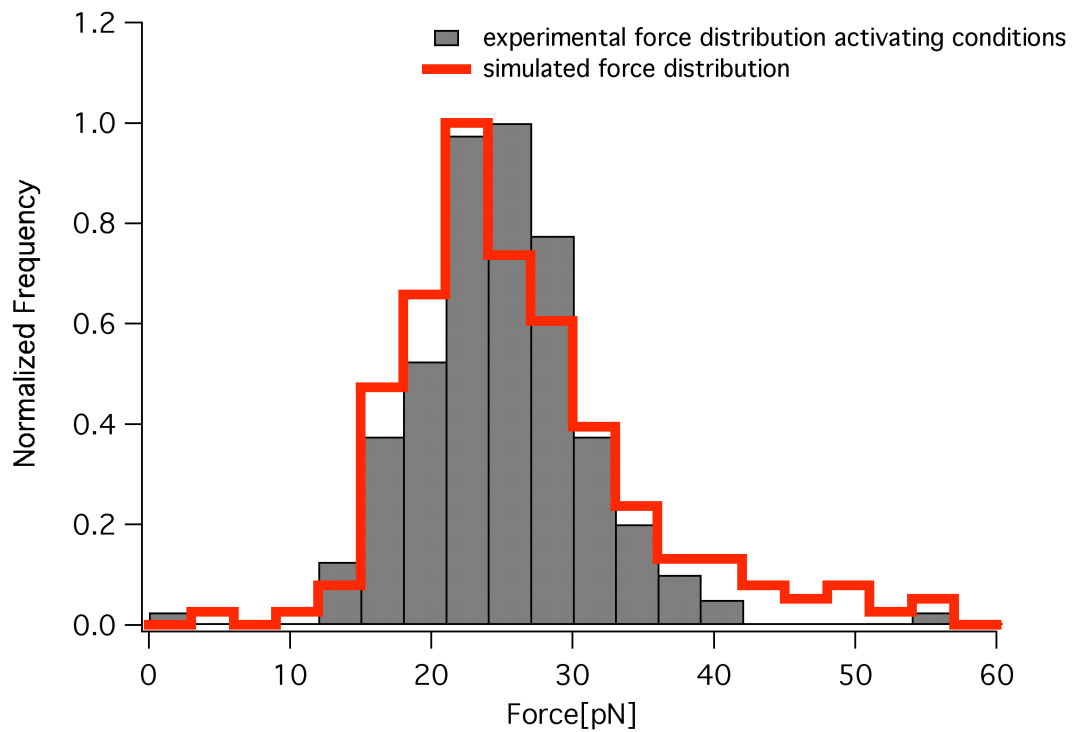
Figure 6

A

B

Figure 7

26
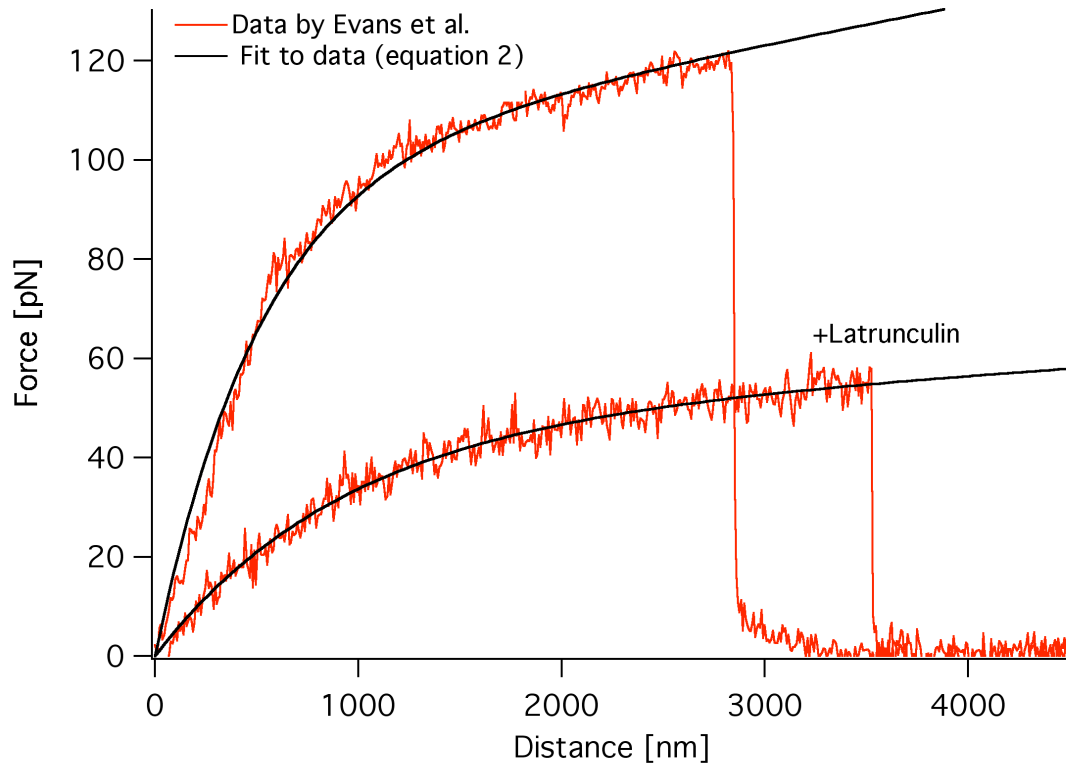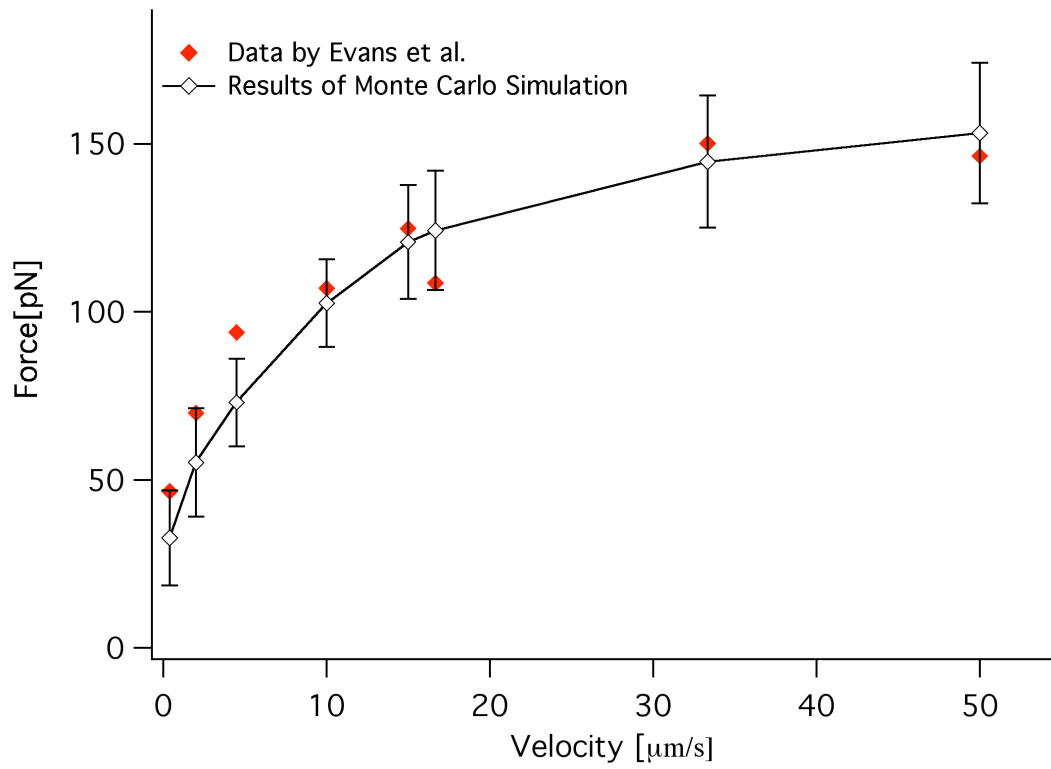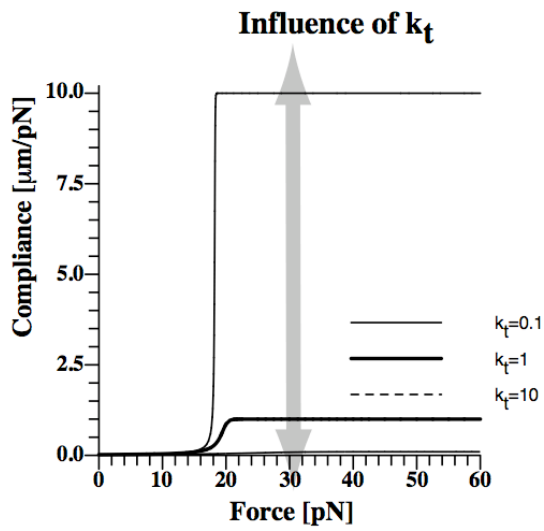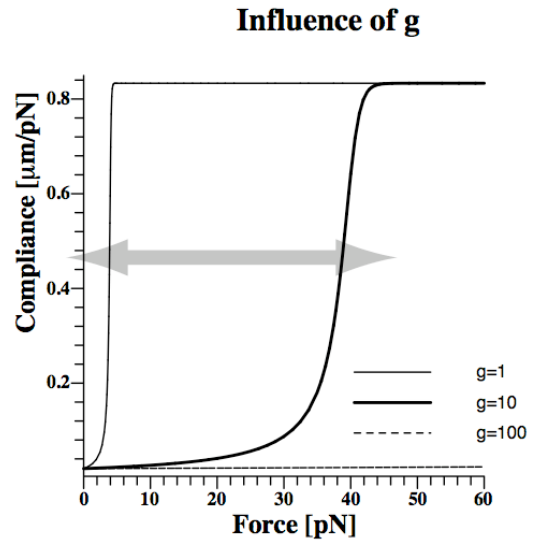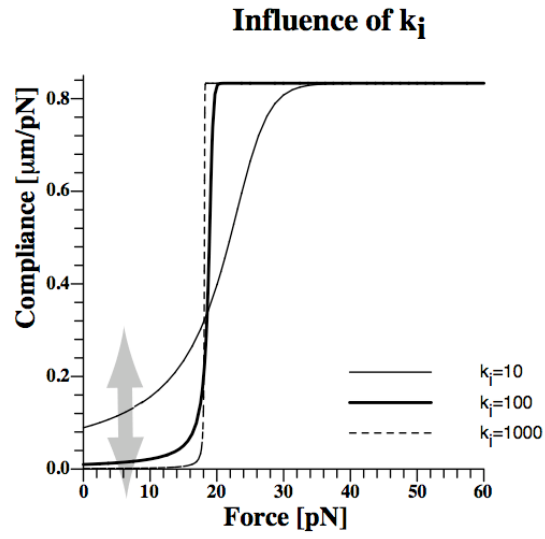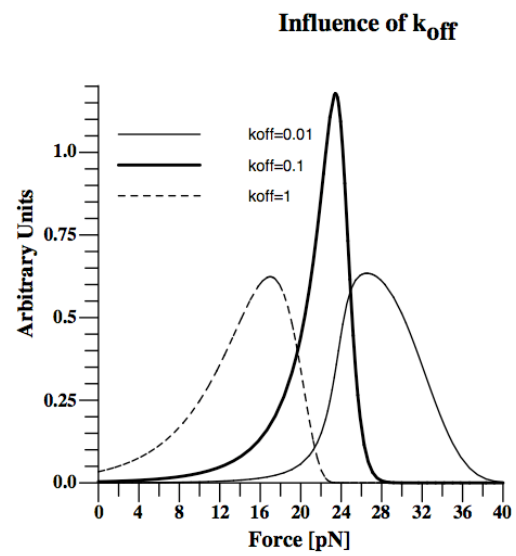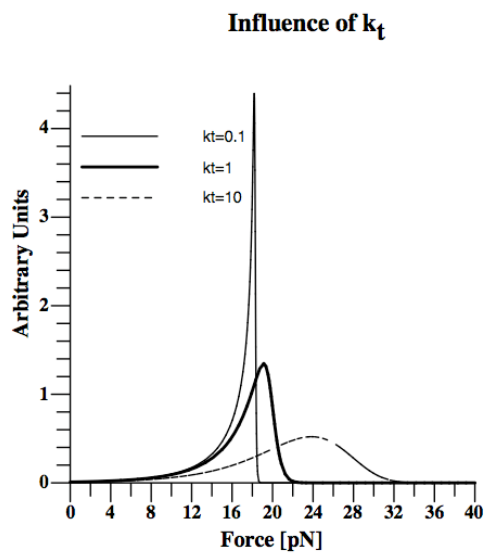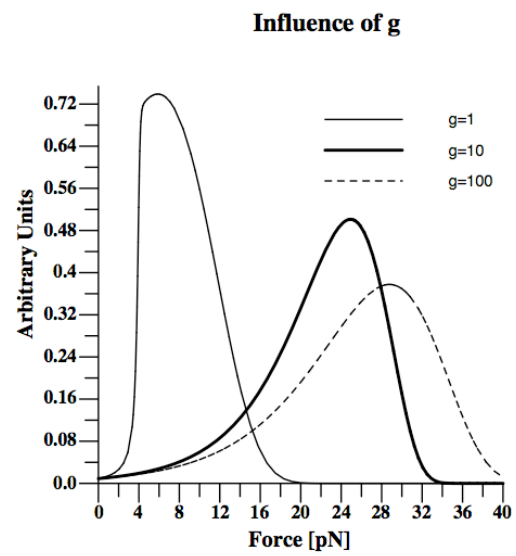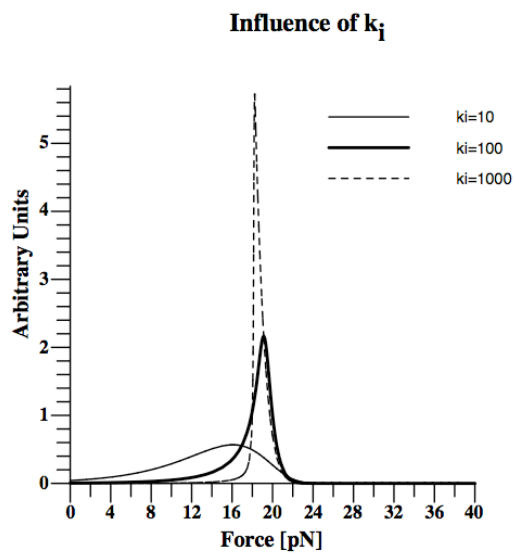
Figure 8

Figure 9

Mechanical Regulation of Cell Adhesion

Julia Schmitz

Kay-Eberhard Gottschalk*

Applied Physics, LMU München, Amalienstr. 54, 80799 München, Germany

Cellular adhesion against external forces is governed by both the equilibrium affinity of the involved receptor-ligand bonds and the mechanics of the cell. Certain receptors like integrins change their affinity as well as the mechanics of their anchorage to tune the adhesiveness. Whereas in the last few years the focus of integrin research has lied on the affinity regulation of the adhesion receptors, more recently the importance of cellular mechanics became apparent. Here, we focus on different aspects of the mechanical regulation of the cellular adhesiveness.

1 Introduction

Cellular adhesion is a crucial step in inflammation, migration and other multi-cellular events. Adhesion is modulated in different ways by chemical stimuli like chemokines, by external forces, and by the geometry and the rigidity of the substrate [1–6]. Epithelial cells are constitutively adhesive and induce apoptosis if detached from adhesive substrates. Blood cells in contrast must not randomly stick to surfaces or other cells. Though, both cell types can actively regulate their adhesiveness according to the situation. Lymphocytes are a cell type, that shows an intriguingly complex variety of different adhesive states. In a resting state, they circulate freely in the blood stream. From time to time they randomly contact the endothelium. The lymphocytes can then start rolling along the vessel walls resisting the force of the blood stream. During rolling, they investigate the surface of the endothelial cells for signalling molecules. At sites of inflammation, chemokines expressed on the surface of the endothelial cells are presented to the lymphocytes [7]. These signal molecules activate the lymphocytes, so that they stop and adhere firmly to the endothelium [8, 9]. Now, the cells extravasate to the injured or inflamed tissue [10]. Rolling and firm adhesion involves a variety of proteins from both the selectin and integrin families [11–14]. This complex process has different requirements in affinity and force persistance. Rolling, for instance, requires a fast bond formation and an equally fast bond breakage, whereas firm adhesion requires low off-rates and the persistance against the strong shear forces of the blood stream. Hence, the cell needs a way to regulate both the affinity and the persistance to external forces [15].

The affinity describes the equilibrium binding properties of a single receptor molecule to a specific ligand. The kinetic properties of the receptor-ligand bond are defined by the on-rate and the off-rate, which can be regulated separately. The affinity can change after a conformational rearrangement of the receptor, mostly located in the ligand binding pocket [16–19]. The avidity, in contrast, describes the overall cellular adhesiveness [16, 20], which not only depends on the single molecule properties. A raise in avidity

---

*Corresponding author. kay.gottschalk@physik.uni-muenchen.de

might be due to receptor clustering [5, 6, 21, 22], thereby changing the valency of the interaction. Other possibilities to influence avidity are the receptor redistribution via lateral diffusion to the site of adhesion or the enhanced expression of the receptor on the cell surface. Furthermore, a reservoir of binding-incompetent receptors can be rendered binding competent [23]. The coexistence of the same receptor in different states and of different receptors with concerted adhesive properties is regulated in a dynamic equilibrium and might have synergistic effects on the cell adhesion.

2 Adhesion Molecules

A variety of adhesion molecules is involved in the different steps of cellular adhesion events [11, 12, 14]. The most prominent classes of adhesion molecules are selectins, integrins and cadherins. These molecules have specialized functions and fine-tuned properties to meet the mechanical and kinetic demands of regulated adhesion. For instance, selectins and integrins play both important roles in the extravasation of lymphocytes. Conceptually, lymphocyte adhesion can be divided into fast rolling, slow rolling and firm adhesion [14]. Often, these steps are consecutive. For each of these steps, different kinetics and different responses to force are needed. The adhesion molecules are adapted to the different demands of rolling or firm adhesion. The kinetics as well as the response to external forces is governed by the energy-landscape of the receptor-ligand bond (Figure 1). This energy landscape determines the bond formation and bond breakage. Bond breakage can be described as a thermally activated escape from a well in this complex landscape under overdamped conditions [24]. At equilibrium conditions, the system chooses with high probability a trajectory with a low energy barrier. An externally applied force reduces the available phase space and can change the trajectory. Therefore, different barriers may be crossed under the influence of force [25, 26].

For simplification, the complex energy landscape is commonly reduced to a projection along a reaction coordinate (Figure 1). This simplified energy landscape contains only the major barriers and is described by the distance of each barrier to the ground state (the potential width x_β) and by the height of the barrier [27]. The barrier height is directly related to the equilibrium off-rate of the bond. While x_β does not influence the equilibrium affinity, it determines the response of the bond to forces (discussed in greater detail in section 3). Caused by external forces, the energy landscape tilts (Fig. 1). The transition barrier of a potential landscape with a small potential width is less reduced by external forces than the barrier of a wide potential landscape (Figure 1) [28–30]. In a complex energy landscape, inner small barriers might become rate-determining in the presence of forces. Since adhesion molecules resist external forces, the adhesion strength is determined by both the equilibrium off-rate and the potential width of the involved adhesion molecules. What is the task of the major adhesion molecules, and how do the kinetic parameters reflect these tasks?

Three types of selectins support lymphocyte rolling: E-selectin, L-selectin and P-selectin. Lymphocyte rolling over the endothelium needs a fast bond formation at the leading front of the lymphocyte, and an equally fast bond breakage at the rear end of the cell. The selectins meet this demand with high on- and off-rates (Table 1) [31, 32]. Furthermore, the potential widths are exceptionally short. This implicates that the bond is only marginally susceptible to external forces. Hence, selectins are ideally suited for their task: they form bonds very quickly; these bonds can resist strong forces; yet, the bonds open up fast. All these features enable rolling in the presence of even very strong forces. Strikingly, the parameters appear to be dependent on the experimental setup. Only under shear forces, the unusually short potential width is noticable. Under vertically applied forces, selectins display values similar to other molecules [26, 33–35] (Table 1). Thus, the geometry of force application apparently is an important factor in determining the bond strength under force. This is plausible from an energetic point of view: different force vectors will enforce different trajectories through the energy

2

landscape (Figure 1) and therefore alter the observed properties of the receptor-ligand bond. These differences might also be caused by multiple, cooperative interactions in the shear force setup [35]. Interestingly, P-selectins and L-selections do not support adhesion in the absence of external forces [36, 37]. Starting from these observations, it has been postulated that under certain conditions, the bond strength of selectins to their ligand actually increases under the influence of external forces. This is the hallmark of a so-called catch bond [38]. Interestingly, P-selectins switch the pathway through the energy-landscape depending on the force application [25, 26]. The mechanical work performed on a receptor-ligand bond hence influences the behavior of this bond in a very complex manner.

Members of the second major class of adhesion molecules, the integrins, transmit signals from the outside of the cell to the inside and vice versa [19, 39]. One fascinating feature of integrins is their ability to modify dynamically both their equilibrium affinity through regulated conformational changes [19, 40, 41] as well as their cellular anchorage and clustering state [19, 39, 42–44]. In a hallmark study, it was shown that these structural changes can be induced by computationally designed membrane-spanning peptides, underlining the importance of the transmembrane domains for signal transduction [45]. The ability to switch conformations and to fine-tune the adhesion state turns integrins into nano-switches, which adapt their properties according to the circumstances. Different integrins are involved in different adhesive steps. VLA-4 is involved both in rolling and firm adhesion [46], while LFA-1 supports mainly firm adhesion [14]. These functional differences between the two classes of integrins are reflected in their kinetic properties: In its resting state, VLA-4 has a twofold to threefold higher off-rate than LFA-1 [30, 47], as required for rolling interactions (Table 1). Under resting conditions, the off-rate of the VLA-4/VCAM-1 bond is comparable to the off-rate observed for P-selectin under shear stress. But it is more susceptible to external forces, caused by the higher potential width x_β. When activated, the off-rate of the integrin VLA-4 is lowered by two orders of magnitude, thus enabling firm adhesion (Table 1). The flow-chamber data on $\alpha_4\beta_7$/MADCAM-1, the pendant to VLA-4/VCAM-1 of the mucosal endothelium, reveal surprisingly low potential widths [48], potentially caused by multiple bindings [35].

Cadherins are Ca^{2+}-dependent adhesion molecules, which predominantly accomplish the adhesion between cells in cellular monolayers lining for example blood vessel walls or the intestine [49]. The mechanical stress on cadherins in the adherens junctions is much lower than the stress on other cell adhesion molecules. Thus, their task is fundamentally different from the tasks of integrins or selectins, which need to capture cells exposed to the shear force of the blood stream. Cadherins have high off-rates and - with the exception of E-cadherin - large potential widths. This comparable weakness of the cadherin-mediated interaction is compensated by lateral association of many cadherins, forming a high avidity surface [49–55].

3 The Bell-Evans model

Avidity and affinity are defined for equilibrium processes. Yet, in the physiological setting of the blood stream, bond dissociation is not an equilibrium process, because the receptor-ligand bond is subjected to external forces. Hence, mechanical work is exerted on the cells and energy is dissipated. Under external forces, the bond strength - defined as the most probable unbinding force of the receptor-ligand bond - becomes dependent on the force loading [28, 56]. Then, the off-rate is not a constant, but a function of the force acting on the receptor-ligand bond and the history of force [57]. An external force which is applied to the molecular bond alters the energy landscape of the equilibrium and reduces the barrier height of the unbinding process (Fig.1). Thus, it raises the frequency of unbinding (k_{off}). This impact of the mechanics on bond kinetics has been described by Bell in 1978 [27]. He related the off-rate to the reduction of the energy barrier by an external force

F:

$$k_{off}^F = \omega \cdot e^{-\beta(E_{barrier} - E_{mech})} \tag{1}$$

with ω being the attempt frequency, $E_{barrier}$ the height of the energy barrier and E_{mech} the work performed by the external force and $\frac{1}{\beta} = k_B T$, the thermal energy of the system.

In the equilibrium, the basal off-rate is determined by $k_{off}^0 = \omega \cdot e^{-\beta(E_{barrier})}$. As shown in Figure 1, the energy barrier is located at position x_β. The work performed on the system at this point is $E_{mech} = F \cdot x_\beta$, if F is the force acting on the system in the direction of the barrier. Hence, equation 1 can be written using the basal off-rate k_{off}^0 and the acting force F:

$$k_{off}^F = k_{off}^0 \cdot e^{\frac{F}{F_\beta}} \tag{2}$$

Here, the characteristic force F_β is scaled with the thermal energy: $F_\beta = \frac{k_B T}{x_\beta}$, where x_β is the position of the transition state in the energy landscape of the bond. In this approach, all properties of the energy landscape are condensed in one parameter x_β. This is only valid for constant forces. Yet in general, the forces acting on the system are not constant, but change with time. This requires an extension of the classical Bell ansatz. On the basis of the Kramers theory, Evans and Ritchie expanded the Bell ansatz to a dynamical theory for the kinetics in an overdamped environment (liquids) and included the deformation of the energy landscape and the spatial variation of the friction between the molecules [28, 58]. Since now the forces are not constant over time, the off-rate becomes dependent on the force loading rate and with this on the time:

$$k_{off}^F = k_{off}^0 \cdot g(F(t)) e^{\Delta E(F(t))} \tag{3}$$

The function $g(F)$ describes the mechanical coupling of the external force F into the potential of the molecular bond and $\Delta E(F)$ the reduction of the energy barrier by the acting force F. As the force F is a function of time with $F = F(t)$, also the barrier height is time dependent. Therefore, the force loading defined as the variation of force over time $\frac{\partial F}{\partial t}$ crucially alters the binding properties.

To describe the strength of a molecular bond, the most probable rupture force under the chosen conditions is a useful parameter. For constant force loading, the probability distribution of rupture forces, from which the strength of the bond and hence the cellular adhesiveness against external forces can be estimated, is given by the well-known relation [28]:

$$p(F, t) = k_{off}^F \cdot e^{-\int_t k_{off}^F(F(t^*)) dt^*} \tag{4}$$

4 The Influence of the Compliance

How can we describe the force loading on the molecular bond? In general, the load on a bond is not linear, even if the velocity of the blood stream which induces the force is constant. The force acting on the receptor-ligand bond is dependent on the mechanical properties of the linker which connects the receptor-ligand pair to the respective surfaces (in lymphocyte adhesion, the receptor is mechanically coupled to the adhering cell and the ligand to the vessel wall). Therefore, to describe the cellular de-adhesion, a formalism for the probability distribution of rupture forces should be used which incorporates the mechanics of this linkage [29]. A good measure for the mechanical properties of the linker is its compliance. The compliance describes how much the linker elongates under an applied force. It is defined as $\frac{\partial z}{\partial F}$, where z is the elongation and F the acting force. If the force changes, the compliance is not necessarily constant. Long, flexible polymers, for instance, which are often used in experiments as linkers for force application to weak bonds [59], display a very different force loading than stiff linkers [60, 61]. Linkers with different compliance result in drastically different rupture force distributions of the same receptor-ligand bond, even under otherwise identical conditions [29]. Evans and Ritchie derived a general expression for the probability distribution of rupture forces for pulling on a bond with constant speed v in-

4

cluding a description of a non-linear elastic linkage [29]:

$$p(F) = k_{off}^F \cdot \frac{1}{v} \cdot c(F) \cdot e^{-\int_f k_{off}^F \cdot \frac{1}{v} \cdot c(F) df} \qquad (5)$$

According to equation 2 and 5, the compliance of the force exerting linker has direct impact on the force persistance of the receptor-ligand bond, similar to the basal off-rate. In the case of cell adhesion, the linker between the force application and the molecular bond is the cell itself and in particular the anchorage of the molecules in the cell or in the substrate. Hence, the cellular mechanics also affects the kinetic properties of cell adhesion and determines the effectiveness of the force absorption.

5 Experimental Techniques

Since the mechanical properties are of such a high importance for the adhesiveness of cells under the influence of external forces, it is desirable to have tools at hand that can thoroughly analyze the receptor properties under load. Many different approaches have been undertaken to investigate the complex phenomena of cell adhesion. With spinning disc experiments and flow chamber assays, the cellular adhesion strength can be quantitatively analysed in ensemble measurements of many cells [62–65]. These assays have a very high throughput and hence a good statistic. Thus, they can examine a multitude of circumstances as for instance mutations or the influence of drugs. But in the ensemble of cells, the molecular aspects of cell adhesion cannot be resolved.

The strength of a single receptor-ligand bond is dependent on the local environment of both interacting molecules. Within a single cell, the local environment can change by redistributing the receptors or by anchoring them to cytoskeletal components. To learn about the local cell mechanics experienced by single adhesion receptors, force spectroscopic experiments can be applied with high temporal and spatial resolution, even on the single-molecule level. Techniques which are capable of specifically administering forces to single molecules on living cells include optical tweezers, micropipette and AFM. These techniques have been used in a variety of experiments: With optical tweezers and video microscopy, Lambert et al. unraveled the dynamics of rapid ligand-induced anchoring of cadherins to the cytoskeleton [66]. Riveline et al. investigated the force-induced formation of focal contacts by using a micropipette assay [67]. Evans et al. measured the local mechanical compliance of a cell surface [68] with a related setup. Micropipette experiments also showed that membrane separation from the cytoskeleton proceeds the rupture of P-selectin/PSGL-1 bonds [26] and that the physical properties of the membrane are actively controlled by the cell metabolism even for simple cells like erythrocytes [69].

AFM has been used to investigate cell-cell adhesion [70–73], cell-substrate adhesion as well as the local and global cellular mechanics [70, 74–76]. In particular, it was used to examine the potential energy landscape of molecular receptor-ligand bonds on living cells by dynamic force spectroscopy [30, 77]. Furthermore, the cellular deformability was compared for different leukemia cells [78] and erythrocytes [79]. Canetta et al. [75] investigated how the intracellular cytoskeletal attachment of ICAM-1 influences the tether formation and the cellular stiffness.

With force spectroscopic techniques like AFM, the experimental conditions can be fine-tuned and chosen to meet different demands: the cell adhesion can be studied on the level of single receptors or of receptor clusters as well as on the level of a small membrane area. Moreover, information of both kinetic and mechanical kind can be obtained in high temporal and spacial resolution. On the whole cell level, these experiments can give insight into the cellular avidity or the cellular elasticity. On the other hand, performed on the single-molecule level, the molecular affinity and anchorage can be adressed. Even different populations of the same receptor on the cell can theoretically be resolved with single-molecule techniques [80, 81]. These populations may differ for instance in their affinity state or in their anchorage in the cell. Integrins are an example for receptors, which coexist in differ-

ent affinity states on the cell surface [82–84]. Furthermore, they also modify their anchorage in the cell, as they can occur either attached to the cytoskeleton [85–87] or diffusing in the membrane.

6 Mechanical Models

The force-distance relationship obtained in force spectroscopic experiments contains information about the elastic properties of the linker, which can be analyzed with the appropriate mechanical model. Using the history of force development, the single-molecule force spectroscopy experiments of isolated molecules have been established as useful tools to examine the mechanical properties of polymers [88–90]. From the force-distance curves, important mechanical properties of the polymers like the persistance length can be obtained. Numerous studies on polymers have been performed and analyzed using models for the entropic elasticity like the worm-like chain model or the freely joined chain model [91–93].

Under the typical experimental conditions of a single-molecule AFM experiment on living cells, the shape of the force-distance curves differs strikingly from the shape of the force-distance curves of stretched polymers [77, 94]. The classical mechanical models used for these polymers are therefore inappropriate to interpret cellular AFM measurements. Since the cell operates as the linker between the applied force and the adhesion receptor, a good assumption on the cellular mechanics is crucial. Thus, models which describe the cellular force-distance relationship are desired.

The great variety of different cell types, force applications and experimental conditions makes it virtually impossible to take a simple mechanical model that describes the response of cells to all circumstances. Every experimental setup needs to find the appropriate simplified mechanical model. This will not only depend on the experimental techniques, but also on the examined cell type.

Different models describing the cellular mechanics have been employed (for a review see [95]).

One class of models treats the cells as solid bodies with elastic or viscoelastic properties. These models are based on different combinations of elastic and viscous elements represented as springs and dashpots. Historic models include the Kelvin body (also called *standard linear solid*), the Maxwell body and the Voigt body (Fig.2) [96]. Bausch et al. used a combination of a Kelvin body in series with a dashpot or a Voigt body to describe the viscoelastic response of cells measured by magnetic bead microrheometry [97, 98]. Koay et al. modeled the creep indentation of single cells with a standard linear solid [99]. Mazzag et al. used different generalized Kelvin bodies to analyze shear stress sensing by cells [100]. In the following, we will focus on the response of cells to pulling forces applied to single receptors in single-molecule force spectroscopic experiments.

The cellular force-distance curves are characterized by a steep initial increase in force, which then levels off at a nearly constant force [74, 101]. The existence of these force plateaus has been interpreted as the result of pulling membranous tubes from the cell, so called tethers [74, 101–104]. These general characteristica depend on both the cell-type and the mode of force application [105]. For lymphocytes and neurons, the force for tether formation does not exceed the plateau force [106, 107]. Endothelial cells and Outer Hair Cells (OHC), on the other hand, show a high tether formation force, which then drops significantly to finally reach the plateau value [74, 104]. For the latter cells, both the tether formation force as well as the plateau force are dependent on the cellular area, at which the force is applied. Theoretical models predict the existence of such a tether formation force [108, 109].

Evans et al. interpreted the initial increase in force as the stretching of intracellular components [106]. This increase follows a linear force-distance dependency and can hence be modelled as a Hookean spring. After the initial increase, a small rupture event was observed, which was then followed by a viscous flow of the tether forming membrane. The viscous flow was modeled as a nonlinear Maxwell-like fluid.

A mechanical model should be able to describe

both, the steep initial increase in force as well as the plateau force. Yet, rupture events in between these two regimes are hard to describe by a continuous model. Still, it is very desirable to have a simple mechanical model, which captures the main features of the experimentally observed force-distance relationship. A good, but necessarily simplified mechanical model for cells is the Kelvin body [110, 111]. When integrating the differential equations under the boundary condition of a constant retract velocity (which is typical for a standard AFM experiment), one obtains the force-distance relationship:

$$F(z) = k_t \cdot z + g \cdot v - g \cdot v \cdot e^{-\frac{k_i \cdot z}{g \cdot v}} \qquad (6)$$

This model does not describe rupture events or tether formation forces. Though, it gives valuable information about the mechanics of the cellular environment around the probed receptor, if the measured interactions between the cell and the substrate are exclusively specific for this receptor. Fitting this force-distance relationship in equation 6 to the experimental force-distance curves yields the viscoelastic parameters of the receptors anchorage, k_t, k_i and g (Fig.3). It has been shown that even subtle differences in the mechanical environment of a single receptor can be detected by using this model [112]. The viscoelastic parameters change for instance after a change in the composition of the surrounding membrane or upon the attachment of the cytoplasmic tails to intracellular proteins (Fig. 4).

7 Influence of the Viscoelastic Parameters on the Adhesion Strength

As shown in equation 5, the compliance of the linker determines the force persistance which is expressed in the rupture force distribution. Yet, the compliance in general is not a constant, but defined as $\frac{\partial z}{\partial F}$. How is a change in force reflected in the compliance? With the force-distance relation in equation 6, a mathematical expression

for the compliance can be given:
$$c(F) = -\frac{g \cdot v}{k_i} \cdot$$

$$\left(\frac{k_i \cdot LambertW(a)}{k_t \cdot g \cdot v \cdot (1 + LambertW(a))} - \frac{k_i}{k_t \cdot g \cdot v} \right) \qquad (7)$$

with
$$a = \frac{k_i}{k_t} \cdot exp\left(\frac{k_i \cdot (g \cdot v - f)}{k_t \cdot g \cdot v} \right).$$

In numerical simulations and with the equations 5, 6 and 7, the influence of the viscoelastic parameters on the force distributions can be gauged (Fig.5). Obviously, the cellular viscosity has the main impact on the force persistance of the transmembrane receptor among the mechanical parameters. In particular, the adjustment of the viscosity affects the rupture force distributions as much as the variation of the off-rate.

Is it possible for cells to influence the membrane viscosity? The viscous dissipation of the membrane originates from three different subprocesses: a) the surface viscosity of each monolayer, b) the viscous slip between the monolayers and c) the viscous slip of the inner monolayer over the cytoskeleton [69, 104, 113, 114]. From the comparison of the experiments on vesicles [115–118] and of those on outer hair cells, it has been proposed that the major contribution to the viscosity is due to the slip of the membrane over the cytoskeleton [107,119–121]. This slip can be influenced in the vicinity of the receptor by changes in the cytoskeletal anchorage of other membrane associated molecules without any changes in the receptor itself (Fig.4). Hence, the persistance to external forces can be regulated even if the receptor itself has the identical affinity and attachment state to the cytoskeleton.

Cells have areas with different membrane viscosity: Outer hair cells display different forces for the pulling of tethers depending on whether the tethers are extruded from the lateral wall or from the basal end of the cell [104]. The higher tether force for the lateral wall can be ascribed to the fact that the lateral membrane is firmly attached to the cytoskeleton, opposed to the membrane on the basal end. It is also expected that in other cells, different membrane

regions will have differing cytoskeletal attachments, for example the membrane areas around focal adhesion points. Focal adhesion points and adherens junctions are known to contain clusters of cytoskeletally attached membrane receptors [122–124].

The importance for the viscous slip of the membrane over the cytoskeleton has further been shown by micropipette experiments on T-lymphocytes. Evans et al [106] extracted membrane tethers on P-selectins from primary T-cells in micropipette experiments. These force-distance curves of normal cells and of cells treated with latrunculin can be fitted with equation 6 in order to determine the viscoelastic parameters (Fig.3). Latrunculin treated cells intriguingly showed a lower viscosity than untreated cells, although latrunculin only inhibits the actin polymerisation and does not affect the membrane composition. Yet, this is in line with the altered viscous flow of the membrane over the impaired cytoskeleton and has also been observed by others [105, 125].

Do cells actively redistribute receptors according to their affinity state in areas with differing membrane environment? Activated integrins are indeed mainly located in lipid rafts [126]. In these membrane areas, also chemokine receptors are located [127]. This clustering of chemokine receptors and integrin effectors into lipid rafts ensures that the proper signalling pathways are activated [128] and the integrity of the raft platforms is mandatory for integrin stimulation [129]. Lipid rafts are rich in cholesterol [128, 130] and in membrane-anchoring molecules [131]. Thus, this environment displays different rheological properties compared with other membrane regions (Fig.4). Due to the importance of the elastic compliance, the integrin relocation after activation becomes as relevant for the adhesive properties against external forces as is the affinity increase. Furthermore, it has been shown that cytoplasmic anchorage of selectins increases the adhesiveness [132, 133].

For the characterisation of the cellular adhesion properties, the influence of the compliance on the distribution of rupture forces as described in equation 5 is fundamental: The cellular compliance, which describes how much the cell elon-

gates under a defined applied force, is very complex and dynamically regulated by the cell. The cell constantly remodels its cytoskeleton, builds stress fibers and thereby reacts actively to its environment [134–136]. This active regulation of the cellular stiffness can be performed in timeframes of less than a second [137]. It has an important impact on the adhesiveness of the cell, even if the equilibrium affinity of the adhesion receptors is unaltered. Integrins are a good example for changes in the mechanical anchorage: they change their cytoskeletal attachment according to the intracellular signalling [44,65,138]. This leads to an increased adhesiveness. Hence, the cellular mechanics and notably the mechanics of the anchorage of the molecular bond determines the force loading and the adhesion strength. These considerations also imply that not only the mechanical properties of the adhering cell itself, but also the elastic compliance of the cellular environment is relevant for the cell behaviour [2, 3, 139–143]. This has recently been impressively demonstrated: the stiffness of the ECM is critical for the differentiation of stem cells [144–146], for the progression of tumour cells [147] and the behaviour of osteoblasts [148].

8 Influence of the kinetic parameters on the velocity dependence of deadhesion

Equation 6 describes the influence of the pulling velocity on the force evolution. To use this for an estimate of the expected rupture force at different velocities, also the kinetic parameters k_{off}^0 and x_β need to be known. With the knowledge of all these parameters - the viscoelastic constants and the kinetic constants - one can simulate the expected ruptures over a variety of velocities using a Monte Carlo Simulation. For P-selectin, the viscoelastic parameters can be obtained from a fit to the data obtained by Evans et al. [106]. Furthermore, Evans et al. [106] investigated the force-velocity dependence of the rupture force with pulling velocities vary-

ing from $0.4\mu m/s$ to $150\mu m/s$ in micropipette experiments. For this cell adhesion receptor, the off-rate and the potential width has been determined by a variety of different techniques. The published parameters varied up to two orders of magnitude: Evans et al. found a potential width of $x_\beta = 2.2\text{\AA}$ and an off-rate of $k_{off}^0 = 0.37s^{-1}$ in micropipette experiments [26]. Alon et al. [31] calculated $x_\beta = 0.3\text{\AA}$ and $k_{off}^0 = 1s^{-1}$ from flow chamber assays. Hanley et al. [34] calculated $x_\beta = 1.4\text{\AA}$ and $k_{off}^0 = 0.2s^{-1}$ from AFM experiments on living cells and Fritz et al. [33] $x_\beta = 2.5\text{\AA}$ and $k_{off}^0 = 0.02s^{-1}$ from AFM experiments on isolated molecules. In figure 3, the expected rupture force for these different parameters, simulated with the presented model in a Monte-Carlo simulation, are shown and compared to the experimental values obtained by Evans et al. [106]. For velocities below $50\mu m/s$, a good fit between model and experiment is observed with the kinetic data obtained by Fritz et al. [33]. The high-velocity regime apparently cannot be described very well by the model. This may reflect a different kinetic regime at high pulling velocities. Interestingly, the kinetic parameters calculated in single-molecule studies on isolated molecules coincide best with the values measured by Evans and co-workers [106]. The kinetic parameters obtained from cells by Evans et al. [26] and by Hanley et al. [34] show a similar trend. The differences between isolated molecules and studies on whole cells might reflect the higher experimental error in the latter studies caused by the complexity of a cell. Whereas the other three studies used force-application, which pull normal to the membrane, Alon et al. [31] exposed the cells to lateral shear forces. The direction of force application has recently been shown to strongly influence the effect of force on a protein complex. The parameters obtained by Alon et al. [31] show a strikingly different behaviour. With these parameters, a much higher rupture force is obtained at high velocities. Hence, the differences in these measurements might reflect that not only the absolute force, but also the vectorial, direction-dependent nature of the force might significantly affect biological systems.

9 Mechanotransduction of signals

Thus, cells react to external forces exerted on them by their environment in a very distinct manner. Forces applied to cell surface receptors can cause intracellular signal cascades [149,150] which regulate the gene expression and other cellular reactions [1, 144, 151]. Force application to transmembrane receptors also controls the strengthening of initial integrin-ECM adhesions to focal adhesion complexes [152]. In another study on the flow-induced response of endothelial cells, it was detected that microtubules transmit the force from the plasma membrane to the nucleus [153]. This leads to nuclear structural changes, which in turn are thought to be important for the modulation of the endothelial growth and metabolism.

To sense the changes in the mechanics of its surroundings, the cell has to probe it either actively or passively. An active sampling, however, would cost energy and the sensitivity would be limited by the sampling frequency. The cell would always have to balance energy consumption versus sensitivity. Passive sampling, in contrast, enables permanent probing, while the energetic dispense is low. It requires a prestressed system, so that the deformation caused by an external force can be transformed directly and immediately to the biochemical effector molecules without the use of long signalling cascades. In addition, a prestressed system does not only provide continuous sensing of the cellular environment, but also guarantees the cellular stability. Hence, a prestressed system is a good design principle for force induced signalling upon mechanical stimuli.

The principle of prestress can also explain the fact, that the cell can design the shape of its environment by exerting forces itself [142]. Integrin mediated forces have been examined for instance during the spreading of endothelial cells and appear even before focal adhesion or stress fiber formation [154]. These cell surface receptors have been found to transmit even sufficient force to bend collagen fibrils [155]. Thus, the cell probes the mechanics of is surroundings as

well as it perceives and reacts to forces exerted by these surroundings.

10 The tensegrity model

Ingber et al. [139, 156, 157] argued that this so-called mechanosensation and the subsequent mechanotransduction of signals is in good agreement with the architectural principle of tensegrity. Tensegrity systems stabilise their shape by continuous tension [156]. They consist of two different kinds of structural elements: stiff parts or struts for the shape stability and elastic parts or cables for the prestress. The stiff parts are put under continuous tension by the elastic parts, thus resulting in a prestressed system. For cells, microtubules and extracellular matrix adhesions are proposed to be the stiff parts, resisting the compression built up by microfilaments and intermediate filaments [158]. This model has been tested computationally [159] and experimentally. In a real-time microscopy analysis, Wang et al. investigated the dislocation of GFP-labeled microtubules and mitochondria after pulling on cell surface integrins and found that the cell behaves as a discrete interconnected network [160]. Furthermore, traction force microscopic experiments indicated that microtubules balance at least a portion of the cellular tensile stress [158, 160–162]. This is in agreement with a priori predictions of the tensegrity model. Kumar et al. combined traction force microscopy, laser nanoscissors and fluorescence photobleaching to confirm that stress fibers in living cells behave as viscoelastic cables tensed by actomyosin motors [163]. Nevertheless all these findings are not totally conclusive [159]. Other discrete models such as the percolation or cellular solid model [164, 165] can also explain most of these findings.

Within the picture of tensegrity, it is easy to imagine that upon modified receptor anchorage the signal outcome is altered (Fig.6). For instance, if integrin receptors are bound to talin via their cytoplasmic ends and thus attached to the cytoskeleton, the force exerted on the extracellular integrin domains is transmitted to different cytoplasmic compartments, as if the integrin is only anchored in the membrane or associated to other cytoplasmic molecules [166]. The energy dissipation to either the cytoskeleton or the membrane cannot only lead to different signalling events, but also to a different alignment of the cell in the force field: In physiology, the lymphocyte adheres to the endothelium despite the forces of the blood stream. If the transmembrane adhesion receptor is only membrane anchored, a membranous tube is pulled from the cell, the so-called tether (Fig.7). With this, the cell can proceed in a slow rolling movement along the endothelium [102] and check for activation signals like chemokines. In the other case, where the cell adhesion receptor is attached to the cytoskeleton, the lateral force from the blood flattens the cell and presses it to the surfaces. Thus, the resulting contact area between the lymphocyte and the ligand-expressing endothelium is increased and the adhesive interaction can be converted from a single receptor-ligand bond to the multiple bond interaction of firm adhesion [167]. In this picture, also the before mentioned dependence of the measured off-rate and potential width on the vectorial nature of the applied force can be explained: If the force is applied perpendicular to the substrate and tether formation occurs, the cell is taken away from the substrate. This is the case in atomic force spectroscopy, optical tweezers or micropipette experiments. If the force though is applied laterally as in the flow chamber, the tether operates like a leash and enables the cell still to contact the substrate.

11 Outlook

Force spectroscopic experiments on single cell surface receptors do not only shed light on the molecular kinetics. With the help of mechanical models like the Kelvin body model, they also give insight into the local cell mechanics and intracellular anchorage events. Thus, transmembrane receptors can be used as nano-probes to examine the mechanical regulation of adhesion by the cell. As discussed above, the anchorage of the adhesive receptor crucially determines the cellular signalling and force persistence.

Tether formation on membrane-anchored receptors leads to a completely different alignment of the cell relative to the substrate (Fig.7), as compared to the force application to cytoskeleton-anchored receptors. The principle of tether formation is a fundamental strategy for adhesive events in nature. To mimic this, several bacteria grow pili, which are tether-like structures with sticky ends [168].

Cell adhesion is important in many physiological and pathophysiological situations, as in morphogenesis, cellular differentiation, immune reactions, cancer metastasis and many more. The manipulation of the cellular mechanics and cell adhesion by biomimetic surface [169–173] or pharmaceutic agents has already been shown [35]. Therefore, the understanding of cell adhesion molecules like integrins are of great medical interest, eg. in the development of protheses [174,175] or in the treatment of cancer [176–180] or asthma [181,182].

References

[1] Viola Vogel and Michael Sheetz. Local force and geometry sensing regulate cell functions. *Nat Rev Mol Cell Biol*, 7(4):265–275, Apr 2006.

[2] Manuel Théry, Victor Racine, Matthieu Piel, Anne Pépin, Ariane Dimitrov, Yong Chen, Jean-Baptiste Sibarita, and Michel Bornens. Anisotropy of cell adhesive microenvironment governs cell internal organization and orientation of polarity. *Proc Natl Acad Sci U S A*, 103(52):19771–19776, Dec 2006.

[3] Ana Kostic and Michael P Sheetz. Fibronectin rigidity response through fyn and p130cas recruitment to the leading edge. *Mol Biol Cell*, 17(6):2684–2695, Jun 2006.

[4] Ronen Alon, Valentin Grabovsky, and Sara Feigelson. Chemokine induction of integrin adhesiveness on rolling and arrested leukocytes local signaling events or global stepwise activation? *Microcirculation*, 10(3-4):297–311, Jun 2003.

[5] V. Grabovsky, S. Feigelson, C. Chen, D. A. Bleijs, A. Peled, G. Cinamon, F. Baleux, F. Arenzana-Seisdedos, T. Lapidot, van Kooyk Y, R. R. Lobb, and R. Alon. Subsecond induction of alpha4 integrin clustering by immobilized chemokines stimulates leukocyte tethering and rolling on endothelial vascular cell adhesion molecule 1 under flow conditions. *J Exp Med*, 192(4):495–506, Aug 2000.

[6] Marco Arnold, Elisabetta Ada Cavalcanti-Adam, Roman Glass, Jacques Blümmel, Wolfgang Eck, Martin Kantlehner, Horst Kessler, and Joachim P Spatz. Activation of integrin function by nanopatterned adhesive interfaces. *Chemphyschem*, 5(3):383–388, Mar 2004.

[7] Magda Kucia, Kacper Jankowski, Ryan Reca, Marcin Wysoczynski, Laura Bandura, Daniel J Allendorf, Jin Zhang, Janina Ratajczak, and Mariusz Z Ratajczak. Cxcr4-sdf-1 signalling, locomotion, chemotaxis and adhesion. *J Mol Histol*, 35(3):233–245, Mar 2004.

[8] G. Constantin, M. Majeed, C. Giagulli, L. Piccio, J. Y. Kim, E. C. Butcher, and C. Laudanna. Chemokines trigger immediate beta2 integrin affinity and mobility changes: differential regulation and roles in lymphocyte arrest under flow. *Immunity*, 13(6):759–769, Dec 2000.

[9] Revital Shamri, Valentin Grabovsky, Jean-Marc Gauguet, Sara Feigelson, Eugenia Manevich, Waldemar Kolanus, Martyn K Robinson, Donald E Staunton, Ulrich H von Andrian, and Ronen Alon. Lymphocyte arrest requires instantaneous induction of an extended lfa-1 conformation mediated by endothelium-bound chemokines. *Nat Immunol*, 6(5):497–506, May 2005.

[10] Guy Cinamon and Ronen Alon. A real time in vitro assay for studying leukocyte

transendothelial migration under physiological flow conditions. *J Immunol Methods*, 273(1-2):53–62, Feb 2003.

[11] P. S. Frenette and D. D. Wagner. Adhesion molecules–part 1. *N Engl J Med*, 334(23):1526–1529, Jun 1996.

[12] P. S. Frenette and D. D. Wagner. Adhesion molecules–part ii: Blood vessels and blood cells. *N Engl J Med*, 335(1):43–45, Jul 1996.

[13] Ronen Alon and Sara Feigelson. From rolling to arrest on blood vessels: leukocyte tap dancing on endothelial integrin ligands and chemokines at sub-second contacts. *Semin Immunol*, 14(2):93–104, Apr 2002.

[14] Klaus Ley, Carlo Laudanna, Myron I Cybulsky, and Sussan Nourshargh. Getting to the site of inflammation: the leukocyte adhesion cascade updated. *Nat Rev Immunol*, 7(9):678–689, Sep 2007.

[15] David M Rose, Ronen Alon, and Mark H Ginsberg. Integrin modulation and signaling in leukocyte adhesion and migration. *Immunol Rev*, 218:126–134, Aug 2007.

[16] Alexandre Chigaev, Gordon Zwartz, Steven W Graves, Denise C Dwyer, Hisashi Tsuji, Terry D Foutz, Bruce S Edwards, Eric R Prossnitz, Richard S Larson, and Larry A Sklar. Alpha4beta1 integrin affinity changes govern cell adhesion. *J Biol Chem*, 278(40):38174–38182, Oct 2003.

[17] Jieqing Zhu, Brian Boylan, Bing-Hao Luo, Peter J Newman, and Timothy A Springer. Tests of the extension and deadbolt models of integrin activation. *J Biol Chem*, 282(16):11914–11920, Apr 2007.

[18] Fang Zhang, Warren D Marcus, Nimita H Goyal, Periasamy Selvaraj, Timothy A Springer, and Cheng Zhu. Two-dimensional kinetics regulation of alphalbeta2-icam-1 interaction by conformational changes of the alphal-inserted

domain. *J Biol Chem*, 280(51):42207–42218, Dec 2005.

[19] Bing-Hao Luo and Timothy A Springer. Integrin structures and conformational signaling. *Curr Opin Cell Biol*, 18(5):579–586, Oct 2006.

[20] Na Ni, Christopher G Kevil, Daniel C Bullard, and Dennis F Kucik. Avidity modulation activates adhesion under flow and requires cooperativity among adhesion receptors. *Biophys J*, 85(6):4122–4133, Dec 2003.

[21] Joana Vitte, Anne-Marie Benoliel, Philippe Eymeric, Pierre Bongrand, and Anne Pierres. Beta-1 integrin-mediated adhesion may be initiated by multiple incomplete bonds, thus accounting for the functional importance of receptor clustering. *Biophys J*, 86(6):4059–4074, Jun 2004.

[22] Jochen Salber, Stefan Gräter, Marc Harwardt, Matthias Hofmann, Doris Klee, Jadranka Dujic, Huang Jinghuan, Jiandong Ding, Stefan Kippenberger, August Bernd, Jürgen Groll, Joachim P Spatz, and Martin Möller. Influence of different ecm mimetic peptide sequences embedded in a nonfouling environment on the specific adhesion of human-skin keratinocytes and fibroblasts on deformable substrates. *Small*, 3(6):1023–1031, Jun 2007.

[23] Alexandre Chigaev, Tione Buranda, Denise C Dwyer, Eric R Prossnitz, and Larry A Sklar. Fret detection of cellular alpha4-integrin conformational activation. *Biophys J*, 85(6):3951–3962, Dec 2003.

[24] M. Bier, I. Derényi, M. Kostur, and R. D. Astumian. Intrawell relaxation of overdamped brownian particles. *Phys Rev E Stat Phys Plasmas Fluids Relat Interdiscip Topics*, 59(6):6422–6432, Jun 1999.

[25] E. Evans, A. Leung, D. Hammer, and S. Simon. Chemically distinct transition

states govern rapid dissociation of single l-selectin bonds under force. *Proc Natl Acad Sci U S A*, 98(7):3784–3789, Mar 2001.

[26] Evan Evans, Andrew Leung, Volkmar Heinrich, and Cheng Zhu. Mechanical switching and coupling between two dissociation pathways in a p-selectin adhesion bond. *Proc Natl Acad Sci U S A*, 101(31):11281–11286, Aug 2004.

[27] G. I. Bell. Models for the specific adhesion of cells to cells. *Science*, 200(4342):618–627, May 1978.

[28] E. Evans and K. Ritchie. Dynamic strength of molecular adhesion bonds. *Biophys J*, 72(4):1541–1555, Apr 1997.

[29] E. Evans and K. Ritchie. Strength of a weak bond connecting flexible polymer chains. *Biophys J*, 76(5):2439–2447, May 1999.

[30] Ewa P Wojcikiewicz, Midhat H Abdulreda, Xiaohui Zhang, and Vincent T Moy. Force spectroscopy of lfa-1 and its ligands, icam-1 and icam-2. *Biomacromolecules*, 7(11):3188–3195, Nov 2006.

[31] R. Alon, D. A. Hammer, and T. A. Springer. Lifetime of the p-selectin-carbohydrate bond and its response to tensile force in hydrodynamic flow. *Nature*, 374(6522):539–542, Apr 1995.

[32] R. Alon, S. Chen, K. D. Puri, E. B. Finger, and T. A. Springer. The kinetics of l-selectin tethers and the mechanics of selectin-mediated rolling. *J Cell Biol*, 138(5):1169–1180, Sep 1997.

[33] J. Fritz, A. G. Katopodis, F. Kolbinger, and D. Anselmetti. Force-mediated kinetics of single p-selectin/ligand complexes observed by atomic force microscopy. *Proc Natl Acad Sci U S A*, 95(21):12283–12288, Oct 1998.

[34] William Hanley, Owen McCarty, Sameer Jadhav, Yiider Tseng, Denis Wirtz, and Konstantinos Konstantopoulos. Single molecule characterization of p-selectin/ligand binding. *J Biol Chem*, 278(12):10556–10561, Mar 2003.

[35] K. E. Edmondson, W. S. Denney, and S. L. Diamond. Neutrophil-bead collision assay: pharmacologically induced changes in membrane mechanics regulate the psgl-1/p-selectin adhesion lifetime. *Biophys J*, 89(5):3603–3614, Nov 2005.

[36] E. B. Finger, K. D. Puri, R. Alon, M. B. Lawrence, U. H. von Andrian, and T. A. Springer. Adhesion through l-selectin requires a threshold hydrodynamic shear. *Nature*, 379(6562):266–269, Jan 1996.

[37] M. B. Lawrence, G. S. Kansas, E. J. Kunkel, and K. Ley. Threshold levels of fluid shear promote leukocyte adhesion through selectins (cd62l,p,e). *J Cell Biol*, 136(3):717–727, Feb 1997.

[38] Bryan T Marshall, Mian Long, James W Piper, Tadayuki Yago, Rodger P McEver, and Cheng Zhu. Direct observation of catch bonds involving cell-adhesion molecules. *Nature*, 423(6936):190–193, May 2003.

[39] Kay E Gottschalk, Paul D Adams, Axel T Brunger, and Horst Kessler. Transmembrane signal transduction of the alpha(iib)beta(3) integrin. *Protein Sci*, 11(7):1800–1812, Jul 2002.

[40] Wei Li, Douglas G Metcalf, Roman Gorelik, Renhao Li, Neal Mitra, Vikas Nanda, Peter B Law, James D Lear, William F Degrado, and Joel S Bennett. A push-pull mechanism for regulating integrin function. *Proc Natl Acad Sci U S A*, 102(5):1424–1429, Feb 2005.

[41] Bing-Hao Luo, Christopher V Carman, Junichi Takagi, and Timothy A Springer. Disrupting integrin transmembrane domain heterodimerization increases ligand binding affinity, not valency or clustering. *Proc Natl Acad Sci U S A*, 102(10):3679–3684, Mar 2005.

[42] Kay-E. Gottschalk and Horst Kessler. The structures of integrins and integrin-ligand complexes: implications for drug design and signal transduction. *Angew Chem Int Ed Engl*, 41(20):3767–3774, Oct 2002.

[43] Kay-Eberhard Gottschalk and Horst Kessler. A computational model of transmembrane integrin clustering. *Structure*, 12(6):1109–1116, Jun 2004.

[44] Carlo Laudanna and Ronen Alon. Right on the spot. chemokine triggering of integrin-mediated arrest of rolling leukocytes. *Thromb Haemost*, 95(1):5–11, Jan 2006.

[45] Hang Yin, Joanna S Slusky, Bryan W Berger, Robin S Walters, Gaston Vilaire, Rustem I Litvinov, James D Lear, Gregory A Caputo, Joel S Bennett, and William F DeGrado. Computational design of peptides that target transmembrane helices. *Science*, 315(5820):1817–1822, Mar 2007.

[46] R. Alon, P. D. Kassner, M. W. Carr, E. B. Finger, M. E. Hemler, and T. A. Springer. The integrin vla-4 supports tethering and rolling in flow on vcam-1. *J Cell Biol*, 128(6):1243–1253, Mar 1995.

[47] Xiaohui Zhang, Susan E Craig, Hishani Kirby, Martin J Humphries, and Vincent T Moy. Molecular basis for the dynamic strength of the integrin alpha4beta1/vcam-1 interaction. *Biophys J*, 87(5):3470–3478, Nov 2004.

[48] M. de Château, S. Chen, A. Salas, and T. A. Springer. Kinetic and mechanical basis of rolling through an integrin and novel ca2+-dependent rolling and mg2+-dependent firm adhesion modalities for the alpha 4 beta 7-madcam-1 interaction. *Biochemistry*, 40(46):13972–13979, Nov 2001.

[49] B. M. Gumbiner. Cell adhesion: the molecular basis of tissue architecture and morphogenesis. *Cell*, 84(3):345–357, Feb 1996.

[50] W. Baumgartner, P. Hinterdorfer, W. Ness, A. Raab, D. Vestweber, H. Schindler, and D. Drenckhahn. Cadherin interaction probed by atomic force microscopy. *Proc Natl Acad Sci U S A*, 97(8):4005–4010, Apr 2000.

[51] Emilie Perret, Anne-Marie Benoliel, Pierre Nassoy, Anne Pierres, Véronique Delmas, Jean-Paul Thiery, Pierre Bongrand, and Hélène Feracci. Fast dissociation kinetics between individual e-cadherin fragments revealed by flow chamber analysis. *EMBO J*, 21(11):2537–2546, Jun 2002.

[52] Porntula Panorchan, Jerry P George, and Denis Wirtz. Probing intercellular interactions between vascular endothelial cadherin pairs at single-molecule resolution and in living cells. *J Mol Biol*, 358(3):665–674, May 2006.

[53] Porntula Panorchan, Melissa S Thompson, Kelly J Davis, Yiider Tseng, Konstantinos Konstantopoulos, and Denis Wirtz. Single-molecule analysis of cadherin-mediated cell-cell adhesion. *J Cell Sci*, 119(Pt 1):66–74, Jan 2006.

[54] Deborah Leckband and Anil Prakasam. Mechanism and dynamics of cadherin adhesion. *Annu Rev Biomed Eng*, 8:259–287, 2006.

[55] Yoshikazu Tsukasaki, Kazuo Kitamura, Kazuya Shimizu, Atsuko H Iwane, Yoshimi Takai, and Toshio Yanagida. Role of multiple bonds between the single cell adhesion molecules, nectin and cadherin, revealed by high sensitive force measurements. *J Mol Biol*, 367(4):996–1006, Apr 2007.

[56] Yu-Jane Sheng, Shaoyi Jiang, and Heng-Kwong Tsao. Forced kramers escape in single-molecule pulling experiments. *J Chem Phys*, 123(9):91102, Sep 2005.

[57] R. Merkel, P. Nassoy, A. Leung, K. Ritchie, and E. Evans. Energy landscapes of receptor-ligand bonds explored with dynamic force spectroscopy. *Nature*, 397(6714):50–53, Jan 1999.

[58] H. A. Kramers. Brownian motion in a field of force and the diffusion model of chemical reactions. *Physica*, 7:284–304, 1940.

[59] A. S M Kamruzzahan, Andreas Ebner, Linda Wildling, Ferry Kienberger, Christian K Riener, Christoph D Hahn, Philipp D Pollheimer, Peter Winklehner, Martin Hölzl, Bernd Lackner, Daniela M Schörkl, Peter Hinterdorfer, and Hermann J Gruber. Antibody linking to atomic force microscope tips via disulfide bond formation. *Bioconjug Chem*, 17(6):1473–1481, 2006.

[60] Kathryn L Brogan and Mark H Schoenfisch. Influence of antibody immobilization strategy on molecular recognition force microscopy measurements. *Langmuir*, 21(7):3054–3060, Mar 2005.

[61] Chad Ray, Jason R Brown, and Boris B Akhremitchev. Correction of systematic errors in single-molecule force spectroscopy with polymeric tethers by atomic force microscopy. *J Phys Chem B*, 111(8):1963–1974, Mar 2007.

[62] Nathan D Gallant and Andrés J García. Quantitative analyses of cell adhesion strength. *Methods Mol Biol*, 370:83–96, 2007.

[63] Fang-Hua Lee, Christopher Haskell, Isreal F Charo, and David Boettiger. Receptor-ligand binding in the cell-substrate contact zone: a quantitative analysis using cx3cr1 and cxcr1 chemokine receptors. *Biochemistry*, 43(22):7179–7186, Jun 2004.

[64] M. J. Smith, E. L. Berg, and M. B. Lawrence. A direct comparison of selectin-mediated transient, adhesive events using high temporal resolution. *Biophys J*, 77(6):3371–3383, Dec 1999.

[65] Ronen Alon, Sara W Feigelson, Eugenia Manevich, David M Rose, Julia Schmitz, Darryl R Overby, Eitan Winter, Valentin Grabovsky, Vera Shinder, Benjamin D Matthews, Maya Sokolovsky-Eisenberg, Donald E Ingber, Martin Benoit, and Mark H Ginsberg. Alpha4beta1-dependent adhesion strengthening under mechanical strain is regulated by paxillin association with the alpha4-cytoplasmic domain. *J Cell Biol*, 171(6):1073–1084, Dec 2005.

[66] Mireille Lambert, Daniel Choquet, and René-Marc Mège. Dynamics of ligand-induced, rac1-dependent anchoring of cadherins to the actin cytoskeleton. *J Cell Biol*, 157(3):469–479, Apr 2002.

[67] D. Riveline, E. Zamir, N. Q. Balaban, U. S. Schwarz, T. Ishizaki, S. Narumiya, Z. Kam, B. Geiger, and A. D. Bershadsky. Focal contacts as mechanosensors: externally applied local mechanical force induces growth of focal contacts by an mdia1-dependent and rock-independent mechanism. *J Cell Biol*, 153(6):1175–1186, Jun 2001.

[68] E. Evans, K. Ritchie, and R. Merkel. Sensitive force technique to probe molecular adhesion and structural linkages at biological interfaces. *Biophys J*, 68(6):2580–2587, Jun 1995.

[69] N. Borghi and F. Brochard-Wyart. Tether extrusion from red blood cells: integral proteins unbinding from cytoskeleton. *Biophys J*, 93(4):1369–1379, Aug 2007.

[70] Xiaohui Zhang, Ewa Wojcikiewicz, and Vincent T Moy. Force spectroscopy of the leukocyte function-associated antigen-1/intercellular adhesion molecule-1 interaction. *Biophys J*, 83(4):2270–2279, Oct 2002.

[71] Martin Benoit and Hermann E Gaub. Measuring cell adhesion forces with the atomic force microscope at the molecular

level. *Cells Tissues Organs*, 172(3):174–189, 2002.

[72] Pierre-Henri Puech, Kate Poole, Detlef Knebel, and Daniel J Muller. A new technical approach to quantify cell-cell adhesion forces by afm. *Ultramicroscopy*, 106(8-9):637–644, 2006.

[73] Anne Simon and Marie-Christine Durrieu. Strategies and results of atomic force microscopy in the study of cellular adhesion. *Micron*, 37(1):1–13, 2006.

[74] Mingzhai Sun, John S Graham, Balazs Hegedüs, Françoise Marga, Ying Zhang, Gabor Forgacs, and Michel Grandbois. Multiple membrane tethers probed by atomic force microscopy. *Biophys J*, 89(6):4320–4329, Dec 2005.

[75] Elisabetta Canetta, Alain Duperray, Anne Leyrat, and Claude Verdier. Measuring cell viscoelastic properties using a force-spectrometer: influence of protein-cytoplasm interactions. *Biorheology*, 42(5):321–333, 2005.

[76] Robert H Eibl and Vincent T Moy. Atomic force microscopy measurements of protein-ligand interactions on living cells. *Methods Mol Biol*, 305:439–450, 2005.

[77] Ewa P Wojcikiewicz, Xiaohui Zhang, Aileen Chen, and Vincent T Moy. Contributions of molecular binding events and cellular compliance to the modulation of leukocyte adhesion. *J Cell Sci*, 116(Pt 12):2531–2539, Jun 2003.

[78] Michael J Rosenbluth, Wilbur A Lam, and Daniel A Fletcher. Force microscopy of nonadherent cells: a comparison of leukemia cell deformability. *Biophys J*, 90(8):2994–3003, Apr 2006.

[79] Shamik Sen, Shyamsundar Subramanian, and Dennis E Discher. Indentation and adhesive probing of a cell membrane with afm: theoretical model and experiments. *Biophys J*, 89(5):3203–3213, Nov 2005.

[80] Reinat Nevo, Vlad Brumfeld, Michael Elbaum, Peter Hinterdorfer, and Ziv Reich. Direct discrimination between models of protein activation by single-molecule force measurements. *Biophys J*, 87(4):2630–2634, Oct 2004.

[81] Jose H Hodak, Christopher D Downey, Julie L Fiore, Arthur Pardi, and David J Nesbitt. Docking kinetics and equilibrium of a gaaa tetraloop-receptor motif probed by single-molecule fret. *Proc Natl Acad Sci U S A*, 102(30):10505–10510, Jul 2005.

[82] A. Jakubowski, M. D. Rosa, S. Bixler, R. Lobb, and L. C. Burkly. Vascular cell adhesion molecule (vcam)-ig fusion protein defines distinct affinity states of the very late antigen-4 (vla-4) receptor. *Cell Adhes Commun*, 3(2):131–142, May 1995.

[83] L. L. Chen, A. Whitty, R. R. Lobb, S. P. Adams, and R. B. Pepinsky. Multiple activation states of integrin alpha4beta1 detected through their different affinities for a small molecule ligand. *J Biol Chem*, 274(19):13167–13175, May 1999.

[84] Alexandre Chigaev, Anna Waller, Gordon J Zwartz, Tione Buranda, and Larry A Sklar. Regulation of cell adhesion by affinity and conformational unbending of alpha4beta1 integrin. *J Immunol*, 178(11):6828–6839, Jun 2007.

[85] S. Liu and M. H. Ginsberg. Paxillin binding to a conserved sequence motif in the alpha 4 integrin cytoplasmic domain. *J Biol Chem*, 275(30):22736–42, 2000. Department of Vascular Biology, The Scripps Research Institute, La Jolla, California 92037, USA.

[86] S. Wiesner, K. R. Legate, and R. Fässler. Integrin-actin interactions. *Cell Mol Life Sci*, 62(10):1081–1099, May 2005.

[87] Seiji Tadokoro, Sanford J Shattil, Koji Eto, Vera Tai, Robert C Liddington, Jose M de Pereda, Mark H Ginsberg,

and David A Calderwood. Talin binding to integrin beta tails: a final common step in integrin activation. *Science*, 302(5642):103–106, Oct 2003.

[88] Rief, Oesterhelt, Heymann, and Gaub. Single molecule force spectroscopy on polysaccharides by atomic force microscopy. *Science*, 275(5304):1295–1297, Feb 1997.

[89] F. Oesterhelt, M. Rief, and H.E. Gaub. Single molecule force spectroscopy by afm indicates helical structure of poly(ethylene-glycol) in water. *New Journal of Physics*, 1:6.1–6.11, 1999.

[90] F. Oesterhelt, D. Oesterhelt, M. Pfeiffer, A. Engel, H. E. Gaub, and D. J. Müller. Unfolding pathways of individual bacteriorhodopsins. *Science*, 288(5463):143–146, Apr 2000.

[91] Wolfgang A Linke and Julio M Fernandez. Cardiac titin: molecular basis of elasticity and cellular contribution to elastic and viscous stiffness components in myocardium. *J Muscle Res Cell Motil*, 23(5-6):483–497, 2002.

[92] Claudio Anselmi, Pasquale DeSantis, and Anita Scipioni. Nanoscale mechanical and dynamical properties of dna single molecules. *Biophys Chem*, 113(3):209–221, Mar 2005.

[93] Huan-Xiang Zhou. Polymer models of protein stability, folding, and interactions. *Biochemistry*, 43(8):2141–2154, Mar 2004.

[94] Julia Morfill, Kerstin Blank, Christian Zahnd, Beatrice Luginbühl, Ferdinand Kühner, Kay-Eberhard Gottschalk, Andreas Plückthun, and Hermann E Gaub. Affinity-matured recombinant antibody fragments analyzed by single molecule force spectroscopy. *Biophys J*, Aug 2007.

[95] C. T. Lim, E. H. Zhou, and S. T. Quek. Mechanical models for living cells–a review. *J Biomech*, 39(2):195–216, 2006.

[96] Yuan-Cheng Fung. *Biomechanics: Mechanical Properties of Living Tissues.* Springer, 1993.

[97] A. R. Bausch, W. Möller, and E. Sackmann. Measurement of local viscoelasticity and forces in living cells by magnetic tweezers. *Biophys J*, 76(1 Pt 1):573–579, Jan 1999.

[98] A. R. Bausch, U. Hellerer, M. Essler, M. Aepfelbacher, and E. Sackmann. Rapid stiffening of integrin receptor-actin linkages in endothelial cells stimulated with thrombin: a magnetic bead microrheology study. *Biophys J*, 80(6):2649–2657, Jun 2001.

[99] Eugene J Koay, Adrian C Shieh, and Kyriacos A Athanasiou. Creep indentation of single cells. *J Biomech Eng*, 125(3):334–341, Jun 2003.

[100] Bori M Mazzag, John S Tamaresis, and Abdul I Barakat. A model for shear stress sensing and transmission in vascular endothelial cells. *Biophys J*, 84(6):4087–4101, Jun 2003.

[101] Basarab G Hosu, Mingzhai Sun, Françoise Marga, Michel Grandbois, and Gabor Forgacs. Eukaryotic membrane tethers revisited using magnetic tweezers. *Phys Biol*, 4(2):67–78, Jun 2007.

[102] Vishwanath Ramachandran, Marcie Williams, Tadayuki Yago, David W Schmidtke, and Rodger P McEver. Dynamic alterations of membrane tethers stabilize leukocyte rolling on p-selectin. *Proc Natl Acad Sci U S A*, 101(37):13519–13524, Sep 2004.

[103] D. W. Schmidtke and S. L. Diamond. Direct observation of membrane tethers formed during neutrophil attachment to platelets or p-selectin under physiological flow. *J Cell Biol*, 149(3):719–30, 2000. Institute for Medicine and Engineering, Department of Chemical Engineering, University of Pennsylvania, Philadelphia 19104, USA.

[104] Zhiwei Li, Bahman Anvari, Masayoshi Takashima, Peter Brecht, Jorge H Torres, and William E Brownell. Membrane tether formation from outer hair cells with optical tweezers. *Biophys J*, 82(3):1386–1395, Mar 2002.

[105] Warren D Marcus, Rodger P McEver, and Cheng Zhu. Forces required to initiate membrane tether extrusion from cell surface depend on cell type but not on the surface molecule. *Mech Chem Biosyst*, 1(4):245–251, Dec 2004.

[106] Evan Evans, Volkmar Heinrich, Andrew Leung, and Koji Kinoshita. Nano- to microscale dynamics of p-selectin detachment from leukocyte interfaces. i. membrane separation from the cytoskeleton. *Biophys J*, 88(3):2288–2298, Mar 2005.

[107] D. Raucher and M. P. Sheetz. Characteristics of a membrane reservoir buffering membrane tension. *Biophys J*, 77(4):1992–2002, Oct 1999.

[108] Ana-Suncana Smith, Erich Sackmann, and Udo Seifert. Pulling tethers from adhered vesicles. *Phys Rev Lett*, 92(20):208101, May 2004.

[109] Ana-Suncana Smith and Udo Seifert. Force-induced de-adhesion of specifically bound vesicles: strong adhesion in competition with tether extraction. *Langmuir*, 21(24):11357–11367, Nov 2005.

[110] David R Murdock, Sergey A Ermilov, Alexander A Spector, Aleksander S Popel, William E Brownell, and Bahman Anvari. Effects of chlorpromazine on mechanical properties of the outer hair cell plasma membrane. *Biophys J*, 89(6):4090–4095, Dec 2005.

[111] A. V. Kondrachuk. Models of the dynamics of otolithic membrane and hair cell bundle mechanics. *J Vestib Res*, 11(1):33–42, 2001.

[112] Julia Schmitz and Kay-Eberhard Gottschalk. The mechanical nanoenvironment of force-resisting integrin receptors measured by atomic force microscopy. *Biophysical Journal (submitted)*, 2007.

[113] L. Bo and R. E. Waugh. Determination of bilayer membrane bending stiffness by tether formation from giant, thin-walled vesicles. *Biophys J*, 55(3):509–517, Mar 1989.

[114] Robert M Hochmuth and Warren D Marcus. Membrane tethers formed from blood cells with available area and determination of their adhesion energy. *Biophys J*, 82(6):2964–2969, Jun 2002.

[115] R. E. Waugh, J. Song, S. Svetina, and B. Zeks. Local and nonlocal curvature elasticity in bilayer membranes by tether formation from lecithin vesicles. *Biophys J*, 61(4):974–982, Apr 1992.

[116] R. E. Waugh. Surface viscosity measurements from large bilayer vesicle tether formation. ii. experiments. *Biophys J*, 38(1):29–37, Apr 1982.

[117] E.A. Evans and A. Yeung. Hidden dynamics in rapid changes of bilayer shape. *Chemistry and Physics of Lipids*, 73:39–56, 1994.

[118] J. Y. Shao and R. M. Hochmuth. Micropipette suction for measuring piconewton forces of adhesion and tether formation from neutrophil membranes. *Biophys J*, 71(5):2892–901, 1996. Department of Mechanical Engineering and Materials Science, Duke University, Durham, North Carolina 27708-0300, USA.

[119] J. Dai and M. P. Sheetz. Mechanical properties of neuronal growth cone membranes studied by tether formation with laser optical tweezers. *Biophys J*, 68(3):988–996, Mar 1995.

[120] J. Dai and M. P. Sheetz. Membrane tether formation from blebbing cells. *Biophys J*, 77(6):3363–3370, Dec 1999.

[121] F. Brochard-Wyart, N. Borghi, D. Cuvelier, and P. Nassoy. Hydrodynamic narrowing of tubes extruded from cells. *Proc Natl Acad Sci U S A*, 103(20):7660–7663, May 2006.

[122] K. Burridge, K. Fath, T. Kelly, G. Nuckolls, and C. Turner. Focal adhesions: transmembrane junctions between the extracellular matrix and the cytoskeleton. *Annu Rev Cell Biol*, 4:487–525, 1988.

[123] A. P. Gilmore and K. Burridge. Regulation of vinculin binding to talin and actin by phosphatidyl-inositol-4-5-bisphosphate. *Nature*, 381(6582):531–535, Jun 1996.

[124] B. Z. Katz, S. Levenberg, K. M. Yamada, and B. Geiger. Modulation of cell-cell adherens junctions by surface clustering of the n-cadherin cytoplasmic tail. *Exp Cell Res*, 243(2):415–424, Sep 1998.

[125] Warren D Marcus and Robert M Hochmuth. Experimental studies of membrane tethers formed from human neutrophils. *Ann Biomed Eng*, 30(10):1273–1280, 2002.

[126] Birgit Leitinger and Nancy Hogg. The involvement of lipid rafts in the regulation of integrin function. *J Cell Sci*, 115(Pt 5):963–972, Mar 2002.

[127] Marcin Wysoczynski, Ryan Reca, Janina Ratajczak, Magda Kucia, Neeta Shirvaikar, Marek Honczarenko, Michael Mills, Jens Wanzeck, Anna Janowska-Wieczorek, and Mariusz Z Ratajczak. Incorporation of cxcr4 into membrane lipid rafts primes homing-related responses of hematopoietic stem/progenitor cells to an sdf-1 gradient. *Blood*, 105(1):40–48, Jan 2005.

[128] Miguel A Del Pozo. Integrin signaling and lipid rafts. *Cell Cycle*, 3(6):725–728, Jun 2004.

[129] Revital Shamri, Valentin Grabovsky, Sara W Feigelson, Oren Dwir, Yvette Van Kooyk, and Ronen Alon. Chemokine stimulation of lymphocyte alpha 4 integrin avidity but not of leukocyte function-associated antigen-1 avidity to endothelial ligands under shear flow requires cholesterol membrane rafts. *J Biol Chem*, 277(42):40027–40035, Oct 2002.

[130] Perttu S Niemelä, Samuli Ollila, Marja T Hyvönen, Mikko Karttunen, and Ilpo Vattulainen. Assessing the nature of lipid raft membranes. *PLoS Comput Biol*, 3(2):e34, Feb 2007.

[131] N. Brdicková, T. Brdicka, L. Andera, J. Spicka, P. Angelisová, S. L. Milgram, and V. Horejsí. Interaction between two adapter proteins, pag and ebp50: a possible link between membrane rafts and actin cytoskeleton. *FEBS Lett*, 507(2):133–136, Oct 2001.

[132] O. Dwir, G. S. Kansas, and R. Alon. Cytoplasmic anchorage of l-selectin controls leukocyte capture and rolling by increasing the mechanical stability of the selectin tether. *J Cell Biol*, 155(1):145–156, Oct 2001.

[133] Ulrich S Schwarz and Ronen Alon. L-selectin-mediated leukocyte tethering in shear flow is controlled by multiple contacts and cytoskeletal anchorage facilitating fast rebinding events. *Proc Natl Acad Sci U S A*, 101(18):6940–6945, May 2004.

[134] Adam J Engler, Maureen A Griffin, Shamik Sen, Carsten G Bönnemann, H. Lee Sweeney, and Dennis E Discher. Myotubes differentiate optimally on substrates with tissue-like stiffness: pathological implications for soft or stiff microenvironments. *J Cell Biol*, 166(6):877–887, Sep 2004.

[135] Till Bretschneider, James Jonkman, Jana Köhler, Ohad Medalia, Karmela Barisic, Igor Weber, Ernst H K Stelzer, Wolfgang Baumeister, and Günther Gerisch. Dynamic organization of the actin system in the motile cells of dictyostelium. *J Muscle Res Cell Motil*, 23(7-8):639–649, 2002.

[136] Benjamin D Matthews, Darryl R Overby, Robert Mannix, and Donald E Ingber. Cellular adaptation to mechanical stress: role of integrins, rho, cytoskeletal tension and mechanosensitive ion channels. *J Cell Sci*, 119(Pt 3):508–518, Feb 2006.

[137] Stefan Diez, Günther Gerisch, Kurt Anderson, Annette Müller-Taubenberger, and Till Bretschneider. Subsecond reorganization of the actin network in cell motility and chemotaxis. *Proc Natl Acad Sci U S A*, 102(21):7601–7606, May 2005.

[138] Tatsuo Kinashi. Intracellular signalling controlling integrin activation in lymphocytes. *Nat Rev Immunol*, 5(7):546–559, Jul 2005.

[139] Donald E Ingber. Mechanosensation through integrins: cells act locally but think globally. *Proc Natl Acad Sci U S A*, 100(4):1472–1474, Feb 2003.

[140] I. Leventals, P.C. Georges, and P.A. Janmey. Soft biological materials and their impact on cell function. *Soft Matter*, 3:299–306, 2007.

[141] Dehong Zeng, Aldo Ferrari, Jens Ulmer, Alexey Veligodskiy, Peter Fischer, Joachim Spatz, Yiannis Ventikos, Dimos Poulikakos, and Ruth Kroschewski. Three-dimensional modeling of mechanical forces in the extracellular matrix during epithelial lumen formation. *Biophys J*, 90(12):4380–4391, Jun 2006.

[142] P.P. Girard, E.A. Cavalcanti-Adam, R. Kemkemer, and J.P. Spatz. Cellular chemomechanics at interfaces: sensing, integration and responses. *Soft Matter*, 3:307–326, 2007.

[143] Aurore Schneider, Grégory Francius, Rodolphe Obeid, Pascale Schwinté, Joseph Hemmerlé, Benoît Frisch, Pierre Schaaf, Jean-Claude Voegel, Bernard Senger, and Catherine Picart. Polyelectrolyte multilayers with a tunable young's modulus: influence of film stiffness on cell adhesion. *Langmuir*, 22(3):1193–1200, Jan 2006.

[144] Donald E Ingber. Cellular mechanotransduction: putting all the pieces together again. *FASEB J*, 20(7):811–827, May 2006.

[145] Adam J Engler, Shamik Sen, H. Lee Sweeney, and Dennis E Discher. Matrix elasticity directs stem cell lineage specification. *Cell*, 126(4):677–689, Aug 2006.

[146] Dennis E Discher, Paul Janmey, and Yu-Li Wang. Tissue cells feel and respond to the stiffness of their substrate. *Science*, 310(5751):1139–1143, Nov 2005.

[147] Muhammad H Zaman, Linda M Trapani, Alisha L Sieminski, Alisha Siemeski, Drew Mackellar, Haiyan Gong, Roger D Kamm, Alan Wells, Douglas A Lauffenburger, and Paul Matsudaira. Migration of tumor cells in 3d matrices is governed by matrix stiffness along with cell-matrix adhesion and proteolysis. *Proc Natl Acad Sci U S A*, 103(29):10889–10894, Jul 2006.

[148] Chirag B Khatiwala, Shelly R Peyton, and Andrew J Putnam. Intrinsic mechanical properties of the extracellular matrix affect the behavior of pre-osteoblastic mc3t3-e1 cells. *Am J Physiol Cell Physiol*, 290(6):C1640–C1650, Jun 2006.

[149] F. G. Giancotti and E. Ruoslahti. Integrin signaling. *Science*, 285(5430):1028–1032, Aug 1999.

[150] Gordon J Zwartz, Alexandre Chigaev, Denise C Dwyer, Terry D Foutz, Bruce S Edwards, and Larry A Sklar. Realtime analysis of very late antigen-4 affinity modulation by shear. *J Biol Chem*, 279(37):38277–38286, Sep 2004.

[151] R. Satcher, C. F. Dewey, and J. H. Hartwig. Mechanical remodeling of the endothelial surface and actin cytoskeleton induced by fluid flow. *Microcirculation*, 4(4):439–453, Dec 1997.

[152] Catherine G Galbraith, Kenneth M Yamada, and Michael P Sheetz. The relationship between force and focal complex development. *J Cell Biol*, 159(4):695–705, Nov 2002.

[153] G. N. Stamatas and L. V. McIntire. Rapid flow-induced responses in endothelial cells. *Biotechnol Prog*, 17(3):383–402, 2001.

[154] Cynthia A Reinhart-King, Micah Dembo, and Daniel A Hammer. The dynamics and mechanics of endothelial cell spreading. *Biophys J*, 89(1):676–689, Jul 2005.

[155] G. M. Lee and R. F. Loeser. Cell surface receptors transmit sufficient force to bend collagen fibrils. *Exp Cell Res*, 248(1):294–305, Apr 1999.

[156] Donald E Ingber. Tensegrity ii. how structural networks influence cellular information processing networks. *J Cell Sci*, 116(Pt 8):1397–1408, Apr 2003.

[157] Donald E Ingber. Tensegrity i. cell structure and hierarchical systems biology. *J Cell Sci*, 116(Pt 7):1157–1173, Apr 2003.

[158] Dimitrije Stamenović, Srboljub M Mijailovich, Iva Marija Tolić-Nørrelykke, Jianxin Chen, and Ning Wang. Cell prestress. ii. contribution of microtubules. *Am J Physiol Cell Physiol*, 282(3):C617–C624, Mar 2002.

[159] K. Yu Volokh, O. Vilnay, and M. Belsky. Cell cytoskeleton and tensegrity. *Biorheology*, 39(1-2):63–67, 2002.

[160] N. Wang, K. Naruse, D. Stamenović, J. J. Fredberg, S. M. Mijailovich, I. M. Tolić-Nørrelykke, T. Polte, R. Mannix, and D. E. Ingber. Mechanical behavior in living cells consistent with the tensegrity model. *Proc Natl Acad Sci U S A*, 98(14):7765–7770, Jul 2001.

[161] Ning Wang, Iva Marija Tolić-Nørrelykke, Jianxin Chen, Srboljub M Mijailovich, James P Butler, Jeffrey J Fredberg, and Dimitrije Stamenović. Cell prestress. i. stiffness and prestress are closely associated in adherent contractile cells. *Am J Physiol Cell Physiol*, 282(3):C606–C616, Mar 2002.

[162] Shaohua Hu, Jianxin Chen, and Ning Wang. Cell spreading controls balance of prestress by microtubules and extracellular matrix. *Front Biosci*, 9:2177–2182, Sep 2004.

[163] Sanjay Kumar, Iva Z Maxwell, Alexander Heisterkamp, Thomas R Polte, Tanmay P Lele, Matthew Salanga, Eric Mazur, and Donald E Ingber. Viscoelastic retraction of single living stress fibers and its impact on cell shape, cytoskeletal organization, and extracellular matrix mechanics. *Biophys J*, 90(10):3762–3773, May 2006.

[164] G. Forgacs. On the possible role of cytoskeletal filamentous networks in intracellular signaling: an approach based on percolation. *J Cell Sci*, 108 (Pt 6):2131–2143, Jun 1995.

[165] R. L. Satcher and C. F. Dewey. Theoretical estimates of mechanical properties of the endothelial cell cytoskeleton. *Biophys J*, 71(1):109–118, Jul 1996.

[166] Eugenia Manevich, Valentin Grabovsky, Sara W Feigelson, and Ronen Alon. Talin 1 and paxillin facilitate distinct steps in rapid vla-4-mediated adhesion strengthening to vascular cell adhesion molecule 1. *J Biol Chem*, 282(35):25338–25348, Aug 2007.

[167] Eilon Woolf, Irina Grigorova, Adi Sagiv, Valentin Grabovsky, Sara W Feigelson, Ziv Shulman, Tanja Hartmann, Michael Sixt, Jason G Cyster, and Ronen Alon.

Lymph node chemokines promote sustained t lymphocyte motility without triggering stable integrin adhesiveness in the absence of shear forces. *Nat Immunol*, Aug 2007.

[168] Robert Lugmaier, Staffan Schedin, Ferdinand Kühner, and Martin Benoit. Dynamic restacking of escherichia coli p-pili. *Eur Biophys J*, Jun 2007.

[169] M. Kantlehner, P. Schaffner, D. Finsinger, J. Meyer, A. Jonczyk, B. Diefenbach, B. Nies, G. Hölzemann, S. L. Goodman, and H. Kessler. Surface coating with cyclic rgd peptides stimulates osteoblast adhesion and proliferation as well as bone formation. *Chembiochem*, 1(2):107–114, Aug 2000.

[170] Ulrich Hersel, Claudia Dahmen, and Horst Kessler. Rgd modified polymers: biomaterials for stimulated cell adhesion and beyond. *Biomaterials*, 24(24):4385–4415, Nov 2003.

[171] E. Lieb, M. Hacker, J. Tessmar, L. A. Kunz-Schughart, J. Fiedler, C. Dahmen, U. Hersel, H. Kessler, M. B. Schulz, and A. Göpferich. Mediating specific cell adhesion to low-adhesive diblock copolymers by instant modification with cyclic rgd peptides. *Biomaterials*, 26(15):2333–2341, May 2005.

[172] Stefan V Graeter, Jinghuan Huang, Nadine Perschmann, Mónica López-García, Horst Kessler, Jiandong Ding, and Joachim P Spatz. Mimicking cellular environments by nanostructured soft interfaces. *Nano Lett*, 7(5):1413–1418, May 2007.

[173] Jörg Auernheimer, Claudia Dahmen, Ulrich Hersel, Andreas Bausch, and Horst Kessler. Photoswitched cell adhesion on surfaces with rgd peptides. *J Am Chem Soc*, 127(46):16107–16110, Nov 2005.

[174] Catherine D Reyes, Timothy A Petrie, Kellie L Burns, Zvi Schwartz, and Andrés J García. Biomolecular surface coating to enhance orthopaedic tissue healing and integration. *Biomaterials*, 28(21):3228–3235, Jul 2007.

[175] Claudia Dahmen, Jörg Auernheimer, Axel Meyer, Anja Enderle, Simon L Goodman, and Horst Kessler. Improving implant materials by coating with nonpeptidic, highly specific integrin ligands. *Angew Chem Int Ed Engl*, 43(48):6649–6652, Dec 2004.

[176] M. A. Dechantsreiter, E. Planker, B. Mathä, E. Lohof, G. Hölzemann, A. Jonczyk, S. L. Goodman, and H. Kessler. N-methylated cyclic rgd peptides as highly active and selective alpha(v)beta(3) integrin antagonists. *J Med Chem*, 42(16):3033–3040, Aug 1999.

[177] M. J. Weyant, A. M. Carothers, M. E. Bertagnolli, and M. M. Bertagnolli. Colon cancer chemopreventive drugs modulate integrin-mediated signaling pathways. *Clin Cancer Res*, 6(3):949–956, Mar 2000.

[178] Luciana Marinelli, Antonio Lavecchia, Kay-E. Gottschalk, Ettore Novellino, and Horst Kessler. Docking studies on alphavbeta3 integrin ligands: pharmacophore refinement and implications for drug design. *J Med Chem*, 46(21):4393–4404, Oct 2003.

[179] L. Marinelli, K. E. Gottschalk, A. Meyer, E. Novellino, and H. Kessler. Human integrin alphavbeta5: homology modeling and ligand binding. *J Med Chem*, 47(17):4166–77, 2004.

[180] A. Meyer, J. Auernheimer, A. Modlinger, and H. Kessler. Targeting rgd recognizing integrins: drug development, biomaterial research, tumor imaging and targeting. *Curr Pharm Des*, 12(22):2723–2747, 2006.

[181] G. T. Bolger. Bio-1211 (biogen). *IDrugs*, 3(5):536–540, May 2000.

[182] W. M. Abraham, A. Gill, A. Ahmed, M. W. Sielczak, I. T. Lauredo, Y. Botinnikova, K. C. Lin, B. Pepinsky, D. R. Leone, R. R. Lobb, and S. P. Adams. A small-molecule, tight-binding inhibitor of the integrin alpha(4)beta(1) blocks antigen-induced airway responses and inflammation in experimental asthma in sheep. *Am J Respir Crit Care Med*, 162(2 Pt 1):603–611, Aug 2000.

Table 1: Bell-parameters of adhesion molecules.

Receptor/Ligand pair	Experimental Technique	$k_{off}^I[s^{-1}]^a$	$k_{off}^O[s^{-1}]^b$	$x_\beta^I[\mathring{A}]$	$x_\beta^O[\mathring{A}]$	Reference
P-selectin/PSGL1	flow chamber[c]		1		0.3	[31]
	micropipette[c]		0.37		2.2	[26]
	AFM[d]		0.02		2.5	[33]
	AFM[c]		0.2		1.4	[34]
	bead collision[c]		0.56		1.0	[35]
L-selectin/PNAd	flow chamber[c]		6.6		0.19	[32]
L-selectin/PSGL1	micropipette[c]	100	3	0.6	4	[25]
E-selectin/ESL	flow chamber[c]		0.7		0.3	[32]
VLA-4/VCAM-1	AFM[d]	59	0.13	1.0	5.9	[47]
	AFM[c], resting	63	1.1	0.93	5.2	[47]
	AFM[c], antibody-activated	75	0.04	0.99	6.2	[47]
LFA-1/ICAM-1	AFM[c], resting	19	0.55	0.49	2.6	[30]
	AFM[c], Mg^{2+}-activated	17	0.02	0.56	3.5	[30]
LFA-1/ICAM-2	AFM[c], resting	10	0.31	1.6	4.5	[30]
	AFM[c], Mg^{2+}-activated	13	0.06	1.5	4.9	[30]
$\alpha_4\beta_7$/MADCAM-1	flow chamber[c], resting		1.28		0.41	[48]
	flow chamber[c], Mg^{2+}-activated		0.05		0.91	[48]
VE-cadherin[e]	AFM[d]		1.8		5.9	[50]
	AFM[c]		0.45		4.2	[52]
N-cadherin[e]	AFM[c]		0.98		7.7	[53]
E-cadherin[e]	AFM[c]	4.0	1.09	1.0	3.2	[53]
	flow chamber[f]		0.45		15	[51]

[a]I: inner barrier

[b]O: outer barrier

[c]cells

[d]isolated molecules

[e]homo-dimer

[f]truncated: only two outermost domains

Fig. 1 Potential landscape: The potential landscape of a receptor-ligand pair is complex. Under equilibrium conditions, the system chooses trajectories with small barriers for unbinding (blue line). The application of force can switch the trajectories and sample different pathways [25,26]. For simplification, normally the projection of the landscape along the reaction coordinate is given. External forces tilt the energy landscape and therefore lower the energy barriers. Energy barriers near the ground state are less affected and might become rate-determining, even if these barriers are lower than the main barrier under equilibrium conditions.

Fig. 2 Mechanical Models: Three standard viscoelastic models, the Maxwell body, the Voigt body and the Kelvin body are shown. They consist of different arrangements of dashpots and springs. With these models, the viscoelastic response of cells to the pulling forces can be approximated.

Fig. 3 Influence of the viscoelastic parameters on the rupture force distributions: The viscoelastic parameters have been varied over several orders of magnitude in numerical simulations to access their influence on the probability distributions of rupture forces. Obviously, the viscosity has the most impact on the force persistance among the mechanical parameters and can adjust it over a wide range of forces analogously to the off-rate.

Fig. 4 **a)** Kelvin body fit: The force-distance relation of a Kelvin body (black) was fitted to the micropipette data of Evans et al. (red) for untreated cells and latrunculin treated cells [106]. Latrunculin lowers the viscosity due to the viscous slip of the membrane over the impaired cytoskeleton. The fit parameters for untreated cells were used for the Monte Carlo Simulations in subfigure 3b.**b)** Monte Carlo Simulation: The simulated force-velocity relations are based on the viscoelastic parameters derived from the Kelvin body fit in subfigure 3a and on the off-rates and potential widths measured with different techniques (lines to guide the eye) [26, 31, 33, 34]. Compared to the data points of Evans et al. (red diamonds) [106], the simulation with the off-rate and potential width of Fritz et al. (empty diamonds) [33] obtained from single-molecule AFM experiments agree best with the experimental data of Evans et al. [106].

Fig. 5 Different possibilities to vary the receptor mechanics: In the middle panel, a transmembrane adhesion receptor holds to a fibre of the extracellular matrix. During receptor clustering (upper panel), the receptors are linked by an intracellular protein at their cytoplasmic tails [5,6,22,124]. If the cytoskletal attachment of the receptor surrounding membrane is enhanced by actin binding proteins (right panel), the viscous slip of the membrane over the cytoskeleton is hindered. After activation, the receptors are often re-distributed into lipid rafts (lower panel) [126], which are stiffened by the inclusion of cholesterol. Many adhesion receptors can also bind to the cytoskeleton via cytoplasmic adaptor proteins (left panel) [15, 166].

Fig. 6 A model for mechanotransduction: **a)** If there is no force applied to the transmembrane receptor R, the inhibitor I blocks the substrate binding pocket of the enzyme E, so that the substrate S cannot be processed. **b)** If a force is applied to the receptor, the inhibitor is moved and the substrate can bind to the enzyme.

Fig. 7 Geometry of cell adhesion in the shear flow: **a)** If the adhesion receptor is attached to the cytoskeleton, the cell is flattened by the flow (arrow) and makes a large contact area

with the substrate. **b)** If the adhesion receptor is only anchored in the cell membrane, a membrane tether is extruded from the cell.

Figure 1:

27

Kelvin body

g　　　k_i

k_t

Maxwell body

g　　　k_i

Voigt body

g

k_t
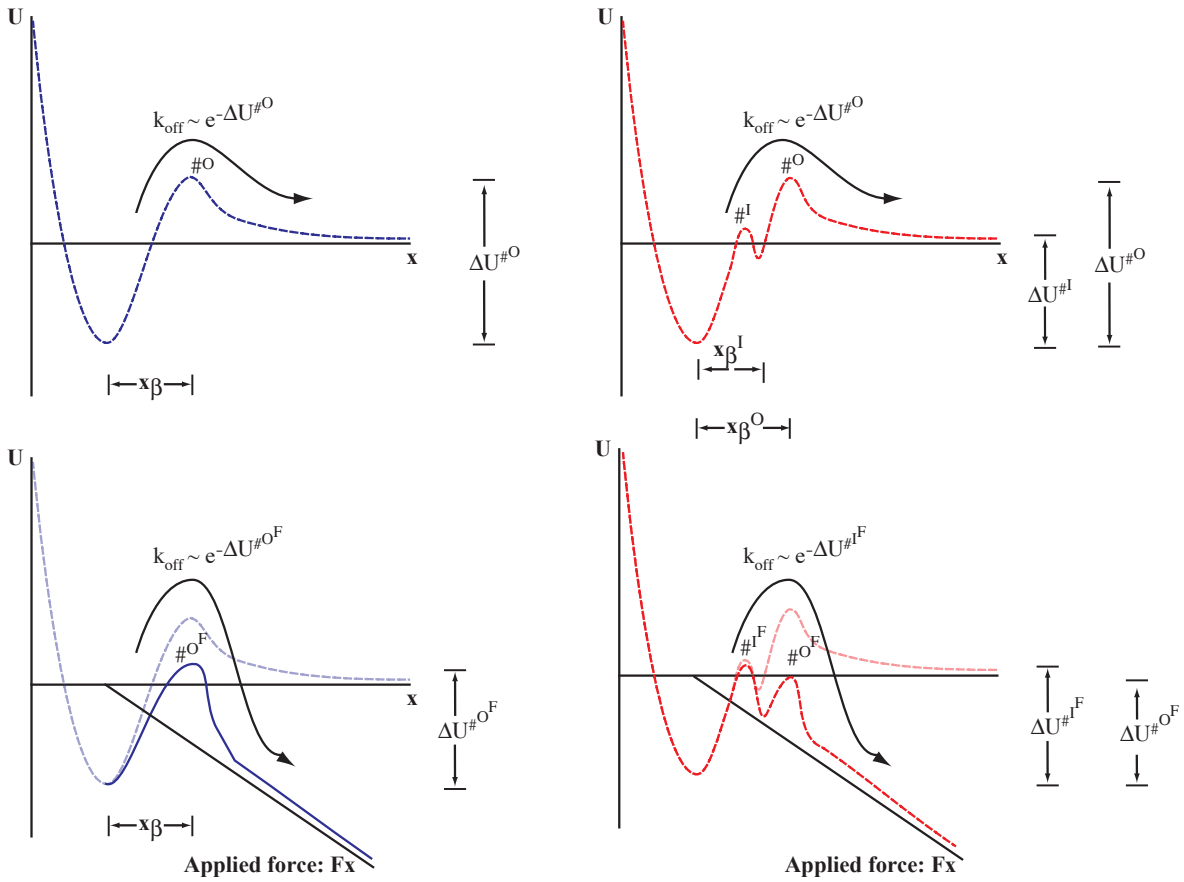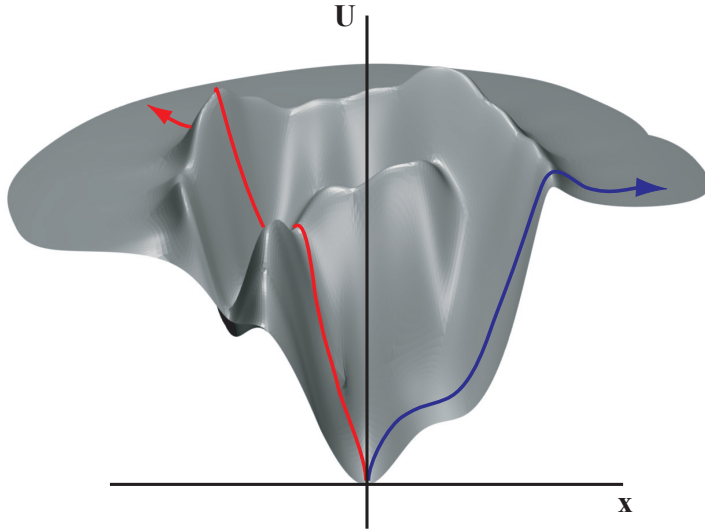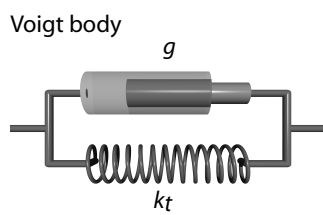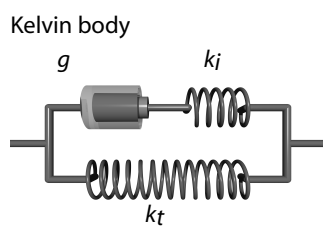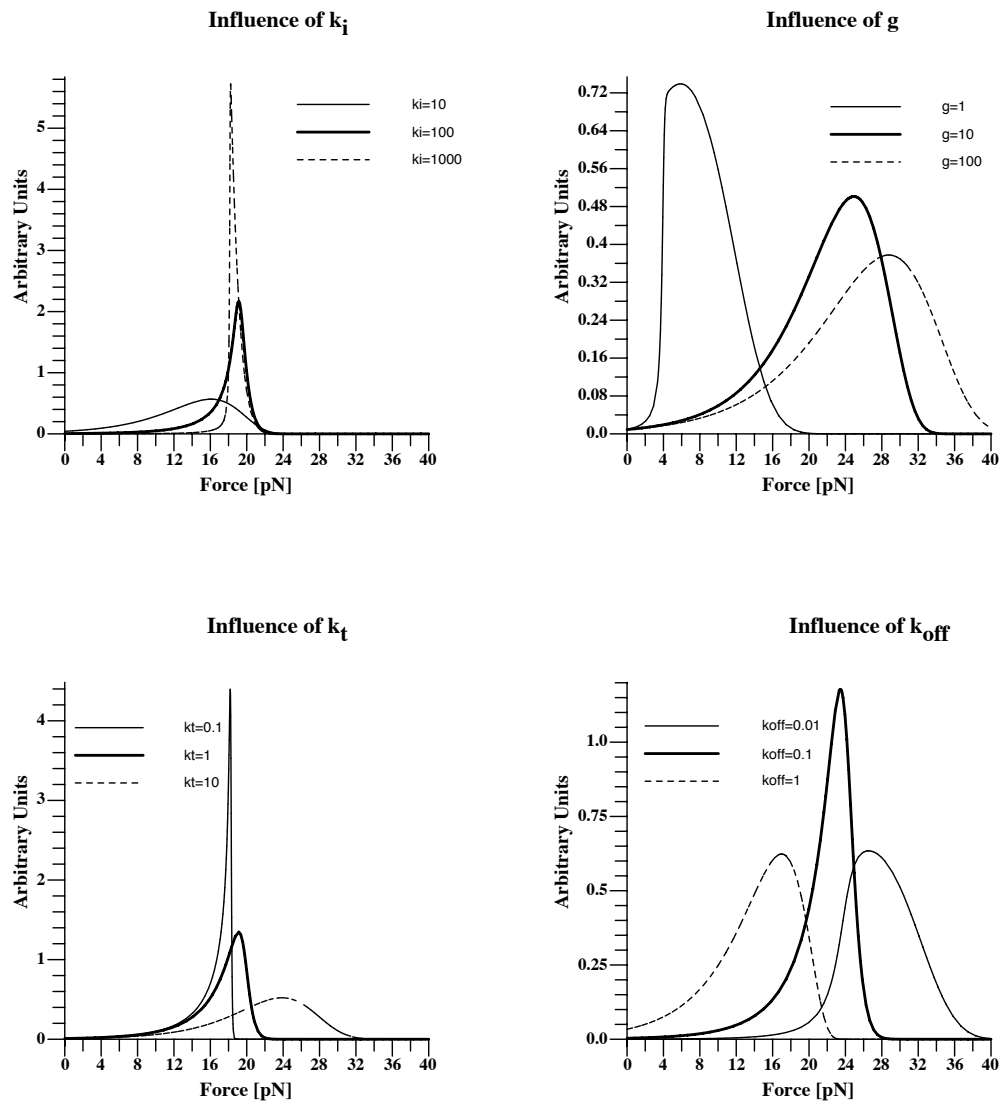
Figure 2:

Figure 3:

Figure 4:

Figure 5:

F
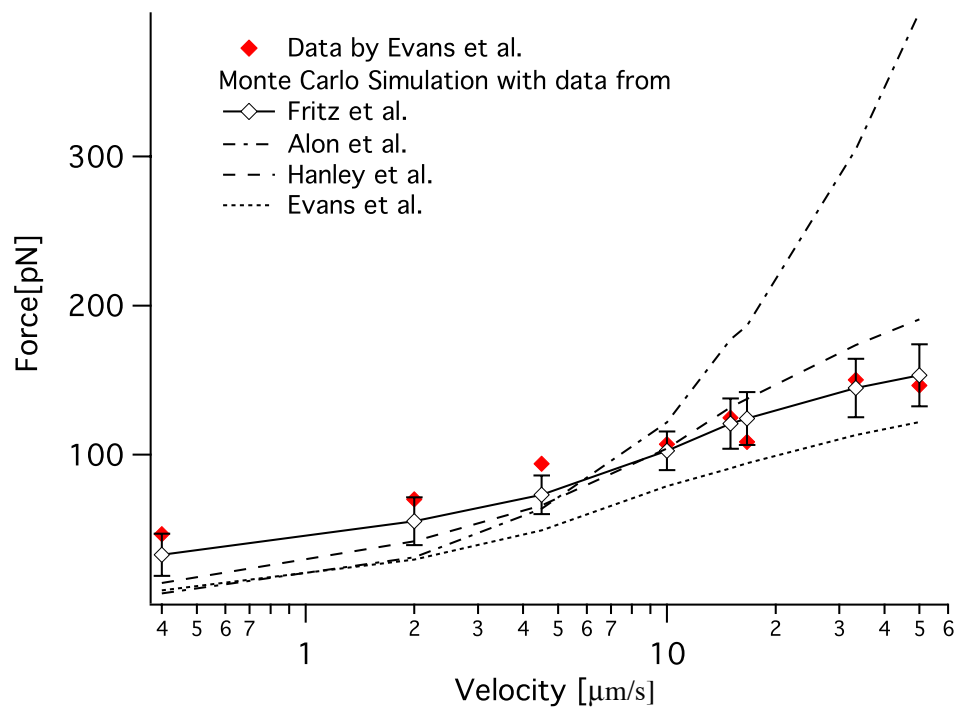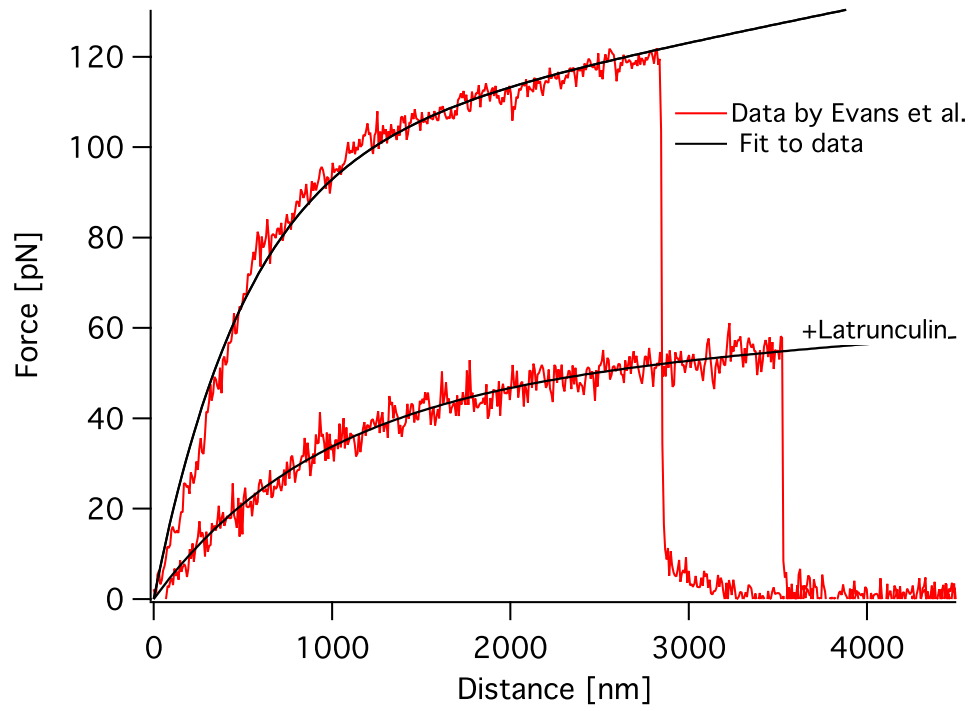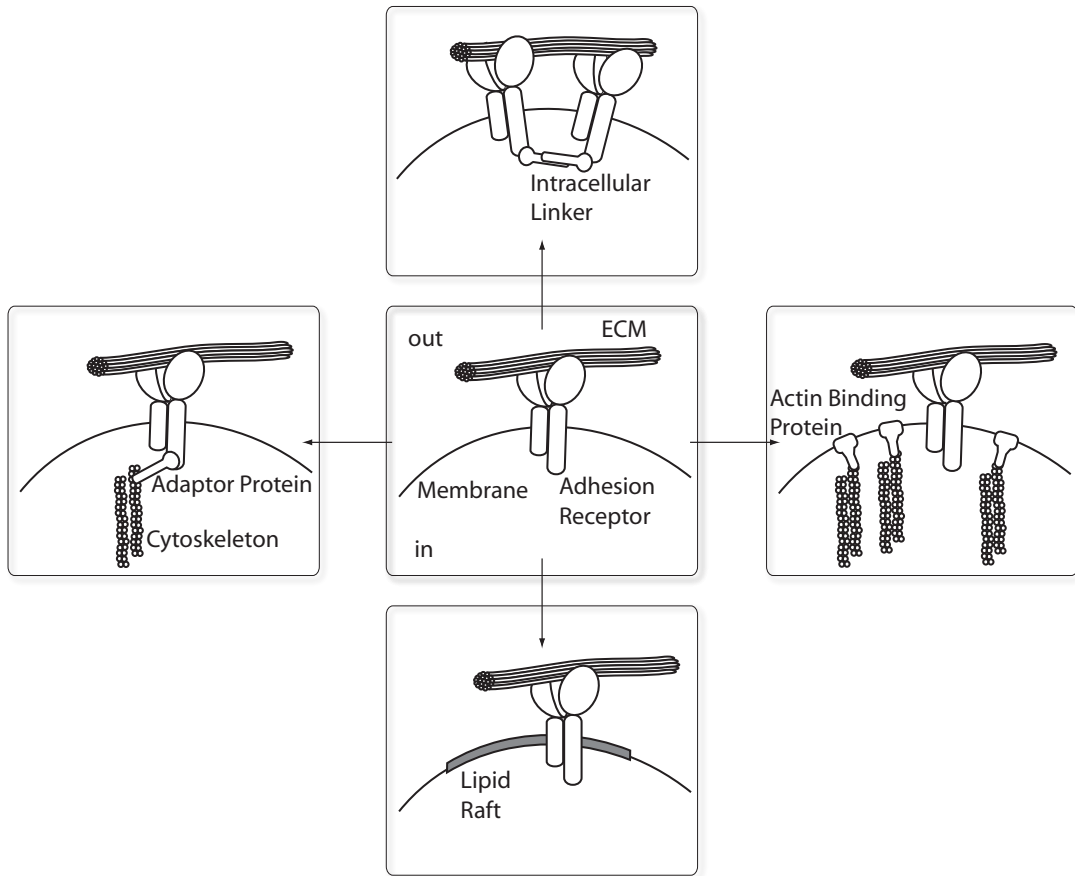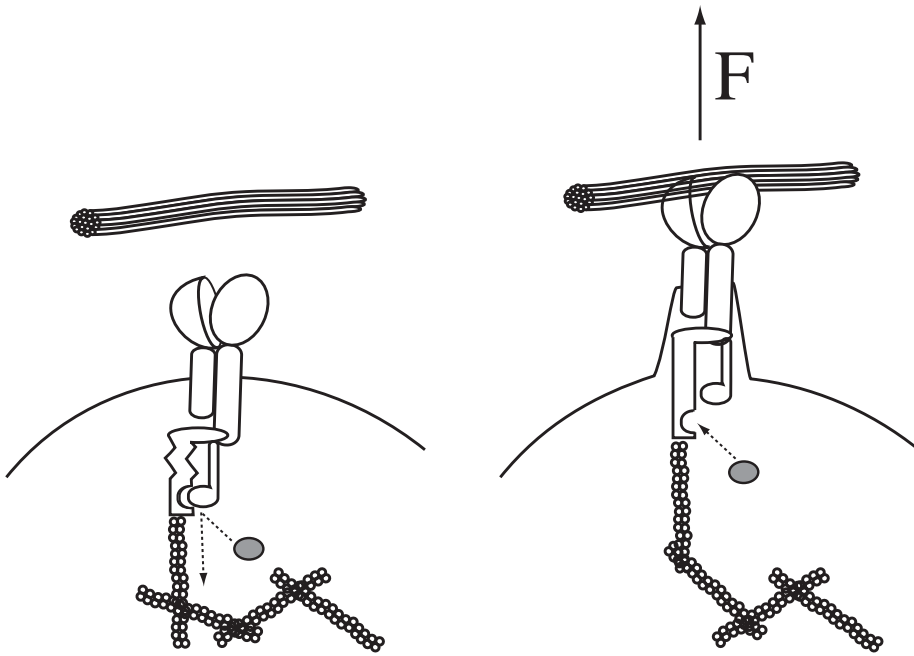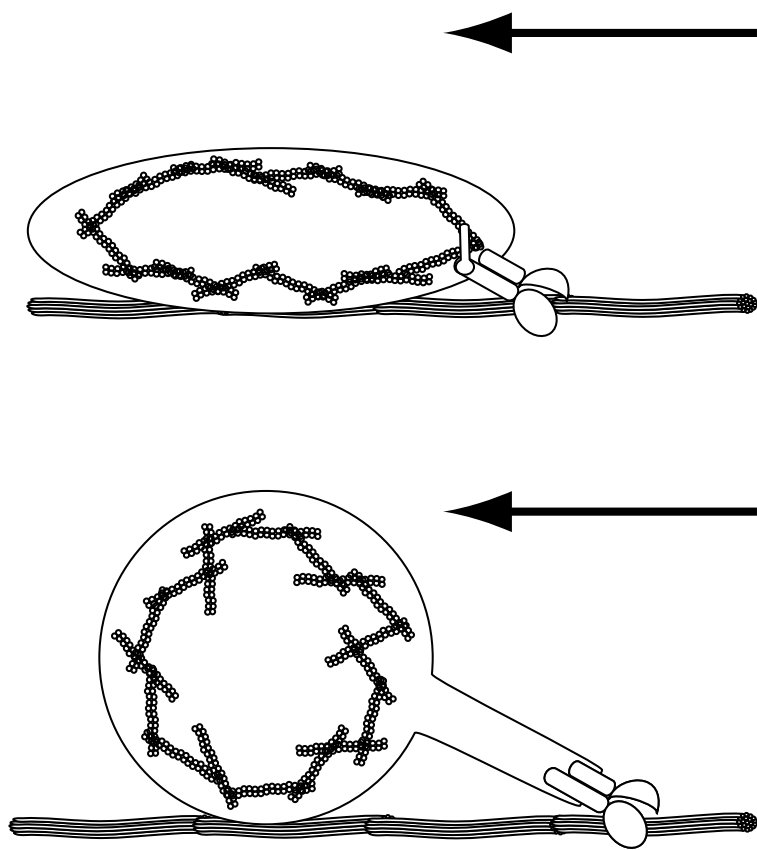
Figure 6:

Figure 7:

Chapter 3

Activation of the Integrin VLA-4 by the Chemokine SDF-1

The recruitment of lymphocytes to the site of inflammation or injury is regulated by the expression of certain adhesion and signal molecules on the adjacent endothelium. During rolling, the lymphocyte integrins are activated in situ by chemokines within subseconds [128, 129]. These signal molecules bind to Gi-protein coupled receptors (GPCRs) on the lymphocytes and initiate intracellular signal cascades aiming at the cytoplasmic tails of the respective integrins. This so-called inside-out signalling induces firm lymphocyte adhesion [130, 131], which is necessary for the subsequent extravasation to the target tissue. Integrins occur in sundry states differing in their conformation, in the affinity to the ligand and in the cellular anchorage of the receptors [14, 132]. All these states coexist in a dynamic equilibrium on the cell surface. Agonistic stimuli as the exogenous activation with divalent cations or the inside-out signalling of chemokines shift the equilibrium between the populations in favour of an adhesion promoting receptor state.

In this chapter, we investigate the activation of the lymphocyte integrin VLA-4 by the chemokine SDF-1 co-immobilised to the integrin ligand VCAM-1. By the means of single-molecule force spectroscopy on living T-lymphocytes, we found that the crosstalk between the chemokine receptor and the integrin implicates mechanical alterations of the VLA-4 anchorage, rather than inducing pre-ligand conformational changes in the integrin ectodomain. In the flow chamber – mimicking the physiological situation of the blood stream – the mechanical stiffening of the VLA-4/VCAM-1 bond precipitated an immediate increase of the cellular adhesiveness.

3.1 Chemokine-Triggered Mechanical Activation of the Integrin VLA-4

The chemokine SDF-1 binds to the Gi-protein coupled receptor CXCR-4 and was found to present a potent stimulator of the integrins LFA-1 and VLA-4 [133, 134, 135]. A common paradigm in integrin research is that the activation by chemokines induces pre-ligand

binding conformational changes such as the integrin extension and the opening of the head group, as observed, e.g., for LFA-1 [131]. However, the integrin VLA-4 activated by SDF-1 neither displayed activation epitopes nor increased affinity to its ligand VCAM-1 [136, 106, 129]. Furthermore, it was shown that surface-bound SDF-1 only promotes the cellular adhesiveness in the presence of external forces [137], thus indicating the involvement of mechanics in the regulation of VLA-4-mediated cell adhesion.

We scrutinised the effect of SDF-1 co-immobilised to VCAM-1 with single-molecule force spectroscopy. Despite a contact time of a mere 100 msec on the substrate, the presence of SDF-1 strengthened the VLA-4/VCAM-1 bond, whilst the rupture lengths were drastically reduced. For substrates functionalised only with the chemokine, SDF-1 on its own showed no adhesive activity for the lymphocytes. Together with blocking experiments with BIO1211 [138], this underlines the specificity of the measured interactions. Co-immobilising P2G instead of SDF-1 with VCAM-1 (a mutant of SDF-1 with retained affinity for the CXCR-4 receptor but lacking signalling activity [139]) had no effect compared with pure VCAM-1 substrates. Furthermore, the change of the mechanical anchorage of VLA-4 in the presence of SDF-1 could be abrogated with pertussis toxin, verifying the dependence on GPCR-signals. Taking a closer look of the distribution of rupture forces, we discovered a bimodal force distribution for the SDF-1-activated lymphocytes. Compared to the force histogram obtained without SDF-1, the distribution of activated cells contained a second peak at higher forces. This indicates the coexistence of two VLA-4 populations on the lymphocyte in the presence of SDF-1 both differing in their bond strength: One integrin population is activated by the chemokine, the other remains unaffected. To examine the mechanical nature of the two populations, we separated the data into a high- and a low-force population. Since the shape of the force curves is governed by the receptor mechanics (see chapter 2), we went on to compare the force evolution of the low- and the high-force population and found the initial slope of the force curves to be markedly higher for SDF-1-stimulated cells. Hence, the physiological activation of the integrin VLA-4 by the chemokine SDF-1 caused a stiffening of the VLA-4 anchorage in the cell.

Whilst we did not notice any agonistic effect of the chemokine on the interaction frequency in the AFM setup, the co-immobilisation of SDF-1 and VCAM-1 drastically enhanced the cellular adhesiveness in the fast-camera flow chamber setup. Remarkably, two populations of interacting cells were observed for co-immobilised chemokine in the shear flow. One population displayed comparable interaction times to those on on pure VCAM-1 substrates, whereas the other population exhibited even shorter times. Since diluting the VCAM-1 density did not lead to a further reduction of the interaction times, this indicates that very few VLA-4 bonds are sufficient for mediating cellular interactions in the shear flow on a substrate with VCAM-1 and SDF-1.

Our experiments demonstrate that the GPCR-dependent intracellular signalling prompted by SDF-1 induces a mechanical regulation of the VLA-4-mediated adhesiveness, rather than affecting the affinity of the integrin or the number of available active receptors. According to the physical theory of bond dissociation under forces (compare equation 1.3), a reduced mechanical compliance raises the force loading on the adhesive bond and increases the bond strength. Hence, the mechanical stiffening of the integrin environment readily

explains the enhanced cellular adhesiveness observed in the flow chamber.

These results have been submitted to the Journal of Cell Biology and are reprinted in section 3.3.

3.2   Conclusions

Our findings reveal a mechanical modulation of the VLA-4-mediated cellular adhesiveness in response to the activation by the chemokine SDF-1. It has been shown that talin is implicated in chemokine-triggered adhesiveness of the integrin VLA-4 and maintains the integrin in the high-affinity conformation [136]. The observed stiffening of the VLA-4 anchorage may thus be due to the association of talin to the cytoplasmic β_1 tail linking the integrin to the actin cytoskeleton [131]. In contrast to an upregulation of the integrin affinity or the integrin number, an intracellular mechanical regulation has the advantage, that the adhesion strengthening is only achieved if the adhesive bond is probed by external forces. The stiffening of the receptor anchorage functions therefore as a force sensor, enabling the cell to identify different environments and to differentiate, e.g., between the shear-free surroundings of the lymphatic tissue and the blood stream. Furthermore, the increased force loading on the adhesive bond may facilitate post-ligand conformational changes in the integrin ectodomain, thus requiring a dual stimulation by forces and ligand binding [106]. This outlines the effectiveness of a mechanical regulation which is indeed exploited by the cell in physiological situations.

3.3   Publications

1. Chemokine-Triggered Modulation of Lymphocyte Adhesion by a Mechanical Integrin Activation (*submitted to the Journal of Cell Biology*)

Chemokine-Triggered Modulation of Lymphocyte Adhesion by a Mechanical Integrin Activation.

Julia Schmitz[1], Eugenia Manevich[2], Martin Benoit[1],

Ronen Alon[2], Kay-Eberhard Gottschalk[1*]

[1]Chair of Applied Physics and Centre for NanoSciences,

Ludwig-Maximilians University,

80799 Munich, Germany.

[2]Department of Immunology,

Weizmann Institute of Science

Rehovot, 76100, Israel.

[*]To whom correspondence should be addressed:

E-mail: kay.gottschalk@physik.uni-muenchen.de.

Number of Characters: 17146

Firm lymphocyte adhesion to the endothelium is mediated by integrins. Endothelial chemokines activate lymphocyte integrins by transducing inside-out signals targeted at the cytoplasmic interface of the integrin. These signals are thought to induce conformational integrin activation due to integrin extension and head-piece activation before the integrin encounters its ligand. This pre-ligand binding conformational activation has not been observed for the lymphocyte integrin VLA-4 despite strongly increased chemokine-triggered VLA-4-mediated cellular adhesion under force, implicating a non-canonical VLA-4 activation. Here, we scrutinize with single-molecule force spectroscopy and fast camera flow chamber studies the VLA-4-activation triggered by the chemokine SDF-1. We observe on the single-molecule level in living cells a strengthened bond of the integrin VLA-4 to its endothelial ligand VCAM-1 caused by a drastically stiffened VLA-4 environment. This implicates chemokine signaling in a new mechanical level of integrin activation, which facilitates conformational changes in the integrin ectodomain post- rather than pre-ligand binding.

Introduction. Integrins are heterodimeric cell adhesion receptors involved in the immune response, hemostasis, cancer metastasis and in auto-immune diseases. Integrin mediated cellular adhesiveness is modulated by intracellular and extracellular signals. The ability of integrins to respond to endothelially presented chemokine signals is crucial for the leukocyte recruitment to the target tissue and their homing to lymph nodes (Alon et al., 2003). This *in situ* activation of lymphocyte integrins initiates firm cell adhesion within subseconds (Grabovsky et al., 2000). Classically, chemokines are thought to modulate integrin affinity via inside-out signaling involving conformational re-arrangements prior to ligand binding (Kinashi, 2005; Laudanna and Alon, 2006). This canonical conformational integrin activation by chemokines was demonstrated for the lymphocyte integrin LFA-1 (Shimaoka et al., 2006). However, for the lymphocyte integrin VLA-4, no activation epitopes were detectable after exposure of cells to prototypic integrin activating chemokines like SDF-1 (CXCL12), and VLA-4 affinity to soluble VCAM-1 was not altered by such exposure (Manevich et al., 2007; Shamri et al., 2005). Therefore, classical models of signal-induced affinity increase of the integrin cannot explain the effect of the chemokine SDF-1 on VLA-4-mediated cellular adhesiveness.

Firm VLA-4 mediated lymphocyte adhesion is physiologically triggered when lymphocytes encounter VCAM-1 in juxtaposition to integrin-stimulatory chemokines displayed on blood vessel endothelial cells (Grabovsky et al., 2000). SDF-1, the ligand of the Gi-protein coupled receptor (GPCR) CXCR-4 (Lapidot et al., 2005), is the most potent VLA-4 stimulatory chemokine tested to date. However, even the potent signals of the chemokine

SDF-1 and other chemokines failed to induce firm T-lymphocyte adhesion in the absence of external forces (Woolf et al., 2007), demonstrating the need for two external stimuli for firm VLA-4 mediated cell adhesion, one biochemical (SDF-1) and the other mechanical (force).

This led us to hypothesize that potent, VLA-4 activating chemokines such as SDF-1, if immobilized to surfaces, induce mechanical changes in the integrin environment, facilitating an enforced conformational activation of the integrin only post-ligand binding rather than pre-ligand binding. To test this hypothesis, we used singe-molecule atomic force microscopy (AFM) on living T-lymphocytes. We found an SDF-1-triggered increase in the strength of the VLA-4/VCAM-1 bond. The increase in bond strengths was accompanied by a decrease in bond-duration together with a stiffer integrin environment as a result of Gi protein signaling. Furthermore, we demonstrated with fast-camera flow chamber studies that the SDF-1 triggered increased bond strength drastically enhances VLA-4 mediated cellular adhesiveness to VCAM-1 under shear flow. Our results on both the single molecule level and on the cellular level suggest that the receptor crosstalk between CXCR-4 and VLA-4 involves a mechanical modulation of VLA-4 adhesiveness. The ability of the cell to influence adhesiveness by specifically altering its mechanics constitutes a new level of chemokine-triggered cellular adhesion regulation.

Results and Discussion. A living lymphocyte presenting and regulating the integrin VLA-4 was attached to the AFM cantilever and gently pushed onto a ligand-functionalized substrate. The indentation force was set to be ~100 pN. After a dwell time of 0.1 s, the cantilever together with the attached T-lymphocyte was retracted (Figure 1). The VCAM-1 density on the substrate was optimized to reach adhesion rates below 30%. This ensured that the majority of ruptures corresponds to single-molecule events (Benoit et al., 2000; Benoit and Gaub, 2002). The VCAM-1 coating density, at which we reached this adhesion rate, corresponds to 100 sites/μm^2. With this density, the average distance between the VCAM-1 molecules on the surface is larger than the average radius of a microvillus, a strong indication for the observation of single-molecular interactions when observing a single rupture in the force-distance curve.

The force-distance curves obtained with the AFM were recorded with pN accuracy and evaluated. Since physiologically, endothelial chemokines are presented in juxtaposition to integrin ligands (Lapidot et al., 2005), we compared the interaction of the lymphocyte integrin VLA-4 and its ligand VCAM-1 in the presence and absence of the chemokine SDF-1 co-immobilized with VCAM-1. Importantly, VCAM-1 density was kept constant with and without co-immobilized SDF-1. During the chosen contact time of 0.1 s, VLA-4 can readily be activated by juxta-posed chemokines, as was shown in previous studies(Grabovsky et al., 2000).

Using AFM, we found that SDF-1 co-immobilized to VCAM-1 exerted significant effects on the distribution of rupture forces. The median of rupture forces increased from 23.9 pN in

the absence of SDF-1 to 30.2 pN in the presence of SDF-1, a highly significant rise (p<0.001). Only in the presence of co-immobilized SDF-1, more than 50% of the ruptures showed rupture forces of >30 pN (Figure 2). In contrast to this chemokine triggered VLA-4 activation, artificial integrin-activation introduced with 5mM Mg^{2+} in the absence of Ca^{2+}, conditions known to activate the integrin ectodomain independent of inside-out signaling, did not strongly influence the distribution of rupture forces (Figure 2).

To test whether the SDF-1 triggered strengthened adhesion is induced by a mere increase of the surface adhesiveness to the T-cell due to the co-immobilization of the chemokine or caused by the signaling of the chemokine through its Gi-protein coupled receptor CXCR4, present in the T-lymphocyte, two controls were performed: first, the cells were pre-treated with pertussis toxin (PTX), a toxin that inhibits Gi-protein signaling and blocks integrin activation(Grabovsky et al., 2000; Shamri et al., 2005), but does not interfere with SDF-1 binding to CXCR4. Second, we co-immobilized P2G, a non-signaling point mutant of SDF-1. P2G binds with similar affinity to the chemokine receptor, CXCR4, but fails to mount any Gi-protein activity (Crump et al., 1997; Grabovsky et al., 2000). Notably, the pre-treatment of the cells with PTX reverted the effect of co-immobilized SDF-1 (Figure 2). Furthermore, the P2G co-immobilized with VCAM-1 had no significant effect on the rupture forces of VLA-4 interacting with VCAM-1 alone. These two findings collectively indicate that the observed increase in rupture force of the VLA-4/VCAM-1 bond triggered by co-immobilized SDF-1 involves G-protein signaling to VLA-4, but is not caused by a mere co-adhesive interaction between CXCR-4 and the immobilized SDF-1.

The rupture forces had a bimodal distribution only after co-immobilization of SDF-1. The lower peak of the bimodal distribution at 19.5 pN compared well with the maximum of the force distribution obtained with VCAM-1 alone at 22.5 pN, while the higher peak at 31.5 pN did not appear without co-immobilized SDF-1. The bimodal distribution is an indicator of the co-existence of at least two populations of the VLA-4 on the surface of T cells after interacting with the VCAM-1/SDF-1 substrate. The detection of these subsets requires the use of studies on the single molecule level. One subset of VLA-4 is activated by SDF-1, while the other subset remains non-activated. The distribution of rupture forces is dependent on the basal off-rate of the integrin-ligand bond. However, the stiffness of the linkage that anchors the integrin to the membrane and the underlying cytoskeleton of the T-lymphocyte has the identical influence on the rupture force as has the basal off-rate (Evans, 2001). Therefore, the bimodal rupture force distribution indicates that for the SDF-1 activated subset of VLA-4 integrins, the kinetics of the VLA-4/VCAM-1 bond or the stiffness of the environment of VLA-4 (or both) are modulated by the co-immobilized SDF-1.

Surprisingly, the duration of the cell-to-substrate adhesion mediated by single VLA-4/VCAM-1 interactions did not increase by SDF-1 triggered G-protein signaling. Rather, SDF-1 induced significantly shorter rupture lengths and short-lived bonds. The rupture length decreased from a median of ~620 nm in the absence of SDF-1 to a median of ~310 nm in the presence of SDF-1 (p<0.001). In contrast to SDF-1 co-immobilization, the treatment of the T-lymphocytes with 5 mM Mg^{2+} did lead to longer rupture lengths with a median of ~1100 nm,

an indication of slower dissociation kinetics of the VLA-4-VCAM-1 bond or of the existence of multiple bonds in the presence of this integrin activating cation (Figure 2).

Taken together, the effect of SDF-1 signaling on rupture force and length of the VLA-4/VCAM-1 bond cannot be explained by a mere chemokine-induced affinity modulation of this bond. A pure decrease in the basal off-rate would stimulate longer ruptures, as observed for the Mg^{2+} activated integrins, in contrast to the here observed effect caused by SDF-1. An increase of the basal off-rate, which would induce shorter ruptures, would on the other hand lower the average rupture force, again in contrast with our findings.

To scrutinize the additional modulatory effects caused by SDF-1 signalling, we examined the mechanical changes stimulated by the ultra-short T-cell interaction with the immobilized SDF-1. To this end, we went on to deduce the mechanical properties of the T-lymphocyte in close vicinity to the probed receptors from the AFM force-distance curves. The shape of the force-distance curves is determined by the integrin anchorage within the cell (Evans and Kinoshita, 2007). Since the bimodal force distribution revealed the existence of at least two receptor populations, we separately analyzed the high- (>25pN) and the low- (<25pN) force population, comparing cells that encountered VCAM-1 alone with cells interacting with SDF-1 co-immobilized to VCAM-1. As a measure for the mechanics of the local VLA-4 environment in the T-lymphocyte, we analyzed the initial slope of the force-distance curve, revealing the early force-loading of the receptor-ligand bond. Only force curves with one single rupture were analyzed. Our measurements show that this initial slope (Figure 3A) was strongly influenced by SDF-1 signaling. Interaction of the cell with SDF-1 co-immobilized to VCAM-1 increased the initial slope from 0.26 pN/nm in the absence of

SDF- to an initial slope of 0.51 pN/nm in the presence of SDF-1 for the high force population. For the non-activated low-force population, on the other hand, the initial slope is significantly less increased from 0.23 pN/nm in the absence of SDF- to an initial slope of 0.38 pN/nm in the presence of SDF-1 (Figure 3).

Although the low-force population displayed unaltered rupture forces compared to the untreated cells, these ruptures still exhibited steeper force curves in cells interacting with SDF-1. The unaltered rupture force of this receptor population indicates that the majority of VLA-4 in this population are non-activated integrins that are less strongly attached to the cytoskeleton compared to the SDF-1 stimulated VLA-4 receptors that mediate the high force population. However, the shorter ruptures show a global cellular stiffening.

AFM measures with high precision the response of a single receptor-ligand bond to force. As the force probe detaches and moves away from the adhesive substrate, it minimizes the probability of rebinding between cell-surface receptors and immobilized ligands on the counter-surface. However, cells adhering to an adhesive substrate under shear flow can stabilize a multifocal contact area usually generated by microvilli, of which each can rebind after local attachment of a neighbor microvillus (Schwarz and Alon, 2004). Notably, the geometry of force application is also different in the AFM setup than in the blood stream: in the AFM, the force is exerted perpendicular to the surface, while in the blood stream, it is exerted parallel to the surface. These two factors may strongly affect the adhesiveness of the cell under force. To examine, how the observed stiffening of the receptor anchorage affects VLA-4 mediated adhesions under shear flow mimicking the blood stream, we performed flow chamber studies using the same T-cells and identical substrates functionalized by VCAM-1

with co-immobilized SDF-1. Cell interactions were monitored by fast camera video-microscopy, which provided a 10 fold higher temporal resolution than previous flow chamber measurements of VLA-4 activation by immobilized SDF-1 (Grabovsky et al., 2000). As reported earlier (Grabovsky et al., 2000), SDF-1 stimulated VLA-4 adhesiveness to VCAM-1 in a PTX sensitive manner (data not shown) and all adhesions were VLA-4-specific, as they could be blocked with the selective VLA-4 blocker, Bio1211. A significant increase in VLA-4 mediated cellular adhesion to VCAM-1 was triggered by co-immobilized SDF-1 (Figure 4). Hence, the adhesion strengthening observed in the AFM experiments correlated with the strong increase in the frequency of successful, VLA-4 mediated interactions in the flow chamber.

Interestingly, in the flow chamber, two cell populations were observed on the adhesive VCAM-1 coated surface, when SDF-1 is co-immobilized: in the ultra-short adhesion regime, VLA-4 stimulated by SDF-1 supported significantly more interactions with VCAM-1 with dwelling times in the range of <0.1 s. These adhesions dissociated faster than the adhesive interactions of VLA-4 with VCAM-1 in the absence of SDF-1 (Fig. 4). In the long adhesion regime, the VLA-4/VCAM-1 mediated cellular off-rates under force were comparable between the SDF-1 stimulated T-lymphocytes and the off-rates of resting cells in the absence of co-immobilized SDF-1 (Figure 4). Hence, also in the flow chamber two subsets of receptors, one activated and one non-activated, can be resolved. Further dilution of VCAM-1 did not further increase the off-rate of VLA-4 mediated interactions. Therefore, the observed distributions of cell attachments suggest that under these experimental conditions of low-density VCAM-1 coating, the flow chamber approaches the single-molecule limit and that

even very few integrin-ligand bonds are sufficient to hold the cell to the VCAM-1 substrate with co-immobilized SDF-1.

Collectively, the flow chamber and AFM data show that a threshold strength of the molecular bond is required to adhere the cell under the influence of the laminar blood flow that prevails in post capillary venules, where most physiological VLA-4/VCAM-1 interactions take place. We describe a new modality of VLA-4 activation whereby SDF-1 increases the VLA-4-VCAM-1 bond strength by stiffening the receptor environment. Thus, the altered force loading of single, SDF-1 stimulated VLA-4/VCAM-1 bonds observed in the AFM is the basis for the dramatic SDF-1 triggered rise in productive VLA-4 attachments to VCAM-1 measured in the flow chamber. Our force-spectroscopic results of single VLA-4 bonds in living T-cells strongly suggest, that at least two populations of this integrin coexist on the surface of cells after *in situ* activation by immobilized SDF-1. As judged from the steep increase in force after cellular stimulation with immobilized SDF-1, we conclude that one set of VLA-4 is directly bound to the cytoskeleton, probably via the association of paxillin and/or talin with the cytoplasmic tails of the alpha4 and beta1 subunits, respectively(Alon et al., 2005; Manevich et al., 2007). The activation of the VLA-4 in living T-lymphocytes occurs in less than 100ms and results in a drastically changed receptor environment.

The attachment of a receptor to the cytoskeleton prevents membrane-tether pulling. However, the actin-rich microvillus becomes stretched, leading to a steep increase in force with time (Evans et al., 2005). The cytoskeletal anchorage detected here to be in situ stimulated by SDF-1 signals has been previously suggested to control the mechanical stability of integrin and selectin bonds(Alon et al., 2005; Brakebusch and Fassler, 2003; Calderwood et

al., 2000; Dwir et al., 2001; Liu et al., 2000; Rosenthal-Allieri et al., 2005; Schwarz and Alon, 2004; Wiesner et al., 2005). Recently, it has been impressively demonstrated how the mechanical properties of the extracellular matrix influence the behavior of cells. Depending on the stiffness of the matrix, stem cells develop differently (Engler et al., 2006). In addition, the migrational properties of cancer cells are dependent on the mechanical properties of the environment (Zaman et al., 2006). Our present work is the first demonstration of a local chemokine signal that stiffens the integrins environment and thereby increases the force loading of the adhesive receptor. Therefore, our results are strong evidence that cells actively modulate their own mechanical properties to influence the effect of force on the cells, and do not only respond to the mechanical properties of the environment.

From a physical point of view, increasing the force-persistence of a molecular bond by environmental stiffening is a general mechanism enhancing adhesiveness in the presence of external forces also for integrins with chemokine-triggered conformational activation: It has been shown (Evans and Ritchie, 1999) that the distribution of forces $p(f)$ needed to break a non-covalent protein-protein bond is equally dependent on the off-rate in the absence of forces k_{off}^{0} and on the mechanical properties of the environment, quantified by its compliance $c(f)=\partial z/\partial f$, where z is the extension of the system and f the applied force (equation 1):

$$p(f) = \exp(f \bullet x_{\beta}/k_B T)/v \bullet k_{off}^{0} \bullet c(f) \bullet \exp(-\int \exp(f \bullet x_{\beta}/k_B T)/v \bullet k_{off}^{0} \bullet c(f) \bullet df) \ (1).$$

Here, f is the acting force, x_{β} the potential width, k_B the Boltzmann constant, v the velocity of force application, T the temperature, k_{off}^{0} the basal off-rate and $c(f)$ the compliance of the system. Stiffening the environment influences $c(f)$, which as shown above has a direct impact on $p(f)$. This impact of the compliance is identical in magnitude to the influence of the basal

off-rate, k_{off}^0. Hence, the cell has at least two means of modulating the force-persistence of the receptor-ligand bond: (1) by altering the basal off-rate k_{off}^0, which mostly can be performed by regulated conformational changes and (2) by altering the mechanical properties of the receptor environment, which changes the cells' extensibility and thereby the compliance $c(f)$. The second possibility has the appeal to influence the receptor-ligand bond only in the presence of external forces. Thus, environmental stiffening is a convenient implementation of an adhesion strengthening force sensor independent of downstream signaling events.

This study opens up a wide field for probing rapid mechanical changes in single transmembrane molecules by AFM, and for deducing the role of specific cytoskeletal associations of the surface receptors in these changes.

Materials and Methods.

Reagents

BSA (fraction V), HSA (fraction V) and HBSS (without calcium/magnesium) were purchased from Sigma-Aldrich. Recombinant human VCAM-1 (sVCAM-1, recombinant ectodomain of the 7 domain human VCAM-1), SDF-1alpha (CXCL12) and anti-human CD43 mAb were purchased from R&D Systems. BIO1211 was a generous gift from Blake Pepinsky (Biogen Inc. Cambridge MA). The SDF-1 mutant P2G was given by Ronen Alon.

Cells

Jurkat T-cells were cultured in RPMI1640 (Biochrom AG) supplemented with 10% heat inactivated FCS, 2mM L-glutamine and penicillin/streptomycin in 5% CO2 at 37°C. Just

before experimentation, the cells were rinsed with 5 mM EDTA and transferred to binding medium (HBSS with 2 mg/ml BSA, 1 mM $CaCl_2$, 1 mM $MgCl_2$, 10 mM HEPES).

Substrate preparation

VCAM-1 was incubated over night at 4°C in the lid of a Petri dish in the concentration of 0.05-0.2 mg/ml together with the carrier protein HSA (2 mg/ml). This gives a VCAM-1 density of 100-400 sites/μm^2 as determined by radioimmunoassay (Grabovsky et al., 2000). After VCAM-1 adsorption, the spots were washed four times with PBS and either blocked with 2% HSA in PBS for >1 h at 4°C or incubated with SDF-1 (2mg/ml in PBS) for 3 h at 4°C. After SDF-1 adsorption, the spots were washed four times with PBS and blocked with 2% HSA in PBS for >1 h at 4°C. To test the mutant P2G, the same coating protocol as for SDF-1 was used.

AFM measurements

The tip of the Si_3Ni_4 cantilever (C lever, Park Scientific Instruments) was pinched off to preclude cell injury. The spring constant was determined by thermal fluctuation analysis. The cantilever was functionalized with 0.1 mg/ml of anti-CD43 mAb for 30 minutes at room temperature.

The force spectroscopy experiments were conducted at 36±1°C in binding medium with a home-built AFM (atomic force microscope). Immediately before the experiment, one cell was immobilized to the cantilever and positioned above the spot coated with VCAM-1 or VCAM-1 and SDF-1. The cell was pressed to the coated surface with a contact force of ca. 100 pN for 100 ms and then retracted with a piezo velocity of 3.4 μm/s. In one experiment, 100-150

force-distance curves were recorded with the same cell. At least 750 force-distance curves per setup were evaluated.

To ensure the specificity of the measured interactions, controls were performed either on plain Petri dish or on VCAM-1 substrate after addition a small peptidomimetic, BIO1211 at a concentration of 1 mg/ml. which blocks the ligand-binding pocket of the integrin VLA-4. It was also tested, whether the chemokine SDF-1 shows adhesive properties in the absence of VCAM-1. Under all these circumstances, hardly any interaction was observed Supplementary Material). Furthermore, measurements on VCAM-1 and co-immobilized P2G, a mutant of SDF-1, were conducted. P2G is known to be unable to induce intracellular signaling, though it has a similar affinity to the CXCR-4 receptor as does wildtype SDF-1. To show the involvement of G-protein signaling, controls with pre-treatment of the cells with pertussis toxin were performed. To this end, the cells were treated with 100 ng/ml PTX for 8-15 h before the experiment.

Laminar flow adhesion assays

Purified ligands were coated alone or with CXCL12 as described above. The polystyrene plates were each assembled on the lower wall of the flow chamber (260 μm gap) as previously described(Feigelson et al., 2001). Cells were perfused through the flow chamber at the desired shear stress. All flow experiments were conducted at 37°C. Tethers were defined as transient if cells attached briefly (< 2 s) to the substrate and as arrests if immediately arrested and remaining stationary for at least 5 s of continuous flow. Frequencies of adhesive categories within differently pretreated cells or rates of cell accumulation on adhesive substrates were determined as a percentage of cells flowing immediately over the

substrates, as previously described(Grabovsky et al., 2000). Over 95% of cellular tethers to

VCAM-1 were blocked by pre-treating cells with BIO1211 (1 μg/ml).

References

Alon, R., S.W. Feigelson, E. Manevich, D.M. Rose, J. Schmitz, D.R. Overby, E. Winter, V. Grabovsky, V. Shinder, B.D. Matthews, M. Sokolovsky-Eisenberg, D.E. Ingber, M. Benoit, and M.H. Ginsberg. 2005. Alpha4beta1-dependent adhesion strengthening under mechanical strain is regulated by paxillin association with the alpha4-cytoplasmic domain. *J Cell Biol*. 171:1073-84.

Alon, R., V. Grabovsky, and S. Feigelson. 2003. Chemokine induction of integrin adhesiveness on rolling and arrested leukocytes local signaling events or global stepwise activation? *Microcirculation*. 10:297-311.

Benoit, M., D. Gabriel, G. Gerisch, and H.E. Gaub. 2000. Discrete interactions in cell adhesion measured by single-molecule force spectroscopy. *Nat Cell Biol*. 2:313-7.

Benoit, M., and H.E. Gaub. 2002. Measuring cell adhesion forces with the atomic force microscope at the molecular level. *Cells Tissues Organs*. 172:174-89.

Brakebusch, C., and R. Fassler. 2003. The integrin-actin connection, an eternal love affair. *Embo J*. 22:2324-33.

Calderwood, D.A., S.J. Shattil, and M.H. Ginsberg. 2000. Integrins and actin filaments: reciprocal regulation of cell adhesion and signaling. *J Biol Chem*. 275:22607-10.

Crump, M.P., J.H. Gong, P. Loetscher, K. Rajarathnam, A. Amara, F. Arenzana-Seisdedos, J.L. Virelizier, M. Baggiolini, B.D. Sykes, and I. Clark-Lewis. 1997. Solution structure and basis for functional activity of stromal cell-derived factor-1; dissociation of CXCR4 activation from binding and inhibition of HIV-1. *Embo J*. 16:6996-7007.

Dwir, O., G.S. Kansas, and R. Alon. 2001. Cytoplasmic anchorage of L-selectin controls leukocyte capture and rolling by increasing the mechanical stability of the selectin tether. *J Cell Biol*. 155:145-56.

Engler, A.J., S. Sen, H.L. Sweeney, and D.E. Discher. 2006. Matrix elasticity directs stem cell lineage specification. *Cell*. 126:677-89.

Evans, E. 2001. Probing the relation between force--lifetime--and chemistry in single molecular bonds. *Annu Rev Biophys Biomol Struct*. 30:105-28.

Evans, E., V. Heinrich, A. Leung, and K. Kinoshita. 2005. Nano- to microscale dynamics of P-selectin detachment from leukocyte interfaces. I. Membrane separation from the cytoskeleton. *Biophys J*. 88:2288-98.

Evans, E., and K. Kinoshita. 2007. Using force to probe single-molecule receptor-cytoskeletal anchoring beneath the surface of a living cell. *Methods Cell Biol*. 83:373-96.

Evans, E., and K. Ritchie. 1999. Strength of a weak bond connecting flexible polymer chains. *Biophys J*. 76:2439-47.

Feigelson, S.W., V. Grabovsky, E. Winter, L.L. Chen, R.B. Pepinsky, T. Yednock, D. Yablonski, R. Lobb, and R. Alon. 2001. The Src kinase p56(lck) up-regulates VLA-4 integrin affinity. Implications for rapid spontaneous and chemokine-triggered T cell adhesion to VCAM-1 and fibronectin. *J Biol Chem*. 276:13891-901.

Grabovsky, V., S. Feigelson, C. Chen, D.A. Bleijs, A. Peled, G. Cinamon, F. Baleux, F. Arenzana-Seisdedos, T. Lapidot, Y. van Kooyk, R.R. Lobb, and R. Alon. 2000. Subsecond induction of alpha4 integrin clustering by immobilized chemokines stimulates leukocyte tethering and rolling on endothelial vascular cell adhesion molecule 1 under flow conditions. *J Exp Med*. 192:495-506.

Kinashi, T. 2005. Intracellular signalling controlling integrin activation in lymphocytes. *Nat Rev Immunol*. 5:546-59.

Lapidot, T., A. Dar, and O. Kollet. 2005. How do stem cells find their way home? *Blood*. 106:1901-10.

Laudanna, C., and R. Alon. 2006. Right on the spot. Chemokine triggering of integrin-mediated arrest of rolling leukocytes. *Thromb Haemost*. 95:5-11.

Liu, S., D.A. Calderwood, and M.H. Ginsberg. 2000. Integrin cytoplasmic domain-binding proteins. *J Cell Sci*. 113 (Pt 20):3563-71.

Manevich, E., V. Grabovsky, S.W. Feigelson, and R. Alon. 2007. Talin 1 and paxillin facilitate distinct steps in rapid VLA-4-mediated adhesion strengthening to vascular cell adhesion molecule 1. *J Biol Chem*. 282:25338-48.

Rosenthal-Allieri, M.A., M. Ticchioni, J.P. Breittmayer, Y. Shimizu, and A. Bernard. 2005. Influence of beta 1 integrin intracytoplasmic domains in the regulation of VLA-4-mediated adhesion of human T cells to VCAM-1 under flow conditions. *J Immunol*. 175:1214-23.

Schwarz, U.S., and R. Alon. 2004. L-selectin-mediated leukocyte tethering in shear flow is controlled by multiple contacts and cytoskeletal anchorage facilitating fast rebinding events. *Proc Natl Acad Sci U S A*. 101:6940-5.

Shamri, R., V. Grabovsky, J.M. Gauguet, S. Feigelson, E. Manevich, W. Kolanus, M.K. Robinson, D.E. Staunton, U.H. von Andrian, and R. Alon. 2005. Lymphocyte arrest requires instantaneous induction of an extended LFA-1 conformation mediated by endothelium-bound chemokines. *Nat Immunol*. 6:497-506.

Shimaoka, M., M. Kim, E.H. Cohen, W. Yang, N. Astrof, D. Peer, A. Salas, A. Ferrand, and T.A. Springer. 2006. AL-57, a ligand-mimetic antibody to integrin LFA-1, reveals chemokine-induced affinity up-regulation in lymphocytes. *Proc Natl Acad Sci U S A*. 103:13991-6.

Wiesner, S., K.R. Legate, and R. Fassler. 2005. Integrin-actin interactions. *Cell Mol Life Sci*. 62:1081-99.

Woolf, E., I. Grigorova, A. Sagiv, V. Grabovsky, S.W. Feigelson, Z. Shulman, T. Hartmann, M. Sixt, J.G. Cyster, and R. Alon. 2007. Lymph node chemokines promote sustained T lymphocyte motility without triggering stable integrin adhesiveness in the absence of shear forces. *Nat Immunol*. 8:1076-85.

Zaman, M.H., L.M. Trapani, A.L. Sieminski, D. Mackellar, H. Gong, R.D. Kamm, A. Wells, D.A. Lauffenburger, and P. Matsudaira. 2006. Migration of tumor cells in 3D matrices is governed by matrix stiffness along with cell-matrix adhesion and proteolysis. *Proc Natl Acad Sci U S A*. 103:10889-94.

Figure Captions.

Figure 1.

Experimental setup. The experimental setup as well as an examp0le of the primary data are shown. **A.** In the AFM, the cell is pushed onto the functionalized surface with a defined indentation force for a pre-set dwell time and then retracted from the surface with a constant velocity. During the dwell time, the cell can react with the proteins immobilized onto the surface. We used two different setups: (1) only VCAM-1 was immobilized to the surface; (2) SDF-1 was immobilized juxtaposed to VCAM-1. The VCAM-1 density was kept constant in both setups. **B.** During retraction, the bonds formed by the cell to the surface break. The force-distance relationship of this event is recorded. **C.** From the force distance curve, the rupture force and the rupture length as well as the initial slope of the force distance curves are determined. These values change when the cell encounters co-immobilized SDF-1.

Figure 2.

Rupture Forces and Rupture Lengths. The results of the AFM measurements are summarized as boxplots. **A:** Boxplots of the rupture force distributions. The grey-shaded region corresponds to the 95% confidence interval of the VLA4/VCAM-1 bond in the absence of SDF-1, while the red-shaded region corresponds to the 95% confidence interval of the force distribution after SDF-1-activation. SDF-1 leads to significantly increased rupture forces, an effect that is reversed by pre-treatement of

the cells with pertussis toxin (PTX). The SDF-1 point mutant P2G, which while binding with similar affinity does not signal, has no significant effect on the rupture forces. **B:** The distribution of rupture forces shows two distinct peaks after integrin-activation by SDF-1. These two peaks are indicative of two different receptor types on the surface. We postulate that the high-force population corresponds to SDF-1 activated integrins, while the low-force population corresponds to non-activated integrins. **C:** Boxplots of the distribution of rupture lengths. The 95% confidence intervals of VCAM alone (grey shade) and VCAM+SDF-1 (red-shade) are shown. SDF-1 shortens the rupture length in a Gi-signaling dependent manner, while Mg2+ elongates it.

Figure 3.

Initial Slope. The initial slope as measure for cellular stiffness is shown. **A:** Typical force-distance curves with (red) and without (black) co-immobilized SDF-1. The slope of the initial part of the force curves was taken as measure for cell-mechanical changes. It is indicated as a dashed line. **B.** SDF-1 leads to a significantly higher initial slopes, indicative of a strong attachment of the probed receptor to the cytoskeleton after SDF-1 triggered signaling.

Figure 4.

Flow-chamber results. Kinetics of formation and dissociation of transient VLA-4-mediated interactions of Jurkat T cells with immobilized VCAM-1 coated alone or in the presence of SDF-1 identically as in figure 2. **A**. The duration of all detectable

interactions were measured at a shear stress of 0.5 dyn/cm^2 and recorded with fast camera at a 2 ms resolution. Shortest interactions yielded a first order dissociation rate constant of 10.2s^{-1} and slow breaking interactions yielded a rate constant of 4.6s^{-1} comparable to that calculated for interactions of resting T cells with VCAM-1 alone with a rate of 4.0s^{-1}. **B.** The frequency of all adhesive interactions to VCAM-1 alone or coimmobilized with SDF-1 determined as outlined in the methods section. A representative experiment of three is shown. The frequency of interactions was expressed as percent of cells passing nearby the substrate as described (Grabovsky et al., 2000).

Supplementary Figure 1.

Relative Adhesion Rates. The absolute adhesion rate VCAM-1 coated surfaces in the absence of SDF was 28%. This was set to 100% for relative rates. BSA coated Petri-dishes or Petri-dishes coated only with SDF-1 showed hardly any interactions. The VCAM-1 mediated interactions were blocked by the peptidomimetic BIO1211. Co-immobilized SDF-1 did not increase the adhesion rate in the AFM.
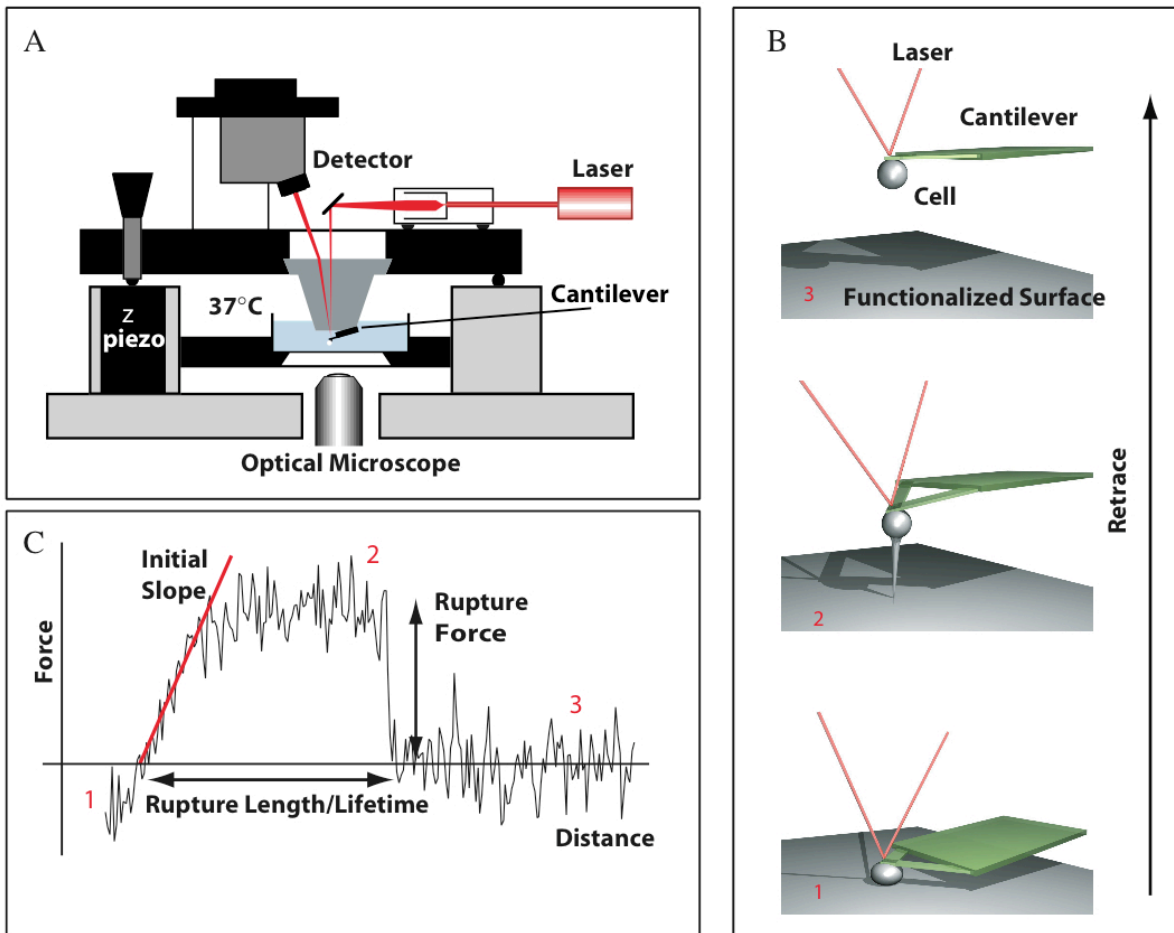
Figure 1.
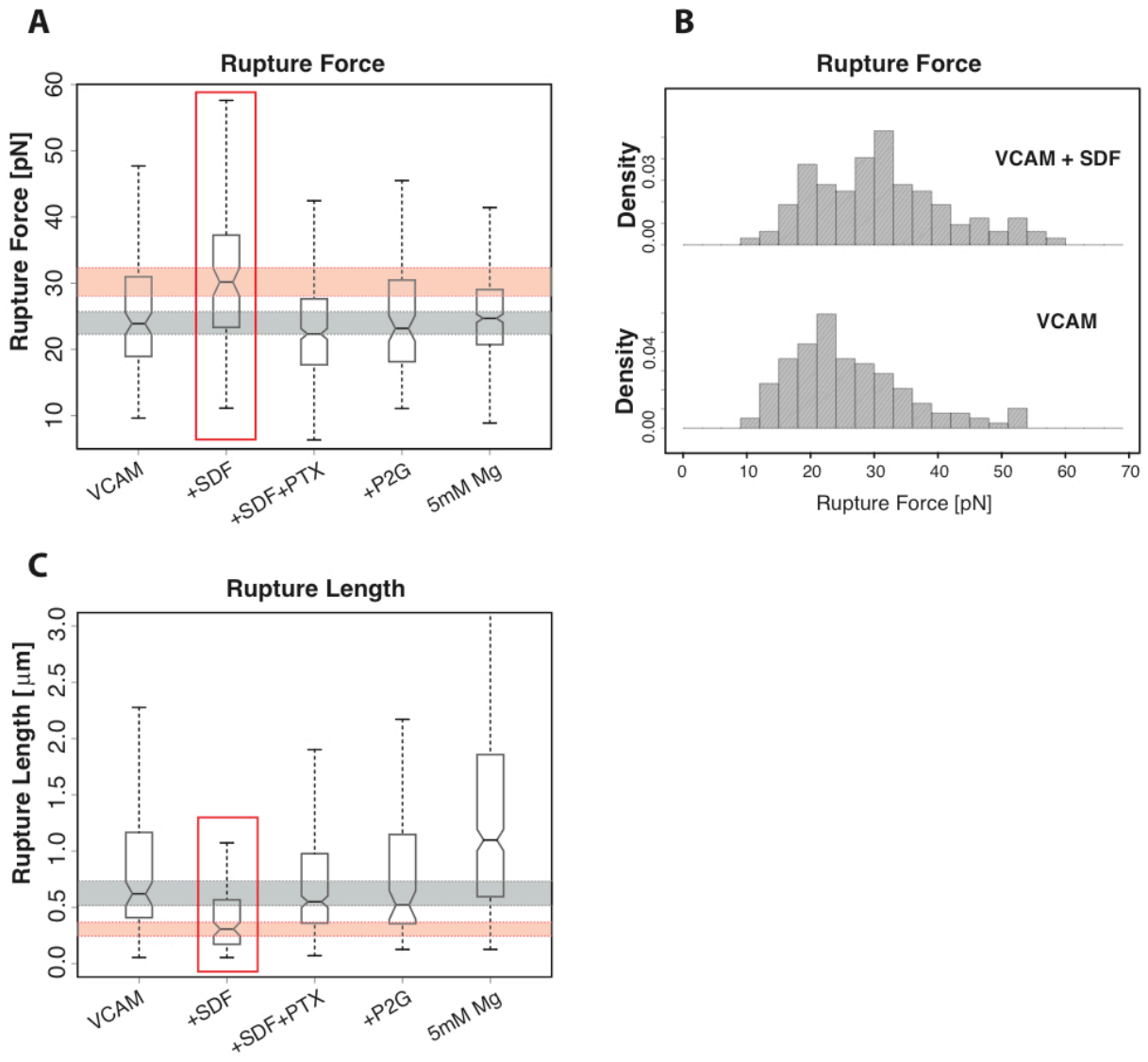
Figure 2
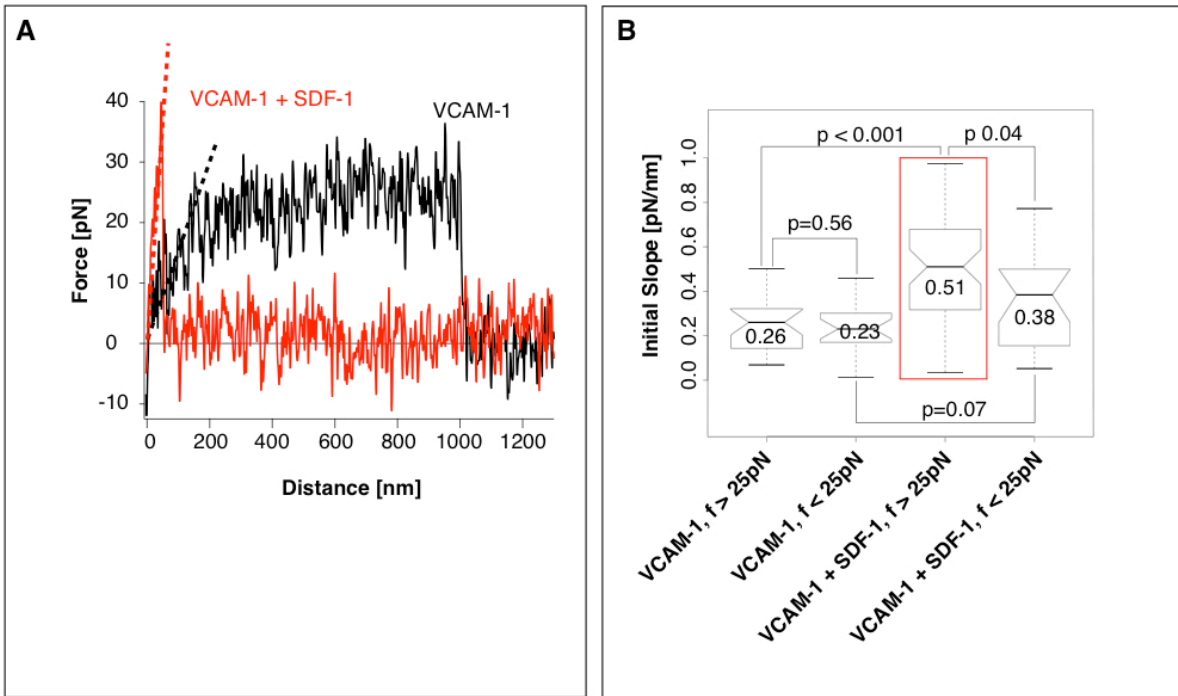
Figure 3.
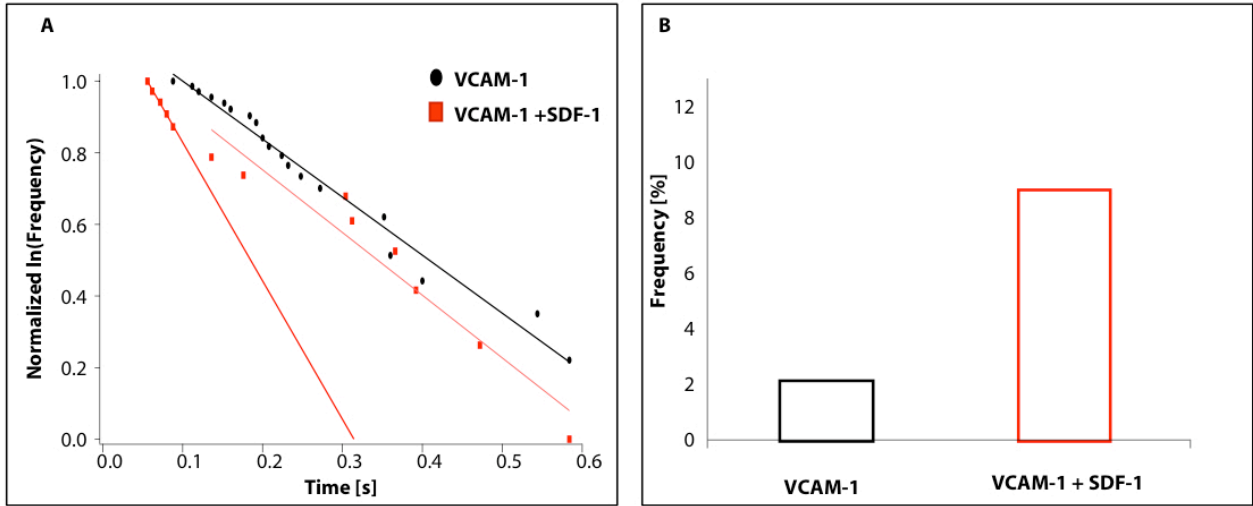
Figure 4

Adhesion Rates
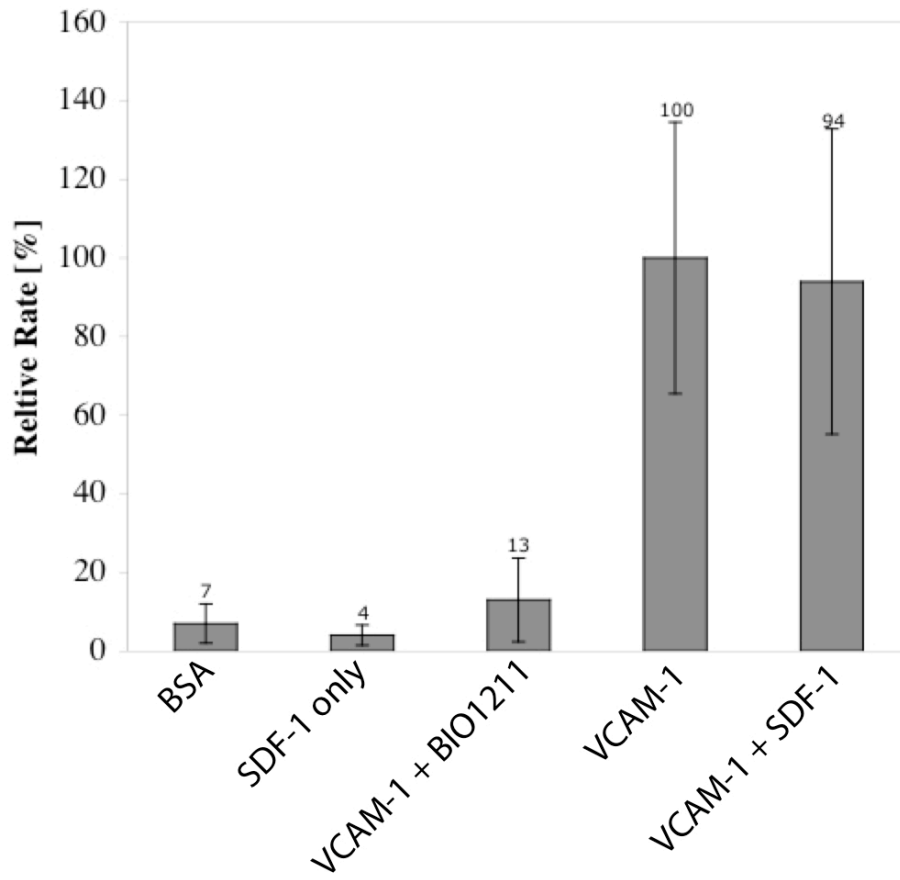
Supplementary Figure.

Chapter 4

Single Molecules and Multiple Bonds

Lymphocyte recruitment from the blood stream begins with an initial adhesive interaction between the lymphocyte and the ligand-presenting endothelium. After the lymphocyte is captured, the force of the blood flow is converted into a momentum on the cell [111]. The cell pivots upon the adhesive bond so that the contact area between the lymphocyte and the endothelium is enlarged and further adhesion receptors on the lymphocyte are given the opportunity to bind to ligands. Hence, the cellular adhesion in the blood stream will be dictated by the binding of multiple bonds [140]. In this setting, a bond may rebind after dissociation, while the adjacent bonds hold the position. The cellular adhesiveness is thus governed by the properties of the individual adhesion molecules, but also by their distribution on and their anchorage in the cell. To fully understand this complex event and to successfully dissect the roles of affinity and avidity within, it is desirable to link the molecular properties to the adhesive behaviour of the whole cell in a bottom-up approach.

Here, we investigated the interaction between the major T-cell integrin VLA-4 and its endothelial ligand VCAM-1 with single-molecule force spectroscopy in combination with flow chamber assays. In the AFM setup, the boundaries are absorbing: If the adhesive bond ruptures, the binding partners are further separated thus preventing rebinding events. In addition, the binding of multiple bonds can be efficiently suppressed by the choice of the experimental parameters, in particular by adjusting the ligand density on the substrate [141]. The flow chamber, however, mimics the physiological situation in the bloodstream. Here, the boundaries are reflecting [142], since rebinding is an important characteristic of cell adhesion in the shear flow. We therefore used AFM experiments on cells to assess the single-molecule properties of VLA-4, whereas the adhesive behaviour of the cell mediated by this integrin was studied in the flow chamber. By extrapolating the adhesive properties of the single receptor to the cellular adhesiveness in the shear flow, we developed a model for the cellular adhesion times observed in the flow chamber. Furthermore, we scrutinised the effect of the exogenous integrin activation with magnesium in both setups (see section 3). Unexpectedly, we found that this activation leads rather to an increased number of active integrins on the cell surface, than to a reduced basal off-rate.

4.1   Single-Molecule Properties and Cell Adhesion in the Shear Flow

In most physiological situations of cell adhesion, the binding partners are both constrained to opposing surfaces. The binding constant governing this process is thus a two-dimensional on-rate [143, 144]. We deduced this rate from AFM experiments performed on different ligand densities by fitting the following relation to the interaction frequency plotted against the ligand density (compare appendix A.1):

$$n_{bonds}(t) = N_{tot} - N_{tot} \cdot e^{-k_{on} \cdot d \cdot t} \qquad (4.1)$$

where N_{tot} is the maximum number of available receptors, d the coated ligand density in the contact area, t the contact time and k_{on} the two-dimensional on-rate in the units *area/time*. From experiments on limiting VCAM-1 density, we derived furthermore the basal off-rate and the potential width of the individual VLA-4/VCAM-1 bond by analysing the distributions of rupture forces and rupture lengths with Monte-Carlo simulations based on the force-distance relation of a Kelvin body (equation 2.1) and on the equation for the off-rate under force (equation 1.1). We next compared the characteristics of the adhesion on low-density VCAM-1 mediated by a single bond with the effect of multiple bonds on higher ligand densities. As expected, only the interaction frequency depends on the ligand density, whereas the off-rate, the potential width, and the most probable rupture force all remained constant for all densities.

The exogenous activation with concentrated magnesium in the absence of calcium drastically raised the interaction frequency compared to that of resting conditions and also increased the potential width of the molecular bond. Surprisingly, we could not detect any effect of the activation on the basal off-rate of the integrin VLA-4 for limiting ligand density. However, the basal off-rate did appeared to be significantly reduced for higher ligand densities on activating conditions. This dependence on the ligand density was attributed to the formation of multiple bonds between the cell and the functionalized surface, even though rebinding is minimised in the AFM setup.

In the flow chamber, stabilising the high-affinity conformation with magnesium increased the frequency of T-cell attachments to VCAM-1 and also prolonged the lifetime of the interactions. In order to interpret the cellular adhesiveness by extrapolating the molecular characteristics from the AFM experiments, we developed a relation based on the on-rate, the basal off-rate and the potential width of the adhesive bond and also accounted for rebinding effects (see appendix A.2):

$$n_{cells}(t) = n_{cells}(0) - n_{cells}(0) \cdot \left(1 - e^{-k_{off}^{F} \cdot t}\right)^{n_{bonds}(t)}$$

Here, $n_{cells}(0)$ is the number of cells bound to the surface at time $t = 0$, k_{off}^{F} is the off-rate under force and the number of bonds $n_{bonds}(t)$ is given by:

$$n_{bonds}(t) = \frac{k_{on}dN_{tot}}{k_{on}d + k_{off}^{F}} + \left(n_{bonds}(0) - \frac{k_{on}dN_{tot}}{k_{on}d + k_{off}^{F}}\right) \cdot e^{-k_{on}dt + k_{off}^{F}t}$$

The model demonstrated that more active receptors are available after the stimulation with magnesium, thus corroborating our observations in the AFM setup. The presence of multiple bonds reduces the effective force acting on the individual receptors. Together with rebinding effects, this explains the prolonged cellular adhesion times and the increased number of productive cellular attachments in the flow chamber setup.

Taken as a whole, our results suggest that the stimulation of the integrin VLA-4 with magnesium increases the cellular avidity, while the intrinsic dissociation rate remains unchanged. On circulating lymphocytes, a pool of resting integrins is expressed on the cell surface [13]. Concentrated magnesium in the absence of calcium shifts the conformational equilibrium in favour of the active structure and thus recruits receptors from the reservoir of inactive integrins. The enhanced presence of functional VLA-4 then leads to the formation of multiple bonds in dependence of the ligand density and to more cellular attachments with a longer duration in the physiological setting.

These results have been submitted to the Biophysical Journal and are reprinted in section 4.3.

4.2 Conclusions

Our results underline the importance of employing single-molecule studies in combination with ensemble studies to dissect avidity and affinity effects in cellular adhesion at short-lived contacts. Based on the molecular binding features, we proposed a model for the cellular adhesiveness on the reflecting boundary conditions of the shear flow. By these means, we discovered the outcome of the exogenous integrin activation with magnesium to be an avidity-related effect rather than a modulation of the basal off-rate.

4.3 Publications

1. Linking Single Integrin Bond Properties to Cell Adhesiveness at Rapid Contacts generated under External Forces (*submitted to the Biophysical Journal*)

Linking single integrin bond properties to cell adhesiveness at rapid contacts generated under external forces.

Julia Schmitz[1], Eugenia Manevich[2], Martin Tschöpe[1], Martin Benoit[1], Ronen Alon[2], Kay-Eberhard Gottschalk[1].*

[1] Applied Physics and Biophysics
Ludwig-Maximilians University of Munich
Amalienstr. 54
80799 Munich, Germany
[2] Depart of Immunology
Weizmann Institute of Science
76100 Rehovot, Israel

- corresponding author
Kay.Gottschalk@physik.uni-muenchen.de
Phone: +49-89-2180 3436
Fax: +49-89-2180

Abstract

Cell adhesion is a complex event dictated by the properties of individual adhesion molecules. It is desirable to link their individual properties to the adhesive behavior of a whole cell. Here, we examine with atomic force microscopic (AFM) and flow chamber experiments how the exogenous activation of the major T cell integrin VLA-4 affects the adhesiveness of T-lymphocytes to the endothelial VLA-4 ligand, VCAM-1. The atomic force measurements are performed on substrates with different VCAM-1 densities to compare the properties of single adhesive bonds on low-density ligands with the effect of multiple bonds on higher ligand densities. We determine the basal off-rate and the potential width of the single adhesive VLA-4/VCAM-1 bond by Monte-Carlo simulations. We show that activating VLA-4 with magnesium increases the potential width of the bond, but does not affect the basal off-rate of single VLA-4-VCAM-1 bonds measured at low VCAM-1 density. At higher VCAM-1 densities, the apparent off-rate of high avidity VLA-4/VCAM-1 interactions is significantly reduced by magnesium. In the flow chamber, both the frequency of T cell attachments to VCAM-1 and their lifetime rise after VLA-4 activation by magnesium. By extrapolating the single-molecule properties to whole cells, we suggest that exogenous stimulation with magnesium increases the rate of VLA-4 rebinding to VCAM-1 rather than the off-rate of single VLA-4-VCAM-1 bonds.

Introduction

Cell-to-surface or cell-to-cell adhesion is of critical importance for a large variety of cellular events, which is governed by adaptive, force-resisting receptors. The integrin family is a prominent subclass of these receptors. Integrins are involved in diverse physiological and patho-physiological events ranging from embryogenesis to tumor metastasis. They operate in a force-exerting environment (1,2). Hence, when probing integrin-ligand interactions, applied forces should be an integral part of the experiments. Integrin adhesiveness is modulated both by affinity and avidity to surface-bound ligands (3): Affinity describes the binding properties of a single molecule, which varies due to different kinetic rates - caused for example by conformational changes. In contrast, avidity characterizes the overall adhesiveness of the whole cell, depending on both the number and the affinity of single receptor molecules (2-8). Approaches that can discriminate between both contributions are desired. Single molecule studies in comparison to ensemble studies are ideally suited for this task. In single molecule studies, avidity effects can be suppressed by design. They are, nevertheless, included in ensemble measurements.

Atomic force spectroscopy is perfectly capable of probing cell adhesion on the single molecule level in a force-exerting environment. It is able to measure and analyze single receptor-ligand bonds in a physiological environment with living cells (9,10). In the AFM setup, the cell is attached to a cantilever and put into contact with a functionalized surface at a pre-defined indentation force and dwell time. During contact, the receptors can diffuse to the ligands and form bonds, depending on the two-dimensional on-rate (Fig. 1). During retraction, both the receptor-ligand rupture forces as well as the cellular adhesion time are measured. When probed by an AFM, the receptor-ligand bonds break in a stochastic Markov process (11). Knowing the time-evolution of the force loading on the bond, important bond properties such as the basal off-rate and the potential width can be determined from Monte-Carlo simulations (12,13).

For dissecting affinity from avidity effects in the ensemble measurements, the single molecule properties as determined by the AFM are mandatory. In order to extrapolate the AFM data to ensemble measurements, a model is needed that describes the cellular behavior in the ensemble measurement starting from the single molecule properties. The AFM operates under an absorbing boundary condition (14): no bond can re-form once broken (Fig. 1). In the blood stream, however, the boundary is reflecting (Fig. 1): individual cell-to-surface bonds can rebind after breakage, as long as the rotating cell encounters ligand and rebinds to the surface (14). Thus, the kinetic analysis of the cellular adhesion times in the blood stream has to take rebinding into account. The blood stream is well approximated by flow chamber experiments. In these experiments, the adhesiveness of the whole cell under the influence of the shear stress of a laminar flow is measured by video microscopy at the desired temporal resolution (Fig. 1), and rebinding can occur unless the ligand is highly diluted (15). For the inclusion of rebinding, the two-dimensional on-rate, which is limited by the diffusion of the receptor through the membrane (16), has to be known.

Here, we probe the interaction of the integrin VLA-4 on Jurkat lymphocytes with its natural ligand VCAM-1 both by AFM and in a flow chamber. Deduced from the AFM measurements conducted with different ligand concentrations, we derive a two-dimensional on-rate of the VLA-4/VCAM-1 bond. By analyzing the distributions of the rupture forces and of the rupture lengths with Monte-Carlo simulations, we determine the basal off-rate and potential width of this bond. We show that on the lowest ligand density the activation by magnesium does not significantly alter the off-rate in comparison to resting conditions. Only for higher ligand densities does the stimulation with magnesium lead to an apparently lowered off-rate. This

dependence on the ligand-density in the AFM setup can be explained by the formation of multiple bonds between the cell and the functionalized surface, even when rebinding is minimized.

With the possibility of rebinding in mind, we derive a simplified model for the cellular adhesion times measured in the flow chamber based on the AFM data. Using this model, we show that the presence of multiple bonds together with rebinding effects can explain the effect of magnesium on VLA-4 adhesiveness observed in the flow chamber. Furthermore, we determine the effective force acting on each single bond in the flow chamber. After magnesium stimulation, multiple bonds share the load of one tether so that the effective force is reduced and the lifetime of the cellular adhesion is prolonged.

Material and Methods

Reagents and antibodies

Recombinant human seven-domain VCAM-1, recombinant anti-human CD43 mAb were purchased from R&D Systems. BSA (fraction V), HSA (fraction V) and Ca^{2+}/Mg^{2+}-free HBSS were obtained from Sigma-Aldrich. Bio1211 was a gift from Blake Pepinsky (Biogen Inc. Cambridge MA).

Cell culture

Jurkat cells were maintained in RPMI1640 medium (Biochrom AG) supplemented with 10% heat-inactivated FCS, 2 mM L-glutamine and penicillin/streptomycin in 5% CO_2 at 37°C. The constant expression of the integrin VLA-4 on the cells was checked by FACS.
Before the AFM measurements, cells were washed with 5 mM EDTA and re-suspended in HBSS medium containing 2 mg/ml BSA, 1 mM $CaCl_2$, 1 mM $MgCl_2$ and 10 mM HEPES (herein referred to as cell binding medium).

Substrate preparation

The lids of Petri dishes were coated by incubating spots over night at 4°C either with 0.2 μg/ml, 0.1 μg/ml, 0.05 μg/ml, 0.025 μg/ml or 0.0125 μg/ml VCAM-1 and carrier protein 2 μg/ml HSA together with an heat-inactivated protein as inert spacer as described earlier (17,18). The site density of the coated VCAM-1 ranged from 50 sites/μm^2 to 800 sites/mm^2 (17). Radioimmunoassays confirmed VCAM-1 coating to be linear to the input ligand over the entire range of coating (19). After adsorption, the spots were washed four times with PBS and blocked with 2% HSA in PBS for >60 minutes at 4°C.

AFM measurements

All force spectroscopy measurements were performed at 36±1°C in cell binding medium using a previously described atomic force microscopy (AFM) apparatus (9). The tip of a Si_3N_4 cantilever (C Lever, Park Scientific Instruments) was removed to prevent cell damage. One leg of the cantilever was broken to reduce the spring constant to ~5.5±1 pN/nm, which was calibrated by thermal fluctuation analysis as reported earlier (20,21). The cantilever was then incubated with 0.1 mg/ml of anti-CD43 mAb for 30 minutes at room temperature. Just before the experiment, a single cell was immobilized on the cantilever and positioned above the coated VCAM-1. The

cantilever was lowered until a contact force of ca. 50-100 pN was reached (Fig. 1). After a contact time of 300 ms, the cell-bearing cantilever was retracted from the surface with the piezo-actuator at a retraction velocity of 3.4 μm/s, which is in the range of physiological velocities for T-lymphocytes (22). For each cell, 50-100 force curves were collected in one experiment; for each setup, at least five cells were measured. A setup is defined as a certain coating density under certain ionic conditions.

To assure that the measured interactions are specific, controls were performed either on an uncoated Petri dish or on VCAM-1 coated substrates by including a VLA-4 blocking agent, Bio1211. This small ligand used at a concentration of 1 μg/ml was found to specifically, saturably and reversibly block the ligand-binding pocket of the lymphocyte integrin VLA-4 (23,24).

Laminar flow adhesion assays

Purified ligands were coated on polystyrene plates as previously described (19). The polystyrene plates were each assembled on the lower wall of the flow chamber (260 μm gap) as previously described (25). Cells were washed with cation-free medium, resuspended in cell binding medium and perfused through the flow chamber at the desired shear stress (Fig. 1). All flow experiments were conducted at 37°C. The shear flow was kept constant at 0.75 dyn/cm^2. The cellular adhesion frequencies were expressed as percentage of cells flowing immediately over the substrates (19,26). The duration of individual adhesive interactions were determined as described (19,26).

Theory

Off-rate and Potential Width

If single, statistically independent bonds are probed, bond breakage forced by the AFM is a stochastic Markov process. Not a single rupture force, but a probability distribution of forces is observed in the experiments (11,27). This distribution can be simulated with Monte-Carlo simulations. During the retraction of the receptor from the ligand-coated surface, the probability of bond rupture $p_{breakage}(t)$ is described by $p_{breakage}(t) = 1 - \exp(-k_{off}^F \cdot t)$. Here, the off-rate under force is:

$$k_{off}^F = k_{off}^0 \cdot \exp\left(\frac{F}{n \cdot f_b}\right) \qquad \text{(equation 1)}$$

k_{off}^0 is the basal off-rate and F the external force distributed over n bonds; $f_b = \dfrac{k_B T}{\gamma}$ is the characteristic force of the bond scaled by the thermal energy $k_B T$ and γ is the potential width of one molecular bond. As the velocity of the retraction v is constant, the time increment dt is equivalent to an increment of distance dz and the probability is $p_{breakage}(z)$. During the retraction, a force F is applied to the receptor-ligand bond. It has been shown that the force-distance relationship when pulling membrane tethers with transmembrane receptors is described by (28):

$$F(z) = k_t \cdot z + g \cdot v - g \cdot v \cdot \exp\left(-\frac{k_i \cdot z}{g \cdot v}\right) \qquad \text{(equation 2)}$$

k_i represents the initial bending elasticity of the membrane, g is the viscosity of the slip of the membrane over cytoskeletal components and k_t is the elasticity of the pulled membrane tether. To simulate the distributions of rupture forces and rupture lengths with Monte-Carlo simulations, we used k_i = 0.26±0.15 pN/nm, k_t = 0.0016±0.0016 pN/nm, g = 5.9±1.5 μN·s/m for resting

conditions and k_i = 0.19±0.1 pN/nm, k_t = 0.0009±0.0009 pN/nm, g = 6.0±0.8 μN·s/m for activating conditions as measured before (28):. In addition, a Gaussian noise of 5 pN was added to the force. With this, the force acting on the bond and the probability of bond breakage $p_{breakage}(z)$ can be calculated at any distance. The probability is then compared to a random number between 0 and 1. If this number is higher than $p_{breakage}(z)$, the bond breaks and the force F and the distance z are registered. If it is lower than $p_{breakage}(z)$, the distance z is increased by an increment dz and the calculation restarts. To obtain a force and a length distribution, we simulated a set of data containing 500 ruptures. After simulating one set of data, the deviation χ^2 between the simulated and the experimental distributions was calculated. The algorithm minimized χ^2 by varying the parameters k_{off}^0 and γ using a genetic algorithm until the experimental distributions were well matched by the simulated ones. We used 10 000 steps to optimize χ^2. With this method, the molecular parameters k_{off}^0 and γ can be estimated from the force and length distributions (27). Due to the stochastic nature of both the rupture processes and the genetic algorithm, not a single solution is found. We averaged over the 20 best solutions and determined the standard deviation of this averaging as error estimate.

In a second scenario, we allowed the number of bonds per tether to increase in order to estimate the effect of multiple bonds ($n \leq 20$). For this, the molecular parameters k_{off}^0 and γ determined from the single-molecule measurements on the lowest ligand density were kept fixed. For each single simulation, a different n with $1 \leq n \leq 20$ was given. Thus, for the 500 simulations of a single set of data as described above, we obtain a distribution of bonds per tether. During the single simulation, the force F was randomly distributed over all bonds, such that every bond was on average loaded with a force of $F_{effective} = \dfrac{F}{n}$. If one bond has ruptured, it cannot rebind in our simulation, (14) and the bond number is reduced to n-1. This procedure is repeated, until all bonds holding the tether have broken and the tether has ruptured. Since now the number of free parameters is effectively 20 (each probability of n with n ≤20 is one degree of freedom), it was too high for an automated adjustment. Therefore, we manually optimized the number of bonds by iteratively altering the distribution of n in order to minimize χ^2 to a value comparable to the automated optimization described above. With this, the average number of bonds n_a per tether can be estimated but not conclusively determined.

On-rate

During the retraction, we record the number of ruptures. As described above, we furthermore estimated the number of bonds per rupture. Therefore, the number of bonds formed can be calculated as the average number of ruptures times the average number of bonds per tether. Since on resting cells, VLA-4 is not attached to the cytoskeleton and is therefore free to diffuse in the membrane, the number of formed bonds is diffusion-limited and depends on the two-dimensional on-rate (27,29,30). With the assumption that the number of bonds breaking during the contact time can be neglected (the contact time is 0.3 s, and, as shown below, the off-rate is 1.2 s^{-1}), and assuming an infinite reservoir of receptors on the cell, the number of bonds is described by the differential equation $\dfrac{dn_{bonds}(t)}{dt} = k_{on} \cdot d \cdot (N_{tot} - n_{bonds}(t))$. For $n_{bonds}(0)=0$, this yields:

$n(t) = N_{tot} - N_{tot} \cdot e^{-k_{on} \cdot d \cdot t}$ (equation 3),

where N_{tot} is the maximum number of available receptors, d the coated ligand density in the contact area, t the contact time and k_{on} the two-dimensional on-rate in the units of *area/time*. Thus, for a given contact time t, k_{on} can be determined by varying the ligand density.

Effective Force in the Flow Chamber

In the flow chamber, rebinding cannot be neglected, since multiple bonds hold the cell and the cell has a chance to rebind to the ligand after bond breakage (Fig. 1) (31). Hence, the appropriate differential equation for the number of receptor-ligand bonds between cell and surface is:

$$\frac{dn_{bonds}(t)}{dt} = k_{on} \cdot d \cdot \left(N_{tot} - n_{bonds}(t)\right) - k_{off}^F \cdot n_{bonds}(t) \quad \text{(equation 4)},$$

where k_{on} is the two-dimensional on-rate, N_{tot} the maximal number of available receptors, $n_{bonds}(t)$ the number of bonds at time t and k_{off}^F the off-rate under the acting force. We approximate that the average force acting on the bonds in the shear flow is constant while the cell is adhering to the surface, so that k_{off}^F is independent of time (31). This yields:

$$n_{bonds}(t) = \frac{k_{on} \cdot d \cdot N_{tot}}{k_{on} \cdot d + k_{off}^F} + \left(n_0 - \frac{k_{on} \cdot d \cdot N_{tot}}{k_{on} \cdot d + k_{off}^F}\right) \cdot \exp\left(-\left(k_{on} \cdot d + k_{off}^F\right) \cdot t\right) \qquad \text{(equation 5)},$$

where n_0 is the number of bonds at time $t = 0$. The force F of the shear flow acting on the cell is shared among all the individual VLA-4/VCAM-1 bonds. Hence, if multiple bonds hold the cell, the effective force on each bond is lower than for a single bond. Therefore, the off-rate k_{off}^F depends on the average effective force on the individual bond $f_{effective} = \dfrac{F}{n}$ following equation 1.

A cell is detaching from the surface after the last bond has broken. This leads to the time dependency for the cell adhesion:

$$n_{cells}(t) = n_{cells}(0) - n_{cells}(0) \cdot (1 - \exp(-k_{off}^F \cdot t))^{n_{bonds}} \quad \text{(equation 6)},$$

where $n_{cell}(0)$ is the number of cells bound at time $t=0$. For cells bound to the surface by a single bond, equation 6 collapses to the kinetic description for a rupture process $n_{cells}(t) = n_{cells}(0) \cdot \exp(-k_{off}^F \cdot t)$. We determine k_{off}^0, f_b and k_{on} by AFM. The bond number of the initial contact was assumed to be $n_0 = 1$ and the contact area between the cell and the surface was estimated to be on the order of 10 μm^2 in the flow chamber (ca. 3% of the total cell surface - Supplementary Fig. 1), neglecting cellular flattening. Since we are analysing short lived, initial contacts, the assumption of round cells seems to be appropriate. The only free parameters in equation 6 are then $n_{cells}(0)$, N_{tot} and k_{off}^F.

Results

Contact Area

From the indentation curves, we determined a median Young modulus of 20 Pa, which is in the reported range (32). With this, we estimated the contact area as previously described (33) (Supplementary Fig. 1). For the contact force of 75±25 pN used here, we calculated an area of 37±5 μm^2. A coated ligand density of 50-800 sites/μm^2 corresponds therefore to a ligand density d (see equation 3 and 5) in the contact area of 185-2960 sites/contact area.

Rupture Forces and Rupture Lengths

To measure the cellular adhesion mediated by the integrin VLA-4 with AFM, we functionalized the surface with different densities of the ligand VCAM-1. Furthermore, we used two different

buffers: first, a buffer with physiological ion concentrations of 1 mM Ca^{2+} and Mg^{2+} and a second integrin-activating buffer supplemented with 5 mM Mg^{2+} and depleted of Ca^{2+} (34,35).

The average of the median rupture length and the median rupture force remained approximately constant for all ligand densities under resting conditions at 1.0±0.24 μm and 19.5±0.62 pN, respectively. In contrast, for activating conditions the median rupture length as well as the median rupture force increased with higher ligand densities from 0.7 μm and 22.0 pN for the lowest density to 4.1 μm and 26.2 pN for the highest density (Fig. 2).

Off-rates and Potential Width assuming a Single Bond

From the distributions of the rupture forces and the rupture lengths, we determined the potential width γ and the basal off-rate k_{off}^0 with Monte-Carlo simulations (Fig. 3). First, the simulations were conducted assuming one single bond ($n = 1$ in equation 1). For resting conditions, the off-rate and the potential width turned out to be both independent of the ligand density (Fig. 2A). The average off-rate for all densities was determined as $k_{off}^0 = 1.2 \pm 0.3$ s^{-1} and the potential width as $\gamma = 0.18 \pm 0.03$ nm. Activating conditions raised the potential width to 0.44±0.07 nm. Interestingly, the off-rate appeared to become dependent on the ligand density after activation. As deduced from the simulations assuming single bonds, the basal off-rate decreased from 0.92 s^{-1} for the lowest measured ligand concentration to 0.04 s^{-1} for the highest concentration. Thus, for the lowest ligand density, the off-rate remained unchanged for magnesium-activated integrins compared to resting integrins. Just for higher ligand densities, the stimulation with magnesium apparently reduced the basal off-rate.

Multiple Bonds.

To test whether multiple bonds on a single tether possibly caused this dependency on the ligand density, we altered the number of bonds n (see equation 1) in the Monte-Carlo simulations for the higher densities under activating conditions. We approximated the setup of 50 sites/μm^2 in the presence of 5 mM magnesium to be in the single-molecule regime. Two arguments favour this approximation: first, the value of the off-rate for the lowest ligand density under activating conditions was in the same order as the values obtained under resting conditions; and second, the adhesion rate was on the order of 30%, rendering single bonds very likely (9,36). Thus, we kept the off-rate and potential width at 0.92 s^{-1} and 0.44 nm of the lowest ligand density under activating conditions and increased the number of bonds n per tether to fit manually the experimental force and length distributions (see *Theory*). With each new set of data, the distribution of the bond numbers were iteratively and interactively adjusted to minimize χ^2. For the higher concentrations under activating conditions, we were able to fit the force and length histograms with similar accuracy as under resting conditions only under the assumption of multiple bonds (Fig. 3). The average number of bonds n_a of our best fit was 4.0 for 100 sites/μm^2 and 7.8 for 200 sites/μm^2.

On-rate

In order to determine the two-dimensional on-rate k_{on} under resting conditions, we fitted the numbers of observed ruptures with equation 3 (Fig. 4) and obtained a k_{on} of $9 \cdot 10^{-4}$ μm^{2}s^{-1} and a N_{tot} of 1.0. Here, we are in the single molecule regime for all ligand densities, therefore the number of recorded ruptures is identical to the number of bonds. To estimate the error in this value stemming from the uncertainty in the contact area and from cellular fluctuations in the bond formation, the minimal on-rate was determined by fitting the minimal number of ruptures

assuming the maximal contact area; vice versa, the maximal on-rate was obtained. This yielded a range for the on-rate of $4 \cdot 10^{-4} - 1.4 \cdot 10^{-3}$ $\mu m^2 s^{-1}$.

Magnesium-activation of the integrins strongly increased the adhesion rate. Due to an accompanying increase in the average rupture length exceeding the instrumental range, we were unable to perform AFM experiments at ligand densities exceeding 200 sites/μm^2 in the presence of magnesium. We could therefore not determine k_{on} for magnesium-stimulated integrins. Howeverl, the measured on-rate for resting integrins is in good agreement with the literature (37,38): Chigaev et al. and Chen et al. measured a three-dimensional on-rate of $2.5 \cdot 10^6$ /M·s and $2.7 \cdot 10^6$ /M·s, respectively. With the factor $\eta = 10^{22}$ /M·m^2 for the conversion of the three-dimensional into a two-dimensional dissociation constant (8,39,40), this corresponds to a two-dimensional on-rate of $3 \cdot 10^{-4}$ $\mu m^2 s^{-1}$, in good agreement with our value. Thus, it is reasonable to approximate a two-dimensional on-rate of $1 \cdot 10^{-4}$ $\mu m^2 s^{-1}$ for the activating conditions, which is calculated from the three-dimensional on-rates reported for the stimulated integrin VLA-4 (37,38) using η. Although we did not reach the saturation level, it is obvious that the saturation plateau is much higher compared to the plateau under resting conditions (Fig. 4). This indicates that the maximum number of available receptors N_{tot} is higher (equation 3).

Flow Chamber Measurements

Next, we investigated the adhesion of cells bearing either resting integrins or magnesium-activated integrins in the flow chamber. This experimental setting resembles more the physiological conditions of the blood stream: in this setup as well as in the blood stream, the force acts horizontally on the cell and the receptors can rebind (reflecting boundary (31)) (Fig. 1). Here, we probed the cells at a VCAM-1 density of 100 sites/μm^2 again under physiological and integrin-stimulating buffer conditions. Below this density, no detectable interactions could be observed under the shear stress used throughout the experiments. The sehar stress used is within the lowest physiological stress range. The total number of adhering cells of the magnesium-treated cells was significantly increased compared to the untreated cells (Fig. 5). Furthermore, a first order kinetic analysis yielded a reduced off-rate under force of $k_{off}^F = 1.2$ s^{-1} for activating conditions as opposed to $k_{off}^F = 3.8$ s^{-1} for resting conditions (Fig. 4). In order to extrapolate the single-molecule properties measured in the AFM setup to the cellular adhesive properties measured in the flow chamber setup, we used equation 6. For this, we estimated the total contact area between cell and surface to be on the order of 10 μm^2 (Supplementary Fig. 1) neglecting cellular flattening for these short contacts, which yields 1000 VCAM-1 sites per contact area at the tested coating density. k_{on}, k_{off}^0 and γ were taken from the single-molecule AFM experiments. For the activating condition, k_{on} was taken from the literature and concerted to 2-dimensional conditions(37,38). k_{off}^0 and γ were taken from the AFM measurements at the lowest ligand concentration, which is still in the single-molecule regime. The fit of the adhesion times in the flow chamber with equation 6 (Fig. 5) yields a molecular off-rate under force of $k_{off}^F = 6.7$ s^{-1} for resting conditions and $k_{off}^F = 2.7$ s^{-1} for activating conditions. The force acting on the cell under the used conditions is on the order of 100 pN. With the relation $k_{off}^F = k_{off}^0 \cdot \exp\left(\dfrac{f_{effective}}{f_b}\right)$ and the

basal off-rates obtained from the AFM experiments, a maximum number of available receptors $N_{tot} = 430$ and an effective force $f_{effective} = 14$ pN is determined for magnesium-treated cells and $N_{tot} = 104$ and $f_{effective} = 41$ pN for untreated cells. Thus, the stimulation with magnesium leads to more frequent adhesive interactions in the flow chamber setup, due to an increased density of active VLA-4 within the contact area. With this, the force from the shear flow is distributed over more

bonds under activating conditions and the effective force on the single bonds is correspondingly lowered allowing longer contact duration and higher rebinding probability.

Discussion

Cell adhesion is influenced by both the on- and the off-rate of the receptor-ligand bond. In ensemble measurements like the flow chamber, the relative contribution of these two parameters is difficult to dissect. In the AFM, on the other hand, we have an exquisite control over the cell-on-surface contact time. Choosing sufficiently short dwelling periods renders the off-reaction during contact negligible. Moreover, during the retraction of the cantilever, rebinding is effectively suppressed, so that the on-rate can be neglected, provided that the experimental conditions are well chosen. Hence, the on-rate can be separated from the off-rate, and the relative contribution of each to the overall cell adhesiveness can be estimated.

On-rates

The importance of two-dimensional on-rates being the relevant rates for physiological situations has been outlined before (8,16,27). Yet, this parameter is not easily accessible as it strongly depends on the contact time and area between the cell and the substrate (see equation 3) (27,29). For resting conditions, the two-dimensional on-rate of $9 \cdot 10^{-4} \, \mu m^2 s^{-1}$ determined in this work agrees well with the literature (37,38), if one converts the reported three-dimensional on-rates into two-dimensional ones (8,39,40). For the activating conditions, we used the on-rates reported in the literature (37,38) and observed a more than ten-fold increase in the number of functional receptors. This suggests that the stimulation of the integrin VLA-4 with magnesium activates a reservoir of otherwise inactive integrins constitutively present on the cell surface.

AFM Measurements under Resting Conditions

From the distributions of rupture forces and rupture lengths, we obtained the potential width and the basal off-rate of the molecular bond between the cellular VLA-4 and its ligand VCAM-1 using Monte-Carlo simulations. We tested two different scenarios emulating 1) one single bond and 2) multiple bonds for the connection between the membrane tether and the surface. If we assume only one single bond ($n = 1$), we obtained for resting VLA-4 a basal off-rate from the simulations with $k_{off}^{0} = 1.2 \pm 0.3 \, s^{-1}$, which is in good agreement with the literature (18,37). For resting conditions, we did not see any trend of these parameters with the ligand density. Furthermore, simulations with multiple bonds ($n > 1$) did not lead to an improved fit compared to the simulations with a single bond, which is based on a simpler model using fewer free parameters. Thus, the assumption of a single bond seems to be valid for all ligand densities under resting conditions.

AFM Measurements under Activating Conditions

The activation with magnesium increased the potential width of the VLA-4/VCAM-1 bond from 0.18±0.03 nm to 0.44±0.07 nm. Hence, the stimulation of integrins with magnesium renders the molecular bond more susceptible to external forces, as described before (18,35,41). Under activating conditions, the potential widths seemed to increase with higher ligand densities. Nevertheless, since the relative deviation from the mean for resting conditions is 19% and for activating conditions 17%, the apparent ligand-density-dependent increase may not be significant. Therefore, we assumed the potential width to be independent of the ligand density both under resting and activating conditions.

Interestingly, at the lowest ligand density under activating conditions, we obtained a basal off-rate of 0.9 s^{-1}. This corresponds to the off rate of the resting integrin within the error of the measurement. With increasing ligand density under activating conditions, however, the off-rate becomes reduced 20-fold to a value of 0.04 s^{-1} at the highest ligand density of 200 sites/μm^2. This means that the activated VLA-4 cannot support prolonged adhesive contact with singular VCAM-1 molecules. Exogenous stimulation with magnesium therefore increases the rate of VLA-4 binding to VCAM-1 rather than the k$_{off}$ of singular VLA-4-VCAM-1 bonds.

Multiple Bonds

The apparent ligand-density-dependent reduction of the off-rate can be economically explained by the probing of multiple bonds (Fig. 6). Different lines of argument support this notion: As shown from the bond formation rate (Fig. 3), the number of binding competent receptors increases strongly after activation of the integrins by highly concentrated magnesium in the absence of calcium. This points to an increased avidity and thus to a higher number of binding-competent receptors, which might lead to multiple bonds per tether. Multiple bonds are known to reduce the off-rate while leaving the potential width unchanged (42,43), in agreement with our results. Furthermore, our Monte-Carlo simulations with multiple bonds described above recaptured the measured force and length distributions well.

From our data, we estimated an average number of bonds of 4.0 and 7.8 for 100 sites/μm^2 and 200 sites/μm^2, respectively, which corresponds to a contact area of $\sim$ 0.04 μm^2 for both cases. For lymphocytes, the area of a microvillus tip can be estimated as 0.008 μm^2 assuming a diameter of 100 nm (44) and the surface area of a whole microvillus was reported to be 0.25 μm^2 (45). Thus, if one accounts for the flattening of the microvillus by the external force and the accompanying increase of the contact area of the microvillus, a contact area of 0.04 μm^2 is plausible. Furthermore, the here deduced average number of bonds n_a might be overestimated: our Monte-Carlo simulations do not account for rebinding effects, although for the here determined bond numbers, rebinding might become important (46). Therefore, even a lower average bond number should be already sufficient to cause the observed increase in the rupture length, as discussed in greater detail below.

Potential Barriers and the Off-rate of the Lowest Density under Activating Conditions

However, if the decrease of the off-rate with the ligand density is due to multiple bonds, the unchanged basal off-rate after activation with magnesium is in contradiction with the literature: in equilibrium measurements on the same receptor/ligand pair, a reduced off-rate of 0.07 s^{-1} was reported (37). The application of an external force, though, may result in a different unbinding path through the energy landscape influencing the barriers. Under equilibrium conditions, the lowest barrier is crossed and the corresponding off-rate should not be lower than an off-rate over a higher barrier enforced by external forces. Hence, the equilibrium off-rate of 0.07 s^{-1} is in conflict with our observed basal off-rate of 0.92 s^{-1} for the lowest density (37). This contradiction can be resolved, if the energy landscape has a transition state, which lies very far from the bound state. In equilibrium, this barrier will be rate determining (Fig. 7). In force exerting experiments, though, due to the tilting of the energy landscape, the transition state will be closer to the bound state and the outer barrier will not be probed (Fig. 7). Thus, in such a potential landscape, the off-rates measured with equilibrium and non-equilibrium experiments may not originate from the same energy barrier. For the interaction between the integrin $\alpha_v\beta_3$ and an RGD peptide, for example, such a far transition state is known from steered molecular dynamic simulations (47). Craig et al. described the position of the dominating transition barrier to be 1 nm away from the

bound state. Furthermore, the presence of force possibly alters the activity and the capability for activation of integrins (2,29,37,48) and therefore koff values measured in force free conditions may considerably vary from those extrapolated from koff values measured under external strain. However, force-applying techniques similar to our experiments have also measured a lower off-rate after integrin activation with magnesium (18,35). Zhang et al. found in AFM studies a basal off-rate of 0.04 s^{-1} for VLA-4 integrins activated with magnesium (18), possibly due to experimental differences in the cell type used, longer dwelling times and higher VCAM-1 densities each contributing to increased rebinding and enhanced avidity.

Multiple Bonds and Rebinding on Higher Densities under Activating Conditions

In the case of multiple bond per tethers, the rupture force is expected to be only slightly larger than the force to break one single bond (49), as we observed for the activating conditions (Fig. 2). The lifetime of the interactions, however, which corresponds in our setup to the rupture lengths due to the constant retract velocity, is known to strongly increase with the number of bonds, in agreement with our results described here (Fig. 2) (42,46).

The estimated average bond numbers n_a reported here are potentially overestimated due to the neglected rebinding effects. Yet, the lifetime of a tether held by two bonds can be approximated with a relation accounting for rebinding (14):

$$T = \frac{1}{2 \cdot k_{off}^0} \left(e^{-\frac{F \cdot \gamma}{2k_b T}} + 2e^{-\frac{F \cdot \gamma}{k_b T}} + \frac{k_{on}^*}{k_{off}^0} e^{-\frac{3 \cdot F \cdot \gamma}{2k_b T}} \right),$$ with k_{on}^* being the rate per time unit for the binding of

receptors and ligands in close proximity (14). For a ligand density of 100 sites/μm^2, a contact area in the AFM of 37 μm^2 and a two-dimensional on-rate under activating conditions of $1 \cdot 10^{-4} \mu m^2 s^{-1}$, this rate k_{on}^* is 0.37 s^{-1}. Assuming that only one of the two bonds is loaded ($F = 20$ pN), the lifetime of a two-bond cluster is 0.34 s for 100 sites/μm^2 of VCAM-1 under activating conditions, which corresponds to 1.1 μm at the here used retract velocity of 3.4 $\mu m/s$. If the load is shared equally between the two bonds ($F = 10$ pN), the lifetime of a two-bond cluster would be $t = 0.75$ s and the expected rupture length $l = 2.6$ μm. This is slightly longer than the median rupture length that we obtained for this ligand density under activating conditions of 2.3 μm. Considering the complexity of the system, the agreement between theory and experiment is striking. Thus, if one takes rebinding into account, on the order of 2 bonds are sufficient for the prolonged tether lifetimes observed in our experiments under activating conditions.

Avidity versus Affinity

Here, we deduce from our measurements that an exogenous activation leads to an increased local density of active VLA-4 at the contact area. This gives rise to multiple bonds with unchanged intrinsic koff, but a reduced off-rate of the high avidity contact. The alternative scenario is that the intrinsic koff is reduced, with an unaltered number of receptors. To compare the influence of the bond number and the impact of an altered off-rate, we simulated the two scenarios: 1) the distributions of rupture forces and rupture lengths with increasing number of bonds (for $n = 1, 2, 5$), but constant off-rate and potential width, thus increasing the avidity; and 2) the same distributions with a single bond, but varying off-rates ($k_{off}^0 = 10, 1.0, 0.1$ s^{-1}), thus increasing the affinity (Fig. 8). While the variation of the off-rate affects both the forces and the lengths, the variation of the bond number predominantly influences the lengths. In our experiments, we observe a strong effect on the rupture lengths and only a slight increase in the forces (Fig. 2). Hence, it appears probable that the apparent dependence of the off-rate on the

ligand density for activating condition may well be due to the presence of multiple bonds of unchanged affinity and not due to altered single-molecule properties.

Flow Chamber

The behaviour of cells in the blood stream is determined by the interplay of single molecules. We analyzed the data from the flow chamber mimicking the blood stream with a model incorporating the parameters observed from the single-molecule measurements. This together with inclusion of rebinding enables us to determine the effective force on the single bonds. This force $f_{effective}$ is reduced after integrin activation. Since the total force acting on the cell remains unchanged, this suggests that the total number of individual VLA-4/VCAM-1 bonds is increased after activation with magnesium. Based on the fit of equation 6 to our data (Fig. 5), the force acting on a single bond in the flow chamber is on the order of 40 pN and 15 pN for resting and activating conditions, respectively. The force acting on individual tethers has been estimated to be on the order of 100 pN for a shear of 0.75 dyn/cm^2 (14,45). Consequently, approximately 2-3 receptor-ligand bonds per tether share this load under resting conditions. For activating conditions, we estimate that there are on the order of 7 bonds per tether. For a ligand density of 100 sites/μm^2, the activation with high-concentrated magnesium increases therefore the number of bonds per tether about four-fold in the flow chamber as well as in the AFM setup. Accordingly, the maximum number of available receptors N_{tot} is also increased for activating conditions indicating a higher number of active VLA-4 on the cell. This is also reflected in the higher number of adhering cells after integrin activation. Hence, the prolonged lifetime of the cell-surface bonds of magnesium-treated cells is at least partially caused by the higher number of binding competent receptors per cell after integrin activation and thus an effect of an increased avidity. Therefore, the analysis of the flow chamber data corroborates the hypothesis of multiple bonds holding a tether after activation with magnesium.

Conclusions

In conclusion, we were unable to detect reduced koff for magnesium activated VLA-4 interacting under limiting VCAM-1 densities. At higher ligand densities, magnesium activated VLA-4, but not resting integrin became sufficiently elevated to support adhesive interactions with decreased off-rate due to multiple bonds. This points out that an avidity increase rather than a modulation of the intrinsic koff is the outcome of the exogenous activation of VLA-4 with magnesium. This increase in higher density of functional VLA-4 results in many more productive cellular attachments in the flow-chamber ensemble, suggesting that rebinding considerations have to be taken into consideration when physiological integrin interactions with adhesive ligands are measured under physiological settings.

Acknowledgements

References

1. Luo, B. H., Carman, C.V., Springer, T.A. 2007. Structural basis of integrin regulation and signaling. Annu Rev Immunol 25:619-647.

2.   Alon, R. and M. L. Dustin. 2007. Force as a facilitator of integrin conformational changes during leukocyte arrest on blood vessels and antigen-presenting cells. Immunity 26:17-27.

3.   Chigaev, A., A. M. Blenc, J. V. Braaten, N. Kumaraswamy, C. L. Kepley, R. P. Andrews, J. M. Oliver, B. S. Edwards, E. R. Prossnitz, R. S. Larson, and L. A. Sklar. 2001. Real time analysis of the affinity regulation of alpha 4-integrin. The physiologically activated receptor is intermediate in affinity between resting and Mn(2+) or antibody activation. J Biol Chem 276:48670-48678.

4.   Gottschalk, K. E. and H. Kessler. 2004. A computational model of transmembrane integrin clustering. Structure 12:1109-1116.

5.   Gottschalk, K. E. 2005. A coiled-coil structure of the alphaIIbbeta3 integrin transmembrane and cytoplasmic domains in its resting state. Structure 13:703-712.

6.   Liu, S., D. A. Calderwood, and M. H. Ginsberg. 2000. Integrin cytoplasmic domain-binding proteins. J Cell Sci 113 (Pt 20):3563-3571.

7.   Ginsberg, M. H., A. Partridge, and S. J. Shattil. 2005. Integrin regulation. Curr Opin Cell Biol 17:509-516.

8.   Iber, D. and I. D. Campbell. 2006. Integrin activation--the importance of a positive feedback. Bull Math Biol 68:945-956.

9.   Benoit, M., D. Gabriel, G. Gerisch, and H. E. Gaub. 2000. Discrete interactions in cell adhesion measured by single-molecule force spectroscopy. Nat Cell Biol 2:313-317.

10. Eibl, R. H. and V. T. Moy. 2005. Atomic force microscopy measurements of protein-ligand interactions on living cells. Methods Mol Biol 305:439-450.

11. Evans, E. and K. Ritchie. 1997. Dynamic strength of molecular adhesion bonds. Biophys J 72:1541-1555.

12. Hanley, W., O. McCarty, S. Jadhav, Y. Tseng, D. Wirtz, and K. Konstantopoulos. 2003. Single molecule characterization of P-selectin/ligand binding. J Biol Chem 278:10556-10561.

13. Hanley, W. D., D. Wirtz, and K. Konstantopoulos. 2004. Distinct kinetic and mechanical properties govern selectin-leukocyte interactions. J Cell Sci 117:2503-2511.

14. Schwarz, U. S. and R. Alon. 2004. L-selectin-mediated leukocyte tethering in shear flow is controlled by multiple contacts and cytoskeletal anchorage facilitating fast rebinding events. Proc Natl Acad Sci U S A 101:6940-6945.

15. Laudanna, C. and R. Alon. 2006. Right on the spot. Chemokine triggering of integrin-mediated arrest of rolling leukocytes. Thromb Haemost 95:5-11.

16.   Bell, G. I. 1978. Models for the specific adhesion of cells to cells. Science 200:618-627.

17.   Alon, R., S. W. Feigelson, E. Manevich, D. M. Rose, J. Schmitz, D. R. Overby, E. Winter, V. Grabovsky, V. Shinder, B. D. Matthews, M. Sokolovsky-Eisenberg, D. E. Ingber, M. Benoit, and M. H. Ginsberg. 2005. Alpha4beta1-dependent adhesion strengthening under mechanical strain is regulated by paxillin association with the alpha4-cytoplasmic domain. J Cell Biol 171:1073-1084.

18.   Zhang, X., S. E. Craig, H. Kirby, M. J. Humphries, and V. T. Moy. 2004. Molecular basis for the dynamic strength of the integrin alpha4beta1/VCAM-1 interaction. Biophys J 87:3470-3478.

19.   Grabovsky, V., S. Feigelson, C. Chen, D. A. Bleijs, A. Peled, G. Cinamon, F. Baleux, F. Arenzana-Seisdedos, T. Lapidot, Y. van Kooyk, R. R. Lobb, and R. Alon. 2000. Subsecond induction of alpha4 integrin clustering by immobilized chemokines stimulates leukocyte tethering and rolling on endothelial vascular cell adhesion molecule 1 under flow conditions. J Exp Med 192:495-506.

20.   Florin, E. L. R., M.; Lehmann, H.; Ludwig, M.; Dornmair, C.; Moy, V.,T.; Gaub, H.-E. 1995. Sensing specific molecular interactions with the atomic force microscope. Biosensors and Bioelectronics 10:895-901.

21.   Butt, H.-J., Jaschke, M. 1995. Calculation of thermal noise in atomic force spectroscopy. Nanotechnology 6:1-7.

22.   Kunkel, E. J., J. L. Dunne, and K. Ley. 2000. Leukocyte arrest during cytokine-dependent inflammation in vivo. J Immunol 164:3301-3308.

23.   Barry, S. T., S. B. Ludbrook, E. Murrison, and C. M. Horgan. 2000. Analysis of the alpha4beta1 integrin-osteopontin interaction. Exp Cell Res 258:342-351.

24.   Lin, K., H. S. Ateeq, S. H. Hsiung, L. T. Chong, C. N. Zimmerman, A. Castro, W. C. Lee, C. E. Hammond, S. Kalkunte, L. L. Chen, R. B. Pepinsky, D. R. Leone, A. G. Sprague, W. M. Abraham, A. Gill, R. R. Lobb, and S. P. Adams. 1999. Selective, tight-binding inhibitors of integrin alpha4beta1 that inhibit allergic airway responses. J Med Chem 42:920-934.

25.   Feigelson, S. W., V. Grabovsky, R. Shamri, S. Levy, and R. Alon. 2003. The CD81 tetraspanin facilitates instantaneous leukocyte VLA-4 adhesion strengthening to vascular cell adhesion molecule 1 (VCAM-1) under shear flow. J Biol Chem 278:51203-51212.

26.   Shamri, R., V. Grabovsky, J. M. Gauguet, S. Feigelson, E. Manevich, W. Kolanus, M. K. Robinson, D. E. Staunton, U. H. von Andrian, and R. Alon. 2005. Lymphocyte arrest requires instantaneous induction of an extended LFA-1 conformation mediated by endothelium-bound chemokines. Nat Immunol 6:497-506.

27.   Zhu, C. 2000. Kinetics and mechanics of cell adhesion. J Biomech 33:23-33.

28.   Schmitz, J., M. Benoit, and K. Gottschalk. in press. The Viscoelasticity of Membrane Tethers and its Relation to Cell Adhesion. Biophys J.

29.   Zhu, C., T. Yago, J. Lou, V. I. Zarnitsyna, and R. P. McEver. 2008. Mechanisms for flow-enhanced cell adhesion. Ann Biomed Eng 36:604-621.

30.   Chesla, S. E., P. Selvaraj, and C. Zhu. 1998. Measuring two-dimensional receptor-ligand binding kinetics by micropipette. Biophys J 75:1553-1572.

31.   Erdmann, T. and U. S. Schwarz. 2004. Stability of adhesion clusters under constant force. Phys Rev Lett 92:108102.

32.   Rosenbluth, M. J., W. A. Lam, and D. A. Fletcher. 2006. Force microscopy of nonadherent cells: a comparison of leukemia cell deformability. Biophys J 90:2994-3003.

33.   Zhang, X., E. P. Wojcikiewicz, and V. T. Moy. 2006. Dynamic adhesion of T lymphocytes to endothelial cells revealed by atomic force microscopy. Exp Biol Med (Maywood) 231:1306-1312.

34.   Chen, J., J. Takagi, C. Xie, T. Xiao, B. H. Luo, and T. A. Springer. 2004. The relative influence of metal ion binding sites in the I-like domain and the interface with the hybrid domain on rolling and firm adhesion by integrin alpha4beta7. J Biol Chem 279:55556-55561.

35.   de Chateau, M., S. Chen, A. Salas, and T. A. Springer. 2001. Kinetic and mechanical basis of rolling through an integrin and novel Ca2+-dependent rolling and Mg2+-dependent firm adhesion modalities for the alpha 4 beta 7-MAdCAM-1 interaction. Biochemistry 40:13972-13979.

36.   Benoit, M. and H. E. Gaub. 2002. Measuring cell adhesion forces with the atomic force microscope at the molecular level. Cells Tissues Organs 172:174-189.

37.   Chigaev, A., G. Zwartz, S. W. Graves, D. C. Dwyer, H. Tsuji, T. D. Foutz, B. S. Edwards, E. R. Prossnitz, R. S. Larson, and L. A. Sklar. 2003. Alpha4beta1 integrin affinity changes govern cell adhesion. J Biol Chem 278:38174-38182.

38.   Chen, C., J. L. Mobley, O. Dwir, F. Shimron, V. Grabovsky, R. R. Lobb, Y. Shimizu, and R. Alon. 1999. High affinity very late antigen-4 subsets expressed on T cells are mandatory for spontaneous adhesion strengthening but not for rolling on VCAM-1 in shear flow. J Immunol 162:1084-1095.

39.   Dustin, M. L., L. M. Ferguson, P. Y. Chan, T. A. Springer, and D. E. Golan. 1996. Visualization of CD2 interaction with LFA-3 and determination of the two-dimensional dissociation constant for adhesion receptors in a contact area. J Cell Biol 132:465-474.

40. Kuo, S. C. and D. A. Lauffenburger. 1993. Relationship between receptor/ligand binding affinity and adhesion strength. Biophys J 65:2191-2200.

41. Wojcikiewicz, E. P., M. H. Abdulreda, X. Zhang, and V. T. Moy. 2006. Force spectroscopy of LFA-1 and its ligands, ICAM-1 and ICAM-2. Biomacromolecules 7:3188-3195.

42. Seifert, U. 2000. Rupture of multiple parallel molecular bonds under dynamic loading. Phys Rev Lett 84:2750-2753.

43. Sulchek, T. A., R. W. Friddle, K. Langry, E. Y. Lau, H. Albrecht, T. V. Ratto, S. J. DeNardo, M. E. Colvin, and A. Noy. 2005. Dynamic force spectroscopy of parallel individual Mucin1-antibody bonds. Proc Natl Acad Sci U S A 102:16638-16643.

44. Fisher, H. W. and T. W. Cooper. 1967. Electron microscope studies of the microvilli of HeLa cells. J Cell Biol 34:569-576.

45. Shao, J. Y., H. P. Ting-Beall, and R. M. Hochmuth. 1998. Static and dynamic lengths of neutrophil microvilli. Proc Natl Acad Sci U S A 95:6797-6802.

46. Tees, D. F., R. E. Waugh, and D. A. Hammer. 2001. A microcantilever device to assess the effect of force on the lifetime of selectin-carbohydrate bonds. Biophys J 80:668-682.

47. Craig, D., M. Gao, K. Schulten, and V. Vogel. 2004. Structural insights into how the MIDAS ion stabilizes integrin binding to an RGD peptide under force. Structure 12:2049-2058.

48. Krammer, A., D. Craig, W. E. Thomas, K. Schulten, and V. Vogel. 2002. A structural model for force regulated integrin binding to fibronectin's RGD-synergy site. Matrix Biol 21:139-147.

49. Williams, P. M. 2003. Analytical descriptions of dynamic force spectroscopy: behaviour of multiple connections. Analytica Chimica Acta 479:107-115.

Figure Legends.

Figure 1: *AFM Setup.*
A) The integrin-expressing T-lymphocyte is attached to a cantilever and placed in contact with a functionalized surface at a pre-defined contact force for a chosen contact time, during which the receptor can diffuse to the ligand. After the contact time, the cantilever is retracted. The force is applied vertically, so that rebinding is effectively suppressed. **B)** A force-time curve is shown. The dotted blue line shows the piezo position (right y-Axis), from which a force-distance curve can be obtained. From the curves, the distribution of rupture forces as well as of the rupture lengths is obtained. The red-boxed part of the force curve is extended in the right panel to show the fit with the force-distance relationship of equation 2. **C)** In the blood stream, the cells are exposed to shear forces generated by a laminar flow. Multiple bonds can hold the cell, some of which can re-bind after breakage (*). If a bond breaks at the rear end, a new bond can be formed at the front end due to the torque experienced by the cell (arrow). The flow chamber mimicks this force application and recors the number of attaching cells as well as the life-time of attachment with videomicroscopy at the desired temporal resolution.

Figure 2: *Effect of Magnesium in AFM Experiments.*
Magnesium leads to a ligand density-dependent increase in the median rupture force and in the median rupture length (*red boxes*). Under resting conditions, both the rupture force and the rupture length are independent of the ligand density (*empty boxes*). The boxes indicate the second and third quartile of the distribution for each condition and the whiskers 1.5 fold of the interquartiles. The median is indicated. For the lowest ligand density, no significant differences between activating and resting conditions can be seen. Yet, with increasing ligand density, the forces and lengths obtained under activating conditions differ significantly from the forces and lengths of the respective ligand density under resting conditions.

Figure 3: *Monte-Carlo Simulations.*
A) The potential width is plotted against the basal off-rate for the different ligand densities (*size of the markers increasing with density*) under activating (*red triangles*) and resting conditions (*black circles*). Both parameters were obtained from the Monte-Carlo simulation assuming single bonds ($n = 1$). **B)** Shown are the histograms of rupture forces and rupture lengths measured under activating conditions at 100 sites/μm^2 (*black bars*) and the simulated lengths and force distributions obtained in Monte-Carlo simulations with $n = 1$ (*light blue*) and with $n > 1$ (*dark blue*).

Figure 4: *Number of Bonds.* **A)** The number of ruptures per force-distance curve is recorded for different ligand densities and fitted with equation 3 for resting integrins (data: black circles, fit: black line). The y-error bars correspond to the standard deviation between the cells and the x-error bars to the deviation in the contact area. The fits for the minimal and maximal on-rates within the errors of the contact area and of the number of ruptures are shown as dotted lines. **B)** Mg-activation leads to a vastly increased number of averaged bonds (red triangles) compared to resting conditions (black circles).

Figure 5: *Flow Chamber*.
A) A comparison of the lifetime measured with the flow chamber is shown for a ligand density of 100 sites/μm^2 for resting VLA-4 (*black*) and for activated integrins (*red*). The solid line is the fit of equation 6, using the parameters determined from the single-molecule measurements. The dashed line is the single-exponential fit according to $\ln(n) = a - k_{off}^F \cdot t$. **B)** The cumulative frequencies of adhesion in the flow chamber are shown for two categories, arrest (empty bars) and transient adhesions (black bars). The total number of adhering cells is increased after VLA-4 activation with magnesium. Furthermore, magnesium leads to significantly higher numbers of arresting cells.

Figure 6: *Effect of Magnesium on Adhesion Determined by AFM.* The cell is retracted with the cantilever from the substrate (arrow). On the lymphocyte, a pool of inactive VLA-4 receptors (blue) is co-existent with a subset of active VLA-4 (red). While only a small fraction of integrins is binding-competent under resting conditions of 1 mM Ca^{2+}/Mg^{2+} (*top*), many more receptors become activated by 5 mM Mg^{2+} (*bottom*). Hence, multiple interactions can distribute the load at high ligand density (*bottom right*), when the cell is pulled away. At low ligand density (*left*), the effects of magnesium are much less pronounced than at high densities (*right*).

Figure 7: *Effect of Force on a Potential Landscape with two Barriers.* **A)** In the equilibrium landscape (*blue*), the outer barrier *#O* is dominant and therefore rate determining. **B)** Under the influence of an external force *F*, the energy landscape is tilted by *-Fx* (*red*) and the inner barrier *#I^F* becomes the transition barrier. Hence, equilibrium experiments and force applying experiments possibly measure different energy barriers in the potential landscape.

Figure 8: *Effect of Bond Number and Off-rate on the Force and Length Distributions.* **A)** With Monte-Carlo simulations, the influence of the bond number on the distributions of rupture force (*left*) and rupture length (*right*) was estimated for n_a = 1, 2 and 5 (no rebinding). In the middle panel, the median values of the force distributions (*top*) and the lengths distributions (*bottom*) are plotted against the bond number. **B)** The influence of the basal off-rate on the distributions of rupture force (*left*) and rupture length (*right*) was estimated for n = 1 with k_{off}^0 = 10, 1 and 0.1 s^{-1}. In the middle panel, the median values of the force distributions (*top*) and the lengths distributions (*bottom*) are plotted against the logarithmical off-rates.

Figure 1

Figure 2.

Figure 3.

Figure 4

Figure 5.

Low ligand density

High ligand density

$1mM$
Ca^{2+}/Mg^{2+}

Cell

force

inactive
VLA-4

Substrate

VCAM-1

$5mM\ Mg^{2+}$

active
VLA-4
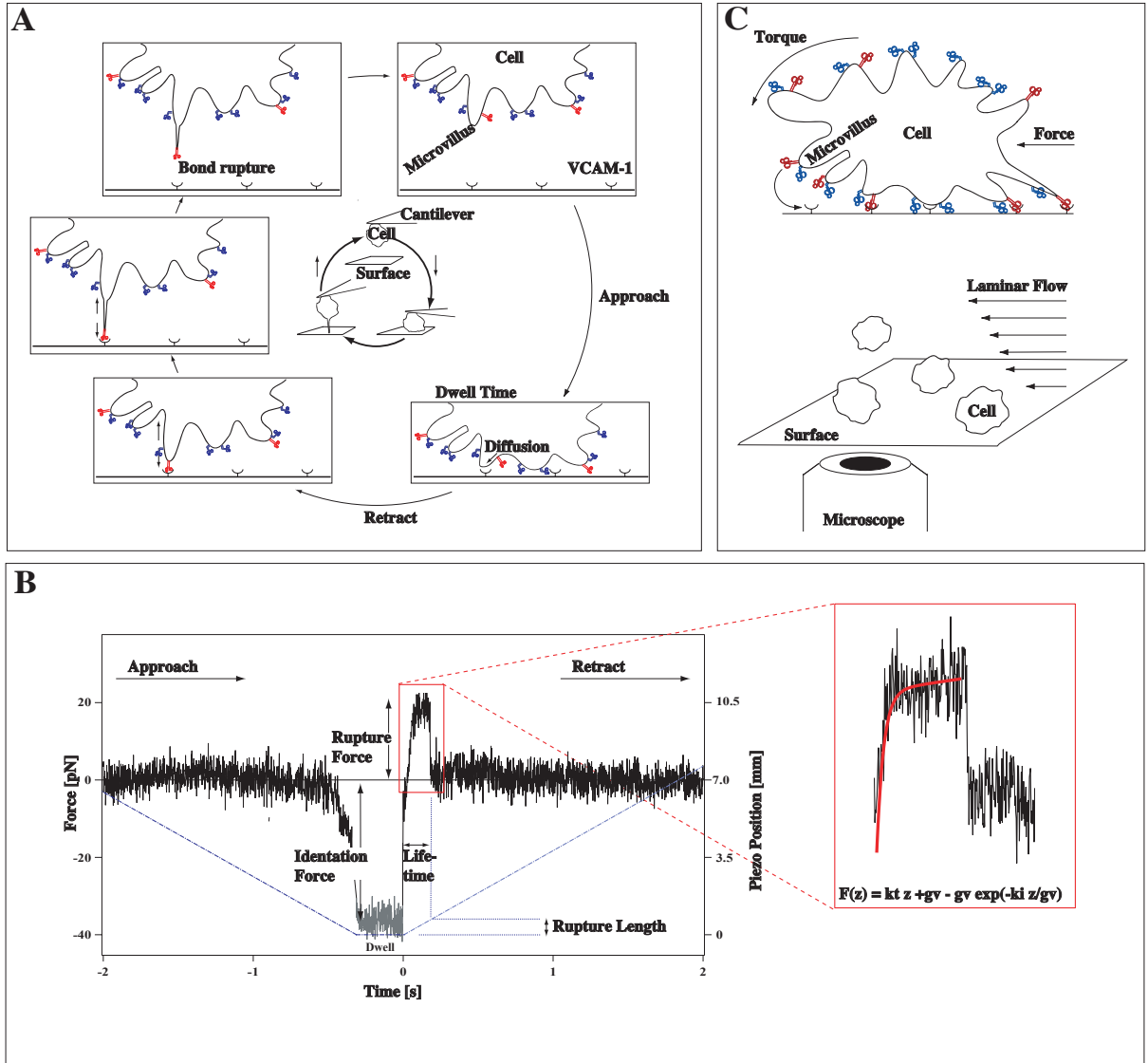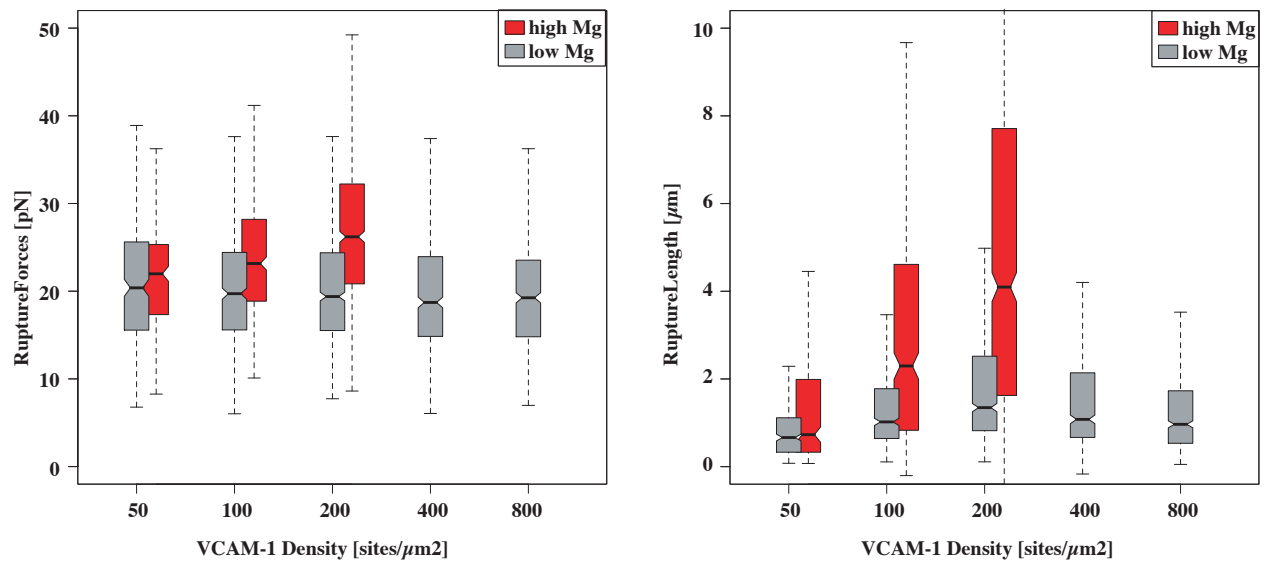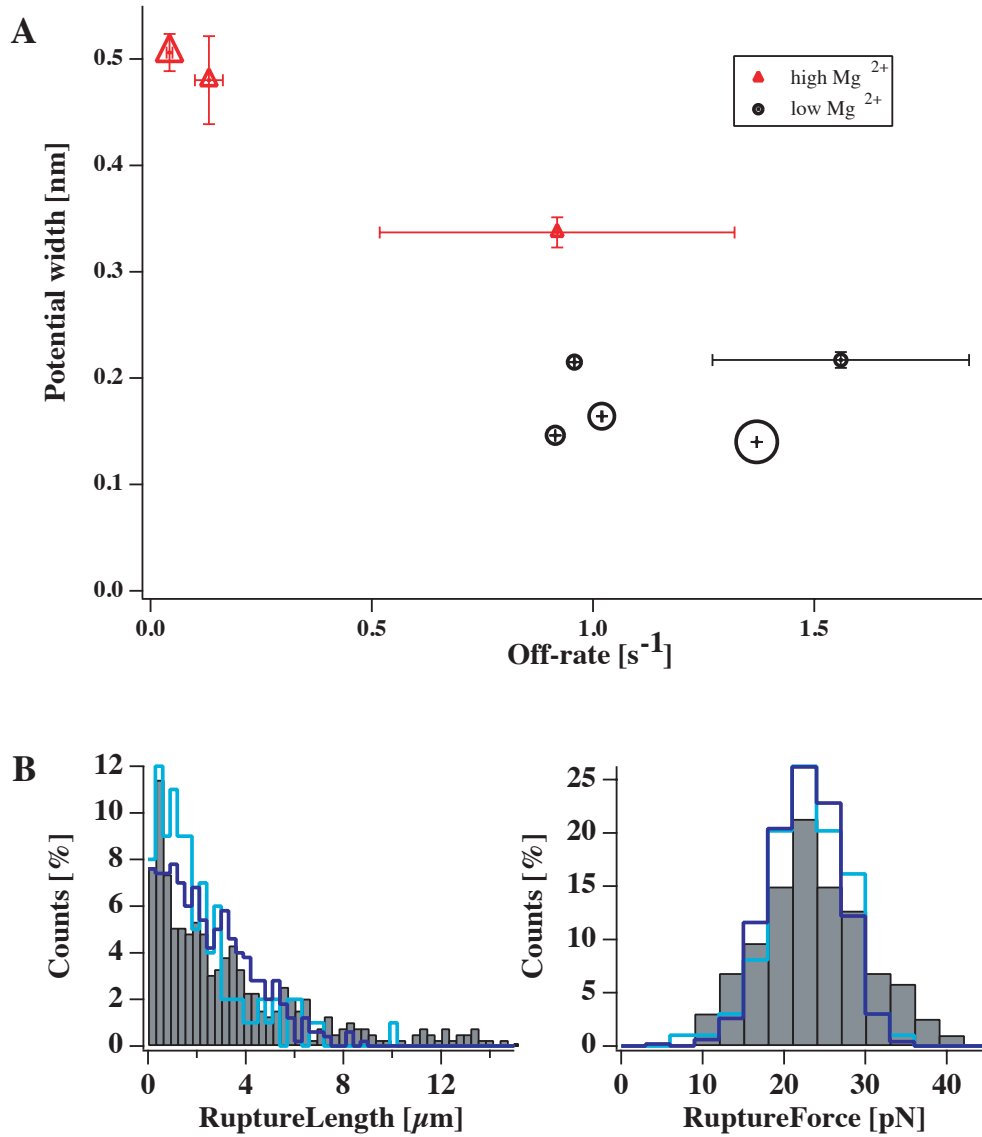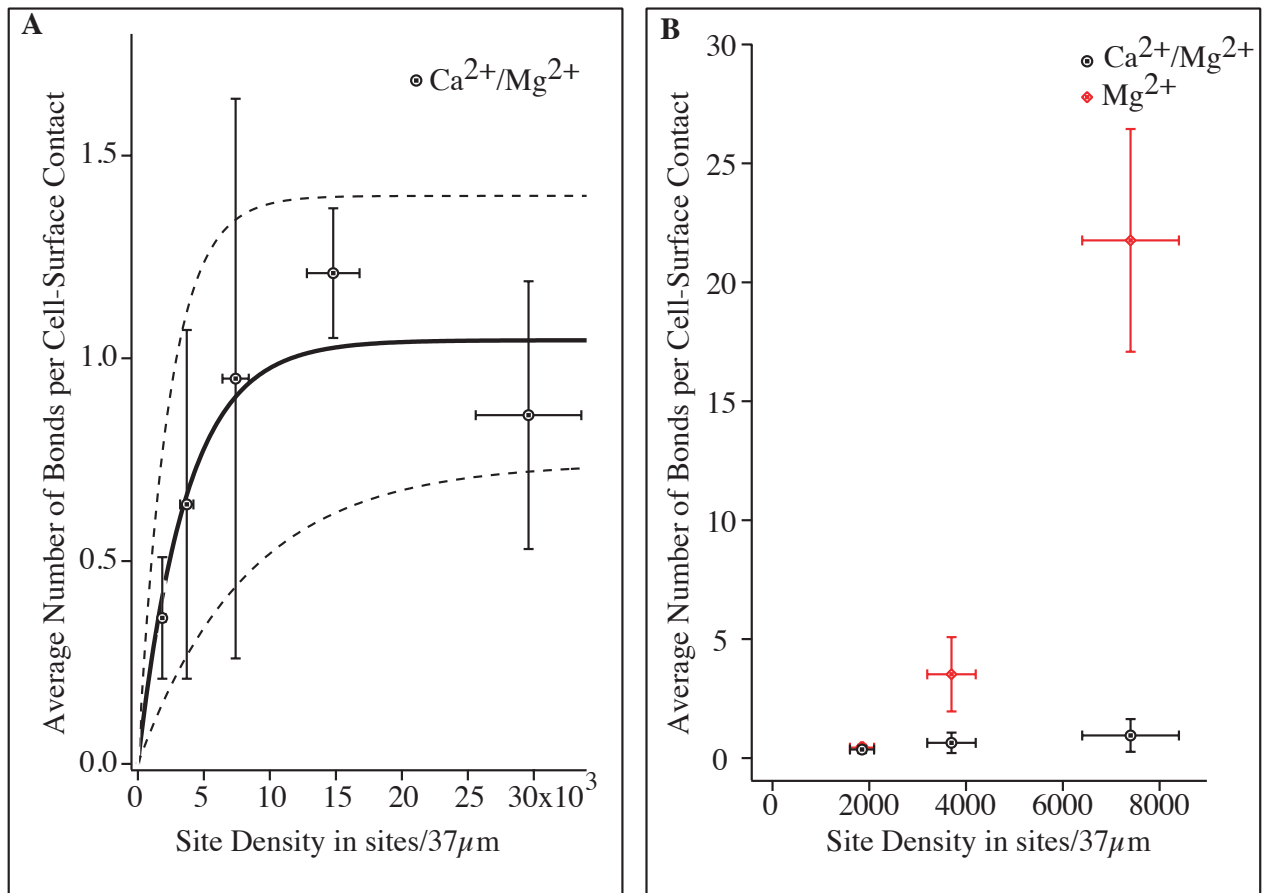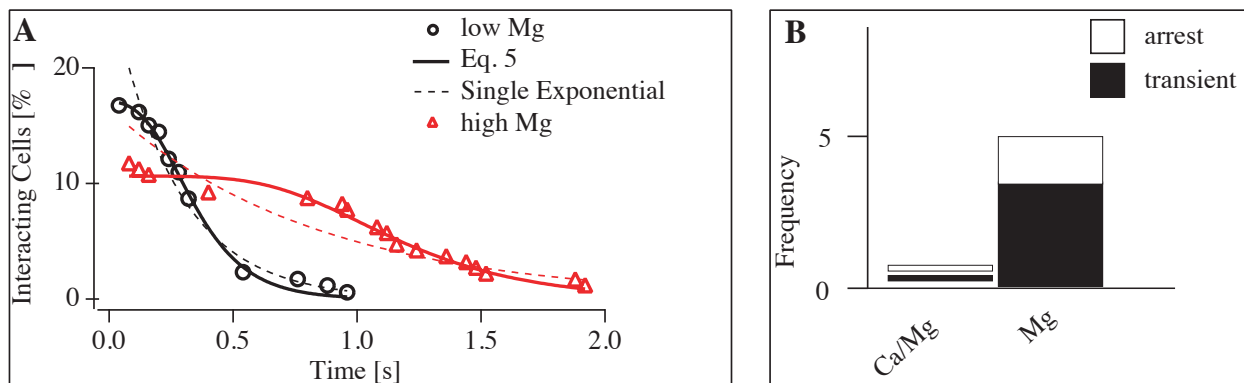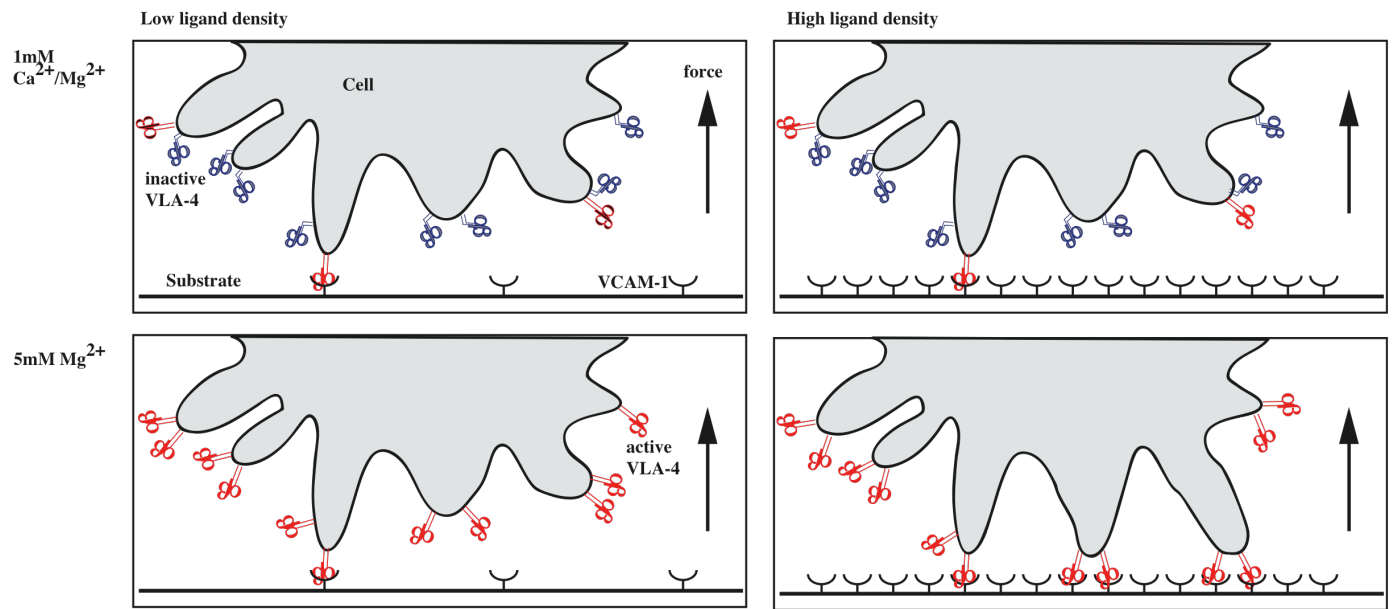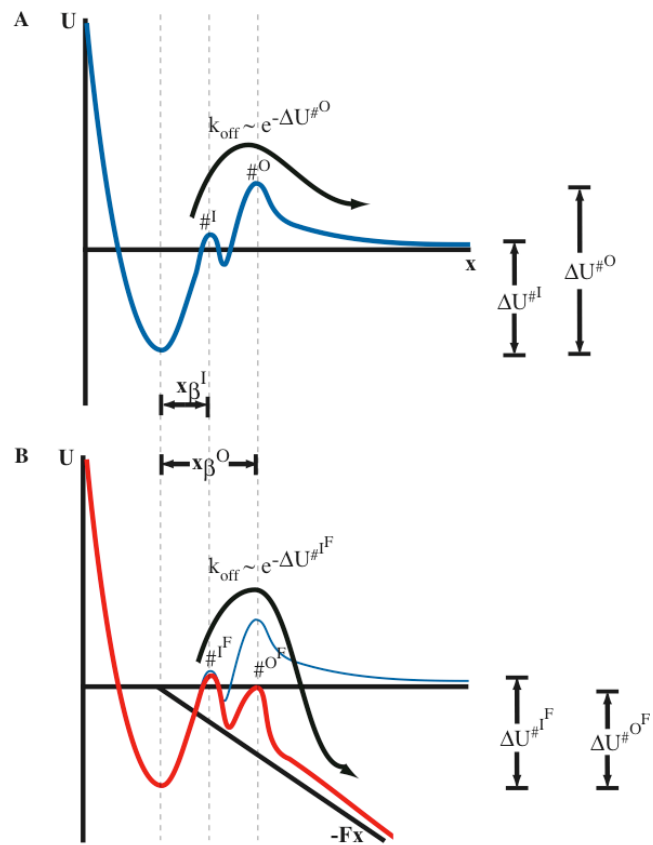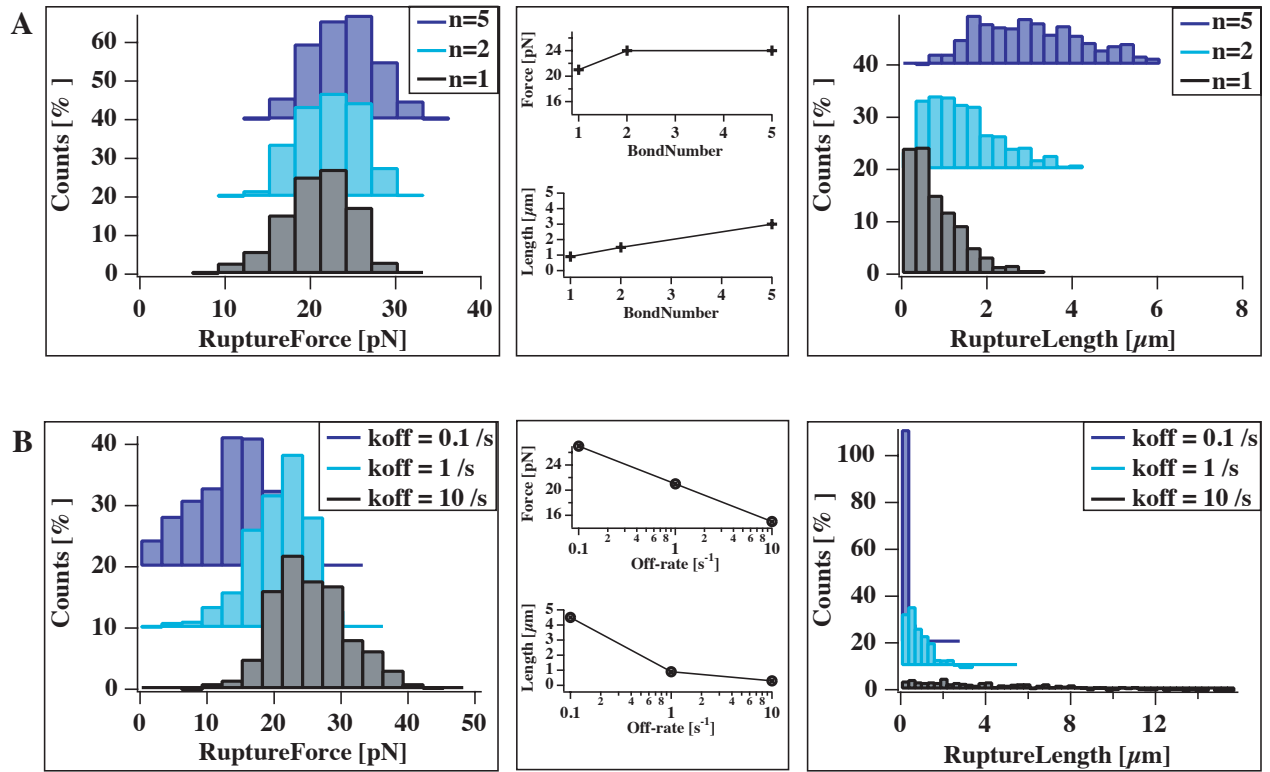
Figure 6.

Figure 7.

Figure 8.

Chapter 5

Opto-Mechanical Studies of Cell Adhesion

Modern optical techniques are widespread in cell biology. In particular, the field of fluorescence microscopy has rapidly expanded during the last few years. In integrin research, FRET studies have helped to observe structural changes. For instance, the separation of the cytoplasmic integrin tails upon activation [28] has been scrutinised by this technique as well as the correlation between the affinity and the extension of the receptor [145]. However, on the one hand, these studies were not conducted on the single-molecule level. For integrins, which occur in different conformations on the cell varying in their structure, their affinity and their anchorage [146], ensemble measurements cannot resolve the different receptor populations, but average over all distributions. On the other hand, it has been sufficiently proven that forces and other mechanical parameters play a crucial role for cell adhesion receptors (see chapter 2). A physiological investigation of integrins implicates a force-exerting setup. A combination of force spectroscopic and optical techniques operating on the single-molecule level will provide answers to many urgent questions in cellular research.

Here, we explored cell adhesion to different surfaces using a home-built combination of an AFM and TIRF microscope. We correlated the rupture of a membrane tether pulled from the fluorescently labelled cell with the force evolution on the molecular bond. Labelling VLA-4 integrins with the affinity-sensitive label BIO1211-Alexa488, we demonstrate that it is possible to detect changes in the receptor affinity induced by activating stimuli.

5.1 The Power of Opto-Mechanical Approaches for the Investigation of Cell Adhesion

Glass surfaces are known to present powerful activators of blood cells provoking strong unspecific adhesion. We used this fact to prove the visualisation of tethers pulled from cells with fluorescently labelled membrane. Indeed, clean glass surfaces unveiled an enormous adhesive activity for lymphocytes in AFM experiments. The membrane tethers adhering

unspecifically to the glass elongated as long as 5 μm and indeed were sometimes difficult to remove within the piezo range of 5 μm. For this reason, several membrane tethers could be glued parallel to the surface and were clearly visible in the TIRF microscope.

Since the observation of membrane tethers was shown to be feasible with our setup, we went on to examine tethers pulled on specific receptor/ligand bonds. For this, we passivated the glass surface with poly-ethylen glycol and coated this substrate covalently with the integrin ligand VCAM-1. This markedly reduced the interaction frequency and lead to much shorter ruptures with lower forces than on the pure glass surface. In fact, the rupture characteristics of this specific adhesive contact correspond well with our previously measured rupture forces and lengths for the VLA-4/VCAM-1 bond. Furthermore, no membranous leftovers could be detected on the functionalised and passivated substrate with the fluorescence microscope. This indicates that for membrane tethers pulled on specific receptor/ligand interactions, the rupture event does not result from the rupture of the tether itself, but rather from the dissociation of the adhesive bond. Since we simultaneously recorded the force evolution with the AFM and the fluorescence intensity in TIRF video microscopy, we were able to correlate the mechanical rupture event with changes in the fluorescence. To align both data sets, we determined the point of the first contact between the cell and the substrate in the force curve and in the fluorescence trace by exploiting the exponential behaviour of the fluorescence intensity in the TIRF setup. The high temporal and spatial resolution of the TIRF video and the force spectroscopic data enabled us not only to relate the mechanical events with the optical observations, but allowed us even to discriminate between adherent tethers and protruding non-interacting microvilli.

As a further application of the TIRF-AFM setup, we showed that affinity changes can be detected using affinity-sensitive fluorescent labels. For this, we utilised the AFM for the positioning of the cell in the TIRF field. The medium contained labelled BIO1211, a peptidomimetic, which specifically binds into the binding pocket of the lymphocyte integrin VLA-4 with an association constant depending on the integrin conformation [138,147,148]. The concentration of the fluorescent marker was adjusted such, that mainly the high-affinity conformation of VLA-4 was labelled. Adding concentrated magnesium to the calcium-free medium induced an increase in the mean fluorescence. This corroborates our observation that integrin activation by magnesium recruits resting low-affinity receptors.

The publication of these data is in preparation and reprinted in section 5.3.

5.2 Conclusions

As discussed before, biochemical and mechanical stimuli influence the cell adhesion and lead to biochemical and mechanical reactions of the cell. In addition, the cellular adhesiveness depends on the attributes of single molecules, such as the affinity state of the receptor molecules, the receptor density on the cell surface and the mechanics of the receptor anchorage in the cell. Hence, opto-mechanical techniques such as the TIRF-AFM, which empower parallel single-molecule studies, open a new field for the experimental investigation of cell adhesion. We outlined the potential of this approach for investigating

both the mechanics of cellular tethers and the affinity changes of single cell-surface receptors. An interesting application for the TIRF-AFM setup complementary to the study area of this thesis would be the opto-mechanical examination of integrin activation by surface-bound chemokines. In such an approach, potential integrin clustering could be observed by single-particle tracking; possible affinity changes could be ascertained with affinity-sensitive labels and structural changes or intracellular anchorage events could be discovered in FRET studies.

Thus, single-molecule force spectroscopy with high-end fluorescent techniques is an efficient tool for unravelling dynamic modifications in the structure or in the conformation of single receptors, which can result in situ from cellular reactions to mechanical or biochemical stimuli.

5.3 Publications

1. Single-Tether Opto-Mechanical Investigation of Cell Adhesion (*in preparation*)

Single-tether opto-mechanical investigation of cell-adhesion

Julia Schmitz[1], Hermann Gumpp[1], Elias Puchner[1], Hermann E. Gaub[1],

Kay-Eberhard Gottschalk[1*]

[1]Department for Applied Physics and Centre for NanoSciences,

Ludwig-Maximilians University,

80799 Munich, Germany.

[*]To whom correspondence should be addressed:

E-mail: kay.gottschalk@physik.uni-muenchen.de.

Regulated cell adhesion is involved in a variety of physiological and patho-physiological events like the immune response or cancer metastasis. State-of-the-art fluorescence techniques are widely used in cell biology, but operate under equilibrium conditions. Recently, force has been identified as a facilitator of cell adhesion. Hence, the application of force is crucial for a molecular understanding of cell adhesion events. Yet, while traditional setups like micropipette experiments or AFM can administer forces even at the single-molecule level, they still lack the ability to use the power of single-molecule optical techniques. Here, we investigate integrin-mediated cell-adhesion by a combination of single-molecule AFM and total-internal reflection fluorescence (TIRF) microscopy. We observe the formation of a single cell-to-surface tether and correlate this to the strength of the individual integrin-ligand interaction. The combination of TIRF with AFM will revolutionise the experimental investigation of cell-adhesion events.

Cell adhesion is regulated by specific interactions of cellular receptors with ligands in the extra-cellular space. The interactions of cell-adhesion receptors are designed to take place in the presence of force. Hence, experimental techniques capable of administering forces are required to gain physiological insight into the function of cell-adhesion receptors. In order to regulate their adhesive properties, cells can fine-tune the conformational state of these receptors (affinity regulation), the number of binding-competent receptors per area (avidity regulation) as well as the attachment state of the receptor to the cytoskeleton. The variety of possible states of a receptor on the cellular surface requires the use of single-molecule studies to dissect individual contributions of these states to overall cell-adhesiveness. Two different lines of research have been employed to study cell-adhesion receptors on the single-molecule level: (1) force spectroscopic techniques have examined the effect of force on single receptor-ligand bonds, and (2)

optical studies have examined lateral mobility and other properties of these receptors. While the force spectroscopic techniques mimic the natural force-resisting function of the receptors, they lack the power to optically investigate the effect of force on the cells. The optical measurements, on the other side, work under equilibrium conditions, and therefore do not probe the physiological setting of force-exposed receptors.

Using a home-built combination of a TIRF microscope with an atomic force microscope, we have merged these two approaches. Here, we report opto-mechanical studies of a cell interacting with surfaces. Figure 1 shows the experimental setup of our system: an AFM is combined with a TIRF setup illuminating the sample from the bottom. In this setup, the AFM can be used to manipulate the cells and to monitor the forces of adhesion, while the optics can be used to observe the interactions on the surface visually.

As a first measurement, we labelled the membrane of T-lymphocytes fluorescently, and used the AFM as a positioning device to push the cells onto un-functionalized glass surfaces, and retract the cells afterwards. Glass surfaces are known to be unspecifically adhesive for blood cells. Indeed, we observed the formation of long membrane tethers, which could be visualised by laterally displacing the cells and pushing it back onto the surface (Figure 2). Due to the non-specificity of the interaction, the glass surface acts as a high avidity surface. This leads to very durable adhesions, and ruptures were hardly observed.

Next, we covalently coated the glass surface with polyethylen-glycole to effectively suppress unspecific binding, and covalently functionalized the PEG-passivated glass surface with diluted VCAM-1, the ligand to the T-lymphocyte integrin VLA-4. The number and duration of adhesions decreased significantly relative to the bare glass. Short ruptures were observed, which allow the investigation of the breakage of a single cell-to-surface tethers.

The fluorescence of the cell showed a strongly curved profile while the cell is approaching the surface (Figure 3). Analysing the time-trace of the total cellular fluorescence shows an

exponential increase in fluorescence intensity with decreasing cell-to-surface distance, as expected for TIRF measurements. Hence, the curvature of the cellular fluorescence is caused by the curved shape of the cell, where certain areas are closer to the surface than others. At a certain point, the average fluorescence strongly deviated from the exponential behaviour, allowing for the identification of the point of first contact (Figure 3). The approach velocity of the cell is known from the piezo velocity. With this, we used the exponential increase in fluorescence during the approach curve together with the knowledge of the point of first contact to calibrate the distance of the cell to the surface at each frame. Since the cell has a curved surface, the brightness of the fluorescence was calibrated at the point of first contact, thus using only a small area at the top of the cell. The frame rate of the CCD camera of 50 ms together with an approach velocity of 3 $\mu m/s$ allows to reach maximum precision of the distance d of $d \pm 75nm$. This maximum precision is further reduced by noise. Despite the inherent inaccuracies, the distance-fluorescence relationship could be well fitted with an inverse exponential relationship (Figure 3). Recalculating the approach velocity v of the cell from the fluorescence intensity yields $v_{calc} = 2.98 \pm 0.05~\mu m/s$, in good agreement with the piezo velocity of $v_{piezo} = 3.0 \mu m/s$.

As known from previous studies, the force required to extract one membrane tether is on the order of 20-30 pN. This indicates that we are observing the rupture of a single cell-to-surface tether here. In order to optically investigate this rupture, we correlated the AFM force-distance curves with the fluorescence images from the TIRF measurements with the knowledge of the contact time in the AFM and the identification of the dwell time in the fluorescence images. From this, we identified two membrane areas, which are still in contact with the substrate in the last frame before the rupture, although we observed only the rupture of a single tether in the AFM. Calculating the distance-time trace of these two contact areas from the distance-fluorescence relationship obtained above showed that one of the contact areas closely follows the retract velocity of the cantilever (Figure 4). Hence, this contact is a non-adhesive protrusion

from the cell, probably a microvillus. The other contact area, however, has a distinct jump in the cell-to-surface distance at the point of rupture, which is then followed by a slow relaxation behaviour. Only $\sim 200ms$ after the rupture, this surface patch retracts with the piezo velocity. Hence, this second area is an adhesive contact, and we observed a single cell-to-surface tether and watched its rupture (Figure 4).

Next, we used a PEG-passivated glass surface and an unlabelled cell, but added fluorescently marked Bio-1211 in access to it so that binding competent integrins were saturated by the labelled marker. We measured under two conditions: without divalent cations and with 5mM Mg^{2+} in the buffer. Without divalent cations, integrins do not bind their ligands, while they are activated by the addition of 5 mM Mg^{2+}. Here, we used the AFM as a positioning tool to push the cell for a defined time at a defined force and watch the activation state of integrins at the same time. We found a good correlation between piezo-position and average fluorescence for the activated integrins. For cells under non-binding conditions, the fluorescence intensity in contact is significantly reduced (Figure 5). This demonstrates that we can detect different activation states of the cell using fluorescently-marked ligands.

With the here-described combination of high-end optical and single molecule force spectroscopy one will be able to analyse in-depth a variety of urgent cell-biological questions. Possible studies involve the correlation of the integrin-structure determined by FRET-based studies with the bond strength of a single integrin-ligand bond or the correlation between integrin-mobility detected by single-particle tracking of integrins while the cell is in contact with the surface and the adhesiveness of the cell. These studies will be instrumental for a in-depth opto-mechanical characterisation of physiological integrin-activation events and downstream signalling events.

1 Figure Captions.

Figure 1: ***Combination of TIRF with AFM.*** In the combination of TIRF with AFM (**A**), a state-of-the-art TIRF setup is combined with an AFM. Using a cell with a fluorescently labelled membrane, we can resolve single cell-to-surface tethers during retraction (B, white circles). This setup is capable of single-molecule fluorescence studies combined with the force readout. Such a combination allows a new approach to cellular signalling involving adhesion events.

Figure 2: ***A T-cell with labelled membrane adheres unspecifically to a glass surface.*** With the AFM, the cell is gently pushed onto the glass surface and then retracted. After retraction, bright spots are visible in the TIRF image. When laterally displacing the cell with the AFM and pushing it back onto the surface, it becomes visible that the three bright spots correspond to membrane tethers pulled from the cell.

Figure 3: ***Correlation between Fluorescence and Cell-to-Surface Distance.*** **A:** Before the cell touches the surface, the fluorescence profile is non-flat (left: fluorescence image; right: surface plot of fluorescence intensity). This reflects the curved surface of the cell. **B:** Initially, the fluorescence intensity follows an exponential increase, as expected from the TIRF measurement for a fluorescent particle approaching the surface with constant velocity. The deviation from exponential behaviour marks the point of first contact (left: all frames; right: zoom into the dashed region indicated left). The error-bars indicate the standard deviation in fluorescence over the averaged area. For this subfigure, we averaged over the ellipse shown in subfigure A. **C:** From the point of contact with the knowledge of the camera's frame rate and the retract velocity of the piezo, we calculated the distance of the cellular surface for each frame, and correlated this to the average fluorescence intensity of the most protruding area indicated in

subfigure A as 'Calibration Area'. The fit of the correlation allows us to calculate distances from the fluorescence intensity. The error bars in the distance stem from the frame-rate of 20 Hz, which leaves at a retract velocity of $3\mu m/s$ an uncertainty of $\pm 75nm$ per frame. The error in fluorescence intensity is the standard deviation within the averaged area. In the right box, we re-calculated the distance for each frame from the fluorescence intensity and performed a line-fit to obtain the average approach velocity. The such determined velocity is in very good agreement with the piezo velocity.

Figure 4: ***Optical observation of a single-molecule rupture event.*** **A:** The cellular force-distance curve was correlated with the fluorescence intensity. This allowed to identify the frames of the rupture event. Two frames before and after the rupture are marked with numbers and shown in B. **B:** Fluorescence images of two frames before and after rupture as indicated in A are shown together with a surface plot of the fluorescence intensity. The last TIRF-image before rupture shows two contact areas. One area corresponds to the adhesive contact, the other to a non-adherent cellular protrusion, probably a microvillus. **C:** Time-distance traces of the two contact areas. The distances were calculated from the average fluorescence intensity of the area according to the measured fluorescence-distance relationship shown in Figure 3. The blue line indicates the expected distance-time relationship from the retract velocity of the piezo of $3\mu m/s$. While the non-adhesive contact closely follows this expected movement, the adhesive contact first shows the rupture as a jump in the contact-area to surface distance, and then relaxes. After relaxation, it retracts from the surface with the expected velocity.

Figure 5: ***Fluorescence intensity of cells with activated integrins (red) vs. cell in non-binding conditions (blue).*** Here, we used the AFM as a positioning tool and tested if we can observed different activation states of the integrin based on the binding of a fluorescent marker.

7

Clearly, activated integrins show a much stronger fluorescent signal then non-binding integrins. Hence, we can detect affinity differences by fluorescence intensity. This will be useful for an opto-mechanical characterisation of physiological integrin-activation mechanism by for instance chemokines. The z-piezo position is indicated by a black line to show the positioning of the cell relative to the surface. High values correlate to an extended piezo, hence to cell-surface contact.

Figure 1:

9

Figure 2:

11

Figure 3:

12
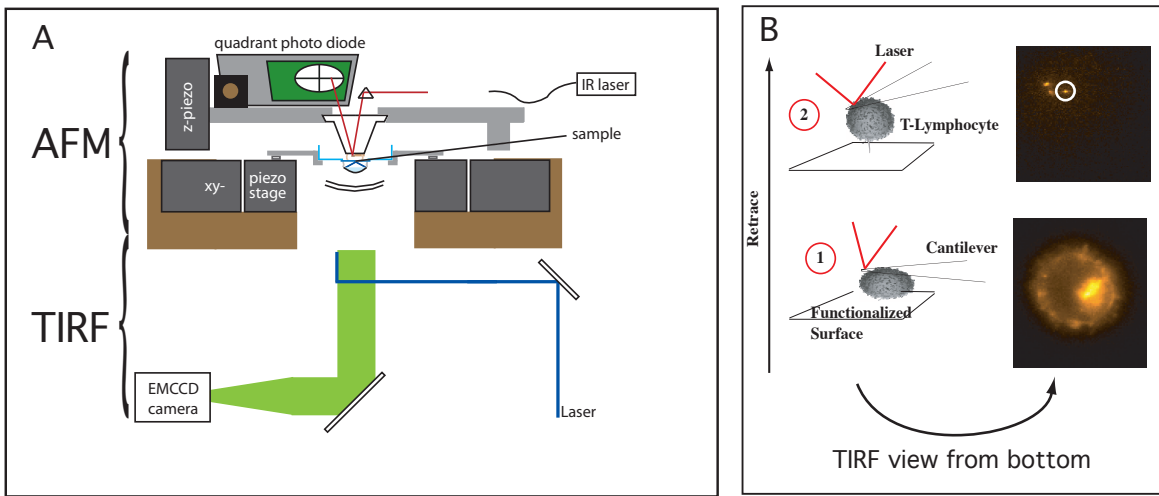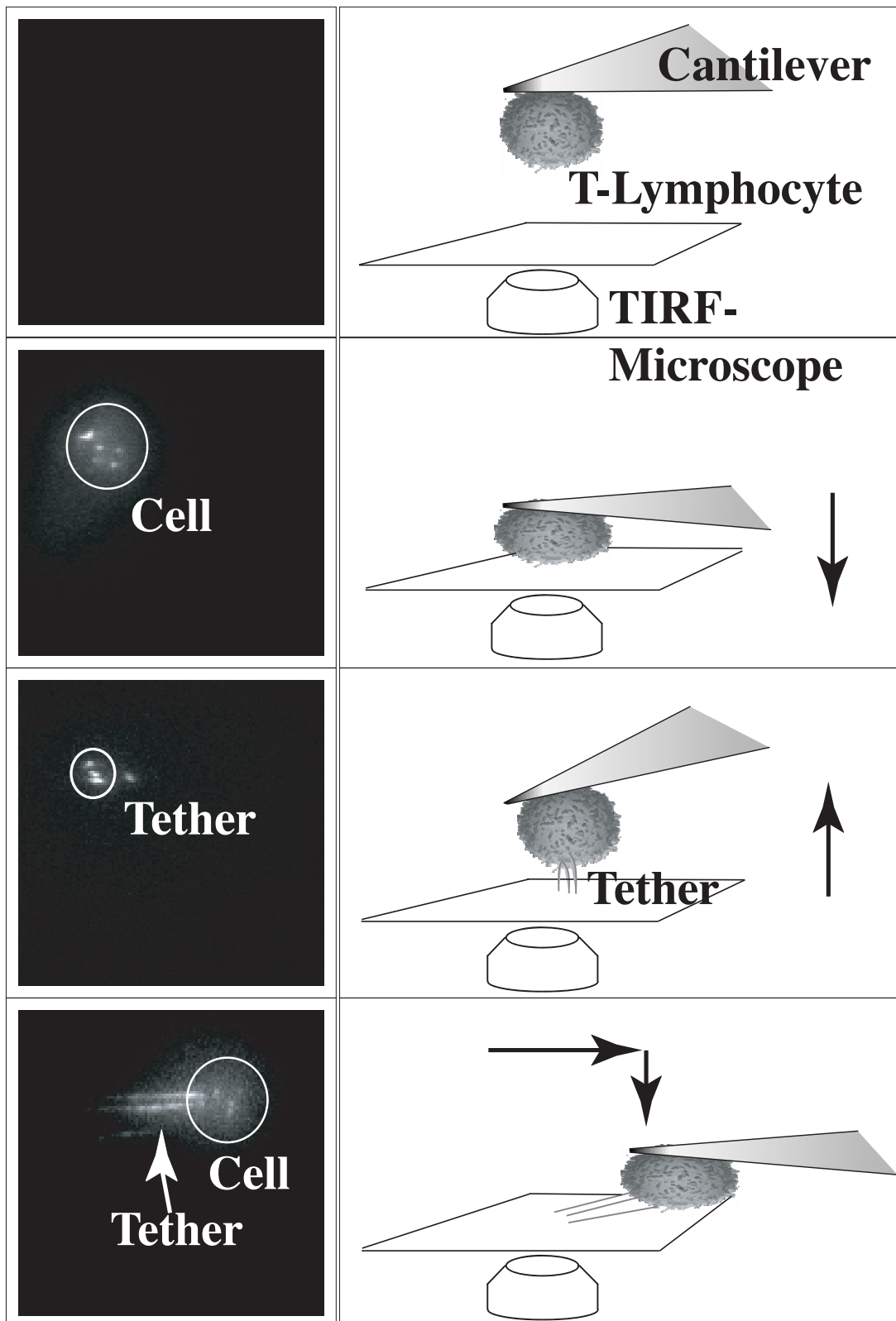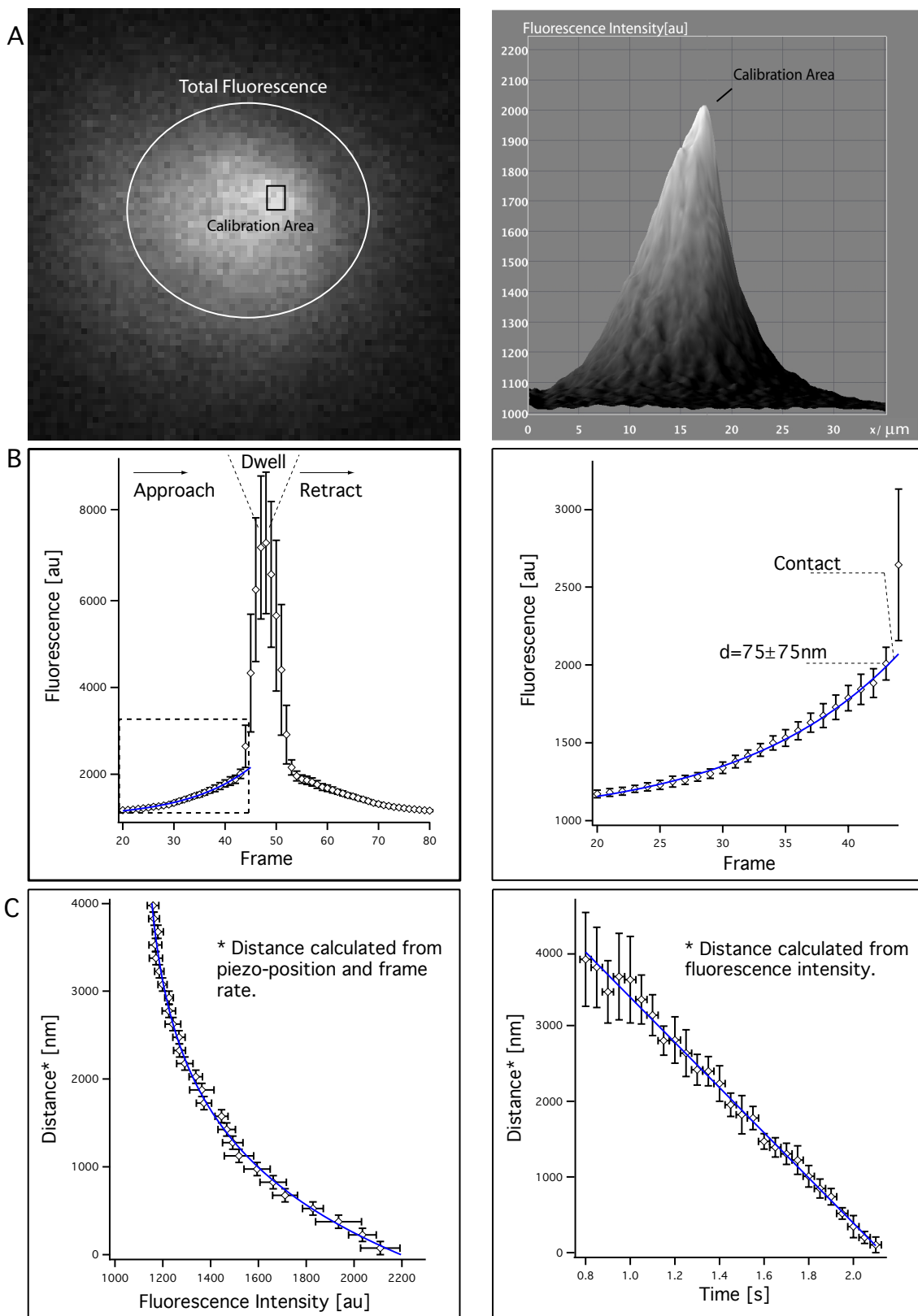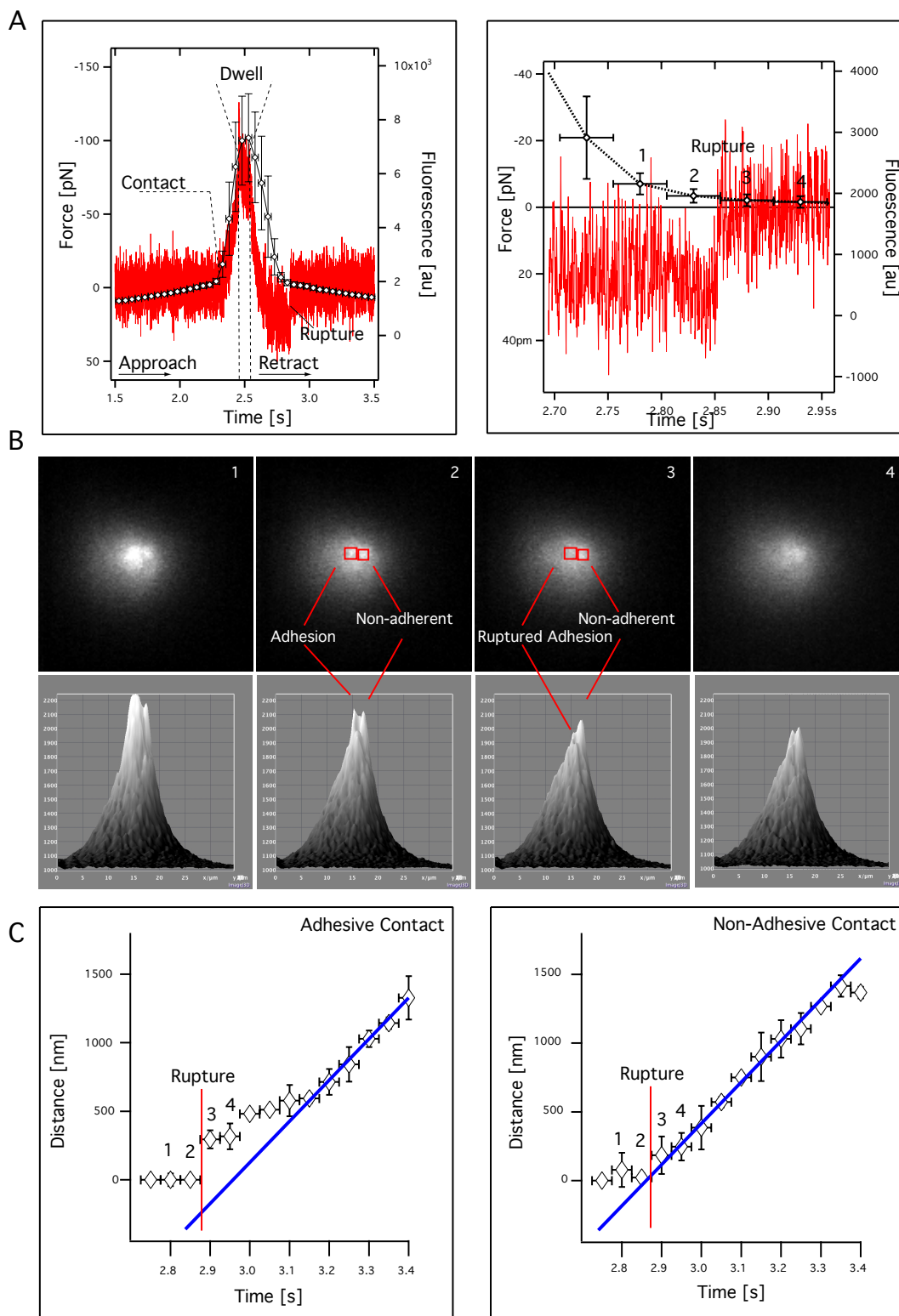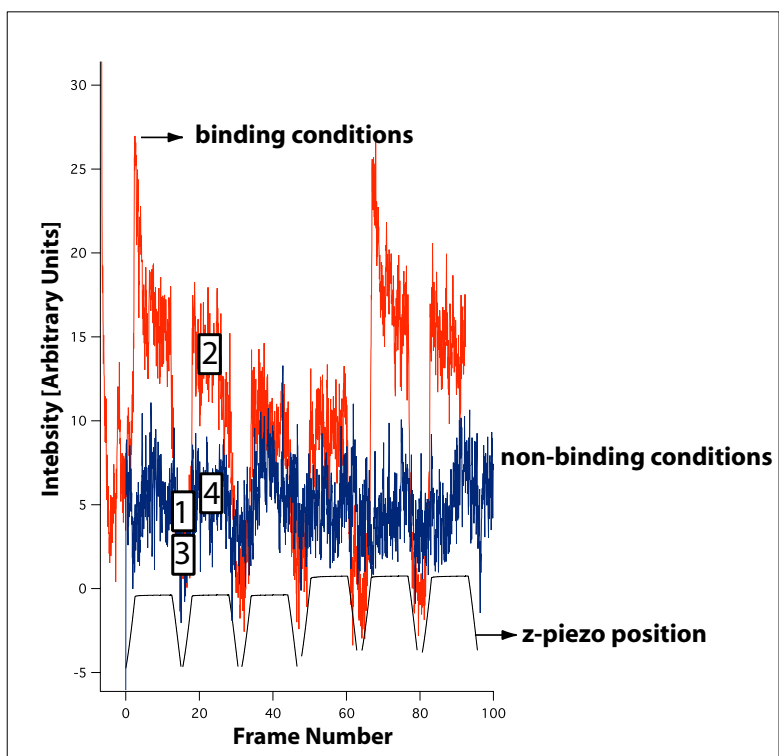
Figure 4:

Binding Conditions **Non-Binding Conditions**

Away from Surface

On Surface

13
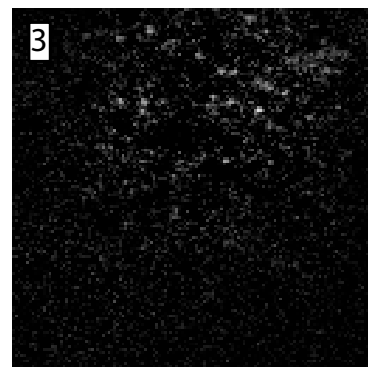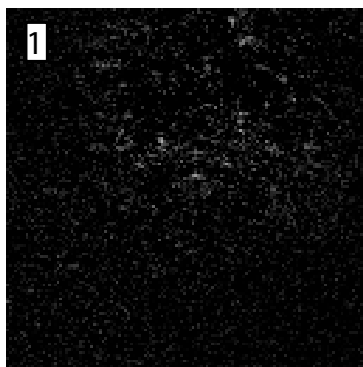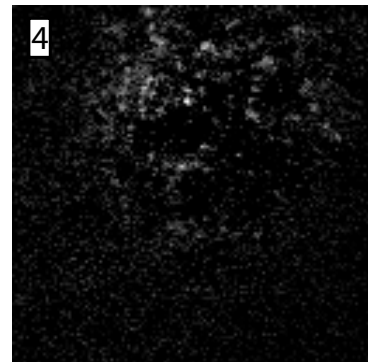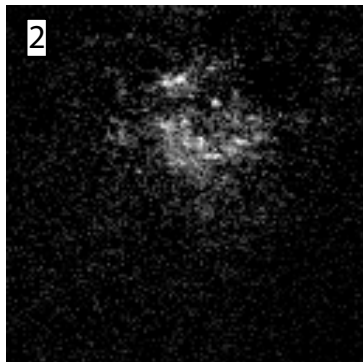
Figure 5:

Chapter 6

Other Projects: The Mechanics of Impacting Nano-Mechanical Single-Electron-Transistors

With the three-dimensional nanostructuring of semiconducting materials becoming feasible, the design of nano-electromechanical systems (NEMS) promises sundry applications as sensors, actuators and signal processing components [149, 150]. These nano-electromechanical systems enthral by their resonance frequency in the microwave range, by their minute effective masses and by quality factors (Q-factor) in the range of 10^4 [149]. The Q-factor characterises the dissipative losses of a system, which limit the sensitivity to signals and the spectral purity of the NEMS. It compares the oscillation frequency with the dissipation rate or, in other words, it compares the energy stored by the system (E_{tot}) with the energy dissipated during one oscillation period (E_{diss}): $Q = 2\pi \frac{E_{tot}}{E_{diss}}$. Running in
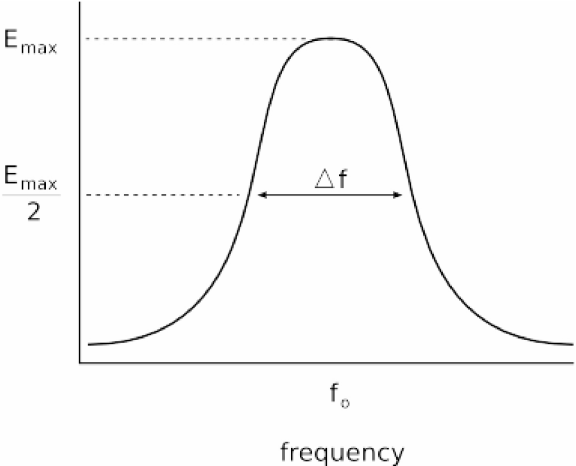
Figure 6.1: The resonance curve

the linear regime, the Q-factor can be directly determined from the Lorenzian resonance curve: $Q = \frac{f_0}{\Delta f}$, with the resonance frequency f_0 and the resonance peak width at half maximimum Δf (Fig. 6.1). For nanomechanical single-electron-transistors (MSET), the determination of the Q-factor is more complicated, since they do not operate in the linear regime [151, 152]. MSETs comprise a metal island on a mechanical element like a string, a beam or a pillar, which is located between a source and a drain electrode. If the mechanical element is excited to sufficiently large amplitudes, single electrons can be shuttled on the metal island from the source to the drain electrode producing an electrical current. Due to the impact of the oscillating island on the electrodes, MSETs are intrinsically non-linear, so that the Q-factor cannot simply be deduced from the resonance curve.

Here, we investigate the Q-factor and the dissipation of an impacting nanomechanical single-electron-transistor with the help of atomic force microscopy.

6.1   Q-factor and Dissipation of Impacting MSETS

The studied nano-electromechanical system consisted of a freely suspended LPCVD silicon nitride string with a gold island at its centre. The string was doubly clamped between a source and a drain electrode under high tensile stress. To tune the eigenfrequency of the system, gold weights were symmetrically attached on both sides of the conducting island. The string was mechanically excited by ultrasonic waves to demonstrate the electrical transport from the source to the drain electrode for sufficiently large amplitudes of the oscillation. However, the system is additionally excited by the force of the electric field between the electrodes on the charged gold island. If the energy added to the system by the source-drain voltage V_{SD} is high enough to compensate for the dissipated energy, a voltage-induced self-oscillation of the string is achieved without the need of ultrasonic driving. Sweeping the voltage to lower values, the self-oscillation collapsed at a threshold voltage, where the input power equalled the dissipated energy. This allowed us to calculate the dissipation per oscillation period. In order to deduce the Q-factor of our MSET, we needed to determine the total energy stored in the system. For this, we used an atomic force microscope. After scanning the chip with the transistors, the tip of the cantilever was positioned on the silicon nitride string of one transistor and the restoring force during the indentation was recorded. The force-indentation curve showed a superlinear behaviour above an indentation of 50 nm and was fitted with a 3rd order polynomial. Due to the fact that the restore force is mainly governed by the tensile stress of the string, the out-of-plane dependence was also assumed to be valid for the in-plane direction. With the force-indentation relationship, the total energy of the system can be calculated for the maximum amplitude of the oscillation, which is restrained by the position of the electrodes with respect to the resting position of the gold island. The obtained Q-factor is lower than expected for non-impacting resonators, thus demonstrating that the main source of the dissipation for impacting systems is the impact of the gold island on the electrodes.

These results are in submission and are reprinted in section 6.3.

6.2 Conclusions

In this project we present a method to determine the Q-factor of non-linear nano-electro-mechanical impacting systems by means of self-oscillation measurements and atomic force microscopy. We show furthermore that the dissipation is mainly caused by the impact of the conducting island on the electrodes.

6.3 Publications

1. Self-excitation of a Nano-Mechanical Single-Electron Transistor at 4 Kelvin (*in submission*)

Version 1.0

Self-excitation of a nano-mechanical single-electron transistor at 4 Kelvin

Daniel R. Koenig, Ralf Jungmann, Julia Schmitz, Eva M. Weig and Jorg P. Kotthaus

Center for NanoScience and Fakultät für Physik der Ludwig-Maximilians-Universität,

Geschwister-Scholl-Platz 1, 80539 München, Germany.

(Dated: April 22, 2008)

We report self-excitation of a nano-mechanical single-electron transistor at 4 Kelvin. By this we demonstrate mechanical shuttling of electrons in a well defined electrical potential a low temperatures. This is a major step towards one-by-one mechanical electron transfer in the Coulomb blockade regime being relevant for the realization of a mechanical current standard. Above this, a dissipation power of 0.7 nW and a Q-factor of 500 for the system is determined.

Suspended nano-electro-mechanical systems (NEMS) have been subject of intense research and development over the last decade. They have become of strong relevance for metrological applications like ultra sensitive displacement, mass, charge and even spin detection [1–6]. One nanomechanical system, which is intended for the application as a current standard, is the mechanical single-electron-transistor (MSET) [7]. It generally consists of a metal island, which is located on a mobile mechanical element like a string, beam or pillar. A source and a drain electrode is placed to both sides of the island. That way, it can shuttle electrons from one contact to the other, once the element is mechanically excited to sufficiently large amplitudes. The ultimate goal of these structures is the mechanical one-by-one electron transfer. This is possible, if the island size and the operation temperature of the MSETs are sufficiently reduced. In this case it can be realized that only one electron is transferred to the island as additional electrons are blocked by the coulomb repulsion of the already charged island. This situation is referred to as Coulomb blockade. Although the progress in nanotechnology has lead to different designs and significant advances of such systems [9–13] the ultimate goal of mechanical electron transport in the Coulomb blockade regime has not yet been achieved. The reason for this is that the systems so far are either fundamentally limited by undesired interactions with their excitation mechanism and/or could just been operated at room temperature. Here we report voltage induced self-excitation of an MSET. By avoiding undesired interaction through operation in a well defined timely constant electrical potential at 4 Kelvin we demonstrate a decisive step towards mechanical electron transport in the Coulomb blockade regime.

Above this we present how the dissipation power P_{diss} of the MSET can be directly calculated by self-excitation measurements. We further determine the mechanical quality factor Q of the system, which is general defined as:

$$Q \equiv 2\pi \frac{E_{\mathrm{tot}}}{E_{\mathrm{diss}}}, \qquad (1)$$

where E_{tot} is the total mechanical energy stored in the system and E_{diss} is the energy, which is dissipated during one oscillation period. For the MSET however it is noch possible to determine Q directly from the Lorentzian resonance curve, like for most NEMS, which can be operated in the linear regime for which $Q = f_0/\Delta f$, where f_0 is the eigenfrequency of

the system and Δf is the full width of the resonance peak at half maximum (FWHM). This is because for MSETs the source and drain constitute impacting boundary conditions to the oscillating island. Therefore, MSETs belong to the class of impacting systems, are intrinsically non-linear and display complicated subharmonic and chaotic behavior [14–17]. We account for the impacting nature of the MSET by employing atomic force microscopy (AFM) in determining Q. The quantitative analysis of E_{diss} and E_{tot} provides fundamental information about the system dissipation, which we are discussing.

The investigated MSET consists of a freely suspended doubly clamped silicon nitride string. The string is fabricated out of LPCVD silicon nitride with an intrinsic tensile stress of 1.38 GPa, which allows for one of the highest Q-factors attainable in NEMS [19]. The string is 14 μm long, 70 nm wide, and 100 nm high. A gold island with dimensions 170 nm in length, 140 nm in width and 60 nm in height is located at the center of the string, as depicted in Fig. 1(a). The gold structures placed symmetrically on the string to either side of the island are gold weights for tailoring the system's eigenfrequency to a value accessible by the piezoelectric driving system. The string can be mechanically excited by voltage-induced self-oscillation [12] as initially proposed by Gorelik et. al. [7] or by ultrasonic waves produced by a piezo actuator, described in detail elsewhere [13]. When excited, the gold island can oscillate and shuttle electrons between the source and drain electrode, placed 80 nm away to either side of the island. Figure 1(b) shows a resonance in the electrical transport measurement for an MSET driven by ultrasonic waves. The time averaged source-drain current $\overline{I_{\mathrm{sd}}}$ is plotted as function of the drive frequency f_{drive}. The measurement was conducted at a temperature of approximately 20 K and a helium exchange gas pressure of 7.5×10^{-4} mbar [20]. The driving power P_{drive} of the signal generator, which drives the piezo actuator, was set to 27.5 dBm, the drive frequency f_{drive} was swept from 3.806 to 3.817 MHz, and the source-drain voltage V_{sd} was set to -2 V. The resonance curve illustrates that the system shuttles electrons between the source and the drain electrode. This happens when the string is excited to sufficiently large amplitudes within its eigenfrequency range. The system however is not exclusively driven by ultrasonic waves, but also by V_{sd}. The voltage V_{sd} causes an electric field E_{sd} between the source and drain electrode, which is given by $E_{\mathrm{sd}} = V_{\mathrm{sd}}/(2d)$, where $d = 80$ nm is the distance between
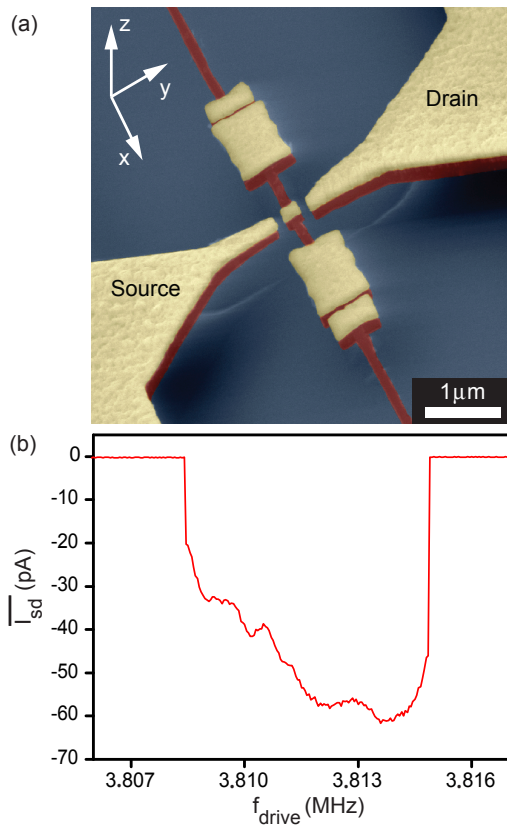
FIG. 1: a) Scanning electron micrograph taken at an angle to reveal the 3D character of the MSET. A gold island is located at the center of a doubly clamped freely suspended silicon nitride string. The gold island can shuttle electrons between the source and drain electrodes when excited to sufficiently large amplitudes. b) Charge transport of the MSET, actuated by ultrasonic waves. The time averaged source-drain-current $\overline{I_{sd}}$ is plotted as function of f_{drive}.


FIG. 2: a) Voltage supported ultrasonic actuation at a drive power $P_{drive} = 22.3$ dBm and $f_{drive} = 3.81$ MHz. Electrical transport is present for $V_{sd} = -1.8$ V and collapses for $V_{sd} = -1$ V. b) Source-drain voltage sweep of self sustained oscillation after the ultrasonic drive is switched off, for sufficiently high source-drain-voltages.

the island and one electrode. The island with charge Q_{island} experiences an additional driving force $F_{sd} = Q_{island}E_{sd}$. The direction of F_{sd} oscillates, as Q_{island} changes its sign with each island-electrode contact. Figure 2(a) illustrates, how F_{sd} supports the ultrasonic actuation at a temperature of 4 K and a helium exchange gas pressure of 3.5×10^{-2} mbar, while $P_{drive} = 22.3$ dBm and $f_{drive} = 3.81$ MHz [20]. For $V_{sd} = -1$ V and a driving power $P_{drive} = 22.3$ dBm of the ultrasonic drive the system is in the state of no transport ($\overline{I_{sd}} = 0$). If $V_{sd} = -1.8$ V, the overall energy put into the resonator is sufficient to compensate for the dissipated energy and the MSET shows electrical transport ($\overline{I_{sd}} \neq 0$).

If V_{sd} is sufficiently large, the system can undergo voltage-induced self-excitation while the ultrasonic drive is completely switched off. This is illustrated in Fig. 2(b) for a V_{sd}-swept from 6 to 8 Volts without ultrasonic excitation. If V_{sd} is continuously reduced, the self-exitation eventually collapses at a threshold voltage V_{th}. For the system presented here $V_{th} = 4.2$ Volts is determined (data not shown). If 1-periodic motion of the system is assumed the source-drain-current is given by:

$$\overline{I_{sd}} = 2Q_{island}f_{drive} = 2\langle n\rangle e f_{drive}, \qquad (2)$$

where $\langle n\rangle$ is the expectation value of the number of island excess charges [7]. The factor 2 comes in as the number of charge carriers transferred to and from the island is twice the number of excess charges, accounting for holes and electrons. For V_{th} we find $\langle n\rangle \simeq 130$. This is still more than two orders of magnitude higher than for single electron transfer. However, by investigating different MSET designs using ultrasonic excitation at room temperature we found for system with an island-electrode distance $d = 30$ nm that P_{drive} could be reduced by more than one order of magnitude for successful electron transport. This indicates a decrease of dissipation and therefore allowing for lower values of $\langle n\rangle$. A further reduction of $\langle n\rangle$ should be possible with operation at even lower temperatures as it is generally found that this significantly reduces the dissipation of NEMS [1, 21, 22]. Above this it should be noted that mechanical electron transport in the Coulomb blockade regime is not necessarily limit to the charing state $n = 1$. Addressing the operation temperature , we determine

a value of 0.2 Kelvin for which an onset of Coulomb blockade for the presented MSET can be expected [13].

Having demonstrated successful self-excitation we are now going to investigate the dissipation of the MSET. As noted, self-excitation collapses below a certain source-drain-voltage. At this threshold voltage V_{th}, the dissipation power P_{diss}, caused by the sum of all underlying loss mechanisms, is equal to the power put into the system. For the system presented here P_{diss} can therefore be calculated:

$$
\begin{aligned}
P_{diss} &= E_{sd}(V_{th})Q_{island}(V_{th})4df_{drive} \\
&= \frac{V_{th}}{2d}\frac{\overline{I_{sd}}(V_{th})}{2f_{drive}}4df_{drive} \\
&= V_{th}\overline{I_{sd}}(V_{th}) = 0.7\,\text{nW}.
\end{aligned} \tag{3}
$$

This analysis assumes that the charging process of the island exclusively occurs at the point of maximum deflection. This is not exactly true as it does not account for tunneling. Taking the maximum tunneling distance to be 1 nm [8] and assuming that the energy the electrons gain over this distance is not at all contributing to the mechanical excitation we estimate the upper limit of the error in equation (3) to be $(4 \times 1\,\text{nm})/(4 \times d\,\text{nm}) \simeq 1\%$. Together with the frequency of the system the energy dissipated per oscillation period T, yields:

$$
E_{diss} = \int_{y(0)}^{y(T)} F_{sd}dy = P_{diss}/f_{drive} = 1.8 \times 10^{-16}\text{J}. \tag{4}
$$

The oscillation period was calculated using $f_{drive} = 3.81\,\text{MHz}$, which was initially applied to trigger the self-oscillation by ultrasonic waves.

In order to calculate the Q-factor in addition to E_{diss} we now determine E_{tot}, the total energy stored in the system. This is accomplished by using an AFM in force spectroscopy mode. The AFM cantilever is used as a reference cantilever against the freely suspended string [23–25]. Figure 3(a) shows an AFM-image of the gold island on the silicon nitride string along with the source and drain electrode taken with a Nanowizard II AFM (JPK Instruments, Berlin, Germany) in noncontact mode, using Pointprobe NCH-W cantilevers (Nanosensors, Neuchatel, Switzerland). For the measurements of E_{tot} the AFM-tip was positioned in the center of the silicon nitride string and the restoring force $F_{restore}$ was measured as function of the out-of-plane deflection in the z-direction. The data are illustrated in Fig. 3(b) and are almost undistinguishable from the coinciding fit. The force $F_{restore}$ follows a superlinear behavior above a z-deflection of 50 nm. The measurement curve is fitted to a 3rd order polynomial of the form $F_{restore} = az + bz^3$ [26]. From the fit, the coefficients a $= 1.8\frac{N}{m}$ and b $= 5.0 \times 10^{12}\frac{N}{m^3}$ were determined, with an error of 40%. We estimate this functional dependence to be equally valid for the in-plane/y-direction with an error of 10%. This is due to the fact that in the limit of high tensile stress, $F_{restore}$ is mainly governed by the tensile force of the string rather than by the Young's modulus and geometry factors [19]. Furthermore, we assume in the calculation of E_{tot} that the functional dependence $F_{restore}$, which was measured at room temperature, also applies for 4 K. Taking the different thermal expansion coefficients of silicon nitride $\alpha_{SiN} = 1.67 \times 10^{-6}/K$ [27] and the silicon substrate
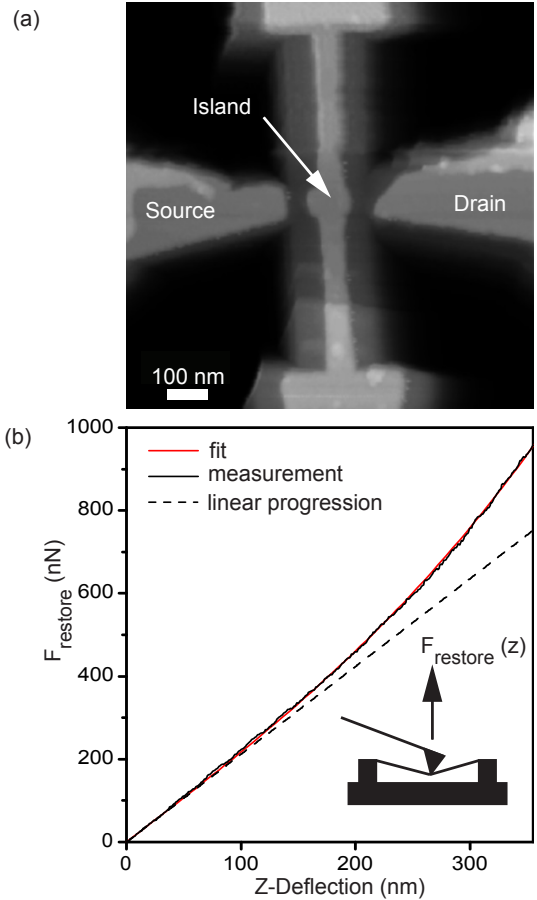
FIG. 3: a) AFM-image of an MSET, which shows the gold island at the center of the silicon nitride string and parts of the source and drain electrode. b) Restoring force $F_{restore}$ of the silicon nitride string as function of its out-of-plane deflection. The functional dependence was measured with an atomic force microscope (see inset).

$\alpha_{Si} = 2.3 \times 10^{-6}/K$ [28] we find this assumption to be valid with an error of 4%. With this, E_{tot} of the MSET system can be calculated:

$$
E_{tot} = F_{restore}\Delta y = \int_0^{125nm} (ay + by^3)dy. \tag{5}
$$

For the integration distance 125 nm is chosen instead of $y_{max} = 80\,\text{nm}$, which corresponds to the maximum amplitude, constrained by the source and drain electrode. This is because the string shape under MSET operation has a sinusoidal instead of a triangular shape as in the case of atomic force spectroscopy measurements. Therefor the length difference $\Delta L = L - S$ of the string due to stretching is different for the dynamic and static case, where L is the length without deflection and S is the length under deflection. Numerical analysis show that ΔL for a static deflection of 125 nm is equivalent with a dynamic deflection of 80 nm as illustrated in figure 4. Therefor 125 nm is applied for the integration distance in equation (5). With this the evaluated integral in

(a) Dynamic string deflection

$\Delta L = L - S = 2.26$ nm

S

y = 80 nm

L = 14 μm

(b) Static string deflection

$\frac{S}{2}$

$\Delta L = L - S = 2.26$ nm

y = 125 nm

$\frac{S}{2}$

L = 14 μm
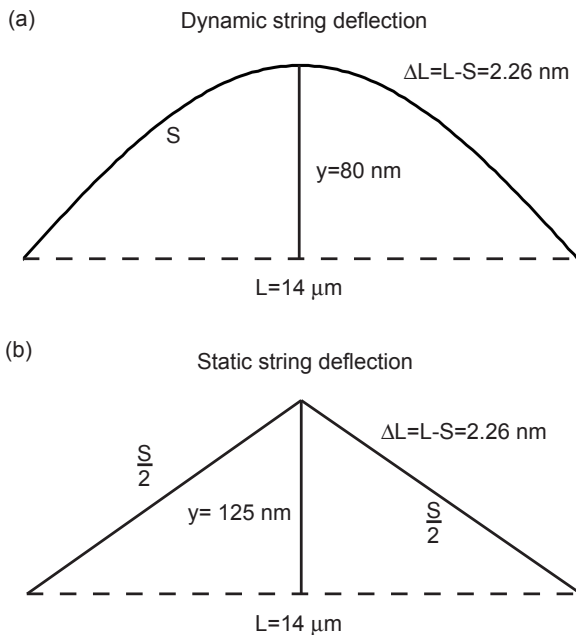
FIG. 4: a) Resonator shape at the point of maximal deflection in the case of MSET operation. The curve follows a sinusoidal behavior as expected for a string unter tensile stress. b) Shape of the resonator string for the static deflection in the case of atomic force spectroscopy.

equation (5) yields $E_{\text{tot}} = 1.4 \times 10^{-14}$ J. Combining equation (1) with the results from equation (4) and (5), we obtain a Q-factor of approximately 500. As we are now going to analyze, this value is far below what would be expected for a non-impacting doubly clamped resonator. The presented system is operated in the so called molecular regime for which the mean free path of the gas molecules is much larger than the device dimensions. In this situation the quality factor due to gas dissipation is given by [18]:

$$Q_{\text{gas}} \approx \frac{m_{\text{eff}} 2\pi f_{\text{drive}} \upsilon}{pA}, \qquad (6)$$

where $m_{\text{eff}} = 3.22 \times 10^{-15}$ Kg is the effective mass of the MSET, $\upsilon = \sqrt{k_{\text{B}}T/m_{\text{He}}} = 91$ m/s is the thermal velocity of the helium molecules each with mass $m_{\text{He}} = 1.7 \times 10^{-27}$ Kg, $p = 3.5 \times 10^{-2}$ mbar is the surrounding gas pressure, and $A \approx 1 \times 10^{-11}$ m^2 is the surface area of the resonator. It is found that $Q_{\text{gas}} > 1 \times 10^7$ and hence can not explain a Q-factor of 500. Other limiting factors are for example clamping losses, surface effects, thermo elastic damping and dissi-

pation caused by the metallization of the gold weights. The contribution of these effect can be approximated by a comparison with similar system. For completely metal coated doubly clamped resonators fabricated from nanocrystalline-diamond the lowest Q-factors under similar operation conditions was found to be > 7000 [21]. The MSETs investigated here however should have Q-factors significantly higher than this lower limit. First of all their clamping points are not metal coated. Secondly the MSETs are fabricated from silicon nitride under high tensile stress which has been demonstrated to enable unprecedented high Q-Factors in NEMS [19, 29, 30]. That the Q-factor of the MSET falls short by more than one order of magnitude compared to the lower limit of the expected value can be explained by additional dissipation factors. Compared to other, non-impacting resonators the MSET has two additional dissipation sources, the radiation power of the accelerated and charged island and phonon excitation due to the impacting island. Estimating the radiation power using the Larmor-formula:

$$P_{\text{radiation}} = \frac{e^2 a^2}{6\pi\epsilon_0 c^3}, \qquad (7)$$

where $a \approx y_{\text{max}}\omega^2 \simeq 4.6 \times 10^7 \frac{\text{m}}{\text{s}^2}$ is the acceleration of charge carriers, ϵ_0 the permittivity of free space and c the speed of light shows a negligible contribution. Therefore, we attribute the main source of dissipation to phonon excitations caused by the impacts between the gold island and the side electrodes, not being present in non-impacting resonators.

In conclusion, we present self-excitation of a nanomechanical single-electron-transistor at 4 K. This demonstrates an important step towards mechanical one-by-one electron transport in the Coulomb blockade regime as it allows for transport in a well defined timely constant electrical potential at low temperatures. We demonstrate transport for a charge state as low as $\langle n \rangle \simeq 130$. Further we quantitatively determine $E_{\text{diss}} = 0.7$ nW and $E_{\text{tot}} 1.4 \times 10^{-14}$ J from which we calculate a Q-factor of approximately 500. By this we determine fundamental system parameters being important indicators for further progress in this field of research. Based on these parameters we discuss the dissipation of the system and find that a significant reduction of $\langle n \rangle$ and operation in the Coulomb blockade regime should be possible with a modified system design and operation at even lower temperatures.

[1] M. D. LaHaye, O. Buu, B. Camarota, and K. C. Schwab, Science **304**, 74 (2004).

[2] R. G. Knobel, and A. N. Cleland, Nature **424**, 291 (2003).

[3] Mo Li, H. X. Tang, and M. L. Roukes, Nature Nanotechnology **2**, 114 (2007).

[4] Y. T. Yang, C. Callegari, X. L. Feng, K. L. Ekinci, and M. L.

Roukes, Nano Lett. **6**, 583 (2006).

[5] A. N. Cleland, and M. L. Roukes, Nature **392**, 160 (1998).

[6] D. Rugar, R. Budakian, H. J. Mamin, and B. W. Chui, Nature **430**, 329 (2004).

[7] L. Y. Gorelik, A. Isacsson, M. V. Voinova, B. Kasemo, R. I. Shekhter, and M. Jonson, Phys. Rev. Lett. **80**, 4526 (1998).

[8] Sze, S. M. in *Physics of Semiconductor Devices* (eds Sze, S. M.) (John Wiley & Sons, New York, 1981).

[9] A. Erbe, R. H. Blick, A. Tilke, A. Kriele, and J. P. Kotthaus, Appl. Phys. Lett. **73**, 3751 (1998).

[10] A. Erbe, C. Weiss, W. Zwerger, and R. H. Blick, Phys. Rev. Lett. **87**, 096106 (2001).

[11] D. V. Scheible, and R. H. Blick, Appl. Phys. Lett. **84**, 4632 (2004).

[12] H. S. Kim, H. Qin, and R. H. Blick, arXiv/0708.1646 (2007).

[13] D. R. Koenig, E. M. Weig, and J. P. Kotthaus, Ultrasonically driven nano-mechanical single-electron transistor (submitted).

[14] A. Isacsson, Phys. Rev. B **64**, 035326 (2001).

[15] S. W. Shaw, J. Appl. Mech. **52**, 453 (1985).

[16] S. Foale, and S. R. Bishop, Phil. Trans. R. Soc. Lond. A **338**, 547 (1992).

[17] T. Kotera, and M. Shintani, JSME International Journal Series C **46**, 659 (2003).

[18] K. L. Ekinci, and M. L. Roukes, Rev. Sci. Instrum. **76**, 061101 (2005).

[19] S. S. Verbridge, J. M. Parpia, R. B. Reichenbach, L. M. Bellan, and H. G. Craighead, J. Appl. Phys. **99**, 124304 (2006).

[20] The measurements have been corrected for a small offset of the current-voltage amplifier.

[21] Hutchinson,A. B., Truitt, P. A., Schwab, K. C., Sekaric, L., Parpia, J. M., Craighead, H. G., and Butler, J. E., Appl. Phys. Lett. **84**, 972-974 (2004).

[22] Yang, Y. T., Ekinci, K. L., Huang, X. M. H., Schiavone, L. M., Roukes, M. L., Zorman, C. A. and Mehregany, M., Appl. Phys. Lett. **78**, 162-164 (2004).

[23] H.-J. Butt, B. Cappella, and M. Kappl, Surface Science Reports **59** 1-152 (2005).

[24] I. W. Frank, D. M. Tanenbaum, A. M. van der Zande, and P. L. McEuen, J. Vac. Sci. Technol. B **25**, 2558 (2007).

[25] A. S. Paulo, J. Bokor, R. T. Howe, R. He, P. Yang, D. Gao, C. Carraro, and R. Maboudian, Appl. Phys. Lett. **87** 053111 (2005).

[26] M. W. Pruessner, T. T. King, D. P. Kelly, R. Grover, L. C. Calhoun, and R. Ghodssi, Sensors & Actuators A **105** 190 (2003).

[27] Senturai, in *Microsystem Design*, (New York, Kluwer, 2001).

[28] Mohamed Gad-el Hak, in *The MEMS handbook*, (CRC Press, Boca Raton, FL, 2005) 2. ed.

[29] Verbridge, S. S., Shapiro, D. F., Craighead, H. G. and Parpia, M. Nano Lett. **7** 1728-1735 (2007).

[30] Verbridge, S. S., Craighead, H. G. and Parpia, M. Appl. Phys. Lett. **92** 013112 (2008).

Chapter 7

Outlook

It is becoming increasingly obvious that mechanical forces play an important role in bio-chemical processes. For this reason it is beneficial to reflect on established physical inter-dependencies and to develop novel physical models describing biological or physiological problems. This thesis demonstrates that physical principles are exploited by cells in order to mechanically fine-tune the kinetic properties of adhesion receptors. The mechanical adaptation has the advantageous characteristics to be functional only in the presence of forces. Physically speaking, force is a vector quantity with a magnitude and a direction. Thus, on the one hand, the force magnitude can shift the equilibrium between different conformational states of a molecule [106, 153]. The momentary magnitude of force on a force-resisting receptor is determined by the velocity of force loading which itself depends on the mechanical compliance of the receptor anchorage. Thus we see that influencing the receptor environment represents an attractive alternative for medical treatments: Instead of aiming at the whole receptor with blocking agents which might provoke strong side effects, fine corrections of the receptor properties may be achieved by adjusting the association of the receptor with intracellular mechanical adapter proteins.

On the other hand, geometrical differences in the force direction dictate on the effect of the force on molecular complexes and other biological systems [154,155]. The experimental techniques should therefore consider the physiological geometry of forces. This necessitates the combination of single-molecule force spectroscopic studies with theoretical models and more physiological assays of the flow chamber – as undertaken in this study – in order to interpret complex phenomena such as cell adhesion in the blood stream.

Recently, the nano-patterning of surfaces with physiologically relevant ligands has become increasingly sophisticated empowering to control the pattern and the spacing of different molecules on the nano-scale. Together with optical and force spectroscopic techniques (e.g. TIRF and AFM), this allows to investigate, how the geometrical arrangement of signal and/or adhesion molecules influences cellular reactions. It has been shown by means of nano-patterning and microscopy, for instance, that the range between 58-73 nm is a universal length scale for integrin clustering and activation [156]. Regarding the subject of this work, chemokines and integrin ligands could be immobilised with variable spacing and in different geometries by surface nano-patterning. Incorporated in studies with a TIRF-AFM

setup it can thus be investigated by labelling the integrin receptors fluorescently, whether the integrin activation by chemokines is locally restricted. Since the activation requires the co-immobilisation of chemokines and ligands [131], a maximum separation distance for the receptor crosstalk might exist, beyond which no successful activation is achieved. The fluorescent labels may hereby serve either to detect different affinity states of the integrin by changes in the fluorescence intensity or to make apparent a local accumulation or an altered mobility of the integrins (due to cytoskeletal constraints) by single-particle tracking. It should also be possible to resolve the induction of the intracellular attachment of labelled adapter proteins like talin or paxillin with a FRET- based approach.

Furthermore, it has been demonstrated that continuous interaction of the chemokine SDF-1 with its receptor CXCR-4 results in sustained activation of the kinases protein kinase B, ERK-2 and PI3-kinase thereby protecting cells from undergoing apoptosis [139]. This time dependency of the activation by SDF-1 could be easily assessed due to the high temporal and spatial control of the AFM position.

As we can see, the rapid progress in technology and theory offers a plethora of fresh opportunities for the investigation of integrin-mediated cell adhesion and its regulation by mechanical and biochemical stimuli.

Appendix A

Appendix A: The Kinetics of Cell Adhesion extrapolated from Single Molecule Properties

A.1 Bond Formation in the Atomic Force Spectroscopy

To determine the two-dimensional on-rate with atomic force spectroscopy, we evaluated the interaction frequency as a measure for the bond formation in dependence of the ligand density. It can be assumed that the bond dissociation during the contact time can be neglected and that the reservoir of receptors on the cell is infinite. Thus, the number of bonds $n_{bonds}(t)$ is described by the differential equation:

$$\frac{dn_{bonds}(t)}{dt} = k_{on} \cdot d \cdot (N_{tot} - n_{bonds}(t))$$

where N_{tot} is the maximum number of available receptors, d the coated ligand density in the contact area, t the contact time and k_{on} the two-dimensional on-rate in the units *area/time*. With $n_{bonds}(t = 0) = 0$, this yields:

$$n_{bonds}(t) = N_{tot} - N_{tot} \cdot e^{-k_{on} \cdot d \cdot t} \tag{A.1}$$

By fitting this relation A.1 to the measured data, the two-dimensional on-rate can be derived.

In the atomic force spectroscopy, the rebinding of dissociated bonds is sufficiently suppressed by the continuous spatial separation of the binding partners. Thus, the bond dissociation is given by a simple decay relation:

$$n_{bonds}(t) = n_{bonds}(0) \cdot e^{-k_{off}^{F} \cdot t} \tag{A.2}$$

with k_{off}^{F} being the off-rate under the external force F. The kinetic constants k_{off} and k_{on} can therefore be separately examined in force spectroscopic experiments.

A.2   Bond Formation in the Flow Chamber

In the flow chamber, rebinding cannot be neglected and the differential equation for the number of bonds contains both the association and the dissociation rate [142]:

$$\frac{dn_{bonds}(t)}{dt} = k_{on} \cdot d \cdot (N_{tot} - n_{bonds}(t)) - k_{off}^{F} \cdot n_{bonds}(t)$$

With the approximation, that the average force on the bonds is constant throughout the cell adhesion in the shear flow, k_{off}^{F} is constant over time [142]. With the number of bonds at time zero $n_0 = 0$ this gives:

$$n_{bonds}(t) = \frac{k_{on}dN_{tot}}{k_{on}d + k_{off}^{F}} + \left(n_0 - \frac{k_{on}dN_{tot}}{k_{on}d + k_{off}^{F}} \right) \cdot e^{-k_{on}dt + k_{off}^{F}t}$$

Since a cell is connected to the surface, until the last bond is broken, the number of cells $n_{cells}(t)$ follows the time dependency:

$$n_{cells}(t) = n_{cells}(0) - n_{cells}(0) \cdot \left(1 - e^{-k_{off}^{F} \cdot t} \right)^{n_{bonds}(t)} \tag{A.3}$$

Here, $n_{cells}(0)$ is the number of cells bound to the surface at time $t = 0$. If only one bond holds the cell in the shear flow, the equation A.3 decreases to the simple decay relation A.2.

Appendix B

Appendix B: The Force-Distance Relationship of a Kelvin Body

A Kelvin body consists of a spring k_t in parallel to a series of a dashpot μ and a second spring k_i (Fig. B.1). Pulling on the Kelvin body with a constant retraction velocity $v = \frac{dz}{dt}$
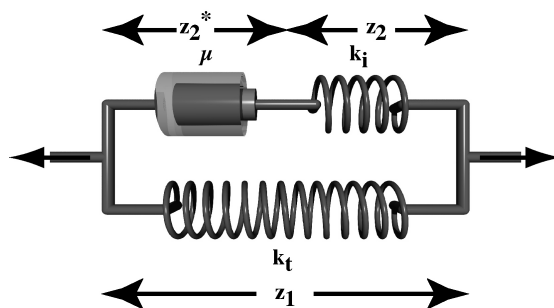
Figure B.1: The Kelvin body: A spring with elasticity k_t is connected in parallel to a series of a second spring with k_i and a dashpot with viscosity μ. The arrows indicate the respective distances affecting the different viscous and elastic elements while stretching the system.

results in a force $F_1(t)$ on the lower part containing the spring k_t:

$$F_1 = k_t \cdot z_1(t)$$

and a force F_2 on the series of the dashpot μ and the spring k_i:

$$F_2 = k_i \cdot z_2(t) = \mu \cdot \frac{dz_2^*}{dt}$$

The total retraction position z is:

$$z = z_1 = z_2 + z_2^*$$

The total force $F(t)$ can be given as:

$$F(t) = F_1(t) + F_2(t) = k_t \cdot z(t) + \mu \cdot \left(\frac{dz}{dt} - \frac{dz_2}{dt} \right) \tag{B.1}$$

From

$$\frac{F(t)}{dt} = k_t \cdot \frac{dz}{dt} + k_i \cdot \frac{dz_2}{dt}$$

follows:

$$\frac{dz_2}{dt} = \frac{1}{k_i} \cdot \frac{dF(t)}{dt} - \frac{k_t}{k_i} \cdot \frac{dz}{dt} \tag{B.2}$$

Substituting equation B.2 into equation B.1 yields:

$$F(t) = k_t \cdot z + \mu \cdot \left(1 + \frac{k_t}{k_i} \right) \cdot \frac{dz}{dt} - \frac{\mu}{k_i} \cdot \frac{dF(t)}{dt}$$

From this, one can derive the time-dependency of the force [157]:

$$\frac{dF(t)}{dt} = -\frac{k_i}{\mu} \left(F(t) - k_t \cdot z - \mu \cdot \left(1 + \frac{k_t}{k_i} \right) \cdot \frac{dz}{dt} \right)$$

If the retract velocity v is constant, the time t can be expressed in terms of the position z as $t = \frac{z}{v}$. With the additional boundary condition $F(z = 0) = 0$, the differential equation can be integrated to:

$$F(z) = k_t \cdot z + \mu \cdot v - \mu \cdot v \cdot e^{\frac{-k_i \cdot z}{\mu \cdot v}} \tag{B.3}$$

This equation B.3 corresponds to equation 2.1 and was used to analyse the force-distance curves recorded in atomic force spectroscopic experiments on living cells.

Glossary

AFM	atomic force microscope
DAG	diacylglycerol
FAK	focal adhesion kinase
FRET	fluorescence resonance energy transfer
GEF	guanine nucleotide exchange factor
GTPases	guanosine triphosphate hydrolase enzymes
IP3	inositol-2,4,5-triphosphate
LFA-1	lymphocyte function associated antigen 1 (also called $\alpha_L\beta_2$)
MSET	mechanical single electron transistor
NEMS	nano-electromechanical system
PAK	kinase family
PEG	poly-ethylen glycol
PI3-kinase	phosphatidylinositol 3 kinase
PIP2	phosphatidylinositol-4,5-bisphosphate
PKC	phosphokinase C
PLC	phospholipase C
PMA	phorbol 12-myristate 13-acetate
RAP1	RAS-related protein 1
RAS	familiy of GTPases
Src	kinase family
TIRF	total internal reflection microscope
VCAM-1	vascular cell adhesion molecule 1
VLA-4	very late antigen 4 (also called $\alpha_4\beta_1$)

Bibliography

[1] Klaus Ley, Carlo Laudanna, Myron I Cybulsky, and Sussan Nourshargh. Getting to the site of inflammation: the leukocyte adhesion cascade updated. *Nat Rev Immunol*, 7(9):678–689, Sep 2007.

[2] J. Schmitz and K. E. Gottschalk. Mechanical regulation of cell adhesion. *Soft Matter*, X:in press, 2008.

[3] M. Amin Arnaout. Integrin structure: new twists and turns in dynamic cell adhesion. *Immunol Rev*, 186:125–140, Aug 2002.

[4] Jian-Ping Xiong, Thilo Stehle, Rongguang Zhang, Andrzej Joachimiak, Matthias Frech, Simon L Goodman, and M. Amin Arnaout. Crystal structure of the extracellular segment of integrin alpha vbeta3 in complex with an arg-gly-asp ligand. *Science*, 296(5565):151–155, Apr 2002.

[5] Tsan Xiao, Junichi Takagi, Barry S Coller, Jia-Huai Wang, and Timothy A Springer. Structural basis for allostery in integrins and binding to fibrinogen-mimetic therapeutics. *Nature*, 432(7013):59–67, Nov 2004.

[6] Tim Lmmermann and Michael Sixt. The microanatomy of t-cell responses. *Immunol Rev*, 221:26–43, Feb 2008.

[7] T. Kinashi. Intracellular signalling controlling integrin activation in lymphocytes. *Nat Rev Immunol*, 5(7):546–59, 2005. Department of Molecular Genetics, Graduate School of Medicine, Institute of Liver Research, Kansai Medical School, 10-15 Fumizono-cho, Moriguchi, Osaka 570-8506, Japan. kinashi@takii.kmu.ac.jp.

[8] A. D. Luster, R. Alon, and U. H. von Andrian. Immune cell migration in inflammation: present and future therapeutic targets. *Nat Immunol*, 6(12):1182–90, 2005. Center for Immunology and Inflammatory Diseases, Division of Rheumatology, Allergy and Immunology, Department of Medicine, Massachusetts General Hospital, Harvard Medical School, Boston, Massachusetts 02114, USA. luster.andrew@mgh.harvard.edu.

[9] C. Laudanna, J. Y. Kim, G. Constantin, and E. Butcher. Rapid leukocyte integrin activation by chemokines. *Immunol Rev*, 186:37–46, 2002. Section of General

Pathology, Department of Pathology, Faculty of Medicine, University of Verona, 37138, Verona, Italy. carlo.laudanna@univr.it.

[10] Michael Sixt, Martina Bauer, Tim Lämmermann, and Reinhard Fässler. Beta1 integrins: zip codes and signaling relay for blood cells. *Curr Opin Cell Biol*, 18(5):482–490, Oct 2006.

[11] Y. van Kooyk and C. G. Figdor. Avidity regulation of integrins: the driving force in leukocyte adhesion. *Curr Opin Cell Biol*, 12(5):542–547, Oct 2000.

[12] C. V. Carman and T. A. Springer. Integrin avidity regulation: are changes in affinity and conformation underemphasized? *Curr Opin Cell Biol*, 15(5):547–56, 2003. Center for Blood Research, Harvard Medical School, Department of Pathology, 200 Longwood Avenue, Boston, MA 02115, USA.

[13] E. C. Butcher and L. J. Picker. Lymphocyte homing and homeostasis. *Science*, 272(5258):60–66, Apr 1996.

[14] M. L. Dustin, T. G. Bivona, and M. R. Philips. Membranes as messengers in t cell adhesion signaling. *Nat Immunol*, 5(4):363–72, 2004. Program in Molecular Pathogenesis, Skirball Institute of Biomolecular Medicine and the Department of Pathology, NYU School of Medicine, New York, New York 10016, USA. dustin@saturn.med.nyu.edu.

[15] C. Brakebusch, R. Grose, F. Quondamatteo, A. Ramirez, J. L. Jorcano, A. Pirro, M. Svensson, R. Herken, T. Sasaki, R. Timpl, S. Werner, and R. Fssler. Skin and hair follicle integrity is crucially dependent on beta 1 integrin expression on keratinocytes. *EMBO J*, 19(15):3990–4003, Aug 2000.

[16] M. A. Williams and J. S. Solomkin. Integrin-mediated signaling in human neutrophil functioning. *J Leukoc Biol*, 65(6):725–736, Jun 1999.

[17] Kay E Gottschalk, Robert Gnther, and Horst Kessler. A three-state mechanism of integrin activation and signal transduction for integrin alpha(v)beta(3). *Chembiochem*, 3(5):470–473, May 2002.

[18] Luciana Marinelli, Antonio Lavecchia, Kay-E. Gottschalk, Ettore Novellino, and Horst Kessler. Docking studies on alphavbeta3 integrin ligands: pharmacophore refinement and implications for drug design. *J Med Chem*, 46(21):4393–4404, Oct 2003.

[19] L. Marinelli, K. E. Gottschalk, A. Meyer, E. Novellino, and H. Kessler. Human integrin alphavbeta5: homology modeling and ligand binding. *J Med Chem*, 47(17):4166–77, 2004. Dipartimento di Chimica Farmaceutica e Tossicologica, Universita di Napoli "Federico II", Via D. Montesano, 49-80131 Napoli, Italy.

[20] M. Amin Arnaout, Simon L Goodman, and Jian-Ping Xiong. Structure and mechanics of integrin-based cell adhesion. *Curr Opin Cell Biol*, 19(5):495–507, Oct 2007.

[21] J. P. Xiong, T. Stehle, B. Diefenbach, R. Zhang, R. Dunker, D. L. Scott, A. Joachimiak, S. L. Goodman, and M. A. Arnaout. Crystal structure of the extracellular segment of integrin alpha vbeta3. *Science*, 294(5541):339–345, Oct 2001.

[22] Vineet Gupta, Jos Luis Alonso, Takashi Sugimori, Makram Issafi, Jiang-Ping Xiong, and M. Amin Arnaout. Role of the beta-subunit arginine/lysine finger in integrin heterodimer formation and function. *J Immunol*, 180(3):1713–1718, Feb 2008.

[23] Brian D Adair and Mark Yeager. Three-dimensional model of the human platelet integrin alpha iibbeta 3 based on electron cryomicroscopy and x-ray crystallography. *Proc Natl Acad Sci U S A*, 99(22):14059–14064, Oct 2002.

[24] Kay-Eberhard Gottschalk. A coiled-coil structure of the alphaiibbeta3 integrin transmembrane and cytoplasmic domains in its resting state. *Structure*, 13(5):703–712, May 2005.

[25] Kay-Eberhard Gottschalk and Horst Kessler. Evidence for hetero-association of transmembrane helices of integrins. *FEBS Lett*, 557(1-3):253–258, Jan 2004.

[26] Kay E Gottschalk, Paul D Adams, Axel T Brunger, and Horst Kessler. Transmembrane signal transduction of the alpha(iib)beta(3) integrin. *Protein Sci*, 11(7):1800–1812, Jul 2002.

[27] Bing-Hao Luo, Christopher V Carman, Junichi Takagi, and Timothy A Springer. Disrupting integrin transmembrane domain heterodimerization increases ligand binding affinity, not valency or clustering. *Proc Natl Acad Sci U S A*, 102(10):3679–3684, Mar 2005.

[28] M. Kim, C. V. Carman, and T. A. Springer. Bidirectional transmembrane signaling by cytoplasmic domain separation in integrins. *Science*, 301(5640):1720–5, 2003. CBR Institute for Biomedical Research, Department of Pathology, Harvard Medical School, 200 Longwood Avenue, Boston, MA 02115, USA.

[29] Junichi Takagi and Timothy A Springer. Integrin activation and structural rearrangement. *Immunol Rev*, 186:141–163, Aug 2002.

[30] P. E. Hughes, F. Diaz-Gonzalez, L. Leong, C. Wu, J. A. McDonald, S. J. Shattil, and M. H. Ginsberg. Breaking the integrin hinge. a defined structural constraint regulates integrin signaling. *J Biol Chem*, 271(12):6571–6574, Mar 1996.

[31] S. Liu, D. A. Calderwood, and M. H. Ginsberg. Integrin cytoplasmic domain-binding proteins. *J Cell Sci*, 113 (Pt 20):3563–3571, Oct 2000.

[32] S. Wiesner, K. R. Legate, and R. Fssler. Integrin-actin interactions. *Cell Mol Life Sci*, 62(10):1081–1099, May 2005.

[33] Jieqing Zhu, Brian Boylan, Bing-Hao Luo, Peter J Newman, and Timothy A Springer. Tests of the extension and deadbolt models of integrin activation. *J Biol Chem*, 282(16):11914–11920, Apr 2007.

[34] Junichi Takagi, Benjamin M Petre, Thomas Walz, and Timothy A Springer. Global conformational rearrangements in integrin extracellular domains in outside-in and inside-out signaling. *Cell*, 110(5):599–511, Sep 2002.

[35] Anthony W Partridge, Shouchun Liu, Sanguk Kim, James U Bowie, and Mark H Ginsberg. Transmembrane domain helix packing stabilizes integrin alphaiibbeta3 in the low affinity state. *J Biol Chem*, 280(8):7294–7300, Feb 2005.

[36] M. A. Arnaout, B. Mahalingam, and J. P. Xiong. Integrin structure, allostery, and bidirectional signaling. *Annu Rev Cell Dev Biol*, 21:381–410, 2005. Structural Biology Program, Leukocyte Biology and Inflammation Program, Nephrology Division, Department of Medicine, Massachusetts General Hospital and Harvard Medical School, Charlestown, Massachussetts 02129, USA. arnaout@receptor.mgh.harvard.edu.

[37] Eileen Puklin-Faucher, Mu Gao, Klaus Schulten, and Viola Vogel. How the headpiece hinge angle is opened: New insights into the dynamics of integrin activation. *J Cell Biol*, 175(2):349–360, Oct 2006.

[38] J. Chen, J. Takagi, C. Xie, T. Xiao, B. H. Luo, and T. A. Springer. The relative influence of metal ion binding sites in the i-like domain and the interface with the hybrid domain on rolling and firm adhesion by integrin alpha4beta7. *J Biol Chem*, 279(53):55556–61, 2004. The CBR Institute for Biomedical Research and Department of Pathology, Harvard Medical School, 200 Longwood Avenue, Boston, MA 02115, USA.

[39] Junichi Takagi, Konstantin Strokovich, Timothy A Springer, and Thomas Walz. Structure of integrin alpha5beta1 in complex with fibronectin. *EMBO J*, 22(18):4607–4615, Sep 2003.

[40] A. Paul Mould, Emlyn J H Symonds, Patrick A Buckley, J. Gnter Grossmann, Paul A McEwan, Stephanie J Barton, Janet A Askari, Susan E Craig, Jordi Bella, and Martin J Humphries. Structure of an integrin-ligand complex deduced from solution x-ray scattering and site-directed mutagenesis. *J Biol Chem*, 278(41):39993–39999, Oct 2003.

[41] Kay-E. Gottschalk and Horst Kessler. The structures of integrins and integrin-ligand complexes: implications for drug design and signal transduction. *Angew Chem Int Ed Engl*, 41(20):3767–3774, Oct 2002.

[42] JianFeng Chen, Azucena Salas, and Timothy A Springer. Bistable regulation of integrin adhesiveness by a bipolar metal ion cluster. *Nat Struct Biol*, 10(12):995–1001, Dec 2003.

[43] Carman C.V. Springer T.A. Luo, B. H. Structural basis of integrin regulation and signaling. *Annu Rev Immunol*, 25:619–47, 2007. 3708124928o-viscoelasticity.enl.

[44] David Craig, Mu Gao, Klaus Schulten, and Viola Vogel. Structural insights into how the midas ion stabilizes integrin binding to an rgd peptide under force. *Structure*, 12(11):2049–2058, Nov 2004.

[45] Richard O Hynes. Integrins: bidirectional, allosteric signaling machines. *Cell*, 110(6):673–687, Sep 2002.

[46] Jian-Ping Xiong, Thilo Stehle, Simon L Goodman, and M. Amin Arnaout. New insights into the structural basis of integrin activation. *Blood*, 102(4):1155–1159, Aug 2003.

[47] Kay-Eberhard Gottschalk and Horst Kessler. A computational model of transmembrane integrin clustering. *Structure*, 12(6):1109–1116, Jun 2004.

[48] Bing-Hao Luo, Timothy A Springer, and Junichi Takagi. A specific interface between integrin transmembrane helices and affinity for ligand. *PLoS Biol*, 2(6):e153, Jun 2004.

[49] X. Du, M. Gu, J. W. Weisel, C. Nagaswami, J. S. Bennett, R. Bowditch, and M. H. Ginsberg. Long range propagation of conformational changes in integrin alpha iib beta 3. *J Biol Chem*, 268(31):23087–23092, Nov 1993.

[50] A. Paul Mould. Analyzing integrin-dependent adhesion. *Curr Protoc Cell Biol*, Chapter 9:Unit 9.4, Aug 2002.

[51] A. Paul Mould, Stephanie J Barton, Janet A Askari, Susan E Craig, and Martin J Humphries. Role of admidas cation-binding site in ligand recognition by integrin alpha 5 beta 1. *J Biol Chem*, 278(51):51622–51629, Dec 2003.

[52] Wei Yang, Motomu Shimaoka, Azucena Salas, Junichi Takagi, and Timothy A Springer. Intersubunit signal transmission in integrins by a receptor-like interaction with a pull spring. *Proc Natl Acad Sci U S A*, 101(9):2906–2911, Mar 2004.

[53] Bing-Hao Luo and Timothy A Springer. Integrin structures and conformational signaling. *Curr Opin Cell Biol*, 18(5):579–586, Oct 2006.

[54] A. Armulik, I. Nilsson, G. von Heijne, and S. Johansson. Determination of the border between the transmembrane and cytoplasmic domains of human integrin subunits. *J Biol Chem*, 274(52):37030–37034, Dec 1999.

[55] Martin J Humphries. Insights into integrin-ligand binding and activation from the first crystal structure. *Arthritis Res*, 4 Suppl 3:S69–S78, 2002.

[56] Y. Takada and W. Puzon. Identification of a regulatory region of integrin beta 1 subunit using activating and inhibiting antibodies. *J Biol Chem*, 268(23):17597–17601, Aug 1993.

[57] J. Tsuchida, S. Ueki, Y. Saito, and J. Takagi. Classification of 'activation' antibodies against integrin beta1 chain. *FEBS Lett*, 416(2):212–216, Oct 1997.

[58] David M Rose, Ronen Alon, and Mark H Ginsberg. Integrin modulation and signaling in leukocyte adhesion and migration. *Immunol Rev*, 218:126–134, Aug 2007.

[59] Magda Kucia, Kacper Jankowski, Ryan Reca, Marcin Wysoczynski, Laura Bandura, Daniel J Allendorf, Jin Zhang, Janina Ratajczak, and Mariusz Z Ratajczak. Cxcr4-sdf-1 signalling, locomotion, chemotaxis and adhesion. *J Mol Histol*, 35(3):233–245, Mar 2004.

[60] A. Chigaev, G. Zwartz, S. W. Graves, D. C. Dwyer, H. Tsuji, T. D. Foutz, B. S. Edwards, E. R. Prossnitz, R. S. Larson, and L. A. Sklar. Alpha4beta1 integrin affinity changes govern cell adhesion. *J Biol Chem*, 278(40):38174–82, 2003. Department of Pathology and Cancer Center, University of New Mexico HSC, Albuquerque, New Mexico 87131, USA.

[61] Guoying Jiang, Grgory Giannone, David R Critchley, Emiko Fukumoto, and Michael P Sheetz. Two-piconewton slip bond between fibronectin and the cytoskeleton depends on talin. *Nature*, 424(6946):334–337, Jul 2003.

[62] Grgory Giannone, Guoying Jiang, Deborah H Sutton, David R Critchley, and Michael P Sheetz. Talin1 is critical for force-dependent reinforcement of initial integrin-cytoskeleton bonds but not tyrosine kinase activation. *J Cell Biol*, 163(2):409–419, Oct 2003.

[63] Olga Vinogradova, Algirdas Velyvis, Asta Velyviene, Bin Hu, Thomas Haas, Edward Plow, and Jun Qin. A structural mechanism of integrin alpha(iib)beta(3) "inside-out" activation as regulated by its cytoplasmic face. *Cell*, 110(5):587–597, Sep 2002.

[64] David A Calderwood, Boxu Yan, Jose M de Pereda, Begoa Garca Alvarez, Yosuke Fujioka, Robert C Liddington, and Mark H Ginsberg. The phosphotyrosine binding-like domain of talin activates integrins. *J Biol Chem*, 277(24):21749–21758, Jun 2002.

[65] B. Yan, D. A. Calderwood, B. Yaspan, and M. H. Ginsberg. Calpain cleavage promotes talin binding to the beta 3 integrin cytoplasmic domain. *J Biol Chem*, 276(30):28164–28170, Jul 2001.

[66] Seiji Tadokoro, Sanford J Shattil, Koji Eto, Vera Tai, Robert C Liddington, Jose M de Pereda, Mark H Ginsberg, and David A Calderwood. Talin binding to integrin beta tails: a final common step in integrin activation. *Science*, 302(5642):103–106, Oct 2003.

[67] Bernhard Nieswandt, Markus Moser, Irina Pleines, David Varga-Szabo, Sue Monkley, David Critchley, and Reinhard Fssler. Loss of talin1 in platelets abrogates integrin activation, platelet aggregation, and thrombus formation in vitro and in vivo. *J Exp Med*, 204(13):3113–3118, Dec 2007.

[68] Kate L Wegener, Anthony W Partridge, Jaewon Han, Andrew R Pickford, Robert C Liddington, Mark H Ginsberg, and Iain D Campbell. Structural basis of integrin activation by talin. *Cell*, 128(1):171–182, Jan 2007.

[69] M. H. Ginsberg, A. Partridge, and S. J. Shattil. Integrin regulation. *Curr Opin Cell Biol*, 17(5):509–16, 2005. Department of Medicine, University of California San Diego, La Jolla, California 92093, USA.

[70] Binnig, Quate, and Gerber. Atomic force microscope. *Phys Rev Lett*, 56(9):930–933, Mar 1986.

[71] Julia Morfill, Kerstin Blank, Christian Zahnd, Beatrice Luginbhl, Ferdinand Khner, Kay-E. Gottschalk, Andreas Plckthun, and Hermann E Gaub. Affinity-matured recombinant antibody fragments analyzed by single-molecule force spectroscopy. *Biophys J*, 93(10):3583–3590, Nov 2007.

[72] X. Zhang, A. Chen, D. De Leon, H. Li, E. Noiri, V. T. Moy, and M. S. Goligorsky. Atomic force microscopy measurement of leukocyte-endothelial interaction. *Am J Physiol Heart Circ Physiol*, 286(1):H359–67, 2004. Dept. of Physiology and Biophysics, Univ. of Miami School of Medicine, Miami, FL 33101-6430, USA.

[73] R. H. Eibl and V. T. Moy. Atomic force microscopy measurements of protein-ligand interactions on living cells. *Methods Mol Biol*, 305:439–50, 2005. Department of Physiology and Biophysics, University of Miami School of Medicine, Miami, FL, USA.

[74] M. Benoit and H. E. Gaub. Measuring cell adhesion forces with the atomic force microscope at the molecular level. *Cells Tissues Organs*, 172(3):174–89, 2002. Center for Nano Science, Ludwigs-Maximilians-Universitat, Munich, Germany. Martin.Benoit@physik.uni-muenchen.de.

[75] M. Kessler, K. E. Gottschalk, H. Janovjak, D. J. Muller, and H. E. Gaub. Bacteriorhodopsin folds into the membrane against an external force. *Journal of Molecular Biology*, 357:644–654, 2006.

[76] S. K. Kufer, E. M. Puchner, H. Gumpp, T. Liedl, and H. E. Gaub. Single-molecule cut-and-paste surface assembly. *Science*, 319(5863):594–596, Feb 2008.

[77] G.I. Bell. Models for the specific adhesion of cells to cells. *Science*, 200:618–627, 1978.

[78] H. A. Kramers. Brownian motion in a field of force and the diffusion model of chemical reactions. *Physica*, 7:284–304, 1940.

[79] E. Evans and K. Ritchie. Dynamic strength of molecular adhesion bonds. *Biophys J*, 72(4):1541–55, 1997. Department of Physics, University of British Columbia, Vancouver, Canada. evans@physics.ubc.ca.

[80] Nathan D Gallant and Andrs J Garca. Model of integrin-mediated cell adhesion strengthening. *J Biomech*, 40(6):1301–1309, 2007.

[81] E. Evans. Probing the relation between force–lifetime–and chemistry in single molecular bonds. *Annu Rev Biophys Biomol Struct*, 30:105–28, 2001. Physics and Pathology, University of British Columbia, Vancouver, V6T 2A6, Canada. evans@physics.ubc.ca.

[82] E. Evans and K. Ritchie. Strength of a weak bond connecting flexible polymer chains. *Biophys J*, 76(5):2439–47, 1999. Physics and Pathology, University of British Columbia, Vancouver, British Columbia V6T 1Z1, Canada. evans@physics.ubc.ca.

[83] Bryan T Marshall, Krishna K Sarangapani, Jizhong Lou, Rodger P McEver, and Cheng Zhu. Force history dependence of receptor-ligand dissociation. *Biophys J*, 88(2):1458–1466, Feb 2005.

[84] Evan A Evans and David A Calderwood. Forces and bond dynamics in cell adhesion. *Science*, 316(5828):1148–1153, May 2007.

[85] Philippe P. Girard, Elisabetta A. Cavalcanti-Adam, Ralf Kemkemer, and Joachim P. Spatz. Cellular chemomechanics at interfaces: sensing, integration and response. *Soft Matter*, 3:307–326, 2007.

[86] R. Alon, S. W. Feigelson, E. Manevich, D. M. Rose, J. Schmitz, D. R. Overby, E. Winter, V. Grabovsky, V. Shinder, B. D. Matthews, M. Sokolovsky-Eisenberg, D. E. Ingber, M. Benoit, and M. H. Ginsberg. Alpha4beta1-dependent adhesion strengthening under mechanical strain is regulated by paxillin association with the alpha4-cytoplasmic domain. *J Cell Biol*, 171(6):1073–84, 2005. Department of Immunology, The Weizmann Institute of Science, Rehovot 76100, Israel. ronen.alon@weizmann.ac.il.

[87] P. E. Hughes and M. Pfaff. Integrin affinity modulation. *Trends Cell Biol*, 8(9):359–364, Sep 1998.

[88] S. Liu, S. M. Thomas, D. G. Woodside, D. M. Rose, W. B. Kiosses, M. Pfaff, and M. H. Ginsberg. Binding of paxillin to alpha4 integrins modifies integrin-dependent biological responses. *Nature*, 402(6762):676–81, 1999. Department of Vascular Biology, The Scripps Research Institute, La Jolla, California 92037, USA.

[89] S. Liu and M. H. Ginsberg. Paxillin binding to a conserved sequence motif in the alpha 4 integrin cytoplasmic domain. *J Biol Chem*, 275(30):22736–42, 2000. Department of Vascular Biology, The Scripps Research Institute, La Jolla, California 92037, USA.

[90] J. Han, S. Liu, D. M. Rose, D. D. Schlaepfer, H. McDonald, and M. H. Ginsberg. Phosphorylation of the integrin alpha 4 cytoplasmic domain regulates paxillin binding. *J Biol Chem*, 276(44):40903–40909, Nov 2001.

[91] Lawrence E Goldfinger, Jaewon Han, William B Kiosses, Alan K Howe, and Mark H Ginsberg. Spatial restriction of alpha4 integrin phosphorylation regulates lamellipodial stability and alpha4beta1-dependent cell migration. *J Cell Biol*, 162(4):731–741, Aug 2003.

[92] D. M. Rose, S. Liu, D. G. Woodside, J. Han, D. D. Schlaepfer, and M. H. Ginsberg. Paxillin binding to the alpha 4 integrin subunit stimulates lfa-1 (integrin alpha l beta 2)-dependent t cell migration by augmenting the activation of focal adhesion kinase/proline-rich tyrosine kinase-2. *J Immunol*, 170(12):5912–8, 2003. Division of Rheumatology, Allergy, and Immunology, Department of Medicine, University of California, San Diego, La Jolla, CA 92093, USA. drose@vapop.ucsd.edu.

[93] J. R. Chan, S. J. Hyduk, and M. I. Cybulsky. Alpha 4 beta 1 integrin/vcam-1 interaction activates alpha l beta 2 integrin-mediated adhesion to icam-1 in human t cells. *J Immunol*, 164(2):746–753, Jan 2000.

[94] C. E. Turner. Paxillin. *Int J Biochem Cell Biol*, 30(9):955–959, Sep 1998.

[95] C. E. Turner, M. C. Brown, J. A. Perrotta, M. C. Riedy, S. N. Nikolopoulos, A. R. McDonald, S. Bagrodia, S. Thomas, and P. S. Leventhal. Paxillin ld4 motif binds pak and pix through a novel 95-kd ankyrin repeat, arf-gap protein: A role in cytoskeletal remodeling. *J Cell Biol*, 145(4):851–863, May 1999.

[96] D. F. Kucik, M. L. Dustin, J. M. Miller, and E. J. Brown. Adhesion-activating phorbol ester increases the mobility of leukocyte integrin lfa-1 in cultured lymphocytes. *J Clin Invest*, 97(9):2139–2144, May 1996.

[97] R. L. Yauch, D. P. Felsenfeld, S. K. Kraeft, L. B. Chen, M. P. Sheetz, and M. E. Hemler. Mutational evidence for control of cell adhesion through integrin diffusion/clustering, independent of ligand binding. *J Exp Med*, 186(8):1347–1355, Oct 1997.

[98] M. Kim, C. V. Carman, W. Yang, A. Salas, and T. A. Springer. The primacy of affinity over clustering in regulation of adhesiveness of the integrin alphalbeta2. *J Cell Biol*, 167(6):1241–53, 2004. The CBR Institute for Biomedical Research and Department of Pathology, Harvard Medical School, Boston, MA 02115, USA.

[99] Birgit Leitinger and Nancy Hogg. The involvement of lipid rafts in the regulation of integrin function. *J Cell Sci*, 115(Pt 5):963–972, Mar 2002.

[100] R. Shamri, V. Grabovsky, S. W. Feigelson, O. Dwir, Y. Van Kooyk, and R. Alon. Chemokine stimulation of lymphocyte alpha 4 integrin avidity but not of leukocyte function-associated antigen-1 avidity to endothelial ligands under shear flow requires cholesterol membrane rafts. *J Biol Chem*, 277(42):40027–35, 2002. Department of Immunology, Weizmann Institute of Science, Rehovot, 76100 Israel.

[101] Sharon J Hyduk, Jiwon Oh, Haiyan Xiao, Mian Chen, and Myron I Cybulsky. Paxillin selectively associates with constitutive and chemoattractant-induced high-affinity alpha4beta1 integrins: implications for integrin signaling. *Blood*, 104(9):2818–2824, Nov 2004.

[102] Julia Schmitz, Benoit Martin, and Kay Eberhard Gottschalk. The visocelasticity of membrane tethers and its importance for cell adhesion. *Biophys J*, X:in press, May 2008.

[103] Viola Vogel and Michael Sheetz. Local force and geometry sensing regulate cell functions. *Nat Rev Mol Cell Biol*, 7(4):265–275, Apr 2006.

[104] Manuel Thry, Victor Racine, Matthieu Piel, Anne Ppin, Ariane Dimitrov, Yong Chen, Jean-Baptiste Sibarita, and Michel Bornens. Anisotropy of cell adhesive microenvironment governs cell internal organization and orientation of polarity. *Proc Natl Acad Sci U S A*, 103(52):19771–19776, Dec 2006.

[105] Ana Kostic and Michael P Sheetz. Fibronectin rigidity response through fyn and p130cas recruitment to the leading edge. *Mol Biol Cell*, 17(6):2684–2695, Jun 2006.

[106] R. Alon and M. L. Dustin. Force as a facilitator of integrin conformational changes during leukocyte arrest on blood vessels and antigen-presenting cells. *Immunity*, 26(1):17–27, 2007. Department of Immunology, Weizmann Institute of Science, Rehovot, Israel. ronen.alon@weizmann.ac.il.

[107] Ilya Leventhal, Penelope C. Georges, and Paul A Janmey. Soft biological materials and their impact on cell function. *Soft Matter*, 3:299–306, 2007.

[108] Paul A Janmey and Christopher A McCulloch. Cell mechanics: integrating cell responses to mechanical stimuli. *Annu Rev Biomed Eng*, 9:1–34, 2007.

[109] Moonsoo Jin, Ioan Andricioaei, and Timothy A Springer. Conversion between three conformational states of integrin i domains with a c-terminal pull spring studied with molecular dynamics. *Structure*, 12(12):2137–2147, Dec 2004.

[110] Nathan S Astrof, Azucena Salas, Motomu Shimaoka, JianFeng Chen, and Timothy A Springer. Importance of force linkage in mechanochemistry of adhesion receptors. *Biochemistry*, 45(50):15020–15028, Dec 2006.

[111] Cheng Zhu, Tadayuki Yago, Jizhong Lou, Veronika I Zarnitsyna, and Rodger P McEver. Mechanisms for flow-enhanced cell adhesion. *Ann Biomed Eng*, 36(4):604–621, Apr 2008.

[112] Jizhong Lou, Tadayuki Yago, Arkadiusz G Klopocki, Padmaja Mehta, Wei Chen, Veronika I Zarnitsyna, Nicolai V Bovin, Cheng Zhu, and Rodger P McEver. Flow-enhanced adhesion regulated by a selectin interdomain hinge. *J Cell Biol*, 174(7):1107–1117, Sep 2006.

[113] W. S. Somers, J. Tang, G. D. Shaw, and R. T. Camphausen. Insights into the molecular basis of leukocyte tethering and rolling revealed by structures of p- and e-selectin bound to sle(x) and psgl-1. *Cell*, 103(3):467–479, Oct 2000.

[114] Donald E Ingber. Tensegrity ii. how structural networks influence cellular information processing networks. *J Cell Sci*, 116(Pt 8):1397–1408, Apr 2003.

[115] R. Satcher, C. F. Dewey, and J. H. Hartwig. Mechanical remodeling of the endothelial surface and actin cytoskeleton induced by fluid flow. *Microcirculation*, 4(4):439–453, Dec 1997.

[116] Catherine G Galbraith, Kenneth M Yamada, and Michael P Sheetz. The relationship between force and focal complex development. *J Cell Biol*, 159(4):695–705, Nov 2002.

[117] Sabrena Noria, Feng Xu, Shannon McCue, Mara Jones, Avrum I Gotlieb, and B. Lowell Langille. Assembly and reorientation of stress fibers drives morphological changes to endothelial cells exposed to shear stress. *Am J Pathol*, 164(4):1211–1223, Apr 2004.

[118] K. Hayakawa, N. Sato, and T. Obinata. Dynamic reorientation of cultured cells and stress fibers under mechanical stress from periodic stretching. *Exp Cell Res*, 268(1):104–114, Aug 2001.

[119] A. M. Collinsworth, C. E. Torgan, S. N. Nagda, R. J. Rajalingam, W. E. Kraus, and G. A. Truskey. Orientation and length of mammalian skeletal myocytes in response to a unidirectional stretch. *Cell Tissue Res*, 302(2):243–251, Nov 2000.

[120] Rumi De, Assaf Zemel, and Samuel A. Safran. Dynamics of cell orientation. *Nature Physics*, 3:655–659, 2007.

[121] Alexandre Saez, Marion Ghibaudo, Axel Buguin, Pascal Silberzan, and Benot Ladoux. Rigidity-driven growth and migration of epithelial cells on microstructured anisotropic substrates. *Proc Natl Acad Sci U S A*, 104(20):8281–8286, May 2007.

[122] Chirag B Khatiwala, Shelly R Peyton, and Andrew J Putnam. Intrinsic mechanical properties of the extracellular matrix affect the behavior of pre-osteoblastic mc3t3-e1 cells. *Am J Physiol Cell Physiol*, 290(6):C1640–C1650, Jun 2006.

[123] Muhammad H Zaman, Linda M Trapani, Alisha L Sieminski, Alisha Siemeski, Drew Mackellar, Haiyan Gong, Roger D Kamm, Alan Wells, Douglas A Lauffenburger, and Paul Matsudaira. Migration of tumor cells in 3d matrices is governed by matrix stiffness along with cell-matrix adhesion and proteolysis. *Proc Natl Acad Sci U S A*, 103(29):10889–10894, Jul 2006.

[124] Adam J Engler, Shamik Sen, H. Lee Sweeney, and Dennis E Discher. Matrix elasticity directs stem cell lineage specification. *Cell*, 126(4):677–689, Aug 2006.

[125] F. G. Giancotti and E. Ruoslahti. Integrin signaling. *Science*, 285(5430):1028–1032, Aug 1999.

[126] G. N. Stamatas and L. V. McIntire. Rapid flow-induced responses in endothelial cells. *Biotechnol Prog*, 17(3):383–402, 2001.

[127] Donald E Ingber. Cellular mechanotransduction: putting all the pieces together again. *FASEB J*, 20(7):811–827, May 2006.

[128] Jeffrey A DiVietro, David C Brown, Larry A Sklar, Richard S Larson, and Michael B Lawrence. Immobilized stromal cell-derived factor-1alpha triggers rapid vla-4 affinity increases to stabilize lymphocyte tethers on vcam-1 and subsequently initiate firm adhesion. *J Immunol*, 178(6):3903–3911, Mar 2007.

[129] V. Grabovsky, S. Feigelson, C. Chen, D. A. Bleijs, A. Peled, G. Cinamon, F. Baleux, F. Arenzana-Seisdedos, T. Lapidot, Y. van Kooyk, R. R. Lobb, and R. Alon. Sub-second induction of alpha4 integrin clustering by immobilized chemokines stimulates leukocyte tethering and rolling on endothelial vascular cell adhesion molecule 1 under flow conditions. *J Exp Med*, 192(4):495–506, 2000. Department of Immunology, The Weizmann Institute of Science, Rehovot, 76100 Israel.

[130] G. Constantin, M. Majeed, C. Giagulli, L. Piccio, J. Y. Kim, E. C. Butcher, and C. Laudanna. Chemokines trigger immediate beta2 integrin affinity and mobility changes: differential regulation and roles in lymphocyte arrest under flow. *Immunity*, 13(6):759–769, Dec 2000.

[131] R. Shamri, V. Grabovsky, J. M. Gauguet, S. Feigelson, E. Manevich, W. Kolanus, M. K. Robinson, D. E. Staunton, U. H. von Andrian, and R. Alon. Lymphocyte arrest requires instantaneous induction of an extended lfa-1 conformation mediated

by endothelium-bound chemokines. *Nat Immunol*, 6(5):497–506, 2005. Department of Immunology, Weizmann Institute of Science, Rehovot 76100, Israel.

[132] C. Chen, J. L. Mobley, O. Dwir, F. Shimron, V. Grabovsky, R. R. Lobb, Y. Shimizu, and R. Alon. High affinity very late antigen-4 subsets expressed on t cells are mandatory for spontaneous adhesion strengthening but not for rolling on vcam-1 in shear flow. *J Immunol*, 162(2):1084–95, 1999. Department of Immunology, The Weizmann Institute of Science, Rehovot, Israel.

[133] F. Sanz-Rodriguez, A. Hidalgo, and J. Teixido. Chemokine stromal cell-derived factor-1alpha modulates vla-4 integrin-mediated multiple myeloma cell adhesion to cs-1/fibronectin and vcam-1. *Blood*, 97(2):346–51, 2001. Department of Immunology, Centro de Investigaciones Biologicas, Madrid, Spain.

[134] C. C. Bleul, R. C. Fuhlbrigge, J. M. Casasnovas, A. Aiuti, and T. A. Springer. A highly efficacious lymphocyte chemoattractant, stromal cell-derived factor 1 (sdf-1). *J Exp Med*, 184(3):1101–1109, Sep 1996.

[135] A. Peled, O. Kollet, T. Ponomaryov, I. Petit, S. Franitza, V. Grabovsky, M. M. Slav, A. Nagler, O. Lider, R. Alon, D. Zipori, and T. Lapidot. The chemokine sdf-1 activates the integrins lfa-1, vla-4, and vla-5 on immature human cd34(+) cells: role in transendothelial/stromal migration and engraftment of nod/scid mice. *Blood*, 95(11):3289–3296, Jun 2000.

[136] Eugenia Manevich, Valentin Grabovsky, Sara W Feigelson, and Ronen Alon. Talin 1 and paxillin facilitate distinct steps in rapid vla-4-mediated adhesion strengthening to vascular cell adhesion molecule 1. *J Biol Chem*, 282(35):25338–25348, Aug 2007.

[137] Eilon Woolf, Irina Grigorova, Adi Sagiv, Valentin Grabovsky, Sara W Feigelson, Ziv Shulman, Tanja Hartmann, Michael Sixt, Jason G Cyster, and Ronen Alon. Lymph node chemokines promote sustained t lymphocyte motility without triggering stable integrin adhesiveness in the absence of shear forces. *Nat Immunol*, 8(10):1076–1085, Oct 2007.

[138] L. L. Chen, A. Whitty, D. Scott, W. C. Lee, M. Cornebise, S. P. Adams, R. C. Petter, R. R. Lobb, and R. B. Pepinsky. Evidence that ligand and metal ion binding to integrin alpha 4beta 1 are regulated through a coupled equilibrium. *J Biol Chem*, 276(39):36520–9, 2001. Biogen, Inc., Cambridge, Massachusetts 02142, USA.

[139] B. Tilton, L. Ho, E. Oberlin, P. Loetscher, F. Baleux, I. Clark-Lewis, and M. Thelen. Signal transduction by cxc chemokine receptor 4. stromal cell-derived factor 1 stimulates prolonged protein kinase b and extracellular signal-regulated kinase 2 activation in t lymphocytes. *J Exp Med*, 192(3):313–324, Aug 2000.

[140] U. S. Schwarz and R. Alon. L-selectin-mediated leukocyte tethering in shear flow is controlled by multiple contacts and cytoskeletal anchorage facilitating fast rebinding events. *Proc Natl Acad Sci U S A*, 101(18):6940–5, 2004. Theory Division, Max Planck Institute of Colloids and Interfaces, 14424 Potsdam, Germany. urlich.schwarz@mpikg-golm.mpg.de.

[141] M. Benoit, D. Gabriel, G. Gerisch, and H. E. Gaub. Discrete interactions in cell adhesion measured by single-molecule force spectroscopy. *Nat Cell Biol*, 2(6):313–7, 2000. Centre for Nanoscience, Ludwig Maximilians Universitat Munchen, Amalienstrabetae 54, D-80799 Munchen, Germany. Martin.Benoit@physik.uni-muenchen.de.

[142] T. Erdmann and U. S. Schwarz. Stability of adhesion clusters under constant force. *Phys Rev Lett*, 92(10):108102, Mar 2004.

[143] S. E. Chesla, P. Selvaraj, and C. Zhu. Measuring two-dimensional receptor-ligand binding kinetics by micropipette. *Biophys J*, 75(3):1553–72, 1998. George W. Woodruff School of Mechanical Engineering, Georgia Institute of Technology, Atlanta 30332-0405, USA.

[144] C. Zhu. Kinetics and mechanics of cell adhesion. *J Biomech*, 33(1):23–33, 2000. George W. Woodruff School of Mechanical Engineering and Department of Biomedical Engineering, Georgia Institute of Technology, Atlanta 30332-0363, USA. cheng.zhu@me.gatech.edu.

[145] Alexandre Chigaev, Tione Buranda, Denise C Dwyer, Eric R Prossnitz, and Larry A Sklar. Fret detection of cellular alpha4-integrin conformational activation. *Biophys J*, 85(6):3951–3962, Dec 2003.

[146] Motomu Shimaoka and Timothy A Springer. Therapeutic antagonists and conformational regulation of integrin function. *Nat Rev Drug Discov*, 2(9):703–716, Sep 2003.

[147] Gordon Zwartz, Alexandre Chigaev, Terry Foutz, Richard S Larson, Richard Posner, and Larry A Sklar. Relationship between molecular and cellular dissociation rates for vla-4/vcam-1 interaction in the absence of shear stress. *Biophys J*, 86(2):1243–1252, Feb 2004.

[148] A. Chigaev, A. M. Blenc, J. V. Braaten, N. Kumaraswamy, C. L. Kepley, R. P. Andrews, J. M. Oliver, B. S. Edwards, E. R. Prossnitz, R. S. Larson, and L. A. Sklar. Real time analysis of the affinity regulation of alpha 4-integrin. the physiologically activated receptor is intermediate in affinity between resting and mn(2+) or antibody activation. *J Biol Chem*, 276(52):48670–8, 2001. Department of Pathology and Cancer Center, University of New Mexico Health Sciences Center, Albuquerque, New Mexico 87131, USA.

[149] K. L. Ekinci. Electromechanical transducers at the nanoscale: actuation and sensing of motion in nanoelectromechanical systems (nems). *Small*, 1(8-9):786–797, Aug 2005.

[150] D.V. Scheible, A. Erbe, and R.H. Blick. Tunable coupled nanomechanical resonators for single-electron transport. *New Journal of Physics*, 4:86.1–86–7, 2002.

[151] A. Isacsson. Dynamics of a three-terminal mechanically flexible tunneling contact. *Physical Review Letters*, 64:035326, 2001.

[152] S. Foale and S.R. Bishop. Dynamical complexities of forced impacting systems. *Philosophical Transactions: Physical Sciences and Engineering*, 338:547–556, 1992.

[153] Rodger P McEver and Cheng Zhu. A catch to integrin activation. *Nat Immunol*, 8(10):1035–1037, Oct 2007.

[154] Christian H Albrecht, Gregor Neuert, Robert A Lugmaier, and Hermann E Gaub. Molecular force balance measurements reveal that dsdna unbinds under force in rate dependent pathways. *Biophys J*, Mar 2008.

[155] Hendrik Dietz, Felix Berkemeier, Morten Bertz, and Matthias Rief. Anisotropic deformation response of single protein molecules. *Proc Natl Acad Sci U S A*, 103(34):12724–12728, Aug 2006.

[156] Marco Arnold, Elisabetta Ada Cavalcanti-Adam, Roman Glass, Jacques Blmmel, Wolfgang Eck, Martin Kantlehner, Horst Kessler, and Joachim P Spatz. Activation of integrin function by nanopatterned adhesive interfaces. *Chemphyschem*, 5(3):383–388, Mar 2004.

[157] A. I. Barakat. A model for shear stress-induced deformation of a flow sensor on the surface of vascular endothelial cells. *J Theor Biol*, 210(2):221–36, 2001. Department of Mechanical and Aeronautical Engineering, University of California, One Shields Avenue, Davis, CA 95616, USA. abarakat@ucdavis.edu.

Thanks

In the end, I wish to say "thank you" to the people, who contributed to my work:

Curriculum Vitae

Address

Julia Schmitz
Ludwig-Maximilians-University
Amalienstr. 54
80799 Munich, Germany
phone: +49-89-21803133
email: juliaschmitz@lmu.de

Personal Details

Date of Birth: 14.06.1980
Place of Birth: Gräfelfing
Nationality: German

Education

05/2005 to present:	**PhD in Physics** Thesis advisor: Dr. Kay-Eberhard Gottschalk Chair for Applied Physics (Prof. Dr. Hermann E. Gaub) Ludwig-Maximilians-University, Munich, Germany
09/1999 to 02/2005:	**Diploma in Physics (grade: very good)** Diploma thesis: Force Spectroscopy on Human T-Lymphocytes Thesis advisor: Dr. Martin Benoit Chair for Applied Physics (Prof. Dr. Hermann E. Gaub) Ludwig-Maximilians-University, Munich, Germany
07/1999:	**Abitur (grade: 1.0)** Grammar school Starnberg